UNVEILING STRATEGIES FOR CHIKUNGUNYA VIRUS ATTENUATION AND ANTIVIRAL THERAPY

By

Alison Whitney Ashbrook

Dissertation

Submitted to the Faculty of the

Graduate School of Vanderbilt University

in partial fulfillment of the requirements

for the degree of

DOCTOR OF PHILOSOPHY

in

Microbiology and Immunology

August, 2015

Nashville, Tennessee

Approved:

Christopher R. Aiken, Ph.D.

Terence S. Dermody, M.D.

D. Borden Lacy, Ph.D.

James W. Thomas, M.D.

John V. Williams, M.D.

Sandra S. Zinkel, M.D., Ph.D.

To my father, Andrew,
for his humor and passion for life
No one lives like you

To my mother, Carla,
for her strength and caring heart
No one loves like you

ACKNOWLEDGEMENTS

I am grateful for the financial support provided by Public Health Service grants U54 AI057157 from the Southeast Regional Center of Excellence for Emerging Infections and Biodefense Development and T32 HL007751 from the National Heart, Lung, and Blood Institute. Additional support was provided by the Elizabeth B. Lamb Center for Pediatric Research and a Dissertation Enhancement Grant from the Vanderbilt University Graduate School that supported my studies conducted in the laboratory of Dr. Thomas E. Morrison at the University of Colorado.

I am forever indebted to Terry Dermody for the opportunity to complete my training in his laboratory and under his mentorship. His dedication to his trainees is unparalleled, and I am so appreciative of all of the support and kindness he has shown me over the past 5 years. I have learned so much about science and life from the wonderful example he sets as a leader, mentor, and friend.

I thank all past and present members of the Dermody lab. Long work days were always made better by having friends close by. I am grateful for having had the chance to work with such collaborative and creative individuals. In particular, I would like to thank Laurie Silva for her generous mentorship and help with all things CHIKV, including my training to work in the BSL3 laboratory. I also would like to thank Bernardo Mainou for his insatiable excitement for science and scientific conversations, which were almost always the highlight of my day. I am grateful to Paula Zamora and Anthony Lentscher for their assistance with experiments presented in this thesis and for the creative ideas and suggestions they have offered me during my graduate work.

I am thankful to Dr. Tem Morrison for hosting me to perform animal studies during my training. It was a wonderful experience to train with such enthusiastic and talented individuals. I learned a great deal from Tem and his students, Kristina Stoermer, David Hawman, and Henri Jupille, and am exceedingly grateful. I would also like to thank Dr. Mark Heise at the University of North Carolina for his assistance with design of experiments and manuscript review.

Members of my thesis committee have provided useful ideas and important suggestions that have greatly improved the quality of my thesis work. I thank Chris Aiken, Borden Lacy, Tom Thomas, John Williams, and Sandy Zinkel for their critical assessments of my work and for their generous support. I have so appreciated the time spent in their company. Additionally, I would like to thank all members of the Pathology, Microbiology, and Immunology and Pediatric Infectious Diseases departments. The fellow graduate students, postdocs, residents, fellows, faculty members, and administrators have made these departments a wonderful place to call home.

Finally, I would like to thank my family, whose love and devotion are without limit. I am eternally grateful for their encouragement and support throughout every step I have taken in life. It is purely having them in my life that makes anything else matter. Thank you for all you have given me.

TABLE OF CONTENTS

Page

LIST OF TABLES

LIST OF FIGURES

LIST OF ABBREVIATIONS

5-NT	5-nonyloxytryptamine
αMEM	Minimum essential medium alpha
ANOVA	Analysis of variance
BCS	Bovine calf serum
BHK	Baby hamster kidney
BMDC	Bone marrow-derived dendritic cell
BSA	Bovine serum albumin
BSL3	Biological safety level 3
Cas9	CRISPR-associated protein 9
CCL	Chemokine (C-C motif) ligand
cDNA	Complementary deoxyribonucleic acid
CHIKV	Chikungunya virus
CHO	Chinese hamster ovary
CRISPR	Clustered regularly interspaced short palindromic repeats
CRP	C-reactive protein
CPE	Cytopathic effect
CXCL	Chemokine (C-X-C motif) ligand
DNA	Deoxyribonucleic acid
DAPI	4’,6’-diamidino-2-phenylindole
DENV	Dengue virus
DLN	Draining lymph node
DMEM	Dulbecco’s Modified Eagle Medium

DMSO	Dimethyl sulfoxide
dNTPs	Deoxynucleoside triphosphates
EC_{50}	Half maximal effective concentration
ECSA	Eastern, central, southern African
EDTA	Ethylenediaminetetraacetic acid
EEA1	Early endosome antigen 1
EEEV	Eastern equine encephalitis virus
eGFP	Enhanced green fluorescent protein
EM	Electron microscopy
ER	Endoplasmic reticulum
FACS	Fluorescence-activated cell sorting
FBS	Fetal bovine serum
FFU	Fluorescent focus unit
FFWA	Fusion-from-without assay
FISH	Fluorescence *in situ* hybridization
GAG	Glycosaminoglycan
GAPDH	Glyceraldehyde-3-phosphate dehydrogenase
GM-CSF	Granulocyte-macrophage colony-stimulating factor
GMK	Green monkey kidney
h	Hour
H&E	Hemotoxylin and eosin
HBMEC	Human brain microvascular endothelial cell
HCV	Hepatitis C virus

HEPES	4-(2-hydroxyethyl)-1-piperazineethanesulfonic acid
HIV-1	Human immunodeficiency virus-1
HSF	Human synovial fibroblast
IC_{50}	Half inhibitory concentration
IFN	Interferon
IFNAR	Interferon α/β receptor
Ig	Immunoglobulin
IL	Interleukin
IOL	Indian Ocean lineage
IP-10	Interferon gamma-induced protein 10
ISG	Interferon stimulated gene
ISVP	Infectious subvirion particle
IU	Infectious unit
Kb	Kilobase
kDa	Kilodalton
KO	Knock-out
LAV	Live attenuated vaccine
LPS	Lipopolysaccharide
LR	La Réunion
mAB	Monoclonal antibody
MAD	Mean absolute deviation
MAVS/IPS-1	Mitochondrial antiviral signaling/IFN-β promoter stimulator
MCP-1	Monocyte chemoattractant protein-1

MDA5	Melanoma differentiation-associated protein 5
MEF	Murine embryonic fibroblasts
MFI	Mean fluorescence intensity
MIG	Monokine induced by interferon gamma
min	Minute
mM	Millimolar
MOI	Multiplicity of infection
MRC	Medical Research Council
NCC	NIH Clinical Collection
NF-κB	Nuclear transcription factor κB
NH_4Cl	Ammonium chloride
NK cells	Natural killer cells
nm	Nanometer
nM	Nanomolar
NSAID	Non-steroidal anti-inflammatory drug
nsP	Nonstructural protein
ONNV	O'nyong-nyong virus
ORF	Open reading frame
PAGE	Polyacrylamide gel electrophoresis
PBMC	Peripheral blood mononuclear cell
PBS	Phosphate-buffered saline
PBS-T	Phosphate-buffered saline with Tween 20
PCR	Polymerase chain reaction

PDB	Protein data bank
PDI	Protein disulfide isomerase
PFA	Paraformaldehyde
PFU	Plaque forming unit
p.i.	Postinfection
PI	Propidium iodide
PRR	Pattern recognition receptor
PVDF	Polyvinylidene fluoride
qRT-PCR	Quantitative real time PCR
RA	Rheumatoid arthritis
RACE	Rapid amplification of cDNA ends
RANKL	Receptor activator of nuclear factor kappa-B ligand
RANTES	Regulated on activation, normal T cell expressed and secreted
RIG-I	Retinoic acid-inducible gene 1
RLR	RIG-like receptor
RNA	Ribonucleic acid
RPMI-1640	Roswell Park Memorial Institute-1640
RRV	Ross River virus
RT-PCR	Reverse transcriptase-polymerase chain reaction
s	Second
s.c.	Subcutaneous
SD	Standard deviation
SDS	Sodium dodecyl sulfate

SEATO	Southeast Asia Treaty Organization
SEM	Standard error of the mean
SFV	Semliki Forest virus
SIM	Structured illumination microscopy
SINV	Sindbis virus
siRNA	Small-interfering RNA
ssRNA	Single-stranded RNA
STAT1	Signal transducer and activator of transcription 1
STS	Staurosporine
T1L	Reovirus strain type 1 Lang
TAE	Tris acetate EDTA
TBS	Tris-buffered saline
TLR	Toll-like receptor
TP	Tryptose phosphate
TX	Triton X-100
USAMRIID	United States Army Medical Institute of Infectious Disease
UTR	Untranslated region
VDB	Virus dilution buffer
VEEV	Venezuelan equine encephalitis virus
VLP	Virus-like particle
WA	Western African
WEEV	Western equine encephalitis virus
WNV	West Nile virus

WRAIR	Walter Reed Army Institute of Research
WT	Wildtype
µl	Microliter

CHAPTER I

INTRODUCTION

Thesis Overview

The tropism of viruses for discrete sites within the host contributes importantly to viral pathogenesis. Viral attachment receptors and cellular restriction factors are important determinants of viral tropism. Attachment to target cells is the first step in viral replication and depends on tissue-specific expression of viral receptors. Cell-intrinsic restriction factors also influence tropism by limiting replication of virus in specific cell types. Elucidating determinants of viral tropism provides insight into mechanisms of virus dissemination and pathogenesis.

Chikungunya virus (CHIKV) is an arthritogenic alphavirus that has reemerged to cause sudden and severe epidemics throughout sub-Saharan Africa, India, Southeast Asia, and the Caribbean. No vaccines or specific therapies to prevent or mitigate disease are available. CHIKV causes a debilitating musculoskeletal inflammatory disease that can persist for months to years after virus is cleared. However, the pathogenesis of CHIKV infection is not well understood. Additionally, viral and host determinants of CHIKV tropism have not been well characterized.

In Chapter I, I provide a review of CHIKV epidemiology, the replication cycle, pathogenesis, host responses, and current antiviral and vaccine strategies. In Chapter II, I identify CHIKV E2 residue 82 as a critical determinant of viral replication in cell culture that influences interactions with glycosaminoglycans (GAGs). In Chapter III, I report that

E2 residue 82 modulates CHIKV dissemination and arthritis in mice, and interactions with GAGs can influence CHIKV tropism. Chapter IV describes a new function for digoxin, an inhibitor of the sodium-potassium ATPase, in blockade of CHIKV infection. Inhibition by digoxin occurs at both entry and post-entry steps in the CHIKV replication cycle. In Chapter V, I demonstrate that PSME2, a regulator of the immunoproteasome, restricts CHIKV infection. To date, the immunoproteasome has not been implicated in alphavirus infection or restriction and may serve as a new target for development of CHIKV-specific antivirals. Finally, in Chapter VI, I summarize my thesis studies and describe future studies for the continuation of this work. Collectively, my dissertation research has identified new determinants of CHIKV infection and tropism. This work reveals new strategies for CHIKV attenuation and development of antiviral agents.

Alphaviruses

Alphaviruses are members of the *Togaviridae* family and include numerous human pathogens of global importance (Table I-1). In addition to the alphavirus genus, the *Togaviridae* family also includes the rubivirus genus, whose sole member is rubella virus. The alphavirus genus is composed of 29 members that are subdivided into those associated with encephalitis and those associated with arthritis in humans; these two groups are further divided into seven antigenic complexes (1). Historically, encephalitic alphaviruses have been termed New World alphaviruses and arthritogenic alphavirus have been termed Old World alphaviruses. However, with globalization of mosquito vectors, this terminology no longer encompasses the geographic distributions observed for these viruses.

Table I-1 Medically important alphaviruses, antigenic complex, and disease.

Virus (abbreviation)	Antigenic complex	Disease
Barmah Forest (BF)	BF	Fever, arthritis, rash
Chikungunya (CHIK)	SF	Fever, arthritis, rash
Eastern equine encephalitis (EEE)	EEE	Fever, encephalitis
Everglades (EVE)	VEE	Fever, encephalitis
Getah (GET)	SF	Fever
Mayaro (MAY)	SF	Fever, arthritis, rash
O'nyong-nyong (ONN)	SF	Fever, arthritis, rash
Ross River (RR)	SF	Fever, arthritis, rash
Semliki Forest (SF)	SF	Fever, encephalitis
Sindbis (SIN)	WEE	Fever, arthritis, rash
Tonate (TON)	VEE	Fever, encephalitis
Venezuelan equine encephalitis (VEE)	VEE	Fever, encephalitis
Western equine encephalitis (WEE)	WEE	Fever, encephalitis

Adapted from Griffin et al. (2013).

Chikungunya Virus (CHIKV)

CHIKV is an arthritogenic alphavirus and member of the Semliki Forest antigenic complex along with the closely related O'nyong-nyong virus (ONNV), Ross River virus (RRV), and Semliki Forest virus (SFV) (1). The name chikungunya is derived from the Makonde language and translates to "that which bends up" to describe the contorted posturing and pain associated with the disease caused by CHIKV (2). Retrospective case reports suggest that CHIKV has been circulating to cause epidemics as early as 1779 (3). However, CHIKV was not isolated until 1952 from an infected individual in Tanganyika (now Tanzania) (2). Prior to its identification, the similarity in CHIKV-induced disease to that caused by dengue virus (DENV) led to the frequent misdiagnoses of CHIKV cases. It was not until an outbreak of dengue-like illness on the Makonde Plateau of Tanganyika, in which DENV was uncommon, that CHIKV was first distinguished as a separate entity. Electron microscopy studies of CHIKV revealed characteristic alphavirus morphology (Figure I-1) (4).

Epidemiology

Since its identification, CHIKV outbreaks have been documented throughout Africa and Asia (Figure I-2) and include three distinct clades or lineages: East/Central/South African (ECSA), Western African (WA), and Asian (Figure I-3) (5). The recent CHIKV epidemics began in June of 2004 with a reemergence of the virus in Kenya and led to the identification of a fourth clade termed the Indian Ocean lineage (IOL). Between January and March of 2005, the virus spread to the Comoros islands just off the East African coast, causing more than 5,000 cases (6). By November of that year

the virus began circulating among several other islands of the Indian Ocean including Seychelles, Mauritius, Mayotte, and La Réunion, infecting thousands of individuals on each island by April of 2006 (7). Significantly devastated by this epidemic was the island of La Réunion with an estimated 244,000 cases of CHIKV, nearly one-third of the total population, between March of 2005 and April of 2006. During the peak of the La Réunion epidemic there were as many as 45,000 cases in a single week. CHIKV spread to India and Southeast Asia to cause overwhelming epidemics affecting millions of people (8). Imported cases of CHIKV disease from travelers returning from these epidemic areas were also reported in Australia, Europe, and the United States (9-13). In some instances, imported cases initiated autochthonous (indigenous or endemic) transmission of CHIKV, as observed in Italy in 2007 and France in 2010 (10, 12). Phylogenetic analysis suggests that strains from the ECSA lineage were responsible for these epidemics (14).

Similar devastation has been observed recently in the Caribbean beginning in October of 2013 with the occurrence of the first local transmission of CHIKV in the Western Hemisphere (15). Since the initial cases of CHIKV on the island of Saint Martin, CHIKV has spread autochthonously to more than 35 countries in Central and South America (16). To date, there have been more than 1.4 million suspected cases in the Americas, including confirmed, locally acquired cases in Florida. Interestingly, sequence analysis of CHIKV strains responsible for the outbreak on Saint Martin demonstrate that these viruses were most closely related to the Asian lineage, in particular to strains isolated in China and the Philippines between 2012 and 2014 (17). Because the mosquito

vectors that transmit CHIKV are globally distributed, CHIKV outbreaks are likely to continue and spread into new geographic areas.

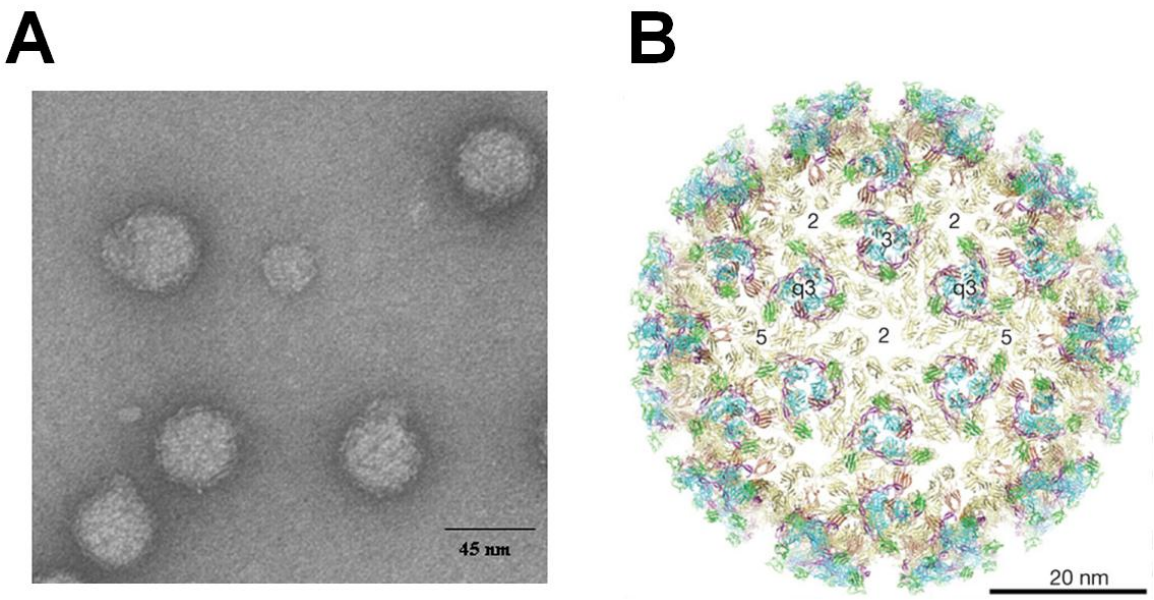

Figure I-1. Electron micrograph and atomic model of CHIKV virions. (A) Electron micrograph of CHIKV strain BaH 306 purified virions. (B) Atomic model of the 240 CHIKV E1/E2 heterodimers arranged as 80 spikes with $T = 4$ icosahedral symmetry. Figures adapted from Simizu et al. (1984) and Voss et al. (2010).

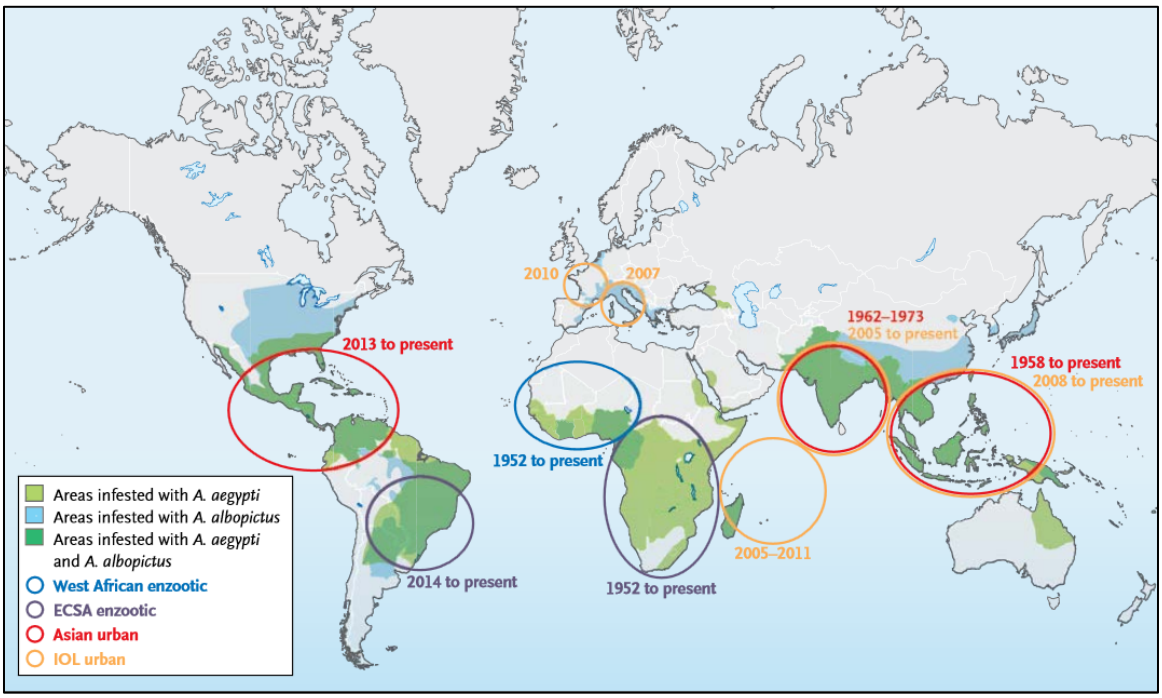

Figure I-2. Distribution and spread of reemerging CHIKV and its mosquito vectors. Adapted from Weaver and Lecuit (2015).

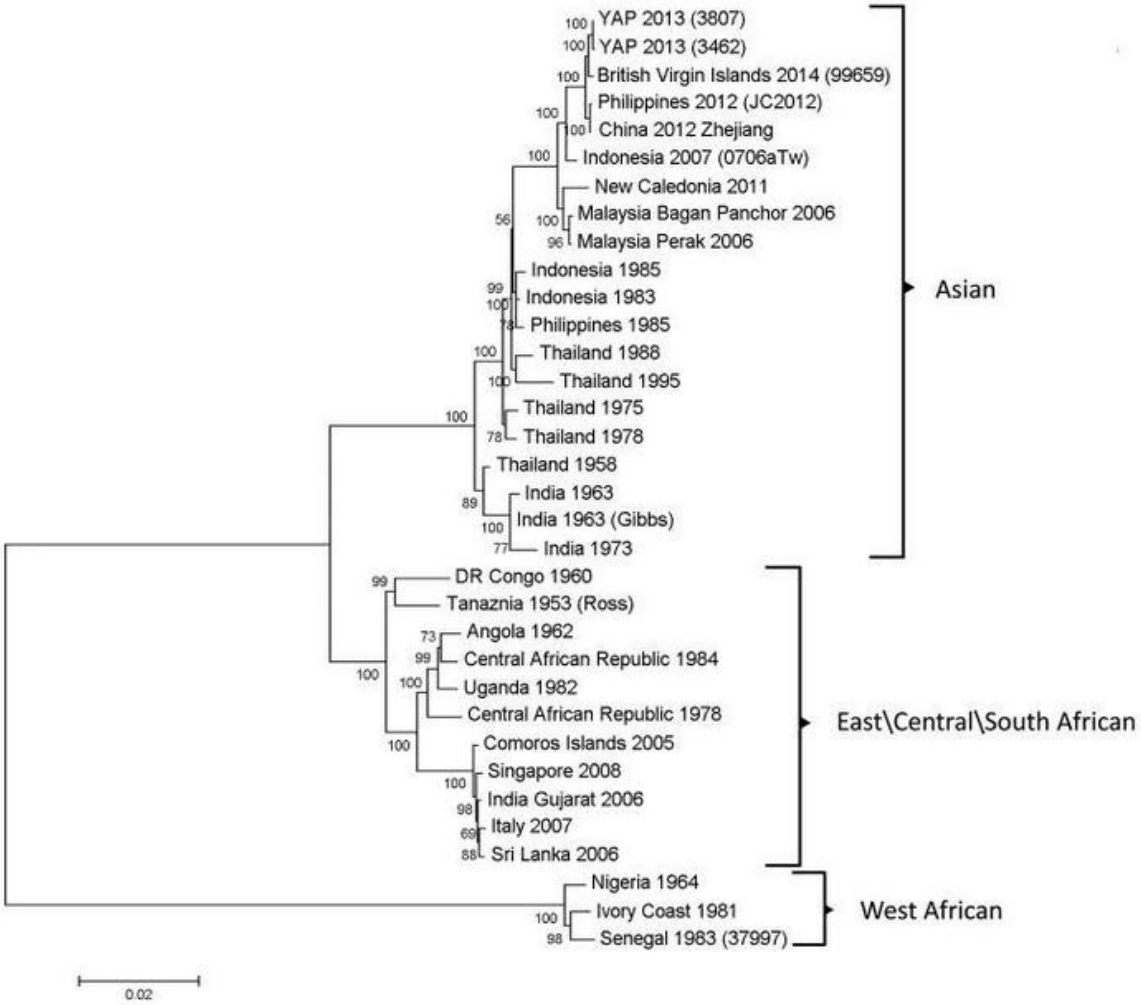

Figure I-3. Phylogeny of CHIKV clades. Phylogenetic organization of CHIKV clades based on complete genomes sequences in the GenBank library. Scale bar represents the number of nucleotide substitutions per site. Figure adapted from Lanciotti and Valadere (2014).

Transmission and Viral Vectors

CHIKV is maintained in both sylvatic, enzootic cycles and urban, epidemic cycles by *Aedes* species of mosquitoes. In the sylvatic or forest cycle, African strains of CHIKV are transmitted between forest-dwelling *Ae. furcifer* and *Ae. africanus* and non-human primates (5). In Asia, CHIKV is primarily maintained in urban cycles. Although, CHIKV-specific antibodies have been detected in wild monkeys (18, 19), a definitive animal reservoir has not been identified. Epidemic transmission of CHIKV occurs through urban cycles between humans and primarily *Ae. aegypti* and *Ae. albopictus* (20). These urban species of mosquitos associate closely with human populations to facilitate rapid spread of the virus.

Sequence analysis of CHIKV strains associated with epidemics in La Réunion revealed an A226V polymorphism in the E1 glycoprotein in greater than 90% of isolates (14). Appearance of this polymorphism in circulating strains of CHIKV coincided with increased transmission by *Ae. albopictus*. Prior to outbreaks of CHIKV in the Indian Ocean, CHIKV was primarily transmitted by *Ae. aegypti*, but this mutation contributed to more efficient replication of CHIKV in *Ae. albopictus* (21). The E1 A226V polymorphism, along with additional mutations in the La Réunion strain, is thought to decrease dependence of strains on cholesterol for replication and influence steps in viral fusion (22).

Adaptation to *Ae. albopictus* likely enhanced CHIKV transmission efficiency during its reemergence and increased the geographic distribution of the outbreak. Whereas *Ae. aegypti* resides in the tropics, the distribution of *Ae. albopictus* extends into more temperate regions, including Europe and the United States (23). This distribution of

these mosquito vectors raises concerns for continued spread into immunologically naïve populations. Interestingly, virus strains responsible for outbreaks in the Caribbean do not encode the E1 A226V polymorphism, suggesting that these strains have not adapted to *Ae. albopictus*. Although the high incidence of CHIKV in these populations could facilitate the selection of *Ae. albopictus*-adapted strains, Asian strains of CHIKV may be constrained from these adaptations (24).

Acute and Chronic CHIKV Disease

CHIKV causes a debilitating musculoskeletal inflammatory disease commonly referred to as chikungunya fever. In contrast to DENV in which the majority of infections are asymptomatic, only 4-28 percent of CHIKV infections are asymptomatic, depending on the study cohort (25, 26). Following a 2- to 6-day incubation period, persons infected with CHIKV experience sudden onset of clinical disease with little to no prodrome (Figure I-4). The acute phase of CHIKV infection is characterized principally by fever, severe polyarthralgia, joint swelling and arthritis, myalgia, skin rash, and digestive symptoms. Most of the acute clinical signs resolve after 7-10 days, but the polyarthralgia and arthritis can recur for months to years after the initial diagnosis (10, 27, 28). The arthralgia is usually symmetrical and primarily affects peripheral joints including the wrists, knees, ankles, and small joints of the hand. Other clinical signs and symptoms experienced by those infected with CHIKV include tenosynovitis, headache, and photophobia.

During recent epidemics, more severe disease and atypical symptoms have been observed (29-31). These severe manifestations, including neurological and cardiac

disease, were reported in neonates, persons greater than 65 years of age, and those with underlying comorbidities. Underlying respiratory and cardiac disease, hypertension, alcohol abuse, and the use of non-steroidal anti-inflammatory drugs (NSAIDs) also correlate with increased disease severity and hospitalization (29). Mother-to-infant transmission of CHIKV during delivery is associated with high rates of infant morbidity (32). Severe illness is observed in 53 percent of newborns, mainly consisting of encephalopathy, with persistent disabilities in 44 percent (33). In neonates, the disease is less frequently rheumatic, but more often characterized by dermatological manifestations and neurological complications (34). Infection is rarely fatal, but reported causes of death include heart, renal, respiratory, and multiple organ failure, encephalitis, bullous dermatosis, pneumonia, toxic hepatitis, acute myocardial infarction, cerebrovascular disease, and septicemia (31).

In contrast to the acute phase, the chronic phase of CHIKV disease has not been extensively studied. Joint and muscle pain are the most common long-lasting symptoms (25). Less frequently reported manifestations include fever, fatigue, headache, rash, joint stiffness, bursitis, tenosynovitis, and synovitis. However, late stages of CHIKV infection also have been associated with neuropathic pain syndrome, cerebral and digestive disorders, and alopecia (35, 36). Increased age correlates with a longer duration of illness and the persistence of joint pain. Pre-existing arthritis also is associated with an increased risk for persistent symptoms. In some cases, the clinical picture is similar to that of rheumatoid arthritis (RA), but an autoimmune causality for chronic CHIKV disease has not been established (37). Moreover, gender has not been clearly associated with disease severity or prevalence as with other autoimmune diseases (36). It remains unclear

whether viral load and antibody titers correlate with prolonged illness and persistent symptoms.

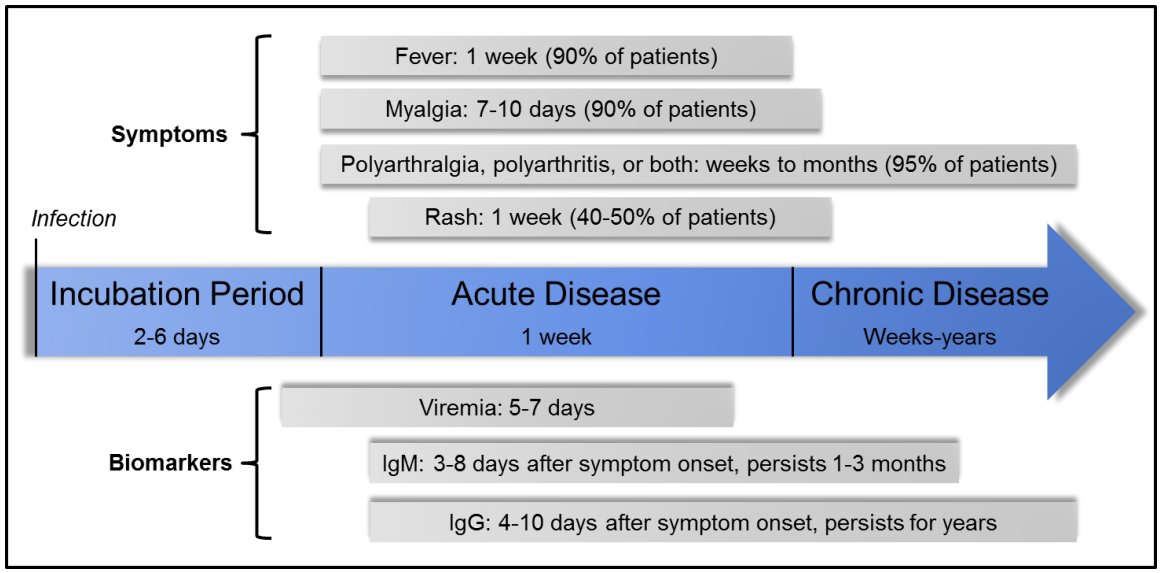

Figure I-4. Timeline of typical CHIKV disease progression. Schematic representation of the phases and duration of CHIKV disease (blue arrow). Grey boxes denote the typical symptoms and biomarkers observed during the progression of disease. Sizes and placements of boxes indicate the time frame and duration of symptom or biomarker presentation. Adapted from Suhrbier et al. (2012).

CHIKV Genome and Replication Cycle

Alphaviruses form icosahedral virions containing a nucleocapsid surrounded by a lipid bilayer envelope (Figure I-1) (38-40). The envelope is studded with heterodimers of the viral E1 fusion and E2 attachment glycoproteins, which associate as trimers (39, 40). E2 mediates attachment to the host cell via binding to cell-surface receptors, which remain unidentified for CHIKV and many other alphaviruses (4, 40). Receptor binding is followed by clathrin-mediated uptake into the endocytic compartment (38, 41). Acidification of endosomes triggers fusion of the viral envelope with the host membrane, which is mediated by E1, a type II fusion protein (42). Type II fusion proteins generate a pore in both membranes through which the nucleocapsid can enter the cytoplasm (43).

The alphavirus genome consists of a single-strand, positive-sense RNA molecule approximately 12 kilobases (kb) in length that contains two open-reading frames (ORFs) (44, 45). The first ORF encodes four nonstructural proteins (nsP1-4) that form the replicase complex and mediate synthesis of viral genomic and subgenomic RNA (1, 44, 45). The subgenomic, second ORF encodes three major structural proteins, capsid, pE2, and E1, and the small peptides, 6K and TF (1, 4, 45-47). Following translation of the subgenomic RNA, the capsid protein is autoproteolytically cleaved from the polyprotein (44, 48). The remainder is transported through the endoplasmic reticulum (ER) and Golgi where the 6K peptide is liberated by cellular proteases, and the E1 and pE2 proteins are glycosylated (4, 49). During egress, the cellular protease, furin, cleaves pE2 to release the E3 peptide and generate the mature heterodimer of E1 fusion and E2 attachment proteins (39, 50, 51). The structural proteins encapsidate the viral genome, forming progeny

virions near the plasma membrane, which bud from the host cell to infect neighboring cells and disseminate throughout the host (52).

CHIKV Tropism and Pathogenesis

CHIKV pathogenesis has been studied using both wildtype and immunodeficient mice (53-58). CHIKV infection of 3-to-4-week-old C57BL/6 mice results in rheumatologic disease after subcutaneous inoculation into the footpad, mimicking many aspects of CHIKV disease in humans (55, 57). Infected mice develop acute metatarsal swelling with histological evidence of arthritis, tenosynovitis, and myositis. Persistent infection in joints is observed for months postinfection in these animals (59, 60). Adult mice lacking type I interferon receptors (*Ifnar1*$^{-/-}$ mice) develop lethal infection, with muscle, joint, and skin serving as primary sites of replication (53).

CHIKV infection elicits inflammatory responses, including cytokine and chemokine production, and immune cell infiltration of tissues that contribute to tissue injury and disease. Elevated levels of IFN-γ, IL-1β, IL-6, CCL2 (monocyte chemoattractant protein-1; MCP-1), CXCL9 (monokine induced by IFN-γ; MIG), CXCL10 (IFN-γ-induced protein 10; IP-10), and macrophage migration inhibitor factor (MIF) have been detected in humans with acute CHIKV infection. Moreover, levels of IL-1β, IL-6, IP-10, MCP-1, MIG, and regulated on activation, normal T cell expressed and secreted (RANTES) are associated with increased disease severity (61-65). Serum levels of IP-10, MCP-1, and MIG correlate with the degree of joint swelling in CHIKV-infected mice (66). These data indicate that specific cytokines and chemokines are critical

mediators of CHIKV pathogenesis, although, the cellular targets of infection that influence the production of these molecules *in vivo* remain undefined.

Production of these cytokines recruits monocytes, macrophages, natural killer (NK) cells, and T cells to musculoskeletal tissues that contribute to CHIKV-induced disease (55). CHIKV-infected *Rag2*$^{-/-}$ and *CD4*$^{-/-}$ mice exhibit reduced joint swelling and pathological injury relative to wildtype mice during the acute phase of disease, suggesting a pathogenic role for CD4^{+} T-cells in CHIKV disease (67). In studies of CHIKV persistence, CHIKV RNA persisted in the spleen, serum, and musculoskeletal tissues of *Rag1*$^{-/-}$ mice longer after infection compared to wildtype mice (59). CHIKV antigen and RNA have also been detected in muscle satellite cells and synovial tissue biopsied from patients suffering from chronic muscle and joint pain (68, 69). These data suggest that chronic CHIKV joint disease may result from persistent CHIKV infection in musculoskeletal tissues.

Vaccine and Antiviral Strategies

There are no licensed, anti-CHIKV therapies or vaccines. Treatment currently is limited to supportive care through the administration of NSAIDs (24, 70). Drugs with known antiviral or antimalarial activity, including chloroquine, interferon, and ribavirin are ineffective in the treatment of CHIKV disease (70-72). During CHIKV outbreaks in La Réunion, some patients received methotrexate, a drug used in the treatment of RA, to ameliorate symptoms of CHIKV-induced arthritis (69, 73). Although potentially effective in alleviating CHIKV arthritis, the immunosuppression associated with methotrexate treatment may exacerbate CHIKV disease or persistence (74). Other therapies are in preclinical development. Treatment of mice with bindarit, an inhibitor of MCP-1,

alleviated CHIKV-associated arthritis and myositis (75), but further studies of this drug in clinical trials are necessary to assess the efficacy in humans. Other antiviral strategies under investigation for CHIKV include furin inhibitors (51), harringtonine, an inhibitor of protein synthesis (76), and viperin, a host interferon-stimulated gene (ISG) (77).

Many CHIKV vaccine candidates are currently being developed. The first CHIKV vaccine was developed from a strain isolated in 1962 from an infected individual in Thailand, strain 15561, which was obtained by the U.S. Army Medical Component at the Southeast Asia Treaty Organization (SEATO) lab (78). Nine years later, the Walter Reed Army Institute of Research (WRAIR) obtained the strain and generated a vaccine by passaging it 11 times in green monkey kidney (GMK) cells followed by formalin-inactivation (78). Sixteen army volunteers were immunized with the formalin-inactivated virus, which resulted in minimal adverse effects (78). In 1985, a live, attenuated vaccine was generated by the United States Army Medical Institute of Infectious Disease (USAMRIID) by passaging the 11^{th} passage of 15561 in GMK cells 18 times in human fetal lung fibroblasts (MRC-5 cells), producing the 181/25 strain (79). The 181/25 strain is attenuated and elicits immune responses in mice that protect against lethal challenge (79). In Phase II trials at the University of Maryland in 2000, volunteers were immunized and monitored for adverse effects for a month following vaccination (80). The vaccine was attenuated in humans and elicited an immune response, but some of the vaccinees experienced transient arthralgia (80). Due to the reactogenicity of this live-attenuated vaccine, current strategies employ virus-like particles (VLPs) and recombinant or chimeric viruses to prevent vaccine-induced disease (81-84). A CHIKV VLP-based vaccine is immunogenic and protective in macaques and has been tested in Phase I

clinical trials in humans (81). This VLP vaccine is a promising candidate, but it requires further testing and development.

Significance of the Research

CHIKV is a reemerging alphavirus of global significance with a high epidemic potential (85). The recent adaptation of CHIKV to another mosquito vector, *Aedes albopictus*, has expanded the host range of the virus (11-13, 86, 87). The immunologically naïve populations in these regions, in addition to the high serum viremia established in infected individuals, supports autochthonous spread as seen over the past year in the Caribbean (17). Currently, there are no licensed CHIKV vaccines or antiviral therapies for infected individuals, and only supportive care for clinical symptoms is available. The severity of CHIKV disease, particularly its high propensity for chronic musculoskeletal manifestations, underscores the need for new targets for vaccine and antiviral development.

The overall goals of this research were to identify virulence determinants of CHIKV infection and define molecular mechanisms of disease. This research used unbiased approaches of chimeric viruses and high-throughput screening to identify viral and cellular determinants of CHIKV virulence, respectively. In the work presented here, I demonstrate that polymorphisms in the E2 attachment protein influence replication in mammalian and mosquito cells, mediate attachment to GAGs, and tissue tropism and pathology in mice. I also define functions for the sodium-potassium ATPase and immunoproteasome in CHIKV infection. Future studies will investigate tissue-specific GAG utilization *in vivo* and the means by which sodium-potassium ATPase blockade and

the immunoproteasome antagonize CHIKV infection. Elucidating viral and cellular factors that mediate tissue tropism and host cell restriction will enhance an understanding of mechanisms of alphavirus pathogenesis.

CHAPTER II

CHIKV E2 RESIDUE 82 INFLUENCES INFECTION OF MAMMALIAN AND MOSQUITO CELLS AND UTILIZATION OF GLYCOSAMINOGLYCANS

Introduction

Arboviruses must replicate efficiently in both their invertebrate and vertebrate hosts to maintain an effective transmission cycle. The viral determinants that promote infection of one species also can promote infection in the other, but more often, a replicative advantage in a species coincides with a fitness cost in the other. In support of this idea, serial passage of CHIKV in either mice or mammalian cell culture diminishes fitness of the virus in mosquitoes and mosquito cell culture (88). However, our understanding of the specific determinants of CHIKV infection and the role of these determinants in infection of mammalian and mosquito cells is limited.

In this study, I defined the importance of sequence polymorphisms displayed by strains 181/25 and AF15561 to CHIKV infectivity in mammalian and mosquito cells. I engineered a panel of CHIKV variants containing these polymorphisms in the genetic background of each parental strain and screened these viruses for differences in infectivity in mammalian and mosquito cells. I found that E2 residue 82 is a determinant of infectivity in both mammalian and mosquito cell culture and contributes to interactions with GAGs. Viruses containing an arginine at E2 residue 82 replicated to higher titers in mammalian cells than viruses containing a glycine at this residue and exhibited increased dependence on GAGs for infection. I conclude that CHIKV utilization of GAGs

facilitates attachment to and infection of mammalian cells, and E2 residue 82 influences this interaction. However, an arginine at E2 residue 82 afforded no advantage in infection of mosquito cells. Instead, a glycine at E2 residue 82 conferred an advantage in infection of these cells, suggesting that this residue mediates different interactions in mosquito cells. These studies identify new determinants of CHIKV infection and provide insights into the species-specific roles of CHIKV E2 residue 82 in infection of mammalian and mosquito cells.

Results

Generation of the CHIKV 181/25 infectious clone. To develop a reverse genetics system to facilitate recovery of wildtype and otherwise isogenic mutant virus stocks, I engineered an infectious clone for strain 181/25. Using this system, mutations can be engineered in a cDNA copy of the viral RNA genome and transcribed *in vitro* to produce infectious, viral RNA. A virus stock is generated by electroporating RNA into cells and harvesting virus from culture supernatants 24-48 h post-electroporation. This viral stock is not passaged in cell culture in order to maintain genome integrity. Deriving virus from the infectious cDNA clone avoids the high mutation rates associated with the error-prone, viral RNA-dependent RNA polymerases in cell culture. The infectious clone successfully produced virus and displayed comparable replication kinetics to that of the original 181/25 virus stock in baby hamster kidney (BHK-21), MRC-5, and green monkey kidney (Vero) cells (Figure II-1).

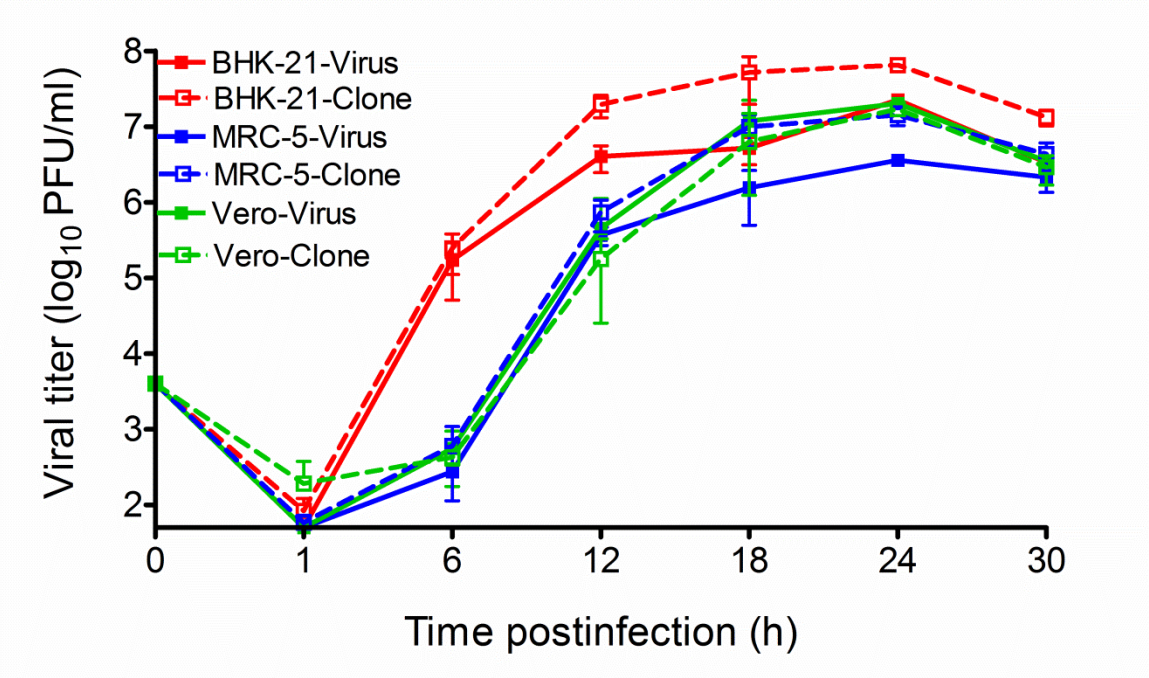

Figure II-1. Infectious clone-derived CHIKV 181/25 replicates with comparable kinetics to 181/25 virus stock. BHK-21 (red), MRC-5 (blue), and Vero (green) cells were adsorbed with CHIKV 181/25 infectious clone-derived virus and 181/25 virus stock at an MOI of 0.01 PFU/cell. At 6-h intervals postinfection, supernatants were harvested, serially diluted, and titered by plaque assay using Vero cells. Results are presented as mean titers for triplicate samples. Error bars indicate standard deviation.

E2 residue 82 is a determinant of CHIKV infectivity in mammalian cell culture. For many viruses, serial passage in mammalian cells enhances viral replicative capacity in cell culture (88-94). To determine whether passage of CHIKV strain AF15561 to generate vaccine strain 181/25 resulted in enhanced replicative capacity, I infected cells with either AF15561 or 181/25, and viral titers in culture supernatants were determined by plaque assay over an infectious time course. Relative to AF15561, 181/25 reached higher titers in several cell lines, including Vero, BHK-21, HeLa, and human brain microvascular endothelial cells (HBMECs) (Figure II-2). These results suggest that strain 181/25 has adapted to mammalian cell culture as a result of cell-culture passage, consistent with observations from other passaged viruses.

Strains 181/25 and AF15561 differ at five nonsynonymous and five synonymous nucleotides across the genome. Polymorphic positions resulting in coding changes in 181/25 are in nsP1 (T301I), E2 (T12I and G82R), 6K (C42P), and E1 (A404V) (Figure II-3). To define residues that contribute to the replication and infectivity differences observed between strains 181/25 and AF15561, Vero cells were infected at an MOI of 1 PFU/cell with either of the parental strains or viruses containing individual polymorphic residues in the reciprocal genetic background (Table II-1). The percentage of infected cells in each case was quantified after a single round of infection by indirect immunofluorescence (Figure II-4). As expected, 181/25 infected a significantly greater percentage of cells relative to AF15561. Substitution of an arginine at E2 residue 82 in the AF15561 background enhanced infectivity to levels even greater than those observed for strain 181/25. Conversely, substitution of a glycine at E2 residue 82 in the 181/25 background significantly diminished 181/25 infectivity. Interestingly, substituting an

isoleucine at E2 residue 12 in the AF15561 background further decreased infectivity relative to AF15561. Introducing any of the other polymorphic residues in either background had no effect on infectivity in these cells. To understand how these findings might compare to previous studies with these viruses in mice, the parental and variant viruses were used to infect murine L929 and NIH 3T3 cell lines (Figure II-5). As observed in experiments using Vero cells, substitution of an arginine at E2 residue 82 in the AF15561 background enhanced infectivity in these murine cell lines, whereas substitution of a glycine at E2 residue 82 in the 181/25 background significantly diminished infectivity. These data suggest that an arginine at residue 82 in the E2 protein confers the enhanced infectivity observed for strain 181/25 in mammalian cells.

Because these virus strains differed substantially in infectivity of Vero cells, I quantified the genome/PFU and genome/FFU ratios for each strain (Table II-2). In Vero cells, parental strains AF15561 and 181/25 had genome/PFU ratios of 6,598 and 176, respectively. Similarly, strains AF15561 and 181/25 had genome/FFU ratios of 9.497×10^7 and 8.000×10^5, respectively. Viral variants containing residues from strain 181/25 in the AF15561 background had reduced genome/PFU and genome/FFU ratios relative to the parental AF15561. Interestingly, introducing the E2 G82R substitution resulted in the most modest reduction in genome/PFU ratio, but the greatest reduction in genome/FFU ratio. In contrast, introducing the E2 R82G substitution in the 181/25 background resulted in increased genome/PFU and genome/FFU ratios, which were the most dramatic increases of any of the viral variants with AF15561 residues in the 181/25 background. Thus, the E2 82 polymorphism serves as a key determinant of CHIKV infectivity in mammalian cell culture.

To determine whether E2 residue 82 contributes to the production of infectious virus over multiple rounds of infection, Vero cells were infected at an MOI of 0.01 PFU/cell, and viral titers in culture supernatants were determined by plaque assay at 6-h intervals (Figure II-4B). Compared with titers of AF15561, titers of AF15561 E2 G82R were increased 10-fold by 6 h postinfection, 7-fold by 12 h postinfection, and 40-fold by 18 h postinfection. Compared with titers of 181/25, titers of 181/25 E2 R82G were reduced 145-fold by 18 h postinfection, 60-fold by 24 h postinfection, and 68-fold by 30 h postinfection. Taken together, these data indicate that E2 residue 82 influences both initial and subsequent rounds of CHIKV infection.

Because this determinant of CHIKV infectivity resides in the viral attachment protein, I tested whether E2 residue 82 influences binding to host cells. For these experiments, Vero cells were adsorbed with each parental strain and the reciprocal E2 82 variant strains, and the percentage of virus-bound cells was quantified using flow cytometry (Figure II-4C). A significantly greater proportion of cells were bound by strain 181/25 than by stain AF15561. In agreement with the infectivity data, introducing the E2 G82R substitution in the AF15561 background significantly enhanced cell-attachment. In contrast, introducing the E2 R82G substitution in the 181/25 background reduced cell-binding to undetectable levels. These data suggest that an arginine at position 82 in the E2 attachment protein is required for the enhanced binding and infectivity observed for strain 181/25 in mammalian cells.

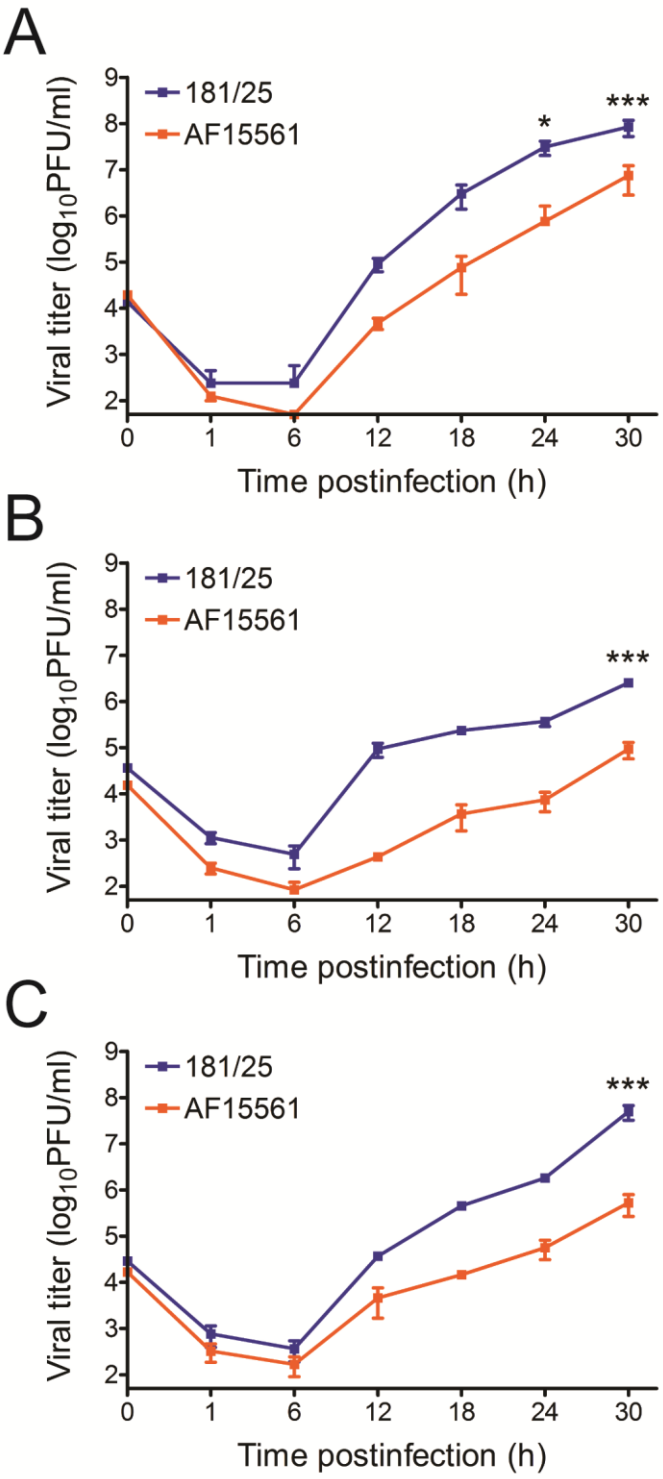
A
181/25
AF15561
*
***
Viral titer (log10PFU/ml)
Time postinfection (h)
B
181/25
AF15561
***
Viral titer (log10PFU/ml)
Time postinfection (h)
C
181/25
AF15561
***
Viral titer (log10PFU/ml)
Time postinfection (h)

Figure II-2. CHIKV strain 181/25 replicates to higher titers in multiple mammalian cell lines than the parental strain AF15561. (A) Vero cells, (B) HeLa cells, and (C) HBMECs were adsorbed with CHIKV strains 181/25 or AF15561 at an MOI of 0.01 PFU/cell. At the times shown, viral titers in culture supernatants were determined by plaque assay using Vero cells. Results are presented as the mean viral titers for triplicate samples. Error bars indicate standard deviation. Titers of 181/25 and AF15561 were significantly different at 24 and 30 h postinfection in Vero cells, 30 h postinfection in HeLa cells, and 30 h postinfection in HBMECs. *, $P < 0.05$, ***, $P < 0.001$, as determined by ANOVA followed by Tukey *post hoc* test.

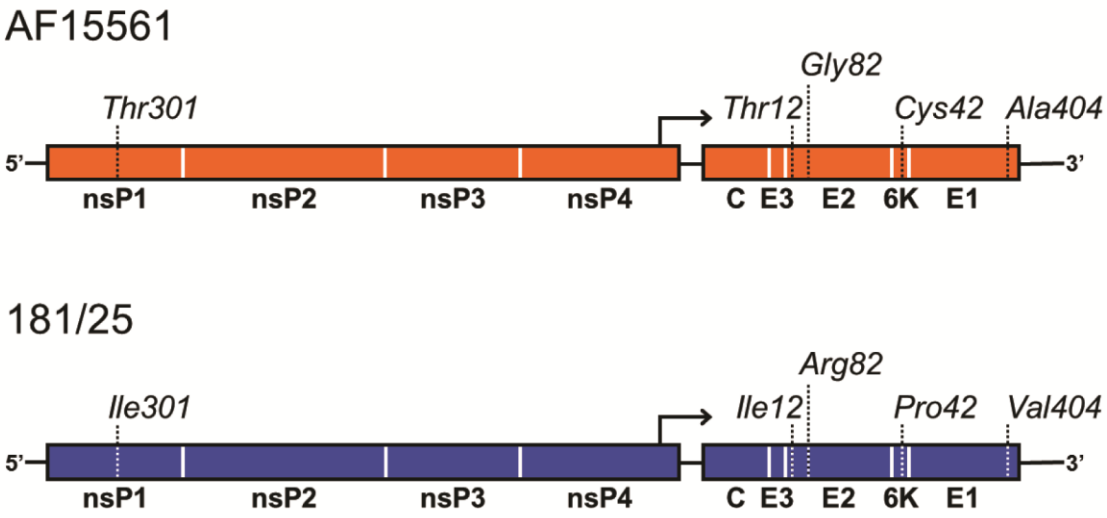

Figure II-3. Schematic depiction of polymorphic residues in CHIKV strains AF15561 and 181/25. Distribution of amino acid polymorphisms between strains AF15561 (top, orange) and 181/25 (bottom, blue) across the ~ 12 kb genome. Numbers correspond to the amino acid position within each protein.

Table II-1. Panel of mutant viruses generated from CHIKV 181/25 and AF15561. Positions of the AF15561 (grey) and 181/25 (white) polymorphisms introduced into the reciprocal backgrounds are shown.

Virus	Background	Residue				
		nsP1 301	E2 12	E2 82	6K 42	E1 404
AF15561	wt	T	T	G	C	A
181/25	wt	I	I	R	P	V
nsP1 T301I	AF15561	I	T	G	C	A
E2 T12I	AF15561	T	I	G	C	A
E2 G82R	AF15561	T	T	R	C	A
6K C42P	AF15561	T	T	G	P	A
E1 A404V	AF15561	T	T	G	C	V
nsP1 I301T	181/25	T	I	R	P	V
E2 I12T	181/25	I	T	R	P	V
E2 R82G	181/25	I	I	G	P	V
6K P42C	181/25	I	I	R	C	V
E1 V404A	181/25	I	I	R	P	A

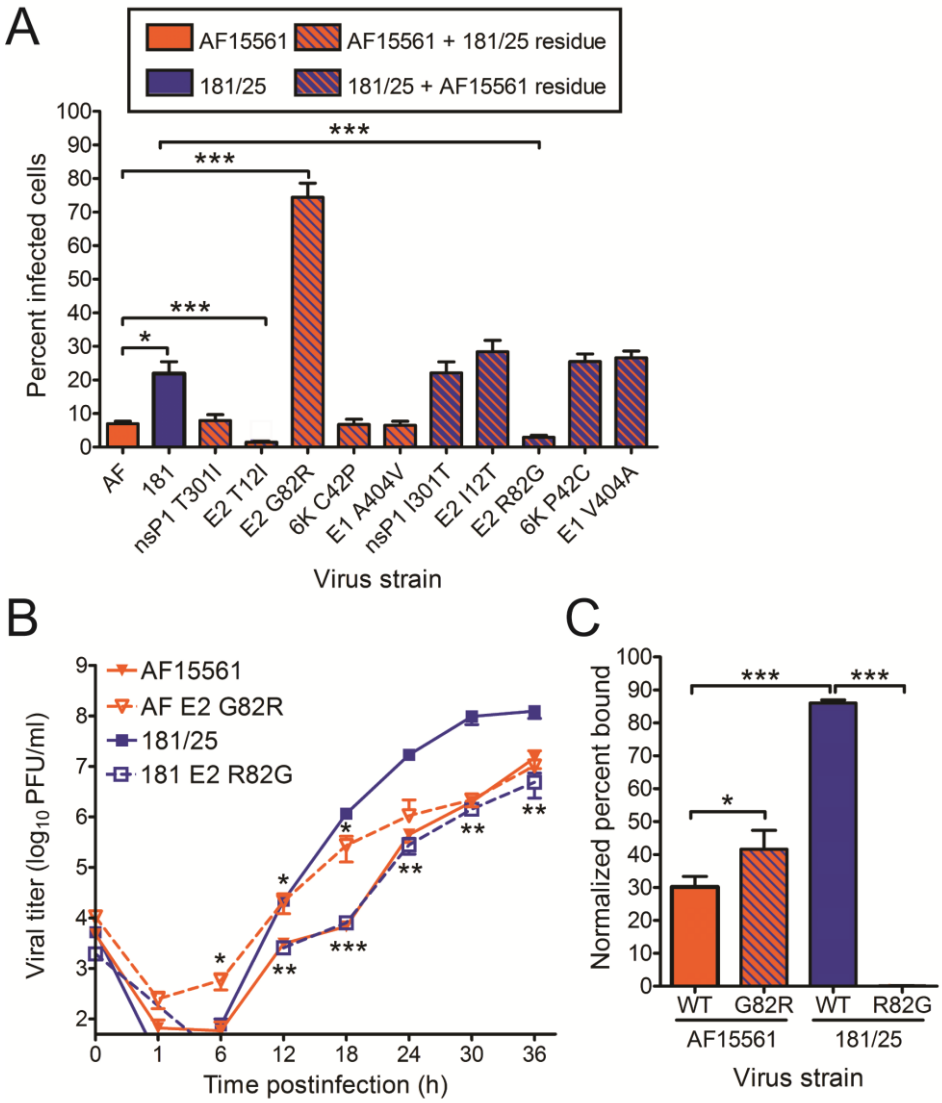
A
AF15561
AF15561 + 181/25 residue
181/25
181/25 + AF15561 residue
Percent infected cells
Virus strain
AF
181
nsP1 T301I
E2 T12I
E2 G82R
6K C42P
E1 A404V
nsP1 I301T
E2 I12T
E2 R82G
6K P42C
E1 V404A
B
AF15561
AF E2 G82R
181/25
181 E2 R82G
Viral titer (log10 PFU/ml)
Time postinfection (h)
C
Normalized percent bound
WT
G82R
WT
R82G
AF15561
181/25
Virus strain

Figure II-4. Residue 82 of the E2 attachment protein is a determinant of CHIKV infectivity in mammalian cells. (A) Vero cells were adsorbed with CHIKV strains AF15561, 181/25, or the variant viruses shown at an MOI of 1 PFU/cell and incubated for 24 h. Cells were stained with CHIKV-specific antiserum and DAPI to detect nuclei and imaged by fluorescence microscopy. Results are presented as percent infected cells for triplicate experiments. Error bars indicate standard error of the mean. (B) Vero cells were adsorbed with AF15561, 181/25, AF15561 E2 G82R, or 181/25 E2 R82G at an MOI of 0.01 PFU/cell. At the times shown, viral titers in culture supernatants were determined by plaque assay using Vero cells. Results are presented as the mean viral titers for triplicate samples. Error bars indicate standard deviation. Titers of AF15561 and AF15561 E2 G82R were significantly different at 6, 12, and 18 h postinfection, and titers of 181/25 and 181/25 E2 R82G were significantly different at 12, 18, 24, 30, and 36 h postinfection. (C) Vero cells were adsorbed with ~ 3 x 10^{10} genomes of AF15561, 181/25, AF15561 E2 G82R, or 181/25 E2 R82G. After 30-min incubation, cells were stained with CHIKV E2-specific mAb, and virus-bound cells were quantified by flow cytometry. Results are presented as percent bound cells for triplicate experiments. No CHIKV-bound cells were detected for 181/25 E2 R82G. Error bars indicate standard deviation. *, $P < 0.05$, **, $P < 0.01$, ***, $P < 0.001$, as determined by ANOVA followed by Bonferroni *post hoc* test (A and C) and Student's *t* test (B).

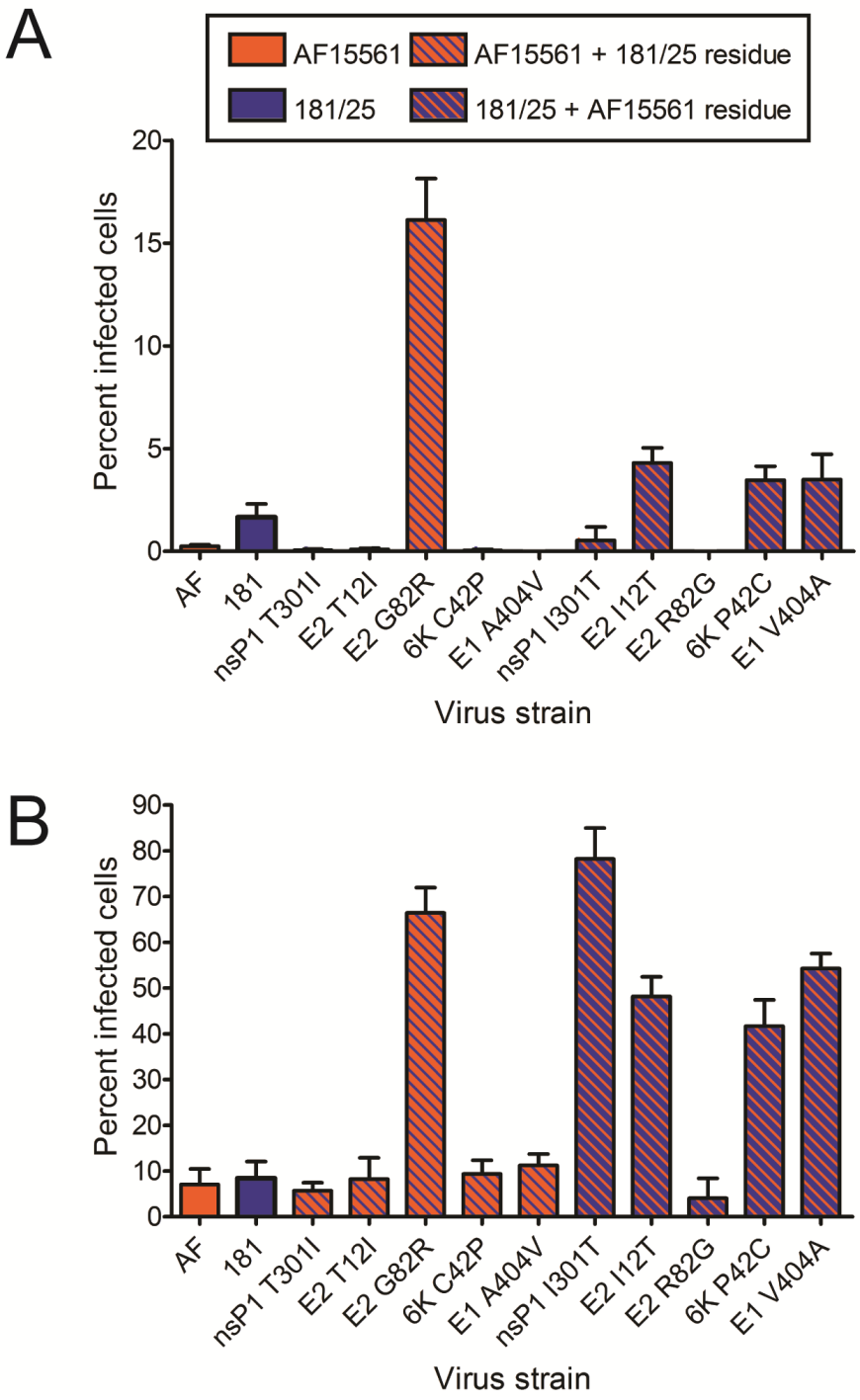

Figure II-5. E2 residue 82 is a determinant of CHIKV infectivity in murine cells. (A) L929 or (B) NIH 3T3 cells were adsorbed with CHIKV strains AF15561, 181/25, or the variant viruses shown at an MOI of 1 PFU/cell and incubated for 24 h. Cells were stained with CHIKV-specific antiserum and DAPI to detect nuclei and imaged by fluorescence microscopy. Results are presented as percent infected cells for triplicate samples from a representative experiment. Error bars indicate standard deviation.

Table II-2. Infectivity of CHIKV parental and mutant viruses by genome equivalents.

Virus strain	Genomes:PFU[a]	Genomes:FFU ($x10^4$)[b]	
		Vero	C6/36
AF15561	6598	9500	750
181/25	176	80	230
AF15561 nsP1 T301I	1113	1410	150
AF15561 E2 T12I	401	2760	280
AF15561 E2 G82R	5656	760	990
AF15561 6K C42P	2533	3750	460
AF15561 E1 A404V	3478	5350	590
181/25 nsP1 I30T	1436	650	1130
181/25 E2 I12T	142	50	110
181/25 E2 R82G	2858	9780	460
181/25 6K P42C	36	10	20
181/25 E1 V404A	89	30	40

[a]Genome copy numbers were determined by triplicate real-time quantitative PCR reactions. Plaque-forming units were determined by plaque assay using Vero cells for three independent stocks for each virus strain.
[b]Fluorescent-focus units were determined by indirect immunofluorescence in triplicate for at least two independent experiments.

E2 residue 82 contributes to CHIKV infectivity in mosquito cells. To determine whether an arginine at E2 residue 82 influences infection and replication in invertebrate cells, I tested the parental and reciprocal E2 82 variant strains for infection and replication in mosquito cells (Figure II-6). *Aedes albopictus* C6/36 cells were infected at an MOI of 1 PFU/cell, and the percentage of infected cells was quantified after a single round of infection by indirect immunofluorescence (Figure II-6A). In sharp contrast to my findings using mammalian cells, strain 181/25 infected significantly fewer C6/36 cells relative to AF15561, and substitution of a glycine at E2 residue 82 in the 181/25 background significantly increased 181/25 infectivity in these cells. However, substitution of an arginine at E2 residue 82 in the AF15561 background did not significantly diminish C6/36 infection. Surprisingly, only substitution of isoleucine for threonine at residue 12 in AF15561 E2 was sufficient to reduce infection in these cells, albeit not to the levels observed for 181/25. Additionally, AF15561 E2 G82R had a similar genome/FFU ratio compared with AF15561, whereas substitutions at the other polymorphic sites with residues from strain 181/25 decreased the genome/FFU ratio. Together, these data indicate that the residue at E2 position 82 provides a fitness advantage for CHIKV infectivity depending on the host cell species.

To assess whether E2 residue 82 affects the production of infectious virus from mosquito cells, C6/36 cells were infected at an MOI of 0.01 PFU/cell, and viral titers in culture supernatants were determined at 6-h intervals (Figure II-6B). Relative to titers of 181/25, titers of 181/25 E2 R82G were increased 29-fold by 12 h postinfection, 8-fold by 18 h postinfection, and 13-fold by 24 h postinfection. However, relative to titers of AF15561, there was no decrease in viral titers when an arginine was introduced at E2 82

in the AF15561 strain. These data indicate that E2 Gly82 in the genetic background of 181/25 enhances infection of mosquito cells. However, polymorphisms exhibited by these strains in addition to E2 Gly82 appear to contribute to the enhanced infectivity of AF15561 in mosquito cells.

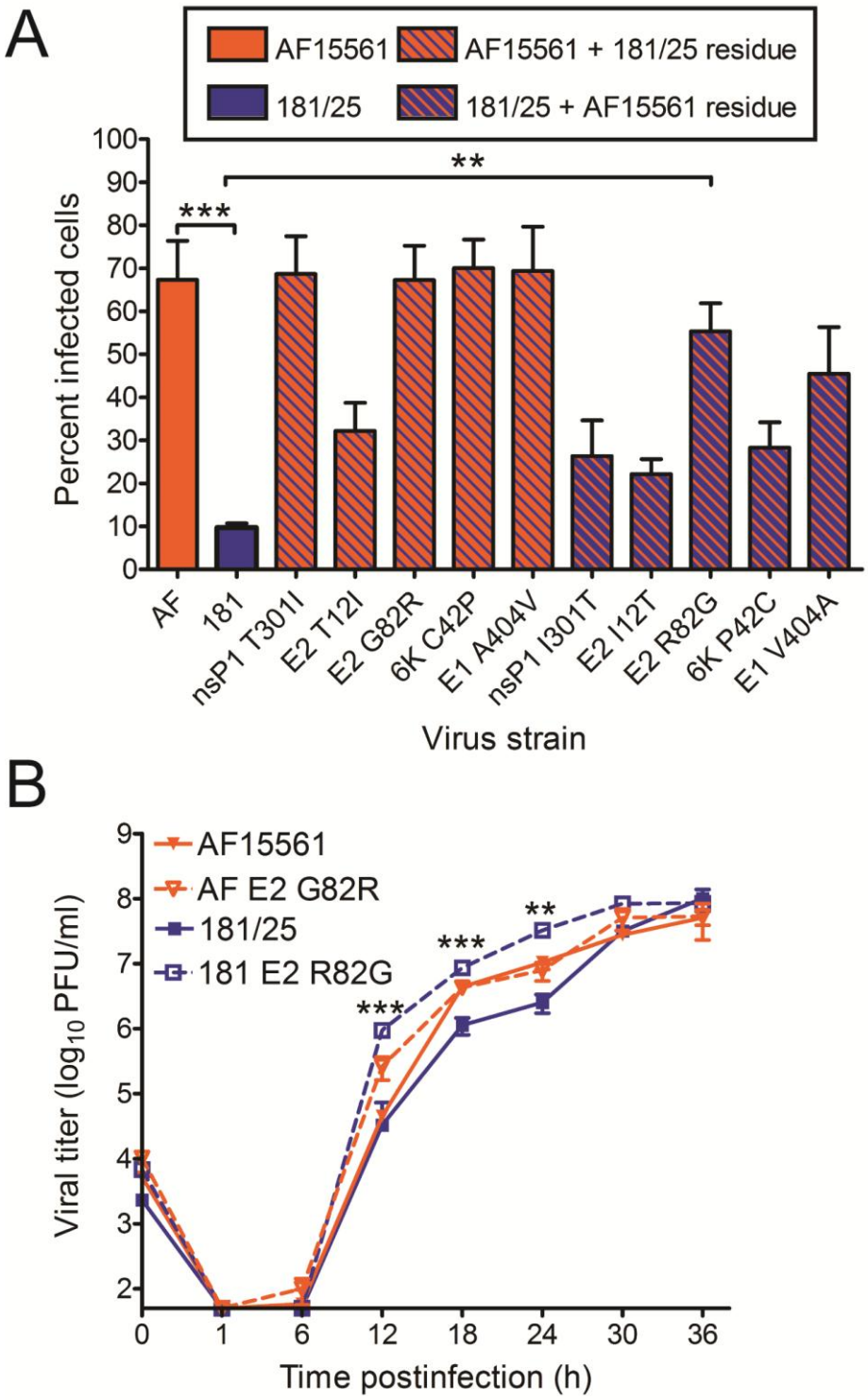
A
AF15561
AF15561 + 181/25 residue
181/25
181/25 + AF15561 residue
Percent infected cells
100
90
80
70
60
50
40
30
20
10
0
***
**
AF
181
nsP1 T301I
E2 T12I
E2 G82R
6K C42P
E1 A404V
nsP1 I301T
E2 I12T
E2 R82G
6K P42C
E1 V404A
Virus strain
B
AF15561
AF E2 G82R
181/25
181 E2 R82G
Viral titer (log10 PFU/ml)
9
8
7
6
5
4
3
2
***
***
**
0
1
6
12
18
24
30
36
Time postinfection (h)

Figure II-6. Residue 82 of the E2 attachment protein is a determinant of CHIKV infectivity in mosquito cells. (A) C6/36 mosquito cells were adsorbed with CHIKV strains AF15561, 181/25, or the variant viruses shown at an MOI of 1 PFU/cell and incubated for 24 h. Cells were stained with CHIKV-specific antiserum and DAPI to detect nuclei and imaged by fluorescence microscopy. Results are presented as percent infected cells for triplicate experiments. Error bars indicate standard error of the mean. (B) C6/36 cells were adsorbed with AF15561, 181/25, AF15561 G82R, or 181/25 E2 R82G at an MOI of 0.01 PFU/cell. At the times shown, viral titers in culture supernatants were determined by plaque assay using Vero cells. Results are presented as the mean viral titers for triplicate samples. Error bars indicate standard deviation. Titers of 181/25 and 181/25 E2 R82G were significantly different at 12, 18, and 24 h postinfection. **, $P < 0.01$, ***, $P < 0.001$, as determined by ANOVA followed by Bonferroni *post hoc* test (A) and Student's *t* test (B).

E2 residue 82 influences utilization of glycosaminoglycans. To understand mechanisms by which E2 residue 82 influences CHIKV attachment to cells, I next investigated the dependence of 181/25 and AF15561 on GAGs for infectivity. Wildtype CHO-K1 and GAG-deficient CHO-pgsA745 cells were infected with purified 181/25, AF15561, 181/25 E2 R82G, or AF15561 E2 G82R at an MOI of 10 PFU/cell. The percentage of infected cells for each virus was quantified after a single round of infection by indirect immunofluorescence (Figure II-7A). The pgsA745 cells were significantly less susceptible to infection by all four viruses relative to infection of CHO-K1 cells ($P < 0.0001$ for 181/25 and AF15561, $P < 0.001$ for AF15561 E2 G82R, and $P < 0.05$ for 181/25 E2 R82G). However, the pgsA745 cells were significantly less susceptible to infection by 181/25 relative to AF15561. Substitution of E2 Gly82 with arginine in the AF15561 background was sufficient to diminish infectivity in these cells to levels observed for 181/25. Furthermore, substitution of E2 Arg82 with glycine in the 181/25 background was sufficient to increase infectivity and mitigate GAG dependence to levels observed for AF15561. These data confirm that strain 181/25 is more dependent on GAGs for infection than is AF15561 and that E2 residue 82 mediates this dependence.

I also assessed infectivity by determining genome/PFU ratios using Vero cells and genome/FFU ratios using both CHO-K1 and pgsA745 cells (Table II-3). I observed a similar trend in the genome/PFU values of purified stocks of the parental and variant viruses used in these experiments. Strain AF15561 had higher genome/PFU ratios than those of 181/25 in both cell lines, and these differences once again segregated with E2 residue 82. Interestingly, all strains had higher genome/FFU ratios in pgsA745 cells relative to the parental CHO-K1 cells. These data support the hypothesis that viruses

containing an arginine at E2 residue 82 are less fit in GAG-deficient cells relative to their glycine-containing counterparts.

Based on these and previously published findings (94-98), the GAG-dependence mediated by this residue likely occurs at an early step in the infectious lifecycle. Therefore, I reasoned that soluble GAGs could act as competitive agonists to block infectivity of GAG-dependent viruses. To test whether competition with soluble GAGs inhibits infection, purified virus was incubated with increasing concentrations of soluble heparin, a highly sulfated GAG, and adsorbed to Vero cells. The percentage of infected cells was quantified after a single round of infection by indirect immunofluorescence (Figure II-7B). Treatment with soluble heparin resulted in a dose-dependent decrease in the percentage of infected cells for all viruses tested. However, this decrease was most substantial for strains 181/25 and AF15561 E2 G82R, for which incubation with the highest concentration of heparin decreased infectivity 15- and 24-fold, respectively. In contrast, incubation of strains AF15561 and 181/25 E2 R82G with the same concentration of heparin resulted in only a 4-fold decrease in infectivity. These findings suggest that CHIKV strains containing an arginine at E2 residue 82 rely on GAGs for efficient cell attachment.

To determine whether the CHIKV strains used in this study directly interact with GAGs, equivalent genome copies of purified parental or variant viruses were incubated with either heparin-conjugated or unconjugated agarose beads. Bound material was resolved by SDS-PAGE and immunoblotted using an E2-specific mAb to detect CHIKV particles (Figure II-7C, left). A significantly greater proportion of strain 181/25 was bound by the heparin-conjugated beads relative to strain AF15561. Substituting AF15561

E2 Gly82 with arginine increased the proportion of this virus that was bound by the heparin-conjugated beads. Concordantly, substituting 181/25 E2 Arg82 with glycine decreased heparin binding. Intensities of the viral protein bands from the particles bound to the heparin-conjugated beads were quantified for three independent experiments and normalized to the intensities of protein bands for input virus (Figure II-7C, right). Approximately 35% and 37% of 181/25 and AF15561 E2 G82R, respectively, were captured by the heparin-agarose beads, whereas only 13% and 16% of AF15561 and 181/25 E2 R82G, respectively, bound to heparin. These results suggest that CHIKV virions directly interact with GAGs and that these interactions are influenced by E2 residue 82.

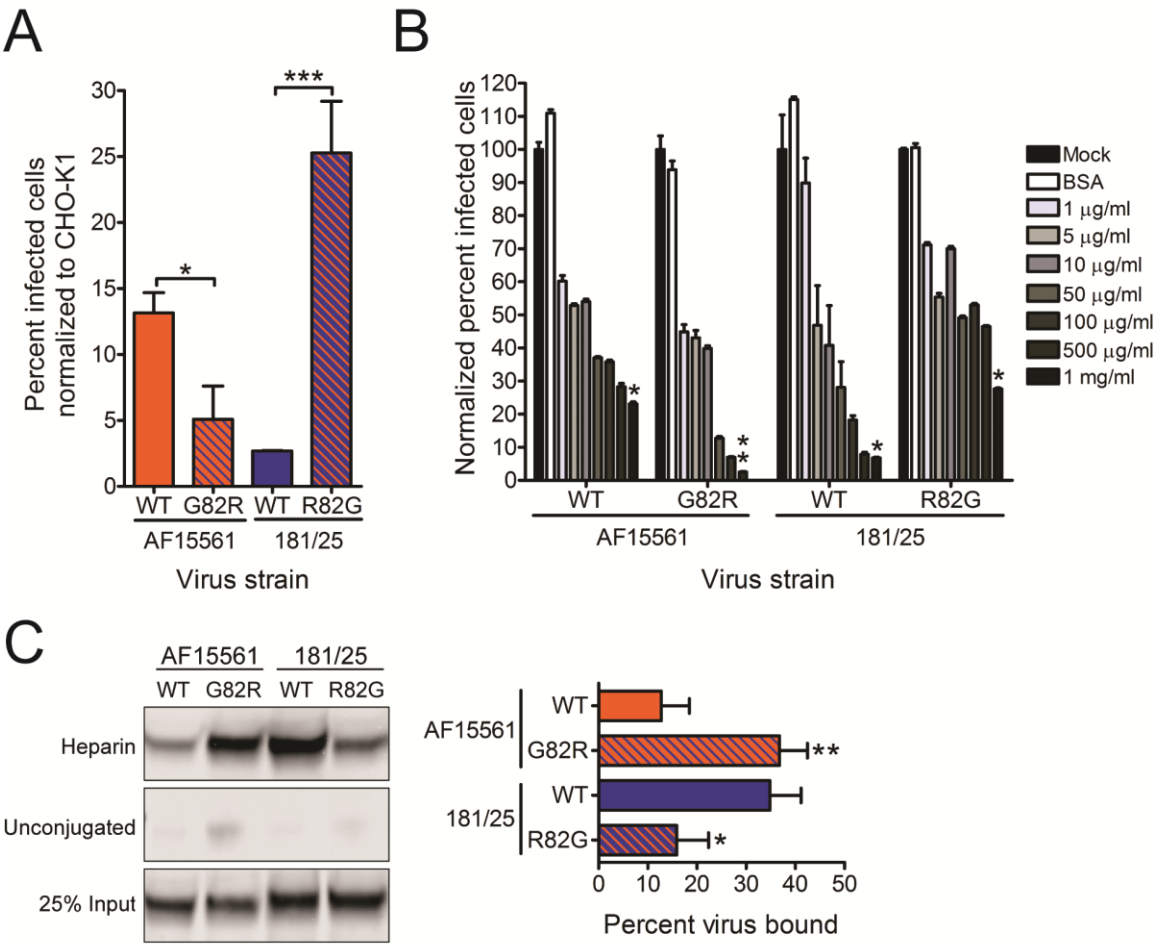
A
Percent infected cells normalized to CHO-K1
30
25
20
15
10
5
0
*
***
WT G82R WT R82G
AF15561 181/25
Virus strain
B
Normalized percent infected cells
120
110
100
90
80
70
60
50
40
30
20
10
0
*
*
*
*
WT G82R WT R82G
AF15561 181/25
Virus strain
Mock
BSA
1 μg/ml
5 μg/ml
10 μg/ml
50 μg/ml
100 μg/ml
500 μg/ml
1 mg/ml
C
AF15561 181/25
WT G82R WT R82G
Heparin
Unconjugated
25% Input
AF15561
WT
G82R
181/25
WT
R82G
**
*
0 10 20 30 40 50
Percent virus bound

Figure II-7. An arginine at E2 residue 82 confers dependence on glycosaminoglycans. (A) CHO-K1 and CHO-pgsA745 cells were adsorbed with AF15561, 181/25, AF1561 E2 G82R, or 181/25 E2 R82G at an MOI of 10 PFU/cell and incubated for 24 h. Cells were stained with CHIKV-specific antiserum and DAPI to detect nuclei and imaged by fluorescence microscopy. Results are presented as percent infected cells for triplicate experiments normalized to the parental CHO-K1 cells. Error bars indicate standard error of the mean. (B) Strains AF15561, 181/25, AF1561 E2 G82R, or 181/25 E2 R82G were treated with BSA at 1000 µg/ml or heparin at the concentrations shown for 30 min and adsorbed to Vero cells at an MOI of 2.5 PFU/cell. After incubation for 24 h, cells were stained with CHIKV-specific antiserum and DAPI to detect nuclei and imaged by fluorescence microscopy. Results are presented as percent infected cells for triplicate experiments. Error bars indicate standard error of the mean. (C) The virus strains shown at 5 x 10^9 genome copies each were incubated with heparin-conjugated or unconjugated agarose beads for 30 min, resolved by SDS-PAGE, and detected by immunoblotting with CHIKV E2-specific mAb (left). Twenty-five percent of input virus is shown as a control. Percent of virus bound to beads was quantified by optical densitometry for triplicate experiments (right). Error bars indicate standard deviation. *, $P < 0.05$, **, $P < 0.01$, ***, $P < 0.001$ as determined by Student's *t* test (A and C) and Kruskal-Wallis followed by Dunn's *post hoc* test (B).

Table II-3. Infectivity of purified CHIKV viruses by genome equivalents.

Virus strain	Genomes:PFU[a]	Genomes:FFU ($x10^4$)[b]	
		CHO-K1	CHO-pgsA745
AF15561	647	1580	11790
AF15561 E2 G82R	498	870	20490
181/25	92	310	2380
181/25 E2 R82G	316	1860	8150

[a]Genome copy numbers were determined by triplicate real-time quantitative PCR reactions. Plaque-forming units were determined by plaque assay using Vero cells for three independent stocks for each virus strain.
[b]Fluorescent-focus units were determined by indirect immunofluorescence in triplicate for at least two independent experiments.

Discussion

In this study, I demonstrate a role for polymorphic residues displayed by strains AF15561 and 181/25 in the differential infection of mammalian and mosquito cells. In particular, I identified E2 residue 82 as the dominant determinant of these differences. Viruses encoding an arginine at E2 residue 82 displayed enhanced infectivity in mammalian cells, and viruses encoding a glycine at this residue displayed enhanced infectivity in mosquito cells. My results indicate that an arginine at E2 residue 82 enhances utilization of GAGs by CHIKV to augment infection of mammalian cells. However, interactions of E2 residue 82 with GAGs in mosquito cells may not occur or may be insignificant for infection of these cells. Data presented here expand our knowledge of how CHIKV E2 residue 82 influences virus-cell interactions to infect mammalian and invertebrate cells.

Vaccine strain 181/25 was developed by passaging a clinical isolate from Thailand, strain AF15561, extensively in mammalian cell culture to produce a highly attenuated, cell culture-adapted virus (79, 80). Accumulation of positively-charged residues within E2 as a consequence of cell culture passage has been demonstrated for other alphaviruses to confer binding to negatively-charged GAGs such as heparan sulfate (94-98). Indeed, I found that strain 181/25 exhibits increased dependence on GAGs for infection of mammalian cells relative to strain AF15561. Selection of an arginine at E2 residue 82 during the passage of strain AF15561 to generate strain 181/25 provided additional positive charge to enhance interactions with GAGs. Since introduction of an arginine at this residue in the AF15561 background was sufficient to enhance GAG dependence to levels observed for strain 181/25, I conclude that the E2 G82R

polymorphism is the sole determinant for differences in GAG utilization between these strains.

E2 residue 82 also may contribute to differences in infectivity by GAG-independent mechanisms. Strains 181/25 and AF15561 differ in GAG-dependence but not to the extent observed for 181/25 and other clinical isolates (66, 99, 100). Strain 181/25 infectivity in CHO-pgsA745 cells, which lack all GAGs, was decreased less than 4-fold relative to strain AF15561 (Figure II-7). In addition, the IC_{50} of heparin inhibition for strains 181/25 and AF15561 were comparable (9.4 and 10.8 μg/ml, respectively). These data suggest that additional mechanisms may underlie decreased infectivity by AF15561 in mammalian cells. Since E2 82 is solvent-exposed and lies within a putative receptor-binding domain of E2 (Figure II-8A) (39), it is possible that this residue participates in interactions with cellular receptors other than GAGs. Substituting AF15561 E2 Gly82 with an arginine enhances infectivity in Vero cells relative to strain AF15561, likely by promoting interactions with GAGs or other cell-surface moieties to mediate attachment. Enhanced viral attachment to the cell surface would facilitate more rapid internalization of the virus and consequent infection. However, infectivity of AF15561 E2 G82R also was significantly greater than that observed for the 181/25 strain in Vero cells (Figure II-4A), although both strains bound heparin-conjugated agarose beads to a similar extent. Furthermore, substituting AF15561 E2 Gly82 with an arginine only modestly enhanced binding to Vero cells. Thus, these findings suggest that an arginine at this residue in the AF15561 background provides a replication advantage in mammalian cell culture in addition to GAG engagement and attachment to host cells.

An arginine at E2 residue 82 does not mediate enhancement of infectivity in mosquito cells as in mammalian cells. These data suggest a GAG-independent function for this residue in invertebrate cells. Several mosquito species express the enzymes capable of synthesizing GAGs (101), but a thorough characterization of GAGs expressed by C6/36 cells has not been reported. Additionally, GAGs are present on the surface of midgut and salivary gland cells of certain mosquito species (101, 102), but it is not clear whether these molecules contribute to CHIKV infection in the invertebrate host. In contrast to mammalian cells, substituting 181/25 E2 Arg82 with glycine enhances infection of C6/36 cells. This enhancement might result from disrupting interactions with negatively-charged GAGs or promoting interactions with other mosquito cell factors either at the cell surface or during later steps in infection. The former possibility would indicate that interactions with GAGs on the surface of C6/36 cells impede CHIKV infection. I think this is not the case, as substituting AF15561 E2 Gly82 with arginine does not diminish infection of these cells. The importance of a glycine at this residue for viral fitness is evidenced by its striking conservation among CHIKV isolates (99), suggesting that it confers an advantage for replication in mosquitoes.

Residues in E2 regulate virion stability by influencing the folding of the protein and by mediating interactions with the E1 and capsid proteins (103-107). Therefore, changes in E2, such as the non-conservative G82R substitution, may alter the stability of the CHIKV virion as demonstrated for other alphaviruses (103-107). When the E2 Arg82 residue was modeled into the crystal structure of the CHIKV E1/E2 heterodimer (Protein Data Bank [PDB] accession code 2XFB [(39)]), this residue closely opposes Glu79, which could result in the formation of a salt bridge between the cationic guanidinium

group of arginine and the anionic carboxylate group of glutamate (Figure II-8B). The formation of this salt bridge may stabilize the E2 protein and, in turn, promote CHIKV infectivity in cell culture and at sites of initial replication in the host but limit dissemination to sites of secondary replication.

The effect of the E2 residue 82 and additional polymorphisms between strains AF15561 and 181/25 on infectivity was largely influenced by the genetic context in which the mutations were introduced. E2 Arg82 resulted in a greater enhancement of infectivity when present in the AF15561 background than in the 181/25 background. This finding was observed in Vero cells and to an even greater extent in murine cells (Figure II-5). Additionally, substitution of AF15561 E2 Thr12 with isoleucine from 181/25, which infects mammalian cells more efficiently, decreased infectivity to levels less than those observed for AF15561. In mosquito cells, substituting AF15561 E2 Thr12 with isoleucine also significantly decreased infectivity, suggesting that the E2 T12I polymorphism negatively influences infection in multiple cell types but only in the context of the AF15561 genetic background. Similar to the E2 R82G polymorphism, substituting 181/25 E1 Val404 with alanine increased infectivity in mosquito cells but not to the levels observed for strain AF15561. Furthermore, substituting AF15561 E1 Ala404 with valine did not decrease infectivity in mosquito cells. Based on these data, I think that multiple polymorphisms between strains AF15561 and 181/25 synergize to provide the replicative advantage observed for strain AF15561. However, the replicative disadvantage of 181/25 in these cells could be attributable to a single polymorphism at E2 residue 12.

Elucidating the viral determinants required for interaction with and infection of host cells is essential for a complete understanding of CHIKV replication and disease. These findings suggest that E2 residue 82 is a determinant of infection in both mammalian and mosquito cells and defines a role for E2 residue 82 in GAG engagement. I demonstrated that viruses containing E2 Arg82 display enhanced infectivity in mammalian cells, while viruses containing E2 Gly82 display enhanced infectivity in mosquito cells. The enhancement provided by an arginine at E2 82 was only partly attributable to increased cell binding, suggesting that this residue promotes interactions with other cell-surface molecules or influences steps in the virus lifecycle following attachment. Studies of GAG-dependent and independent functions of E2 residue 82 will improve our understanding of CHIKV replication and the host interactions required to cause disease.

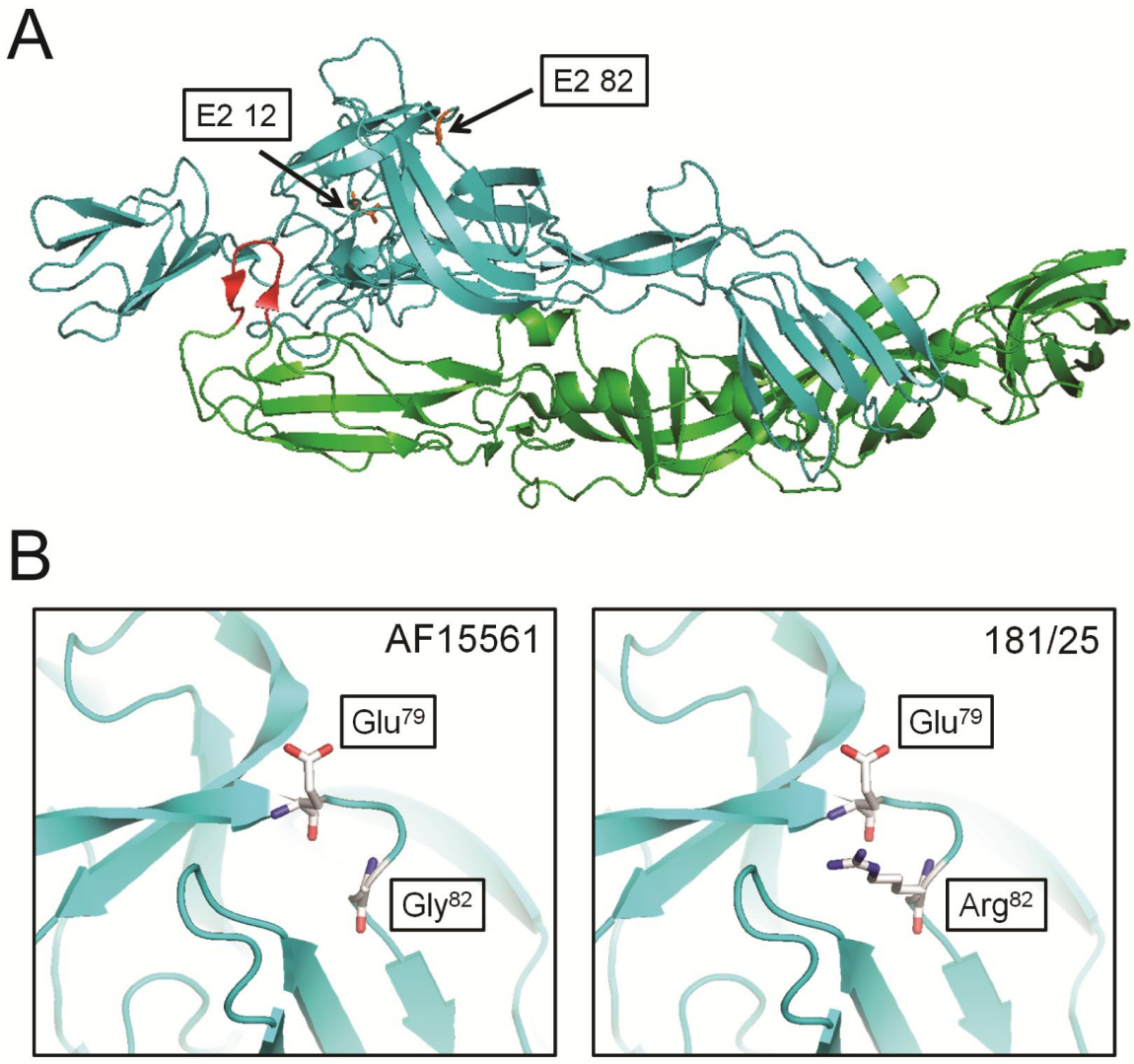

Figure II-8. E2 residue 82 opposes a conserved glutamate at E2 residue 79. (A) Ribbon tracing of the CHIKV E1/E2 heterodimer with E2 depicted in cyan and E1 depicted in green. E2 residues 12 and 82 are shown in orange. The E1 fusion loop is in red. (B) Enlarged regions of E2 with ball and stick representation of glycine (AF15561, left) or arginine (181/25, right) at E2 residue 82 in relation to the highly conserved glutamate at E2 residue 79.

CHAPTER III

CHIKV E2 RESIDUE 82 MODULATES VIRAL DISSEMINATION AND ARTHRITIS IN MICE

Introduction

Virus interactions with host cell-surface molecules serve a critical first step in virus infection. Additionally, interactions with cellular receptors can mediate targeting of virus to discrete sites within the host and contribute to the induction of signaling pathways and immune responses that ultimately affect disease outcome. The specific mechanisms used by CHIKV to disseminate in its host and cause disease have not been well characterized and largely inferred from related alphaviruses. Furthermore, the contributions of specific host attachment molecules and virus entry pathways to CHIKV tissue tropism and immune responses are not known. Understanding the role of attachment molecules during CHIKV infection *in vivo* will provide insight into mechanisms of CHIKV tissue tropism and the host responses that lead to disease.

Previously, I determined that residue 82 in the E2 attachment protein is a critical determinant of infection in mammalian cells and contributes to infection of mosquito cells (Chapter II). Moreover, my studies and others found that E2 residue 82 influences interactions with GAGs in mammalian cells (99, 100). Heparan sulfate-binding viruses often exhibit reduced viral dissemination and attenuation *in vivo* (96, 108-111). However, such viruses can show increased virulence depending on the route of inoculation, as demonstrated for certain strains of eastern equine encephalitis virus (EEEV) and SFV

(112-114). A strategy to introduce attenuating heparan sulfate-binding residues within the CHIKV E2 attachment protein has been established as a model for CHIKV vaccine development (66). Wildtype CHIKV strain LR2006 OPY1 (LR) induces significantly less footpad swelling and proinflammatory cytokine production following substitution of E2 Gly82 with arginine and Glu79 with lysine, the latter of which was identified following serial passage in cell culture (66). Introduction of either substitution enhanced sensitivity to blockade of infection by soluble heparin or salt disruption of ionic interactions (66), suggesting that viruses attenuated by virtue of these mutations exhibit increased dependence on GAGs for infection. However, the roles of E2 residue 82 in CHIKV-induced arthritis and viral tropism are not fully understood. In addition, it is not known whether GAG utilization is the sole mechanism that underlies CHIKV 181/25 attenuation.

To define the role of E2 residue 82 in CHIKV pathogenesis, I inoculated mice with virus strains polymorphic at this site and monitored for disease. Using this mouse model of CHIKV-induced disease, I found that E2 residue 82 influences CHIKV-induced pathology, including footpad swelling and inflammation and necrosis in the metatarsal muscle ipsilateral to the site of inoculation. In addition, this residue regulates viral dissemination to the spleen and establishment of viremia. Viruses containing an arginine at E2 residue 82 were attenuated for musculoskeletal disease, yet substitution of a glycine at this residue was not sufficient to confer virulence. I conclude that CHIKV utilization of GAGs alters viral tropism, tissue inflammation, and tissue injury induced during infection, resulting in attenuated CHIKV disease.

Results

CHIKV E2 residue 82 regulates virus-induced pathology. To determine whether E2 residue 82 influences CHIKV virulence, I tested CHIKV strains polymorphic at the E2 82 residue for the capacity to induce pathology in a mouse model of CHIKV disease (57). In this model, three-week-old mice are inoculated subcutaneously in the left rear footpad. Infected mice develop signs of disease similar to those observed in humans infected with CHIKV, including swelling of the feet and ankles, arthritis, myositis, and tenosynovitis. Mice were inoculated with 10^3 PFU of 181/25, AF15561, 181/25 E2 R82G, or AF15561 E2 G82R, and virulence was assessed by weight gain and swelling of feet (Figure III-1). AF15561-infected mice gained less weight than 181/25-infected mice, indicating that strain AF15561 is more virulent in these animals (Figure III-1A). Mice inoculated with AF15561 E2 G82R gained weight in parallel with mock-infected mice, suggesting that an arginine at E2 residue 82 in the AF15561 background significantly reduces CHIKV virulence. However, mice inoculated with 181/25 E2 R82G did not exhibit impaired weight gain, suggesting that substitution of a glycine at E2 residue 82 in 181/25 is not sufficient to recapitulate the virulent phenotype.

To determine the effect of E2 residue 82 on CHIKV-induced arthritis, I assessed swelling of the left and right feet at 1, 3, 5, and 7 days postinoculation (Figure III-1B). At 3, 5, and 7 days postinoculation, AF15561-infected mice exhibited significant swelling of the left feet. No swelling was observed in the uninoculated feet of any of the animals. Inoculation with AF15561 E2 G82R resulted in reduced swelling in the left hind limb at 3 and 5 days postinoculation relative to AF15561, whereas inoculation with 181/25 E2

R82G only modestly increased swelling at 5 days postinoculation relative to 181/25. Together, these data suggest that a glycine at E2 residue 82 is necessary but not sufficient for full virulence of strain AF15561 as assessed by weight gain and foot swelling.

To determine whether E2 residue 82 influences the magnitude of pathologic injury, left hind limbs of infected mice were processed for histology and assigned a pathology score based on histologic changes by an observer blinded to the conditions of the experiment (Figure III-2). Tissue damage appeared more severe for AF15561-infected mice relative to 181/25-infected mice at day 7 postinoculation (Figure III-2A and B). In particular, there was slightly more inflammation and necrosis in the metatarsal muscle of AF15561-infected mice compared to that of 181/25-infected mice. However, levels of myositis and tendonitis induced by these strains were comparable. Substitution of an arginine at E2 82 in the AF15561 strain led to reduced tissue damage, inflammation, and necrosis compared to mice inoculated with the parental AF15561 strain (Figure III-2B). More dramatically, substitution of a glycine at this residue in the 181/25 strain led to consistently more inflammation and necrosis of the metatarsal muscle as well as more severe tendonitis in the hind limb relative to the hind limbs of 181/25-infected mice. These data suggest that E2 residue 82 modulates CHIKV-induced disease and that a glycine at this residue is sufficient to mediate tissue injury in CHIKV-infected mice.

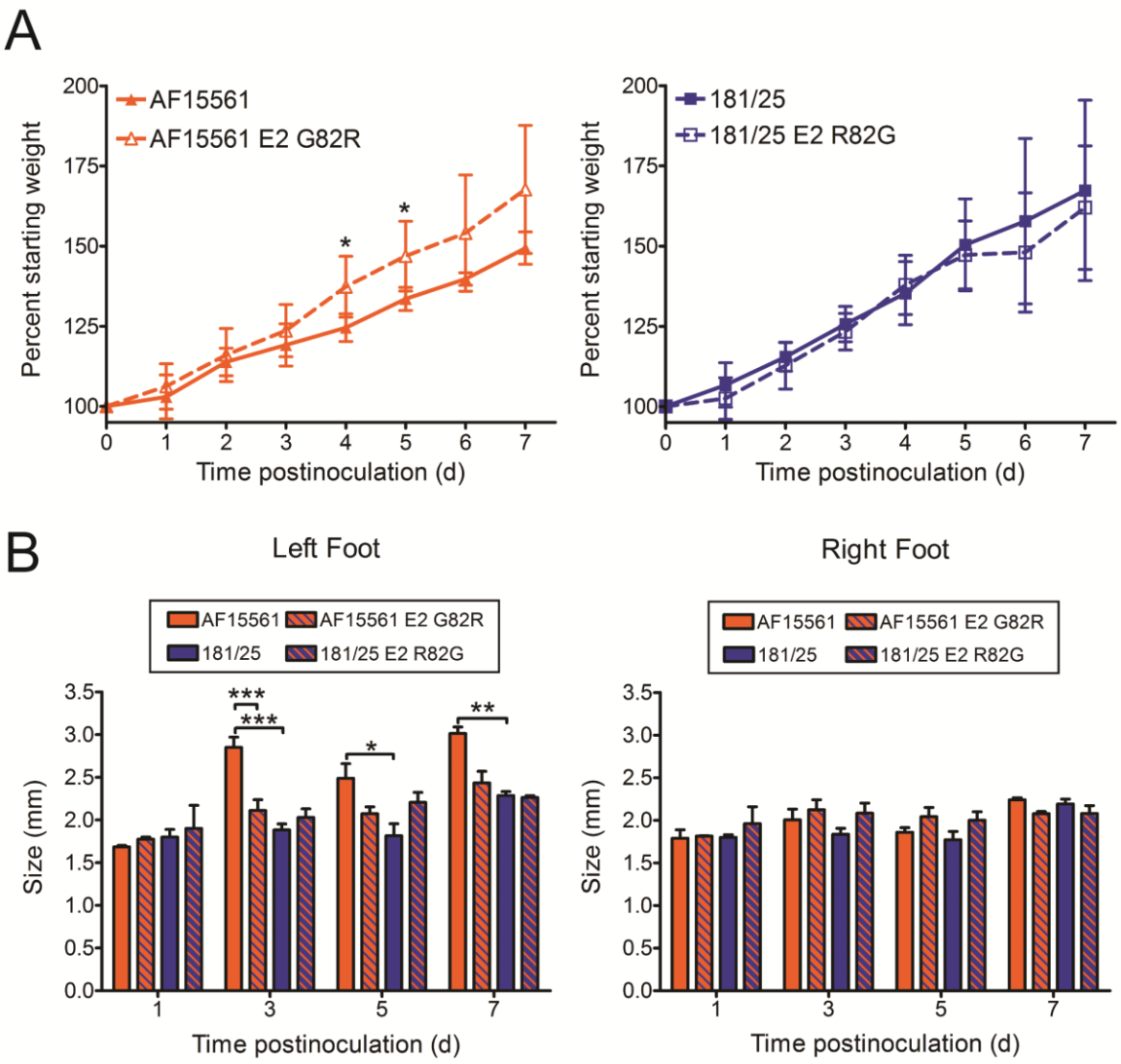

Figure III-1. CHIKV E2 residue 82 modulates virus-induced pathology. C57BL/6J mice (20-22 days old) were inoculated with 10^3 PFU of AF15561, 181/25, AF1561 E2 G82R, or 181/25 E2 R82G in the left rear footpad. (A) Mice were weighed at 24-h intervals postinoculation. Results are presented as the mean percent starting weight (weight on day 0). Error bars indicate standard deviation. (D0-D1, n = 17; D2-D3, n = 15; D4-D5, n = 8; D6-D7, n = 3). (B) Swelling of the left and right hind feet was quantified using calipers at the times shown. Error bars indicate standard deviation. (D1, n = 2; D3, n = 7; D5, n = 5; D7, n = 3). *, $P < 0.05$, **, $P < 0.01$, ***, $P < 0.001$, as determined by ANOVA followed by Bonferroni *post hoc* test.

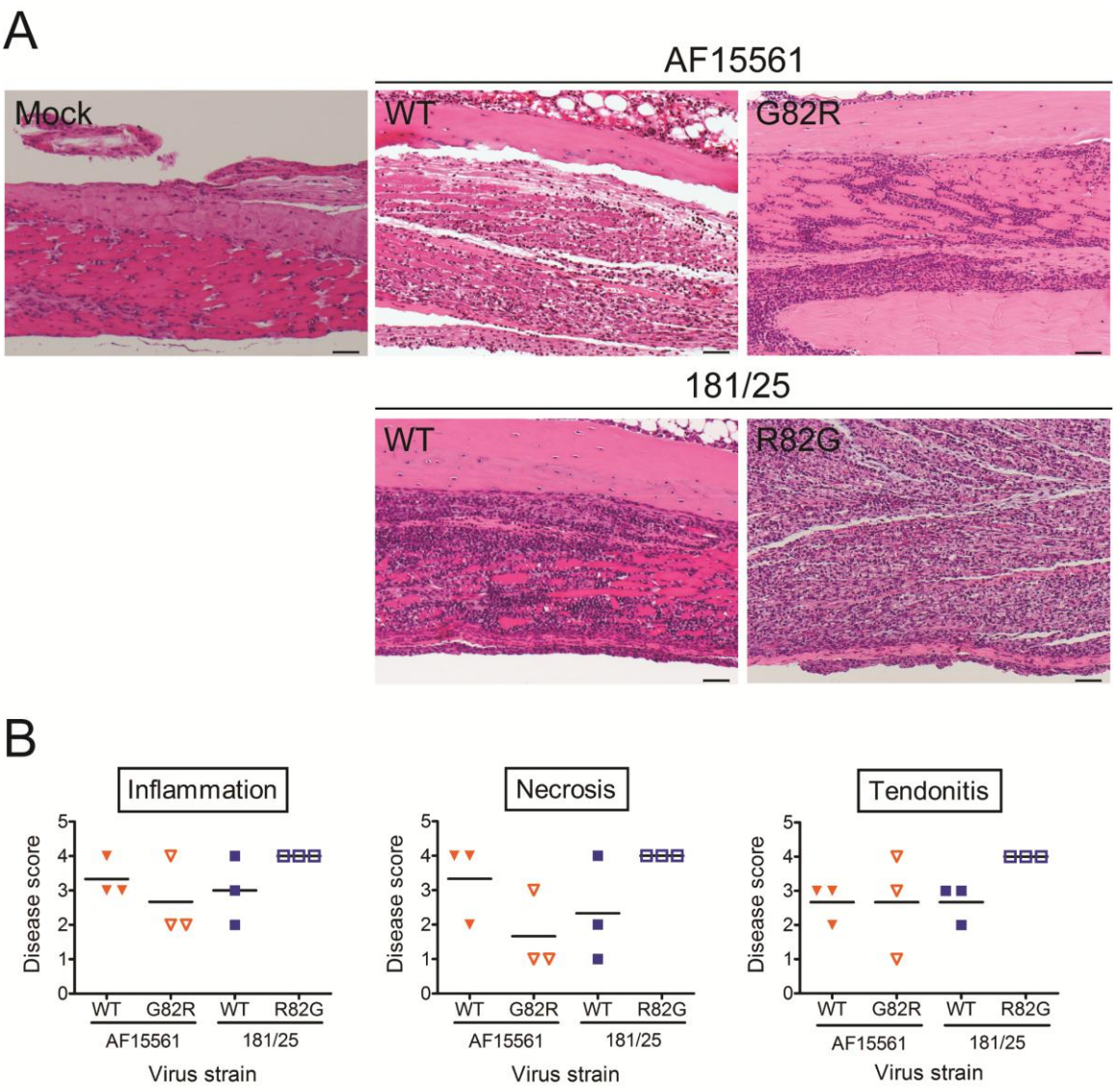

Figure III-2. An arginine at E2 residue 82 diminishes CHIKV-induced arthritis. (A) C57BL/6J mice (20-22 days old) were inoculated with PBS or 10^3 PFU of AF15561, 181/25, AF1561 E2 G82R, or 181/25 E2 R82G in the left rear footpad. At day 7 postinoculation, mice were euthanized and perfused with 4% PFA. Consecutive 5-µm sections of the left hind limb were stained with H&E. (A) Representative sections of three mice per group are shown for mock-infected mice or mice inoculated with the parental strains and the reciprocal E2 82 variant strains. Scale bars, 50 µm. (B) H&E-stained sections were scored for histologic evidence of inflammation and necrosis in the metatarsal muscle and tendonitis. Results are expressed as pathology score of tissues from individual animals. Horizontal black lines indicate mean pathology score. Scores were assigned based on the following scale: 0, no lesions; 1, minimal, 0-24% of tissue affected; 2, mild, 25-49% of tissue affected; 3, moderate, 50-75% of tissue affected; and 4, marked, >75% of tissue affected.

CHIKV titers in the spleen and serum are influenced by E2 residue 82. To determine whether differences in virus-induced pathology are a consequence of differences in viral replication, mice were inoculated subcutaneously in the left rear footpad with 10^3 PFU of 181/25, AF15561, 181/25 E2 R82G, or AF15561 E2 G82R. Tissues were harvested at 1, 3, and 5 days postinoculation, and viral titers were determined by plaque assay (Figure III-3). At 1 day postinoculation, all viruses produced equivalent titers in the left and right hind limbs (Figure III-3A). However, AF15561 produced higher titers in the spleen and serum relative to 181/25. Titers of AF15561 E2 G82R were reduced in the spleen and serum relative to AF15561 at 1 day postinoculation, and 181/25 E2 R82G produced higher titers in the spleen and serum relative to 181/25, although this difference was not statistically significant. These data suggest that a glycine at E2 residue 82 contributes to higher viral titers in the spleen and serum at early times postinoculation.

By 3 days postinoculation, all viruses produced comparable titers in the left ankle, but AF15561 replicated to significantly higher titers in the left quadriceps and right ankle relative to 181/25 (Figure III-3B). However, this difference in replication did not segregate with E2 residue 82, as mice inoculated with AF15561 E2 G82R displayed higher viral titers in the left quadriceps and right ankle relative to 181/25 E2 R82G. Similarly, higher titers of AF15561 E2 G82R were detected in the right quadriceps and serum relative to 181/25 E2 R82G. In the spleen, I observed a trend similar to the day 1 timepoint with AF15561 E2 G82R producing lower titers in that organ relative to AF15561, and 181/25 E2 R82G producing slightly higher titers relative to 181/25.

By 5 days postinoculation, no virus was detected in the serum. In the left and right quadriceps, titers of AF15561 E2 G82R were higher relative to those of AF15561 (Figure

III-3C). In addition, titers of 181/25 were higher in these tissues relative to those of 181/25 E2 R82G. These data suggest that an arginine at E2 residue 82 correlates with higher viral titers in the quadriceps muscles at later times postinoculation. In contrast, viruses containing a glycine at E2 82 produced higher titers in the spleen at earlier times postinoculation. Thus, residue 82 in the E2 glycoprotein contributes to either viral dissemination to or replication within the hind limbs and spleen and influences establishment of viremia.

A glycine at E2 residue 82 is selected in the spleens of CHIKV-infected mice. Since high mutation rates are associated with replication of positive-sense RNA viruses (115, 116), I determined the sequences of viral isolates from CHIKV-infected mice to assess the stability of the engineered mutations. RNA was isolated from the spleens of CHIKV-infected mice at 1 day postinoculation, cDNA was generated, and sequences of the E2 open-reading frame from multiple clones were determined (Figure III-4). Of the clones derived from mice inoculated with strain AF15561 E2 G82R, 21 of 23 clones (91%) encoded a glycine at E2 residue 82. In contrast, only 2 of 13 (15%) of the clones derived from mice inoculated with strain AF15561 encoded an arginine at this position. Viral RNA could not be recovered from the spleens of 181/25-infected animals at this early timepoint, which precluded sequence analysis. To confirm that these mutations were not present in the viral inocula, RNA was isolated from virus stocks, cDNA was generated, and E2 sequences were determined. Of the 20 clones sequenced from each virus stock, all encoded the engineered residues in the E2 open-reading frame. These results suggest that

a glycine at E2 82 is preferentially selected early in CHIKV infection in the spleen, but a residual population of isolates with an arginine at this position is maintained.

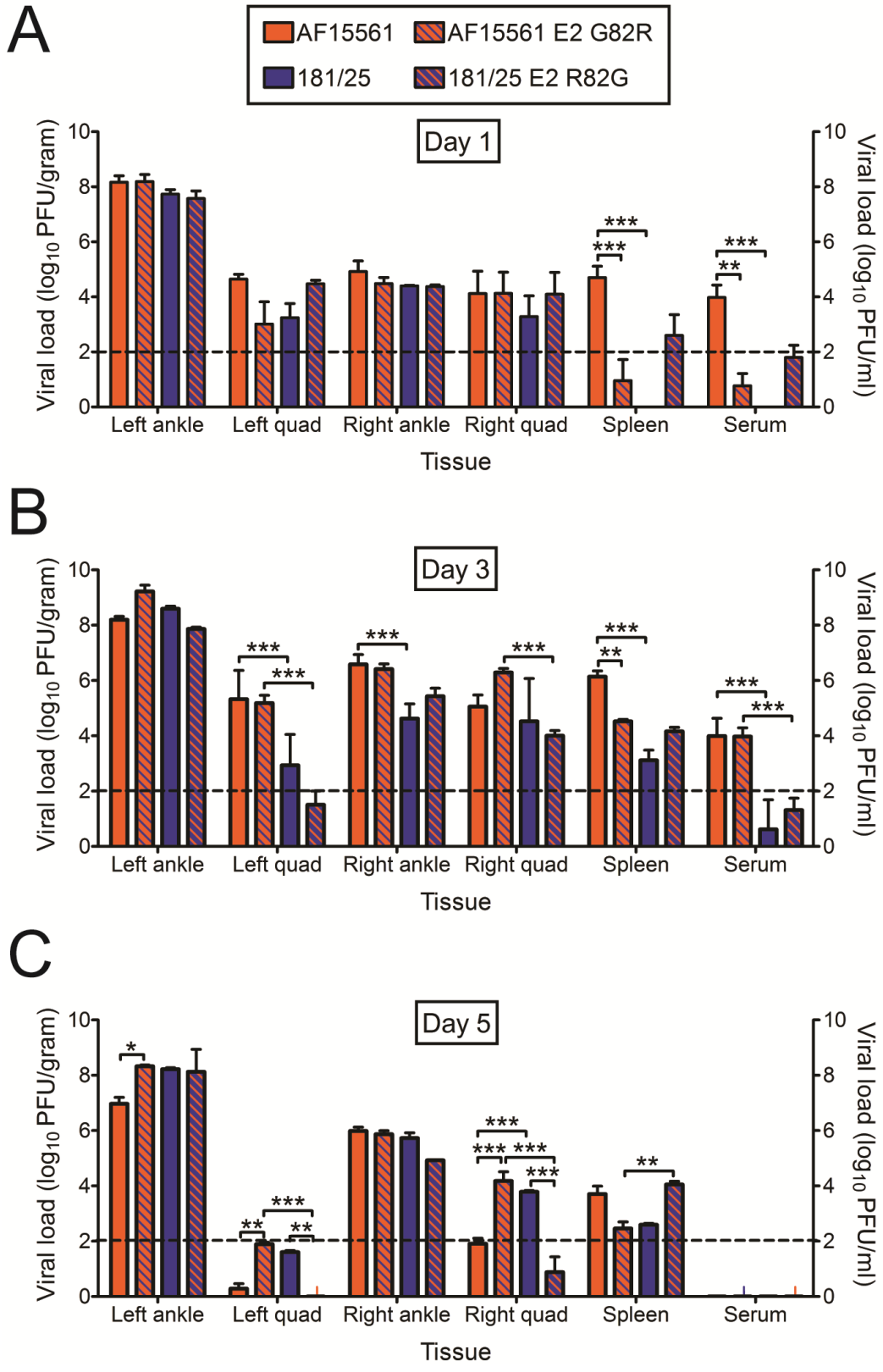
A
AF15561
AF15561 E2 G82R
181/25
181/25 E2 R82G
Day 1
Viral load (log10 PFU/gram)
Viral load (log10 PFU/ml)
Left ankle
Left quad
Right ankle
Right quad
Spleen
Serum
Tissue
B
Day 3
C
Day 5

Figure III-3. Viral loads following inoculation of parental strains and the reciprocal E2 82 variant strains. C57BL/6J mice (20-22 days old) were inoculated with PBS or 10^3 PFU of AF15561, 181/25, AF1561 E2 G82R, or 181/25 E2 R82G in the left rear footpad. At days 1, 3, and 5 postinoculation, mice were euthanized, ankles, quadriceps (quad), and spleen were excised, and serum was collected. Viral titers in tissue and serum homogenates were determined by plaque assay using BHK-21 cells. Results are expressed as the mean PFU/gram (tissue) or PFU/ml (serum). Error bars indicate standard error of the mean. Dashed lines indicate the limit of detection. (D1, n = 5; D3, n = 7; D5, n = 5). **, $P < 0.01$, ***, $P < 0.001$, as determined by ANOVA followed by Bonferroni *post hoc* test.

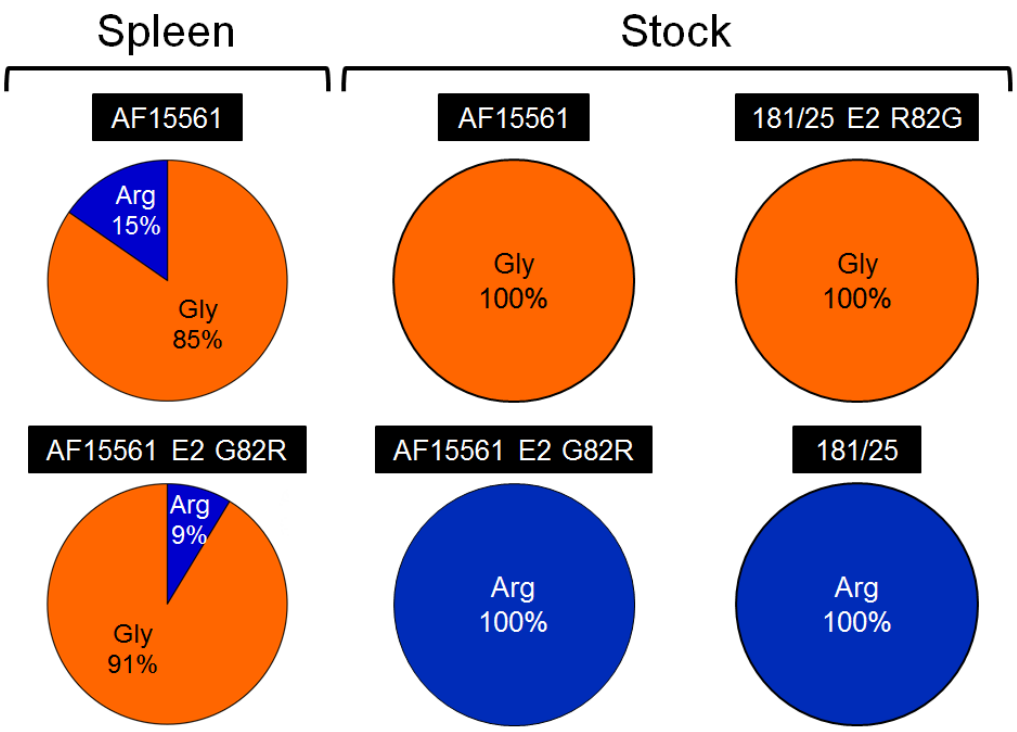

Figure III-4. E2 Gly82 is selected in spleens of CHIKV-infected mice. At 1 day postinoculation, RNA was isolated from spleens of CHIKV-infected mice or from virus stocks used for inoculations. cDNA was generated using random hexamers and amplified using PCR. The mutagenized region of the E2 open-reading frame was sequenced. Shown are the percentages of virus clones encoding either a glycine or arginine at E2 residue 82 for each sample. Number of clones sequenced: Spleen AF15561 = 13; Spleen AF15561 E2 G82R = 23; Stock AF15561 = 19; Stock AF15561 E2 G82R = 18; Stock 181/25 E2 R82G = 23; Stock 181/25 = 17.

Discussion

CHIKV causes both an acute and chronic disease characterized by debilitating joint pain and inflammation (28, 117). However, the viral and host determinants responsible for CHIKV disease have not been fully defined. Additionally, mechanisms of pathogenesis for arthritogenic alphaviruses like CHIKV are not completely understood. CHIKV strain 181/25, which was isolated following serial passage in mammalian cell culture, differs from its closest known parental strain, AF15561, at 5 synonymous and 5 nonsynonymous nucleotide positions. One nonsynonymous polymorphism, G82R in the E2 attachment protein, attenuates virulence in some mouse models (66, 118). In this study, I demonstrate a role for E2 residue 82 in CHIKV-induced musculoskeletal disease. Viruses containing a glycine at E2 82 replicated to higher titers in lymphoid tissues and established higher levels of viremia. Moreover, these viruses induced greater pathologic injury, including inflammation and necrosis, in joint-associated tissues compared with viruses containing an arginine at this position. Data presented here provide new information about the function of CHIKV E2 residue 82 in a mouse model of CHIKV-induced disease.

My results (Chapter II) along with previously published data (66, 99, 118) indicate that an arginine at E2 residue 82 enhances utilization of GAGs by CHIKV to infect cultured cells and attenuates the virus in mice. However, it is not clear how an increase in GAG dependence leads to attenuation of CHIKV. For other alphaviruses, such as Sindbis virus (SINV) and Venezuelan equine encephalitis virus (VEEV), higher-affinity interactions with GAGs prevent viral spread to sites of secondary replication or facilitate viral clearance from the bloodstream (96, 119, 120). I found that CHIKV strains

containing an arginine at E2 82 produce lower titers at sites of secondary replication including the spleen and reduced viremia in immune competent mice. These findings are consistent with those obtained by Gardner et al. using a similar mouse model (66). Thus, it appears that GAG-dependent strains of CHIKV disseminate less efficiently, are cleared more rapidly, or perhaps both.

As early as 1 day postinoculation of strain AF15561 E2 G82R, nucleotide sequences of most isolates detected in the spleens of infected mice encode a glycine at E2 residue 82. Reversion also was observed by Gorchakov et al. (118) in which 100% of isolates in the blood encode a glycine at E2 82 by 3 days postinoculation. In contrast, following inoculation with the E2 T12I variant, only 22% of isolates encoded a threonine at E2 residue 12 (118). E2 82 may mediate viral tropism specifically in lymphoid tissues early in infection, and the presence of an arginine at this residue may limit the capacity of the virus to replicate in lymphoid cells. Consistent with this idea, lower levels of viral RNA were detected in the popliteal lymph nodes of mice inoculated with viruses containing an arginine at E2 82 (data not shown). The rapid selection of a glycine at this residue may explain the higher titers of 181/25 and AF15561 E2 G82R in the spleen and other tissues of infected mice at later times postinoculation and might support a role for this residue early in infection. Although viral isolates from the spleens of AF15561-infected mice encoded a glycine at E2 82, the population was not homogeneous, as a subset of clones encoded an arginine at this residue. These data suggest that selection at this position *in vivo* is not absolute.

Beyond viral attachment and tissue tropism, E2 82 might contribute to host responses to CHIKV early in infection. Although there were significant differences in

swelling and pathology in the left hind limb, titers produced at this site by strains that vary solely at E2 82 were comparable. These data support the hypothesis that differences in pathological injury produced by CHIKV strains with an E2 residue polymorphism result from differences in immune and inflammatory responses. Such responses could be tissue-specific and dependent upon replication efficiency in the discrete cell subsets that are targeted within those tissues. Concordant with this hypothesis, relative to the virulent CHIKV LR strain, LR-E2 Arg82 induces lower levels of proinflammatory cytokines and chemokines (66). These data suggest that E2 residue 82 also modulates the induction of inflammatory pathways that contribute to differences in swelling elicited by these viruses during infection. Despite similar levels of myositis and tendonitis induced by these strains, viruses containing E2 Arg82 induced less necrosis in the hind limb metatarsal muscle compared with viruses containing E2 Gly82. In mice deficient for IFN-α/β receptors or the STAT1 signal transducer, similar levels of inflammatory infiltrates were observed in the hind limbs following infection with CHIKV strains LR and 181/25, despite reduced swelling in 181/25-infected mice (100). These data suggest a correlation between induction of inflammatory pathways and events that contribute to swelling in the infected host, which may occur independently of immune cell infiltration.

Results in this chapter demonstrate that a glycine at E2 82 is required for virulence in the AF15561 background but not sufficient to confer virulence to the attenuated 181/25 strain. Substituting 181/25 E2 Arg82 with glycine failed to recapitulate the virulent phenotype as assessed by weight gain and footpad swelling. However, introducing a glycine at E2 82 was sufficient to induce histopathologic injury in the hind limbs of infected mice to levels induced by the parental AF15561 strain. Therefore, the

effects of this residue are dependent on the genetic background in which the mutations are introduced, as observed with infectivity data presented in Chapter II. Additionally, the AF15561 E2 T12I polymorphism was demonstrated previously to contribute to 181/25 attenuation (118) but was not identified in this study in which I used infectivity in mammalian cells as an *in vitro* correlate of virulence to screen viral variants. Therefore, additional polymorphisms displayed by strains AF15561 and 181/25 likely contribute to attenuation of 181/25 in this mouse model of CHIKV disease.

Understanding mechanisms of virus entry and the interactions that promote dissemination and pathogenesis will illuminate new avenues for development of pathogen-specific therapeutic and prophylactic intervention strategies. This study defines a role for E2 residue 82 in CHIKV tropism and virulence *in vivo*. In infected mice, viruses encoding an arginine at E2 residue 82 exhibit defects in replication in lymphoid tissues, establishment of viremia, and production of pathological injury in joint-associated muscle. A glycine at E2 82 is under strong selective pressure in the spleens of CHIKV-infected mice, but this residue was not static, as an arginine also was selected at low frequency. These findings support new functions for E2 residue 82 in host-specific and GAG-independent processes and in the development of joint swelling through inflammation-mediated events. Future studies to understand mechanisms by which E2 residue 82 influences CHIKV tropism and host responses during infection will reveal both viral and host targets to restrict infection and diminish disease.

CHAPTER IV

ANTAGONISM OF THE SODIUM-POTASSIUM ATPASE RESTRICTS CHIKV INFECTION

Introduction

Viruses require a multitude of host factors to productively infect target cells and must employ strategies to evade host defense to allow for efficient replication. CHIKV displays broad tropism in humans, but many of the host factors required to promote CHIKV infection are not fully understood. Furthermore, the molecules and mechanisms that contribute to virus-induced pathology during disease progression have not been well characterized. Identification of pro- and anti-viral host factors should illuminate interactions essential for CHIKV replication and disease. In turn, such studies may reveal new targets for CHIKV-specific antiviral therapies.

To identify host mediators of CHIKV replication, Laurie Silva and I screened a library of small molecules for the capacity to diminish infection of U-2 OS cells by CHIKV replicon particles expressing an enhanced green fluorescent protein (eGFP) reporter. In this screen, I identified digoxin, a cardiac glycoside that blocks the sodium-potassium ATPase, as a potent inhibitor of CHIKV infection. Pretreatment of U-2 OS cells or primary human synovial fibroblasts with digoxin resulted in a dose-dependent decrease in infection by CHIKV virions. Digoxin treatment of murine cells also inhibited CHIKV infection but only after treatment with significantly higher concentrations, which correspond to the relative transcript levels of the sodium-potassium ATPase α3 subunit.

Overexpression of the human or murine α3 isoform exacerbated digoxin inhibition of CHIKV, suggesting that blockade of the sodium-potassium ATPase by digoxin mediates the antiviral activity. Digoxin also displayed antiviral activity against other alphaviruses, including RRV and SINV, and the unrelated mammalian orthoreovirus (called reovirus here). Digoxin inhibited both entry and post-entry steps in CHIKV infection. Passage of CHIKV in digoxin-treated cells selected for multiple mutations in both nonstructural and structural genes, suggesting multiple mechanisms of CHIKV inhibition by digoxin. These data suggest a role for the sodium-potassium ATPase in CHIKV infection and provide a new target for the development of broad-spectrum antiviral therapeutics.

Results

Identification of digoxin as an inhibitor of CHIKV infection. To identify host factors required for CHIKV infection, Laurie and I screened 727 chemical compounds from the NIH Clinical Collection (NCC) for the capacity to impede or augment infection by CHIKV replicon particles (Figure IV-1A). The NCC library is comprised almost entirely of compounds that have been used in Phase I, II, and III clinical trials in humans. Human osteosarcoma (U-2 OS) cells were incubated with dimethyl sulfoxide (DMSO) as a vehicle control, 100 nM bafilomycin A1 as a positive control, or 1 μM of each NCC compound. Treated cells were adsorbed with CHIKV strain SL15649 replicon particles expressing eGFP and incubated for 24 h. The percentage of infected cells was determined by GFP expression, and robust *Z* scores were calculated for each compound. Seven compounds had average *Z* scores of ≤ -2.0 (inhibited infection) and 20 compounds had

average *Z* scores ≥ 2.0 (enhanced infection) (Figure IV-1B). The largest class of compounds that influenced CHIKV infection alters steroid or other hormonal signaling and biosynthetic pathways (Figure IV-1C). Significant numbers of compounds also targeted ion transporters and neurotransmitter receptors, such as those for serotonin and dopamine. Homoharringtonine, a protein translation inhibitor and known antagonist of CHIKV infection (76), had the largest negative *Z* score, -41.94. Digoxin, an inhibitor of the sodium-potassium ATPase, produced the second-largest negative *Z* score, -26.67, suggesting that a functional sodium-potassium ATPase is required for CHIKV infection.

Digoxin inhibits CHIKV infection in a species-specific manner. To determine whether inhibition of the sodium-potassium ATPase blocks infection by CHIKV virions, I treated a variety of cell lines with DMSO, 5-nonyloxytryptamine (5-NT), a serotonin agonist, as a positive control, or digoxin at increasing concentrations for 1 h prior to adsorption with CHIKV strain SL15649 for 1 h, incubated cells for 5 h in the presence of compound, and scored cells for infection using indirect immunofluorescence (Figure IV-2). Relative to DMSO-treated cells, treatment of U-2 OS cells with digoxin resulted in a dose-dependent decrease in CHIKV infection with a half maximal effective concentration (EC_{50}) of 48.8 nM (Figure IV-2A). Digoxin treatment similarly decreased CHIKV infection of primary human synovial fibroblasts (HSFs) with an EC_{50} of 43.9 nM (Figure IV-2B), suggesting that digoxin can impede CHIKV infection of physiologically relevant target cells in the host. Digoxin treatment also inhibited CHIKV infection of Vero cells (data not shown). Despite inhibition of CHIKV infectivity in multiple human cell types, digoxin treatment of ST2 cells and other murine cell lines at doses sufficient to block infection of human

cells did not decrease CHIKV infection in these cell types (Figure IV-2C and data not shown). In addition, digoxin treatment did not diminish CHIKV infection of *Aedes albopictus* C6/36 cells (Figure IV-2D). Together, these data indicate that digoxin is a potent inhibitor of CHIKV infection and that inhibition occurs in a species-specific manner.

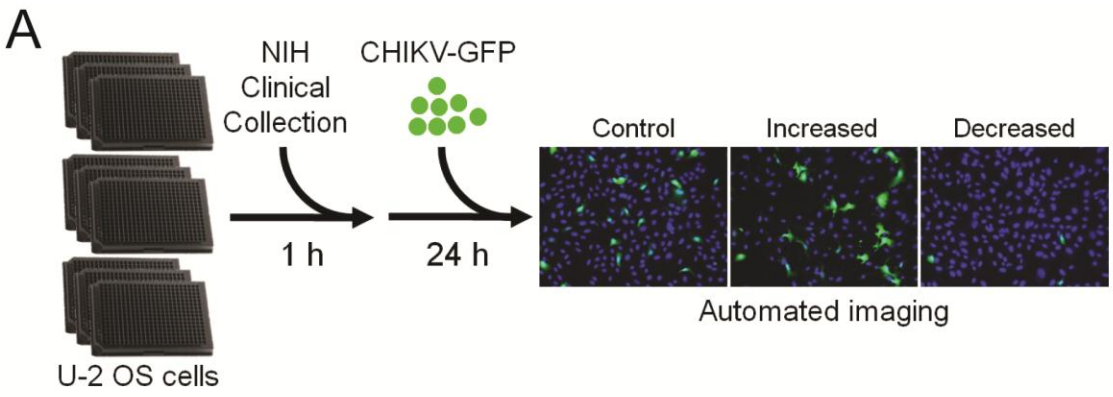

B

Compound Name	Target	*Z* Score
Homoharringtonine	Protein synthesis	-41.94
Digoxin	Sodium-potassium ATPase	-26.67
Goserelin Acetate	LHRH agonist	-3.35
Metyrapone	Cortisol synthesis	-3.22
Vincristine Sulfate	Microtubules	-2.48
Perphenazine	Dopamine antagonist	-2.47
SR 57,227A	Serotonin agonist	-2.31
Dehydrocholic acid	Steroid metabolism	2.00
Benzbromarone	Organic anion transporter	2.00
Anastrozole	Estrogen synthase	2.08
Balsalazide	Prostaglandin synthase and lipoxygenase	2.12
Cefaclor	Bacterial cell wall antibiotic	2.20
SDM25N	Opioid receptor antagonist	2.20
Resveratrol	Phosphodiesterase inhibitor	2.24
Lansoprazole	Proton-pump inhibitor	2.26
Palonosetron	Serotonin antagonist	2.39
Granisetron	Serotonin antagonist	2.71
Haloperidol	Dopamine and glutamate antagonist	2.78
Fluperlapine	Serotonin and α_2-adrenergic antagonist	2.85
Tibolone	Estrogen receptor	2.88
Desoximetasone	Glucocorticoid receptor	2.88
Ropivacaine	Sodium channel	2.89
Corticosterone	Corticoid receptors	2.96
Salmeterol	β_2-adrenergic receptor	3.09
Dehydroepiandrosterone	Steroid precursor	3.15
Cefixime Trihydrate	Bacterial cell wall antibiotic	3.32
5-Methoxytryptamine	Serotonin agonist	3.41
Phenothiazine	Dopamine antagonist	3.86

C

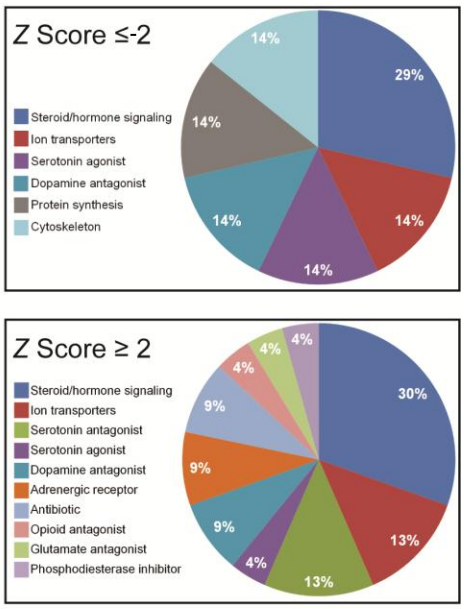

Figure IV-1. High-throughput screening to identify inhibitors of CHIKV infectivity. (A) U-2 OS cells were incubated with DMSO, 100 nM bafilomycin A1, or compounds from the NIH Clinical Collection at a concentration of 1 µM at 37°C for 1 h. Compounds were removed, and cells were adsorbed with SL15649 eGFP replicon particles at an MOI of 5 IU/cell and incubated at 37°C for 20-24 h. Cells were stained with Hoechst stain to detect nuclei and imaged by automated, high-content fluorescence microscopy. Percent infected cells was determined as ratio of infected cells to total cells. (B) Robust *Z* scores were calculated for individual samples. Shown are the average robust *Z* scores for the antiviral or proviral candidate compounds with robust *Z* scores ≤ -2 or ≥ 2 median absolute deviations from the median of each plate identified in three independent screening experiments. (C) Distribution of candidate compounds by known biological target.

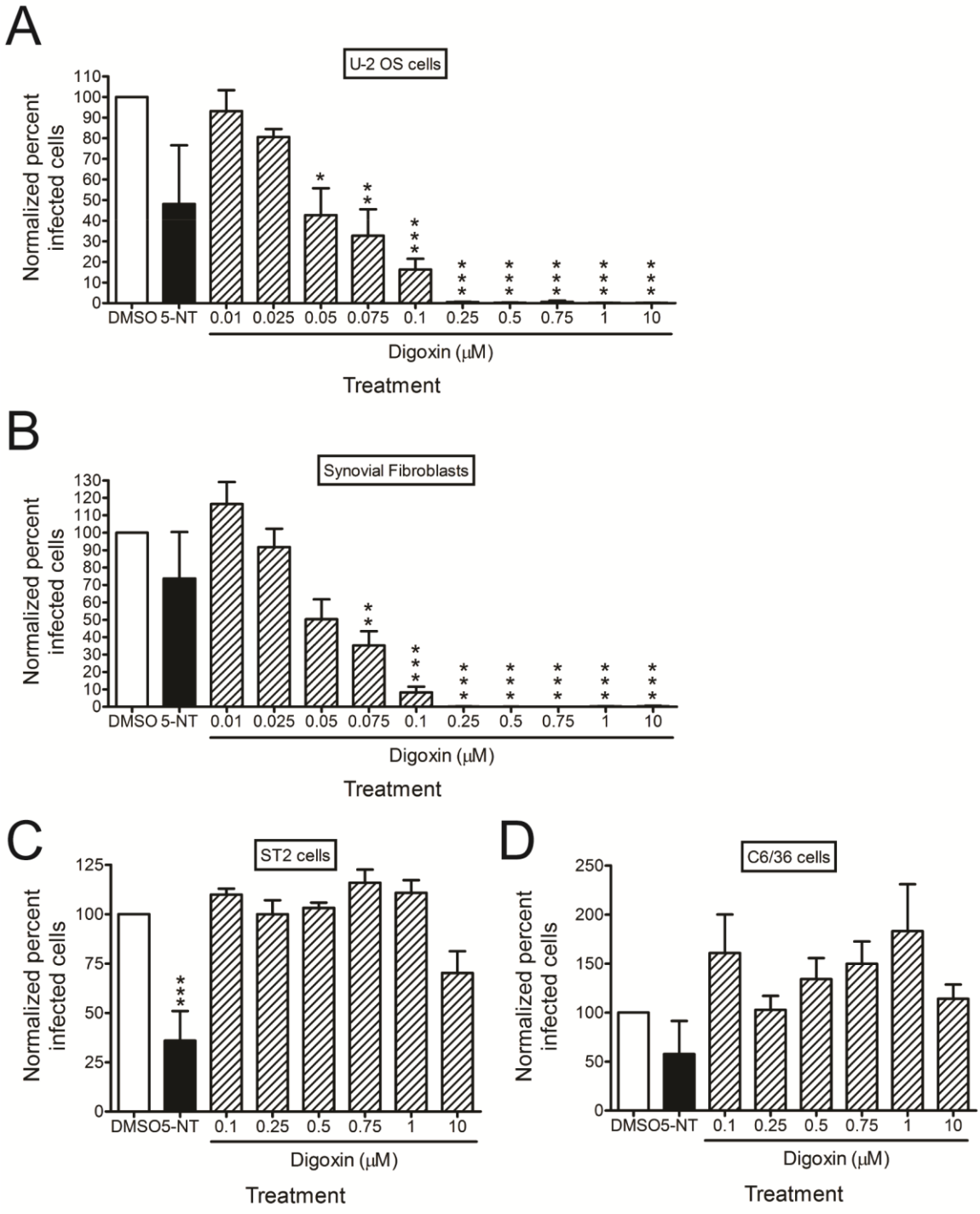
A
U-2 OS cells
Normalized percent infected cells
DMSO 5-NT 0.01 0.025 0.05 0.075 0.1 0.25 0.5 0.75 1 10
Digoxin (μM)
Treatment
B
Synovial Fibroblasts
Normalized percent infected cells
DMSO 5-NT 0.01 0.025 0.05 0.075 0.1 0.25 0.5 0.75 1 10
Digoxin (μM)
Treatment
C
ST2 cells
Normalized percent infected cells
DMSO5-NT 0.1 0.25 0.5 0.75 1 10
Digoxin (μM)
Treatment
D
C6/36 cells
Normalized percent infected cells
DMSO5-NT 0.1 0.25 0.5 0.75 1 10
Digoxin (μM)
Treatment

Figure IV-2. Digoxin potently inhibits CHIKV infectivity in human cells. (A) Human U-2 OS cells, (B) primary human synovial fibroblasts, (C) murine ST2 cells, or (D) mosquito C6/36 cells were incubated with DMSO, 10 µM 5-NT, or increasing concentrations of digoxin for 1 h prior to adsorption with CHIKV strain SL15649 at an MOI of 5 PFU/cell. After 1 h-incubation, virus was removed, and cells were incubated with medium containing the respective concentration of inhibitor for 5 h. Cells were stained with CHIKV-specific antiserum and DAPI to detect nuclei and imaged by fluorescence microscopy. Results are presented as percent infected cells normalized to DMSO-treated cells for triplicate experiments. Error bars indicate standard error of the mean. *, $P < 0.05$, **, $P < 0.01$, ***, $P < 0.001$, as determined by ANOVA followed by Tukey *post hoc* test.

CHIKV inhibition by digoxin is not a result of decreased cell viability. The sodium-potassium ATPase is essential for homeostasis in most multicellular organisms. Therefore, I sought to determine whether inhibition of CHIKV infection by digoxin occurred as a consequence of altered viability of treated cells. To assess the cytotoxic effects of digoxin treatment, cells were stained with either propidium iodide (PI) or PrestoBlue® to assess plasma membrane integrity and mitochondrial metabolic activity, respectively, at 6 h post-treatment with DMSO, STS as an inducer of cell death, or increasing concentrations of digoxin (Figure IV-3). Data presented in Figure IV-3B were generated by Anthony Lentscher during his rotation in the Dermody laboratory. Incubation of U-2 OS cells with digoxin for 6 h did not significantly alter membrane integrity relative to DMSO-treated cells (Figure IV-3A). In keeping with these results, viability of U-2 OS cells was not altered significantly by digoxin treatment at early times post-treatment, as assessed by reduction of the PrestoBlue® substrate (Figure IV-3B). U-2 OS cell viability was only modestly impaired at 24 h following treatment with 1 μM digoxin, a dose 20 times the digoxin EC_{50} for CHIKV antiviral activity in these cells. Digoxin treatment decreased viability of Vero cells at 24 h at all concentrations tested, suggesting that Vero cells are more susceptible to digoxin cytotoxic effects. Although higher concentrations of digoxin induced cytotoxicity at the later times, digoxin effects on CHIKV infection at earlier times were not associated with cytotoxicity. These data suggest that the inhibition of CHIKV by 6 h postinfection is not attributable to cytotoxic effects.

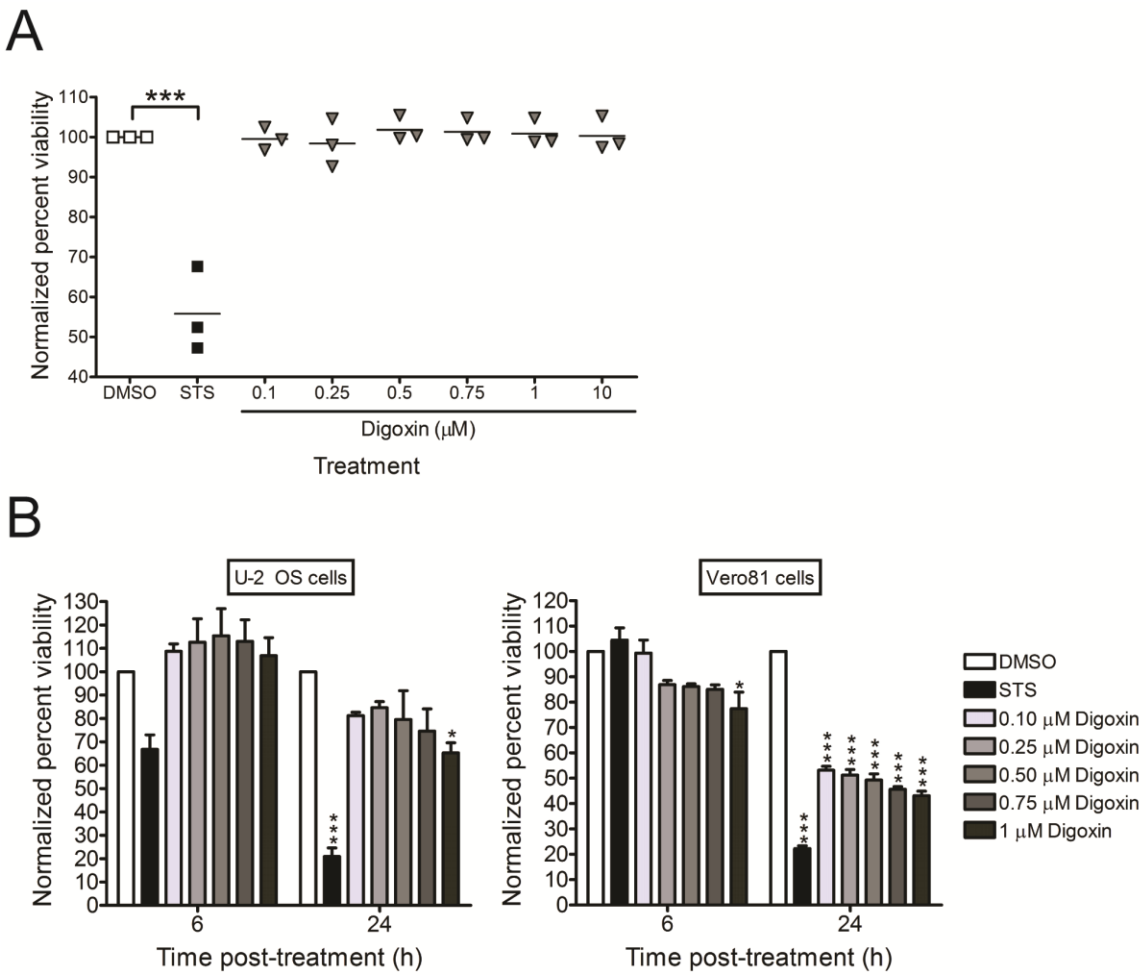

Figure IV-3. CHIKV inhibition by digoxin is not attributable to cytotoxicity. (A) U-2 OS cells were treated with DMSO, 10 μM STS, or increasing concentrations of digoxin for 6 h. Cell viability was quantified by PI staining. Results are expressed as percent viable cells normalized to DMSO-treated cells for individual experiments. Horizontal black lines indicate mean percent viability. (B) U-2 OS cells or Vero cells were treated with DMSO, 10 μM STS, or increasing concentrations of digoxin for 6 or 24 h. Cell viability was quantified by PrestoBlue fluorescence assay. Results are presented as percent viable cells normalized to DMSO-treated cells for triplicate experiments. Error bars indicate standard error of the mean. *, $P < 0.05$, ***, $P < 0.001$, as determined by ANOVA followed by Tukey *post hoc* test.

Digoxin treatment inhibits related and unrelated viruses. To determine whether digoxin blocks infection by other strains of CHIKV as well as related alphaviruses, I determined the effect of digoxin treatment on infection by CHIKV strains SL15649 and 181/25, RRV strain T48, and SINV strain TRSB (Figure IV-4). U-2 OS cells were treated with DMSO, 5-NT, or increasing concentrations of digoxin for 1 h prior to adsorption with CHIKV, RRV, or SINV at an MOI of 1, 10, or 5 PFU/cell, respectively, to adjust for infectivity differences in these cells. At 6 h postinfection, cells were scored for infectivity by indirect immunofluorescence. Digoxin treatment significantly diminished infection by all strains tested with EC_{50} values of 108.9 nM for CHIKV strain SL15649, 100.9 nM for CHIKV strain 181/25, 126.5 nM for RRV, and 198.9 nM for SINV.

To determine whether digoxin exhibits inhibitory effects against diverse virus families, I collaborated with Paula Zamora in the Dermody laboratory to assess the capacity of digoxin to inhibit mammalian reovirus, a nonenveloped, double-stranded RNA virus. Paula generated the data presented in Figure IV-4B. Human brain microvascular endothelial cells (HBMECs) were treated with DMSO, 5-NT, or digoxin prior to adsorption with reovirus virions (left) or infectious subvirion particles (ISVPs) (right). ISVPs are reovirus disassembly intermediates formed following endocytosis and cleavage of the viral outer capsid by intracellular cathepsins or *in vitro* following protease treatment. ISVPs bind to cell-surface receptors and internalize at the plasma membrane, bypassing the disassembly requirements of virions, including acidic pH and protease activity. At 20 h postinfection with either reovirus virions or ISVPs, cells were scored for infection by indirect immunofluorescence. Treatment with digoxin impaired infection by

both virions and ISVPs, indicating that digoxin inhibits infection by broad families of viruses. Furthermore, decreased infectivity of ISVPs by digoxin treatment suggests that digoxin inhibits reovirus infection at one or more steps after internalization.

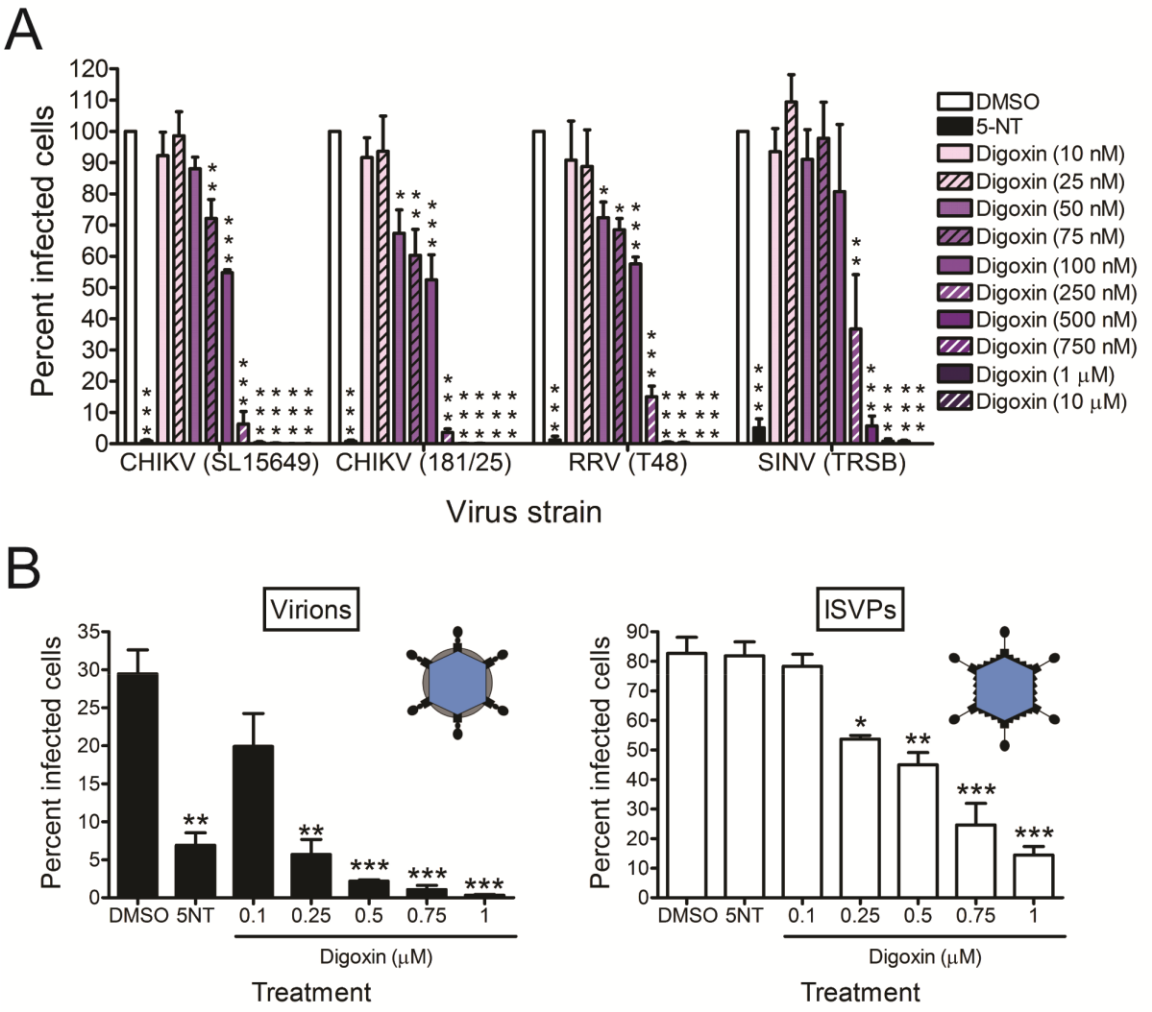

Figure IV-4. Digoxin treatment inhibits multiple alphaviruses and mammalian reovirus. (A) U-2 OS cells were incubated with DMSO, 10 μM 5-NT, or increasing concentrations of digoxin for 1 h prior to adsorption with CHIKV strains SL15649 and 181/25 at an MOI of 1 PFU/cell, RRV strain T48 at an MOI of 10 PFU/cell, or SINV strain TRSB at an MOI of 5 PFU/cell. After 1 h-incubation, virus was removed, and cells were incubated with medium containing the respective concentration of inhibitor for 5 h. Cells were stained with virus-specific antiserum and DAPI to detect nuclei and imaged by fluorescence microscopy. Results are presented as percent infected cells normalized to DMSO-treated cells for triplicate experiments. Error bars indicate standard error of the mean. (B) HBMECs were incubated with DMSO, 10 μM 5-NT, or increasing concentrations of digoxin for 1 h prior to adsorption with reovirus virions (left) or ISVPs (right) at an MOI of 1500 particles/cell. After 1 h-incubation, virus was removed, and cells were incubated with medium containing the respective concentration of inhibitor for 20 h. Cells were scored for infection by indirect immunofluorescence. Results are presented as percent infected cells for duplicate experiments. *, $P < 0.05$, **, $P < 0.01$, ***, $P < 0.001$, as determined by ANOVA followed by Tukey *post hoc* test.

Digoxin impairs CHIKV infection at entry and post-entry steps. I next sought to define the steps in CHIKV replication blocked by digoxin. To determine the timing of digoxin-mediated inhibition of CHIKV infection, U-2 OS cells were treated with DMSO or 1 μM digoxin at 15-min intervals for 1 h prior to adsorption or at 15- or 60-min intervals for 4 h after adsorption (Figure IV-5A). As a control for inhibition of CHIKV entry, 20 mM NH_4Cl was added at the same intervals to block acidification of endocytic compartments. Cells were fixed at 6 h postinfection and scored for infection by indirect immunofluorescence. Maximal impairment of CHIKV infection by digoxin was achieved when added 60 min prior to adsorption. The magnitude of inhibition gradually decreased when drug was added at later times, with only negligible effects observed when it was added 120 min post-adsorption. CHIKV bypassed digoxin inhibition with similar kinetics to bypass of NH_4Cl inhibition, suggesting that digoxin restricts CHIKV infection at early steps in the replication cycle.

If digoxin acts to block CHIKV infection by inhibiting viral entry steps (attachment, internalization, and membrane fusion), then electroporation of digoxin-treated cells with infectious RNA should bypass the inhibition. To test whether RNA electroporation allows CHIKV to replicate in the presence of digoxin, cells were treated with DMSO, 5-NT, or digoxin for 1 h prior to adsorption with CHIKV strain SL15649 (Figure IV-5B) or electroporation with *in vitro*-generated SL15649 RNA (Figure IV-5C). Infected or electroporated cells were cultured in either complete medium (Figure IV-5B and C, left) or in medium containing inhibitor (Figure IV-5B and C, right). Viral titers in supernatants were determined at 6-h intervals after adsorption or electroporation. Pretreatment of cells with digoxin followed by drug washout had no effect on production

of progeny virus (Figure IV-5B, left). However, treatment of cells with 100 nM digoxin before and after adsorption with CHIKV significantly diminished virus production from electroporated cells (Figure IV-5B, right). In contrast to infected cells, pretreatment of cells with either 10 nM or 100 nM digoxin prior to electroporation significantly impaired virus production, as did digoxin treatment before and after electroporation. Remarkably, no virus was detected in supernatants of cells treated with 100 nM digoxin before and after electroporation. These data indicate that electroporation of CHIKV RNA does not bypass digoxin-mediated inhibition and suggest that CHIKV is more sensitive to digoxin at a post-entry step of the replication cycle.

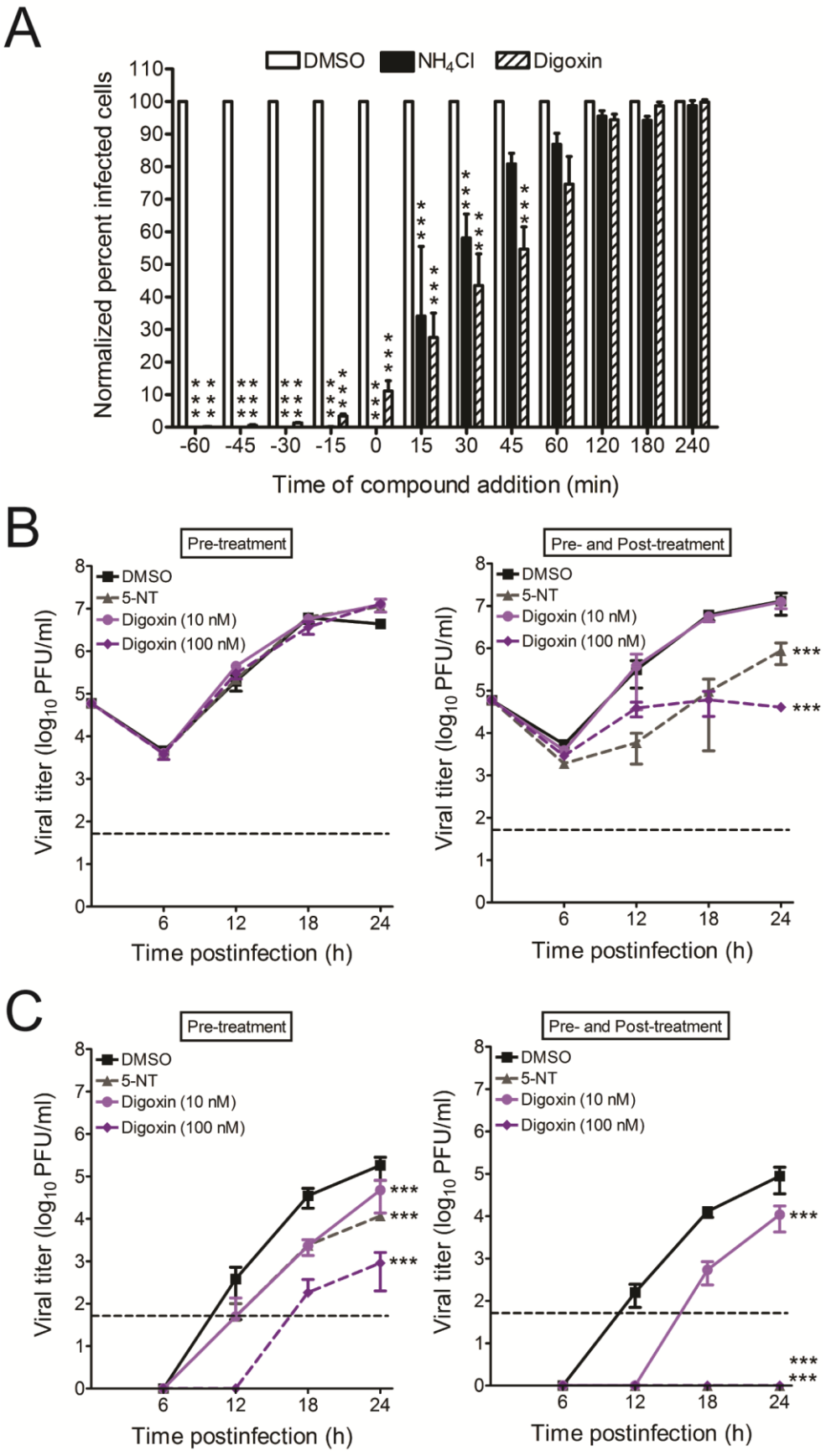
A
DMSO
NH4Cl
Digoxin
Normalized percent infected cells
Time of compound addition (min)
B
Pre-treatment
Pre- and Post-treatment
DMSO
5-NT
Digoxin (10 nM)
Digoxin (100 nM)
Viral titer (log10 PFU/ml)
Time postinfection (h)
C
Pre-treatment
Pre- and Post-treatment
DMSO
5-NT
Digoxin (10 nM)
Digoxin (100 nM)
Viral titer (log10 PFU/ml)
Time postinfection (h)

Figure IV-5. Digoxin inhibits CHIKV at entry and post-entry steps of the replication cycle. (A) U-2 OS cells were incubated with DMSO, 20 mM NH_4Cl, or 1 µM digoxin prior to (-60 to -15), during (0 to +45), or after (+60 to +240) adsorption (in min). Cells were adsorbed with CHIKV 181/25 at an MOI of 5 PFU/cell for 1 h and incubated in the presence or absence of inhibitors for 5 h. Cells were scored for infection by indirect immunofluorescence. Results are presented as percent infected cells normalized to DMSO-treated cells for duplicate experiments. Error bars indicate standard error of the mean. (B and C) U-2 OS cells pretreated with DMSO, 10 µM 5-NT, 10 nM or 100 nM digoxin were either (B) adsorbed with SL15649 virus at an MOI of 0.01 PFU/cell for 30 min or (C) electroporated with SL15649 RNA generated in vitro. Cells were incubated in complete medium (B and C, left) or medium containing DMSO or inhibitor (B and C, right). At the times shown, viral titers in culture supernatants were determined by plaque assay using Vero cells. Results are presented as the mean viral titers for triplicate samples. Error bars indicate standard deviation. Dashed lines indicate the limit of detection. ***, $P < 0.001$, as determined by ANOVA followed by Tukey *post hoc* test.

Species-specific inhibition by digoxin occurs via the sodium-potassium ATPase. Blockade of the sodium-potassium ATPase by cardiac glycosides is less effective in murine cells relative to human cells (121-123), which is attributable to polymorphisms in the sodium-potassium ATPase catalytic α subunit. The murine α1 isoform displays decreased sensitivity to cardiac glycoside treatment relative to the human α1 isoform. Additionally, human and murine α3 isoforms, which are sensitive to cardiac glycoside treatment, can be differentially expressed and might contribute to differences in digoxin sensitivity. Given the species-specific differences in sodium potassium ATPase subunits, I hypothesized that the species-specific antiviral activity mediated by digoxin occurs via polymorphisms in the sodium-potassium ATPase.

To determine whether blockade of the sodium-potassium ATPase specifically mediates CHIKV inhibition, U-2 OS cells were treated with increasing concentrations of digoxin or ouabain, a related cardiac glycoside, for 1 h prior to adsorption with CHIKV at an MOI of 5 PFU/cell. At 6 h postinfection, cells were scored for infectivity by indirect immunofluorescence (Figure IV-6). Similar to digoxin treatment, treatment of cells with ouabain resulted in a dose-dependent decrease in CHIKV infection. Ouabain treatment resulted in 50% reduction of CHIKV infection at a concentration that was 2.5-fold less than the concentration of digoxin required for the same reduction. These data suggest that antagonism of the sodium-potassium ATPase by independent compounds restricts CHIKV infection.

To determine whether higher doses of digoxin are capable of inhibiting CHIKV infection of murine cells, ST2 and C2C12 cells were treated with DMSO, 5-NT, or increasing concentrations of digoxin for 1 h prior to adsorption with CHIKV at an MOI

of 5 PFU/cell. At 6 h postinfection, cells were scored for infectivity by indirect immunofluorescence (Figure IV-7A). At higher concentrations, digoxin treatment significantly diminished infection with EC_{50} values of 16.2 μM in ST2 cells and 23.2 μM in C2C12 cells, values 330 to 475 times the EC_{50} of digoxin in U-2 OS cells. These data indicate that digoxin can inhibit CHIKV infection of murine cells, but significantly higher concentrations are required to produce an inhibitory effect.

I next assessed whether levels of the α1 and α3 ATPase subunits differ in human and murine cells. ATP1A1 (α1) and ATP1A3 (α3) RNA was isolated from mock-infected and CHIKV-infected U-2 OS and ST2 cells, used as a template for cDNA synthesis, and subjected to PCR amplification of the ATP1A1, ATP1A3, and GAPDH as a control (Figure IV-7B). Expression of ATP1A1 was detected in both U-2 OS and ST2 cells and did not differ significantly following infection. In contrast, the ATP1A3 transcript was detected in U-2 OS cells but not in ST2 cells. PCR with two additional primer sets specific for murine ATP1A3 produced similar results, while all primers allowed amplification when a murine ATP1A3 cDNA construct was used as template (data not shown). Although the ATP1A3 transcript was detected in U-2 OS cells, transcript levels were increased in CHIKV-infected cells. Thus, decreased expression of ATP1A3 in murine cells correlates with reduced sensitivity to digoxin-mediated inhibition of CHIKV. In addition, these findings suggest that expression of sodium-potassium ATPase subunits is modulated during CHIKV infection.

To test directly whether the α subunits influence digoxin inhibition of CHIKV, human and murine isoforms of the α1 and α3 subunits were overexpressed in U-2 OS cells. Transfected cells were treated with DMSO or increasing concentrations of digoxin

prior to adsorption with CHIKV, and cells were scored for infectivity by indirect immunofluorescence (Figure IV-7D). Treatment of cells with 50 nM digoxin decreased CHIKV infectivity to a similar extent in cells transfected with the human or murine constructs. However, treatment with higher concentrations of digoxin resulted in greater impairment of CHIKV infection in cells transfected with human ATP1A1, ATP1A3, and murine ATP1A3. Following treatment with 100 nM digoxin, cells transfected with murine ATP1A1 displayed similar impairment of CHIKV infection to that observed for mock-transfected cells. Interestingly, CHIKV infection was least impaired following treatment with 250 nM digoxin in cells transfected with murine ATP1A1. These data indicate that overexpression of the human or murine α3 isoforms or the human α1 isoform of the sodium-potassium ATPase enhance sensitivity to digoxin-mediated effects. Furthermore, these results suggest that the murine α1 isoform is refractory to digoxin inhibition and limits antiviral activity of digoxin in murine cells. Collectively, these findings pinpoint antagonism of the sodium-potassium ATPase as the mechanism of digoxin-mediated inhibition of CHIKV infection.

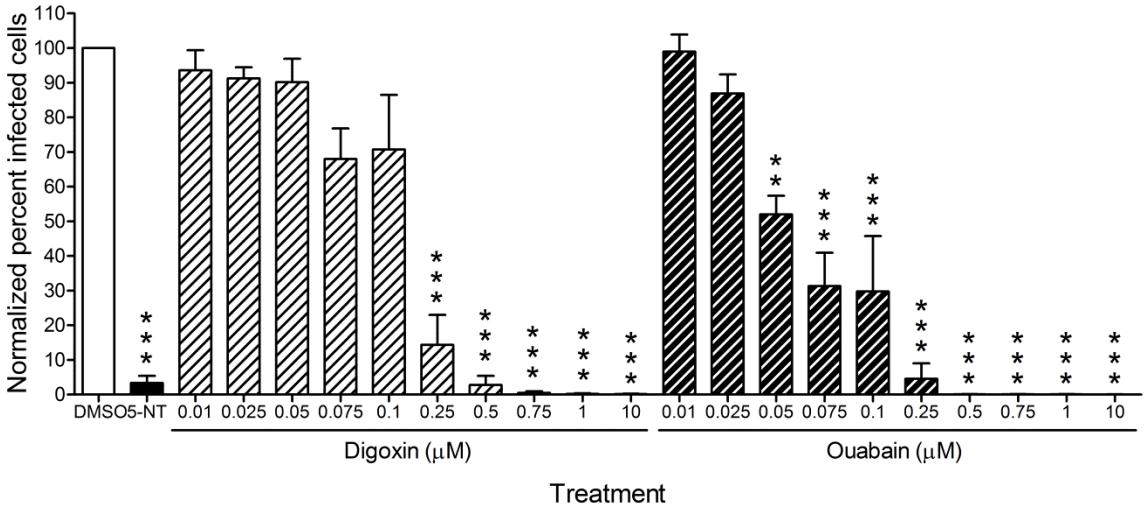

Figure IV-6. Inhibition by digoxin occurs via the sodium-potassium ATPase. U-2 OS cells were incubated with DMSO, 10 μM 5-NT, or increasing concentrations of digoxin or the related cardiac glycoside, ouabain, for 1 h prior to adsorption with CHIKV SL15649 at an MOI of 5 PFU/cell. After 1 h, virus was removed, and cells were incubated with medium containing the concentration of inhibitor shown for 5 h. Cells were scored for infection by indirect immunofluorescence. Results are presented as percent infected cells normalized to DMSO-treated cells for triplicate experiments. Error bars indicate standard error of the mean. ***, $P < 0.001$, as determined by ANOVA followed by Tukey *post hoc* test.

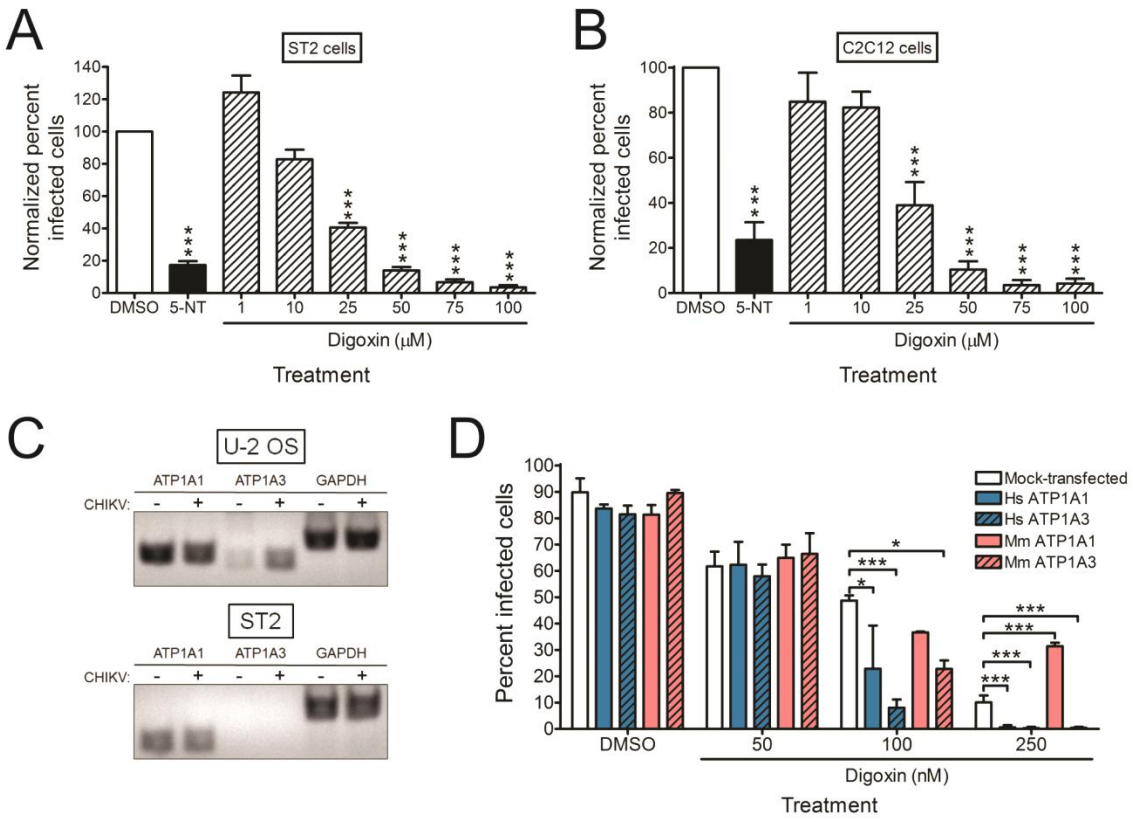

Figure IV-7. Reduced digoxin sensitivity of CHIKV in murine cells is mediated by the alpha subunits of the sodium-potassium ATPase. (A) ST2 cells or (B) C2C12 cells were incubated with DMSO, 10 μM 5-NT, or increasing concentrations of digoxin for 1 h prior to adsorption with CHIKV strain SL15649 at an MOI of 5 PFU/cell. After 1 h, virus was removed, and cells were incubated with medium containing the concentration of inhibitor shown for 5 h. Cells were stained with CHIKV-specific antiserum and DAPI to detect nuclei and imaged by fluorescence microscopy. Results are presented as percent infected cells normalized to DMSO-treated cells for triplicate experiments. Error bars indicate standard error of the mean. (C) RNA was isolated from U-2 OS cells (top) and ST2 cells (bottom) and used for generation of cDNA and amplification of ATP1A1, ATP1A3, and GAPDH transcript. (D) U-2 OS cells were transfected with human (Hs) or mouse (Mm) ATP1A1 or ATP1A3 24 h prior to adsorption with CHIKV strain 181/25 at an MOI of 5 PFU/cell. After 1 h, virus was removed, and cells were incubated with medium containing DMSO or the concentration of inhibitor shown for 5 h. Cells were stained with CHIKV-specific antiserum and DAPI to detect nuclei and imaged by fluorescence microscopy. Results are presented as percent infected cells for triplicate samples. Error bars indicate standard deviation. *, $P < 0.05$, ***, $P < 0.001$, as determined by ANOVA followed by Tukey *post hoc* test.

Digoxin-resistant CHIKV populations encode mutations in the nonstructural proteins. To enhance understanding of mechanisms by which digoxin restricts CHIKV infection, I passaged CHIKV strains SL15649 and 181/25 in cells treated with either DMSO or digoxin to select digoxin-resistant viruses. U-2 OS cells were adsorbed with either SL15649 or 181/25 at an MOI of 0.01 PFU/cell for 1 h. Virus was removed, and cells were incubated with medium containing either DMSO or 100 nM digoxin until comparable CPE was observed. Supernatants from infected cells were used to inoculate fresh cells, and the process was repeated with increasing concentrations of digoxin until CPE was observed with doses 5 times the EC_{50} value in U-2 OS cells. Interestingly, digoxin resistance was only observed with passage of virulent strain SL15649 and not with passage of attenuated strain 181/25. To test whether supernatants of digoxin-treated cells contained drug-resistant viruses, U-2 OS cells were pretreated with DMSO, 10 μM 5-NT, or increasing concentrations of digoxin prior to adsorption with Passage x14 supernatants from DMSO- and digoxin-treated cells. Infected cells were scored for infection by indirect immunofluorescence at 6 h postinfection (Figure IV-9). Treatment of cells with 5-NT prevented infection by both $SL15649_{DMSO}$ and $SL15649_{Digoxin}$ supernatant stocks. However, significantly higher levels of digoxin were required to inhibit infection by $SL15649_{Digoxin}$ compared to $SL15649_{DMSO}$. Treatment of cells with 500 nM digoxin completely inhibited infection by $SL15649_{DMSO}$, but this dose only resulted in approximately 50% inhibition of infection by $SL15469_{Digoxin}$. These data suggest that virus populations present in supernatants of digoxin-treated cells are resistant to inhibition by digoxin.

To determine the genetic basis for digoxin resistance, I determined the full-length nucleotide sequences of virus stocks prepared from the DMSO or digoxin passage series (Table IV-1). Sequence analysis identified 12 nonsynonymous mutations in the virus population of supernatants from digoxin-treated cells. The majority of these polymorphisms (11 of 12) were in the nonstructural cassette and 7 were in nsP3. Two amino acid polymorphisms in nsP2 (P16L and G641A) and in nsP3 (A137V and Stop524C) and 1 polymorphism in E2 (S159R) were identified in multiple virus clones sequenced from digoxin-treated cell supernatants. In addition, several of the mutations resulted in a charge change. These findings indicate that multiple mutations are selected during passage of virus in digoxin-treated cells. Furthermore the selection of mutations in nonstructural and structural proteins provides additional evidence for multiple mechanisms of CHIKV inhibition by digoxin.

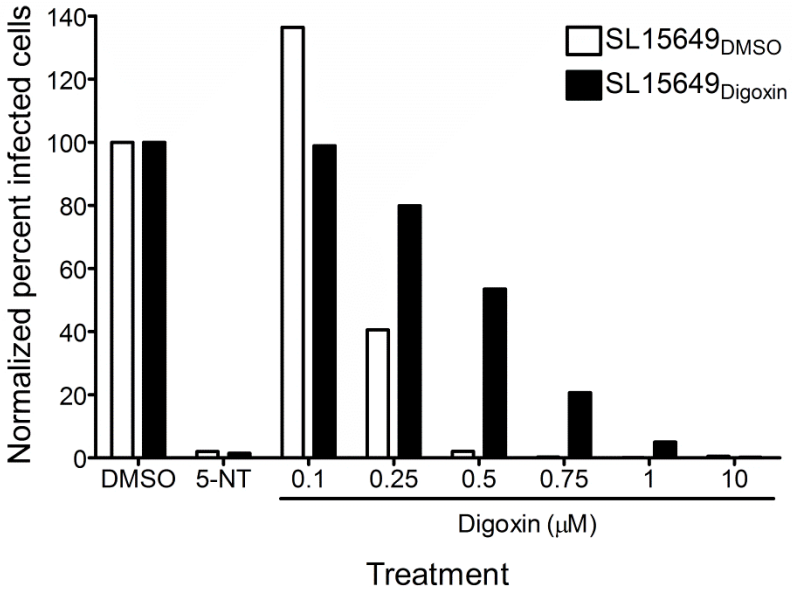

Figure IV-8. Passage of CHIKV in presence of digoxin selects for drug-resistant viruses. U-2 OS cells were incubated with DMSO, 10 μM 5-NT, or increasing concentrations of digoxin for 1 h prior to adsorption with CHIKV strains that had been passaged 14 times in the presence of either DMSO ($SL15649_{DMSO}$) or digoxin ($SL15649_{Digoxin}$) at an MOI of 5 PFU/cell. After 1 h, virus was removed, and cells were incubated with medium containing the concentration of digoxin shown for 5 h. Cells were stained with CHIKV-specific antiserum and DAPI to detect nuclei and imaged by fluorescence microscopy. Results are presented as percent infected cells normalized to DMSO-treated cells.

Table IV-1. Nonsynonymous mutations selected during passage of CHIKV in digoxin-treated cells.

Viral gene	Polymorphism	Number of clones encoding mutation
nsP2	P16L	4/4
	D509N	1/4
	G641A	2/2
nsP3	A137V	3/4
	T412A	1/1
	P435L	1/4
	P463L	1/4
	D486N	1/4
	Stop524C	2/4
	Stop524_L525del	1/4
nsP4	R63K	1/4
E2	S159R	2/2

Discussion

CHIKV has reemerged to cause epidemics of arthritis throughout Africa, South and Southeast Asia, and the Caribbean. The rapid, mosquito-borne transmission of CHIKV has resulted in millions of cases of CHIKV disease in the last decade alone. The high attack rate and global significance of CHIKV infection warrant the development of CHIKV-specific therapeutics and vaccines. Thus far, no therapeutic or prophylactic therapies are available.

To enhance an understanding of the host factors required for CHIKV infection, we screened a library of chemical compounds for the capacity to diminish or enhance CHIKV infection in U-2 OS cells. I identified digoxin, a cardiac glycoside, as a potent inhibitor of CHIKV infection and replication. I demonstrate that digoxin impedes CHIKV infection at both entry and post-entry steps of the replication cycle via antagonism of the sodium-potassium ATPase. Digoxin treatment also inhibited infection by other alphaviruses, including RRV and SINV, and mammalian reovirus. Furthermore, passage of CHIKV in digoxin-treated cells selected for several mutations across the genome, particularly in the nonstructural proteins, nsP2 and nsP3. Taken together, these findings indicate that a functional sodium-potassium ATPase is required for CHIKV infection. Furthermore, antagonism of the sodium-potassium ATPase highlights a new strategy for development of therapeutics to limit CHIKV replication and disease.

The sodium-potassium ATPase is the only known target of cardiac glycosides and, therefore, inhibition of CHIKV likely occurs via antagonism of this ion exchanger. In support of this hypothesis, CHIKV infection also is inhibited by ouabain, a related cardiac glycoside. In addition, sensitivity to cardiac glycoside treatment is species-

specific (121-123), which parallels species-specific differences in susceptibility of CHIKV-mediated inhibition observed in this study. Cardiac glycoside sensitivity is dictated by isoforms of the α subunit (122, 123). The murine α1 isoform is more resistant to cardiac glycoside treatment compared with the human α1 isoform. In the murine cells tested here, higher levels of the α1 isoform were detected relative to the α3 isoform. Overexpression of an α3 isoform (human or mouse) conferred sensitivity to digoxin-treatment (Figure IV-7B and C), as noted previously. Digoxin also did not inhibit CHIKV infection in mosquito cells, likely on the basis of the absence of the sodium-potassium ATPase in these cells. These data indicate that direct and specific blockade of the sodium-potassium ATPase by digoxin impairs CHIKV infection.

Inhibition of the sodium-potassium ATPase disrupts ion transport and alters many cellular biosynthetic, signaling, and vesicular sorting pathways (124). However, the precise alterations that restrict CHIKV infection are not known. The sodium-potassium ATPase is an antiporter-like enzyme that mediates efflux of 3 sodium ions and influx of 2 potassium ions in a single transport cycle. This ion movement functions to maintain cellular resting potential and volume and influences other transporters and signal-transduction pathways. Inhibition of the ATPase increases levels of intracellular sodium, which triggers influx of calcium to allow sodium efflux by the sodium-calcium exchanger, which is responsible for the inotropic effects of digoxin treatment (125). Cardiac glycoside treatment also triggers interactions between the sodium-potassium ATPase and the inositol 1,4,5-trisphosphate receptor (Ins[1,4,5]P_3R) to elicit calcium oscillations and nuclear transcription factor κB (NFκB) transcriptional activation (126, 127).

During viral infection, activation of pattern recognition receptors (PRRs) ultimately leads to NF-κB transcriptional activation (128). However, NF-κB activation is inhibited following CHIKV infection by the induction of miR-146a expression (129). Evasion of NF-κB activation suggests that CHIKV replication is susceptible to NF-κB-dependent restriction if a sufficiently high threshold is reached (i.e., following digoxin treatment). Excess intracellular calcium also contributes to osmotic stress and the induction of apoptotic and necrotic cell death (130). Cardiac glycosides also reduce endosomal pH (131, 132). Optimal fusion of CHIKV with endosomal membranes occurs at a pH of 5.3 (133). However, it is not clear whether a lower pH impedes CHIKV infection. A strongly acidic intracellular environment may induce conformational changes in the E1 or E2 glycoproteins on the virion surface to prevent or prematurely trigger fusion at sites incompatible with productive infection.

I envision two possible mechanisms underlying digoxin-mediated inhibition of CHIKV infection. One possibility is that increased endosomal acidification might destabilize CHIKV glycoproteins and prevent efficient fusion. It is probable that CHIKV requires a particular ion composition for discrete steps of the viral replication cycle, perhaps for coordinating the functions of specific viral proteins. A second possibility is that digoxin may induce stress responses in the cell that induce an antiviral state to prevent CHIKV replication. Digoxin appears to inhibit CHIKV entry and post-entry steps in replication. Treatment of cells with digoxin maximally inhibited CHIKV when added 60 min prior to infection, whereas addition of drug 60 min after CHIKV adsorption had no effect (Figure IV-5A). The temporal window in which digoxin inhibition occurs mirrored that of ammonium chloride, which further supports the hypothesis that digoxin

blocks CHIKV entry. Digoxin treatment does not inhibit viral attachment to cells (data not shown) but instead appears to block internalization, fusion, or release of the viral genome into the cytoplasm. However, electroporation of viral RNA to bypass the digoxin-mediated entry defect was not sufficient to restore viral replication to levels in untreated cells (Figure IV-5C). In an analogous case, proteolytic cleavage of reovirus virions to form ISVPs *in vitro* was sufficient to overcome restriction by the entry inhibitor, 5-NT, but ISVPs failed to produce yields in treated cells comparable to those in untreated cells. ISVPs are thought to enter cells at the plasma membrane and, thus, are not susceptible to inhibition by compounds that inhibit reovirus internalization or disassembly (134-136). Other evidence suggests that ISVPs are internalized via endocytosis, and penetrate into the cytoplasm from a very early endocytic vesicle (137). Ouabain treatment prevents conversion of ISVPs to the subsequent disassembly intermediate, termed ISVP*, which is required for delivery of the viral core into the cytoplasm (138). The digoxin-mediated post-entry block to reovirus replication is undefined. Selection of multiple mutations in nonstructural proteins of the CHIKV genome following passage of virus in digoxin-treated cells also points to inhibition of post-entry steps of the replication cycle.

The complexity of cardiac glycoside-mediated effects on cells likely explains the capacity of digoxin to inhibit CHIKV at multiple steps in the replication cycle. In addition, inhibition of CHIKV by more than one mechanism would make it difficult to select digoxin-resistant mutants. Indeed, passage of CHIKV in digoxin-treated cells led to development of drug resistance only after approximately 14, 72-h passages, suggesting that inhibition of the sodium-potassium ATPase is a favorable candidate for antiviral drug

development. Digoxin is currently FDA-approved for treatment of persons with congestive heart failure and cardiac arrhythmias, but reported side effects of digoxin preclude its widespread clinical use (139-141). Derivatives of digoxin are effective in inhibition of T_H17 cell differentiation in the treatment of autoimmune diseases with reduced toxicity (142). The capacity of ouabain to inhibit CHIKV infection suggests that these analogous compounds also would diminish CHIKV infection in a similar manner.

Identification of CHIKV-specific therapies requires an improved understanding of CHIKV biology and pathogenesis. Findings presented in this chapter elucidate functions of the sodium-potassium ATPase in CHIKV infection. Antagonism of this ion transporter with digoxin inhibited CHIKV infection of human cells and mice. Digoxin inhibited multiple steps of the CHIKV replication cycle as evidenced by time-of-addition and electroporation-bypass experiments. Further studies to delineate mechanisms by which blockade of the sodium-potassium ATPase impedes CHIKV infection will illuminate host factors and pathways required for CHIKV infection. Such factors may serve as additional drug targets.

CHAPTER V

COMPONENTS OF THE IMMUNOPROTEASOME ALTER CHIKV INFECTION

Introduction

Host factors are essential for viral infection and serve critical functions in disease pathogenesis. The host immune response to CHIKV infection contributes to CHIKV-induced tissue injury (61, 143-146). However, little is known about the specific host factors that act during CHIKV infection to impede viral replication. RNAi screens offer an unbiased approach to identify cellular factors that promote or antagonize the replication of several pathogenic viruses including DENV, HCV, HIV, and WNV (147-150) as well as the related alphavirus SINV (151). Identifying host determinants that regulate CHIKV infection may reveal new targets for antiviral therapeutics. As these targets may be host-specific molecules, they would be impervious to the rapid mutation of viral genomes that often leads to treatment failure.

Using high-throughput, RNA interference (RNAi) screening, 18,055 genes of the human genome were screened for the capacity to restrict infection by GFP-expressing CHIKV replicon particles. Silencing of 36 genes resulted in a significant increase in CHIKV infectivity in 3 of 3 biological replicates. Additionally, silencing of 174 genes resulted in a significant increase in GFP-intensity, a correlate of virus replication efficiency, in all replicates. Of the genes that enhanced CHIKV infection, a majority were interferon-regulated. Subsequent validation of these ISG candidates identified PSME2, a

component of the immunoproteasome 11S regulatory complex, as a negative regulator of CHIKV infection. Diminished expression of PSME2 resulted in increased infectivity or GFP intensity in all 3 screens with *Z* scores ≥ 2. Silencing of PSME2 also resulted in increased production of viral progeny at early times postinfection. PSME2 knockdown by siRNA transfection was confirmed by RT-PCR and immunoblotting. Furthermore, knockdown of PSME2 by single siRNAs produced similar increases in CHIKV infection. Treatment of cells with epoxomicin, a proteasome-specific inhibitor, also increased CHIKV infectivity, suggesting broader mechanisms of CHIKV restriction by the proteasome. In support of this idea, siRNA knockdown of PSMF1, an inhibitor of the 11S and 19S complexes, significantly decreased CHIKV infection. These data point to a role for the proteasome in regulating CHIKV infection.

Results

Identification of host genes that impede CHIKV infection. Candidate cellular determinants of CHIKV infection in U-2 OS cells were identified using high-throughput RNAi screening. U-2 OS cells were transfected with pools of gene-specific siRNAs from the Dharmacon ON-TARGET Plus library and seeded into wells of 384-well plates. Cells were transfected with siRNAs specific for luciferase as a non-targeting control and the $6V_0C$ subunit of the vacuolar-type H^+-ATPase (V-ATPase) as a positive control for decreased infectivity. Cells were cultured for 48 h to allow for efficient knockdown and then infected with CHIKV strain SL15649 replicon particles expressing eGFP and incubated for 24 h. The percentage of infected cells and average GFP intensity were

determined, and robust *Z* scores were calculated for each siRNA. Targets of siRNAs that resulted in *Z* scores ≥ 2 from three biological replicates of the screen were compared to identify overlapping genes (Figure V-1). Of the 18,055 genes screened, knockdown of 608 genes resulted in a significant decrease in the percentage of CHIKV-infected cells in at least 2 of the 3 screens. Knockdown of 388 genes resulted in a significant decrease in the average GFP intensity of infected cells in at least 2 of 3 screens. In addition, knockdown of 130 and 555 genes resulted in a significant increase in the percentage of infected cells or GFP intensity, respectively, in at least 2 of 3 screens. To identify potential immune regulators and host cell restriction factors of CHIKV, I focused validation experiments on genes under interferon control in which siRNA knockdown increased CHIKV infection. Of the genes that increased CHIKV infectivity or replication in 3 of 3 screens, 71 are regulated by type I or type II interferon (Table V-I). Knockdown of 16 of these 71 interferon-regulated genes resulted in *Z* scores ≥ 2 by both percent infection and GFP intensity. From this subset of genes, I focused validation studies on PSME2, a component of the immunoproteasome 11S regulatory complex.

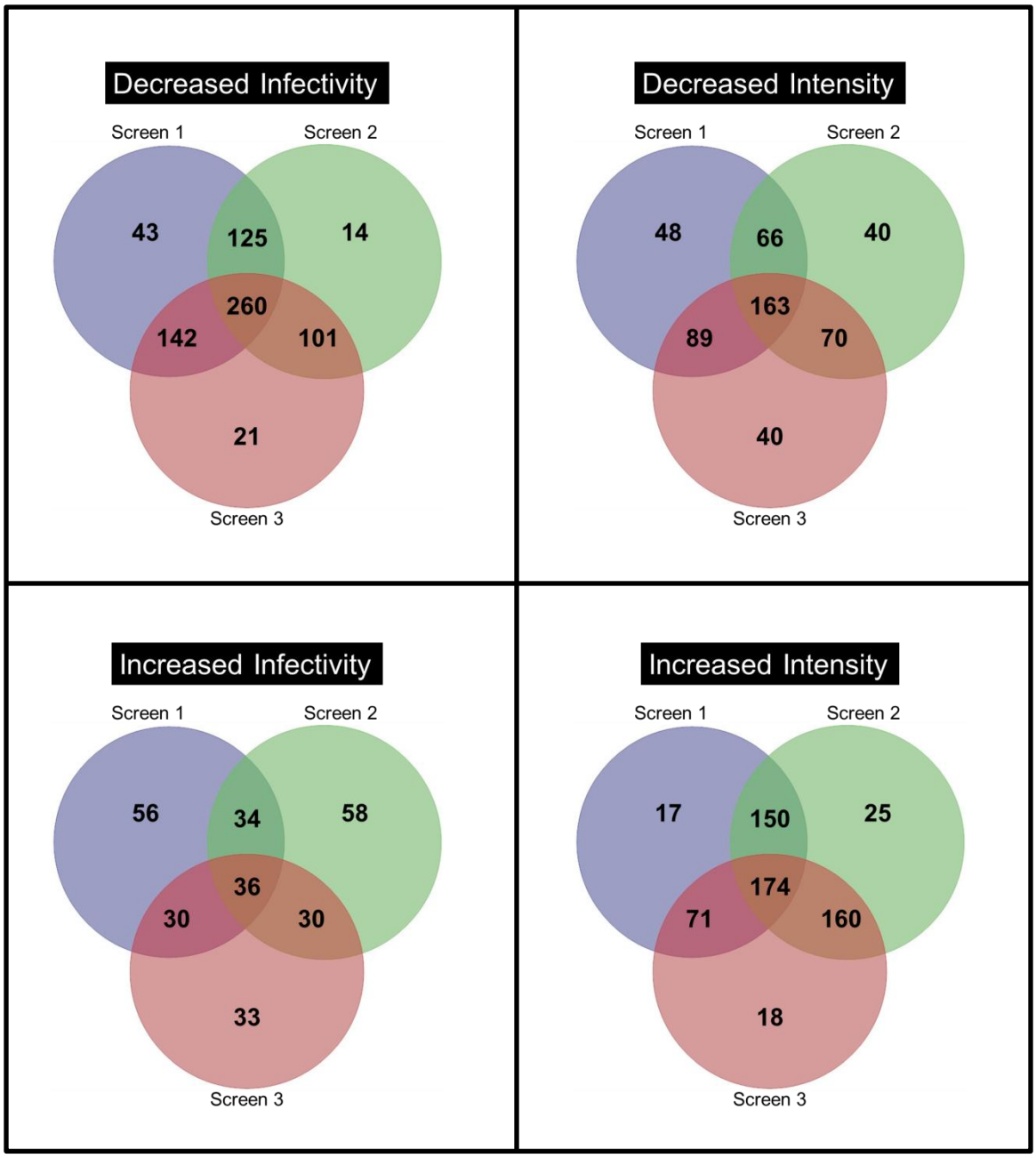

Figure V-1. Number and overlap of gene candidates identified from siRNA screen. Venn diagrams present the number of gene candidates with *Z* scores ≥ 2 or ≤ -2 identified by each screening replicate. Shown are the gene candidates that result in a decrease or increase in the percentage of infected cells or GFP intensity.

Table V-1. *Z* scores for known and predicted interferon-regulated gene candidates identified in 3 of 3 RNAi screen replicates.

Gene Symbol	Entrez Gene ID	NCBI RefSeq	Average *Z* scores (n=3)	
			Infectivity	Intensity
ADORA3	140	NM_020683	**2.12**	**2.15**
AES	166	NM_198970	**2.01**	1.86
ALAD	210	NM_000031	1.23	**2.60**
AMIGO2	347902	NM_181847	**2.09**	1.47
ANLN	54443	NM_018685	1.54	**2.66**
ARHGAP5	394	NM_001173	1.59	**3.44**
ASPA	443	NM_000049	-0.03	**2.25**
AZI1	22994	NM_001009811	0.92	**2.65**
BCL3	602	NM_005178	1.79	**3.55**
BEX2	84707	NM_032621	1.37	**2.56**
BRD2	6046	NM_005104	0.26	**2.41**
CALCRL	10203	NM_005795	0.63	**2.24**
CARD9	64170	NM_052813	1.59	**4.07**
CDH18	1016	NM_004934	**2.33**	1.60
CREB3L3	84699	NM_032607	1.15	**2.59**
CROCC	9696	NM_014675	-0.13	**3.09**
DCT	1638	NM_001922	1.51	**2.66**
DDX42	11325	NM_203499	1.76	**2.45**
DNAJC12	56521	NM_201262	**2.23**	1.18
EFS	10278	NM_032459	0.95	**3.15**
ELF1	1997	NM_172373	**2.50**	**2.74**
ESM1	11082	NM_007036	-0.15	**3.33**
EXOSC9	5393	NM_005033	0.40	**3.08**
FCGR2B	2213	NM_001002273	-0.04	**2.44**
FOXC1	2296	NM_001453	-0.01	**2.43**

GNA12	2768	NM_007353	1.86	**4.24**
GNAI3	2773	NM_006496	**2.26**	**2.78**
GSTK1	373156	NM_015917	**2.28**	**4.43**
GTF2H5	404672	NM_207118	1.84	**3.02**
GUCY1A2	2977	NM_000855	1.55	**2.88**
IL15RA	3601	NM_002189	1.53	**2.74**
IL2RA	3559	NM_000417	1.72	**2.83**
INCENP	3619	NM_020238	**2.86**	**3.18**
LATS1	9113	NM_004690	0.80	**2.67**
LBX2	85474	NM_001009812	1.54	1.10
LIMS3	96626	NM_033514	**2.53**	**2.63**
LTA	4049	NM_000595	**2.19**	1.33
MAP3K5	4217	NM_005923	1.78	**2.31**
MRPL17	63875	NM_022061	1.82	0.73
NAP1L2	4674	NM_021963	1.20	**3.67**
NAT2	10	NM_000015	**2.74**	**3.40**
NCOA7	135112	NM_181782	1.67	1.24
NFAT5	10725	NM_173215	1.40	**3.29**
OPN3	23596	NM_001030011	**2.28**	1.49
PDE7A	5150	NM_002603	0.85	**2.40**
PKIG	11142	NM_007066	**2.44**	**2.93**
POLB	5423	NM_002690	**2.05**	**2.73**
POLR2F	5435	NM_021974	**2.00**	**3.96**
PRICKLE2	166336	NM_198859	**2.06**	**3.03**
PRPS2	5634	NM_002765	1.61	**2.33**
PSME2	5721	NM_002818	**2.18**	**2.90**
RGS18	64407	NM_130782	**2.17**	0.74
RHOV	171177	NM_133639	1.33	**2.76**
RUNX2	860	NM_001015051	1.34	**2.95**

SKI	6497	NM_003036	**2.15**	**3.20**
SLC19A1	6573	NM_194255	1.75	**3.27**
SLC35A3	23443	NM_012243	1.78	**3.30**
SNRP70	6625	NM_003089	0.96	**3.50**
SNURF	8926	NM_022804	1.93	-0.09
SPINT1	6692	NM_001032367	1.33	**2.78**
TARBP1	6894	NM_005646	1.46	**2.74**
TFF3	7033	NM_003226	1.98	**3.16**
TGFBI	7045	NM_000358	**2.13**	1.00
TMEM35	59353	NM_021637	**2.07**	1.95
TOMM7	54543	NM_019059	1.85	1.17
TRIM31	11074	NM_052816	1.30	**3.25**
TUBGCP2	10844	NM_006659	**2.02**	**3.13**
VEGFC	7424	NM_005429	1.76	**2.56**
VIPR1	7433	NM_004624	**2.73**	**3.47**
VPS18	57617	NM_020857	**2.08**	**2.27**
WDFY4	57705	NM_020945	0.84	**3.17**
YARS	8565	NM_003680	1.18	**2.70**

Silencing of PSME2 enhances CHIKV infection. Knockdown of PSME2 in U-2 OS cells resulted in an increase in the percentage of infected cells and in GFP intensity relative to luciferase-transfected cells (Figure V-2A and B). The magnitude of these increases was not as dramatic as the reduction in CHIKV infectivity and GFP intensity observed following knockdown of $6V_0C$ but was similar to increases in infection in previously published reports of virus restriction factors identified using siRNA-based methods (152, 153). To determine whether PSME2 limits the production of infectious virus over multiple rounds of infection, U-2 OS cells were transfected with nonspecific or PSME2-targeting siRNAs and infected with CHIKV strain 181/25 at an MOI of 1 PFU/cell. Viral titers in culture supernatants were determined by plaque assay over a time course (Figure V-2C). Strain 181/25 replicated to higher titers in cells transfected with PSME2-specific siRNAs relative to cells transfected with nonspecific siRNA at early times postinfection. Titers of 181/25 were increased 15-fold by 6 h postinfection following knockdown of PSME2, but this increase did not persist at later time points. These data suggest that silencing of PSME2 enhances CHIKV infection during early rounds of replication, suggesting that PSME2 restriction can be overcome as infection progresses.

To confirm that transfection of PSME2-specific siRNAs results in efficient knockdown, I used RT-PCR and immunoblotting to probe for expression of PSME2 (Figure V-3). Relative to control-transfected cells, little to no PSME2 transcript was detected in cells transfected with PSME2-specific siRNAs, whereas GAPDH transcript levels were unchanged (Figure V-3A). Furthermore, transfection of cells with PSME2-specific siRNA decreased PSME2 protein levels by greater than 95% (Figure V-3B),

suggesting that changes in CHIKV infection correlate with diminished PSME2 expression.

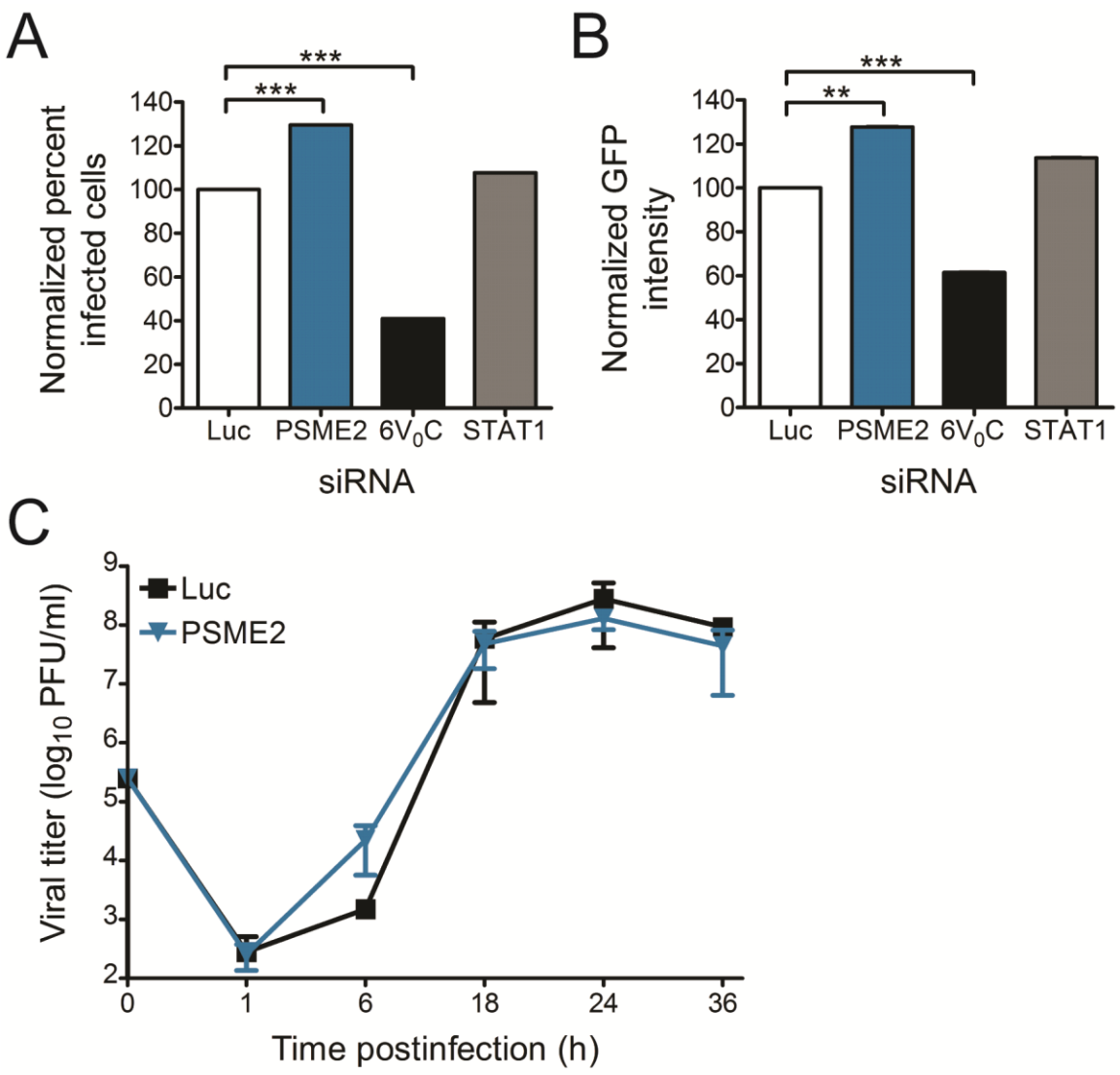

Figure V-2. PSME2 restricts CHIKV infection and replication. U-2 OS cells were transfected with Dharmacon ON-TARGETplus® SMARTpool® siRNAs 48 h prior to infection with CHIKV SL15649 eGFP replicon particles. siRNAs targeting luciferase (Luc), $6V_0C$, and STAT1 were included as nonspecific, positive, and negative controls, respectively. At 24 h postinfection, cells were stained with Hoechst dye to detect nuclei, and GFP-positive cells were quantified by fluorescence microscopy. Results are presented as (A) percent infected cells or (B) GFP intensity normalized to Luc-transfected cells for triplicate experiments. Error bars indicate standard error of the mean, but were not visible. (C) U-2 OS cells were transfected with Luc siRNA or Dharmacon siGENOME® SMARTpool® siRNAs to PSME2 and adsorbed with CHIKV strain 181/25 at an MOI of 1 PFU/cell. At the times shown, viral titers in culture supernatants were determined by plaque assay using BHK-21 cells. Results are presented as the mean viral titers for triplicate samples. Error bars indicate standard deviation. **, $P < 0.01$, ***, $P < 0.001$, as determined by ANOVA followed by Tukey *post hoc* test.

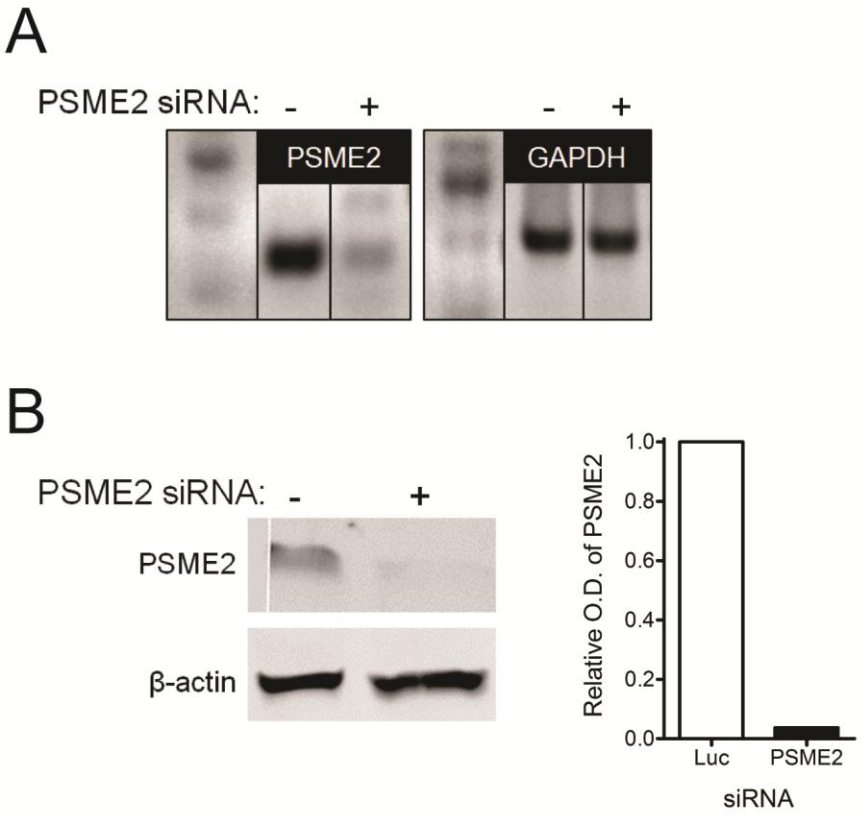

Figure V-3. Expression and siRNA knockdown of PSME2. (A) U-2 OS cells were transfected with nonspecific (-) or siRNA pools targeting PSME2 (+) and incubated for 48 h. RNA from transfected cells was isolated and used for generation of cDNA and amplification of PSME2 or GAPDH transcript by RT-PCR. (B) Cell lysates of transfected cells were resolved by SDS-PAGE and immunoblotted using antibodies to detect PSME2 or β-actin as a loading control (left). Relative PSME2 protein expression was quantified by optical densitometry using ImageJ (right).

Enhancement of CHIKV infection correlates with degree of PSME2 knockdown. Although transfection of a pool of PSME2-specific siRNAs resulted in significant depletion of PSME2 transcript and protein, siRNAs can mediate off-target effects if seed sequences are similar or identical at other loci in the genome. Therefore, I next sought to assess effects of PSME2 knockdown on CHIKV infection and transcript levels using individual siRNAs that target different regions of the PSME2 gene (Figure V-4). U-2 OS cells and HBMECs were transfected with either control siRNAs or individual siRNAs specific for PSME2. Transfected cells were adsorbed with SL15649 replicon particles (U-2 OS cells) or strain 181/25 (HBMECs) and assessed for infection by indirect immunofluorescence (Figure V-4A and B) or subjected to RT-PCR to assess expression of PSME2 (Figure V-4C and D). Transfection of both U-2 OS cells and HBMECs with pooled siRNAs specific for PSME2 resulted in a significant increase in the percentage of infected cells relative to cells transfected with nonspecific siRNA. Once again, transfection of pooled siRNAs specific for PSME2 resulted in decreased PSME2 expression in U-2 OS cells. This finding also was observed in HBMECs, albeit to a lesser extent. In U-2 OS cells, transfection of three of the individual siRNAs (Singles 2-4) resulted in a significant increase in the percentage of infected cells, with the level of the increase corresponding to the extent of PSME2 knockdown. Of these individual siRNAs, transfection of one (Single 2) also significantly enhanced CHIKV infection in HBMECs. Transfection of one of the individual siRNAs (Single 1) produced the opposite phenotype, significantly diminishing infection in both cell types tested. Although this individual siRNA reduced PSME2 expression levels, additional off-target effects likely contribute to the decrease in CHIKV infection observed in these cells. These data suggest

that the enhancement of CHIKV infection mediated by siRNA knockdown of PSME2 are not due to off-target effects and demonstrate a role for PSME2 in multiple cell types.

Proteasome inhibition enhances infectivity of CHIKV. The 26S proteasome is composed of a 20S core and a 19S regulator and functions to degrade proteins and peptides within the cell (154). However during infection or oxidative stress, the constitutive proteasome is modified by replacement of the 19S regulator with the 11S regulator to form the immunoproteasome (155). The immunoproteasome functions in the degradation small peptides and processing of antigen for MHC Class I presentation (155, 156). Because PSME2 encodes one of the three subunits that form the 11S regulator, I reasoned that PSME2 might restrict CHIKV infection through its role in modulating the proteasome. To test this hypothesis, I used the compound epoxomicin to selectively inhibit the 20S proteasome. U-2 OS cells were pretreated with DMSO, 10 μM 5-NT as a positive control for decreased infection, or increasing concentrations of epoxomicin for 2 h prior to adsorption with CHIKV strain SL15649 at an MOI of 5 PFU/cell for 1 h. Cells were assessed for infection at 6 h postinfection by indirect immunofluorescence (Figure V-5). Treatment of cells with epoxomicin resulted in a significant (64%) increase in the percentage of CHIKV infected cells relative to DMSO-treated cells. These data indicate the inhibition of the proteasome enhances CHIKV infection and suggest broad mechanisms of CHIKV restriction by the proteasome.

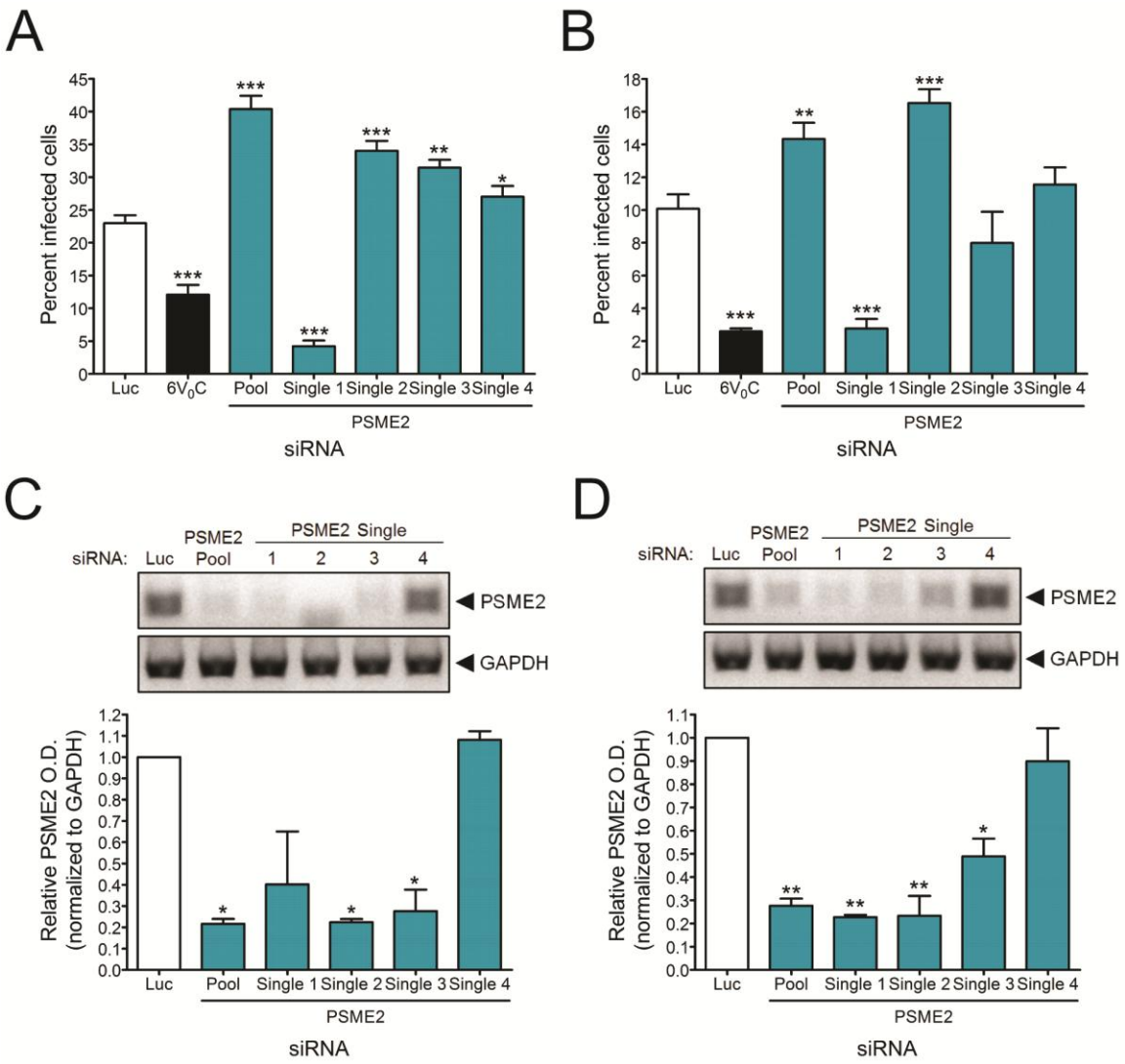

Figure V-4. CHIKV infection is enhanced by PSME2 knockdown with single siRNAs. (A, C) U-2 OS cells and (B, D) HBMECs were transfected with nonspecific (Luc), control ($6V_0C$), or PSME2-specific pooled (Dharmacon siGENOME® SMARTpool®) or single siRNAs and incubated for 48 h. Cells were infected with (A) CHIKV SL15649 eGFP replicon particles for 24 h or (B) CHIKV strain 181/25 for 6 h. Cells were stained with Hoechst (A) or DAPI dye (B) to detect nuclei, and GFP-positive cells were quantified by fluorescence microscopy. Results are presented as percent infected cells for triplicate samples. Error bars indicate standard deviation. RNA from transfected (C) U-2 OS cells and (D) HBMECs was isolated and used for generation of cDNA and amplification of PSME2 or GAPDH transcript. Products were resolved on 1% agarose gels (top), and relative PSME2 RNA levels were quantified by optical densitometry using ImageJ (bottom) for duplicate experiments. Error bars indicate standard deviation. *, $P < 0.05$, **, $P < 0.01$, ***, $P < 0.001$, as determined by ANOVA followed by Tukey *post hoc* test.

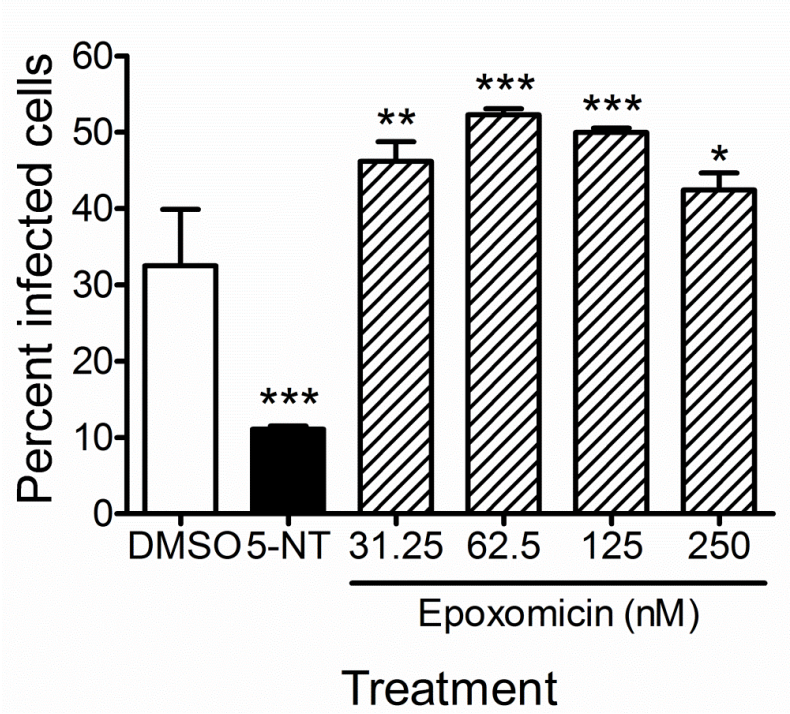

Figure V-5. Proteasome inhibition by epoxomicin treatment enhances CHIKV infection. U-2 OS cells were incubated with DMSO, 10 μM 5-NT, or increasing concentrations of epoxomicin for 2 h prior to adsorption with CHIKV strain SL15649 at an MOI of 5 PFU/cell. After 1 h, virus was removed, and cells were incubated with complete medium for 5 h. Cells were stained with CHIKV-specific antiserum and DAPI to detect nuclei and imaged by fluorescence microscopy. Results are presented as percent infected cells for triplicate samples. Error bars indicate standard deviation. *, $P < 0.05$, **, $P < 0.01$, ***, $P < 0.001$, as determined by ANOVA followed by Tukey *post hoc* test.

Components of the constitutive and immunoproteasome influence CHIKV infection. To determine whether additional components of the constitutive or immunoproteasome contribute to CHIKV infection, U-2 OS cells were transfected with control siRNAs or siRNAs specific for PSME2, PSMA2, or PSMF1. PSMA2 encodes a component of the 20S proteasome, and PSMF1 encodes an inhibitor of 20S proteasome activation by the 11S and 19S regulators. Transfected cells were adsorbed with CHIKV SL15649 eGFP replicon particles at an MOI of 5 IU/cell and assessed for infection at 24 h by indirect immunofluorescence (Figure V-6). Whereas knockdown of PSME2 significantly increased the percentage of infected cells (Figure V-6) and GFP intensity (Figure V-6B), knockdown of PSMA2 significantly decreased CHIKV infection and replication relative to cells transfected with nonspecific siRNA. Infection was decreased to levels even below those observed for cells transfected with siRNAs specific for $6V_0C$. This result suggests that PSMA2 promotes CHIKV infection and is consistent with reports of enhancement of VEEV, EEEV, and WEEV by proteasome activity (157). In addition, transfection of PSMF1-specific siRNAs significantly decreased CHIKV infection and replication. Since PSMF1 is an inhibitor that functions in opposition to PSME2 to prevent activation of the 20S proteasome, one would expect PSMF1 to serve an opposite role in CHIKV infection. These findings indicate a role for components of both the constitutive and immunoproteasome in regulating CHIKV infection.

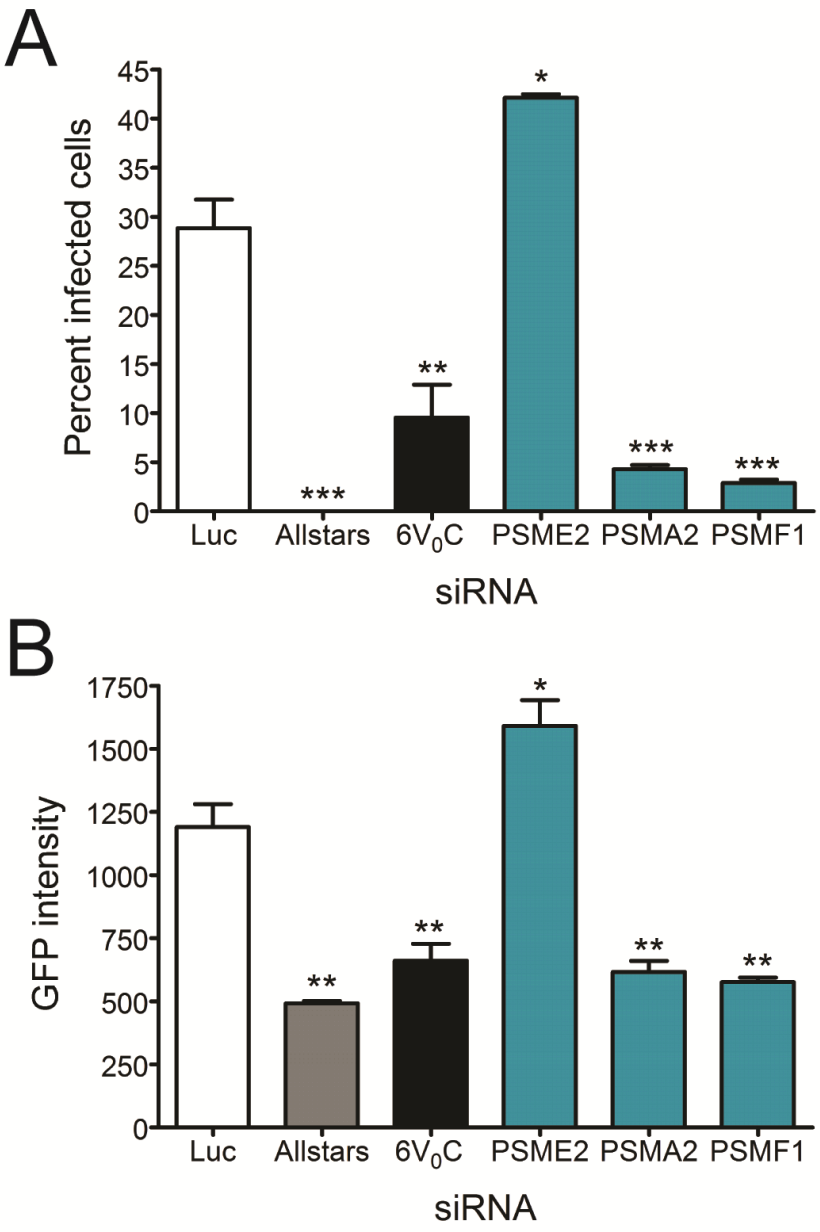

Figure V-6. Components of constitutive and immunoproteasome modulate CHIKV infection. U-2 OS cells were transfected with siRNA pools 48 h prior to infection with CHIKV SL15649 eGFP replicon particles at an MOI of 5 IU/cell. siRNAs targeting luciferase (Luc) and $6V_0C$ were included as non-targeting and positive controls, respectively. AllStars, a proprietary siRNA pool that induces cell death following transfection, was included to assess transfection efficiency. At 24 h postinfection, cells were stained with Hoechst dye to detect nuclei, and GFP-positive cells were quantified by fluorescence microscopy. Results are presented as (A) percent infected cells or (B) GFP intensity for duplicate experiments. Error bars indicate standard error of the mean. **, $P < 0.01$, ***, $P < 0.001$, as determined by ANOVA followed by Tukey *post hoc* test.

Discussion

Host responses during CHIKV infection serve antiviral functions but also result in exacerbation of disease. Elucidating differences in the factors and mechanisms involved in these dichotomous roles will enhance an understanding of CHIKV pathogenesis and shed light on new approaches for antiviral development. To gain mechanistic insights into cell-intrinsic antiviral strategies, I used high-throughput, RNAi screening to identify host genes that impede CHIKV infection. This screen identified 71 interferon-regulated genes as candidate CHIKV restriction factors, including PSME2. siRNA knockdown of PSME2, a component of the immunoproteasome 11S regulatory complex, resulted in significant increases in CHIKV infection and replication. Inhibition of the 20S proteasome by epoxomicin treatment also increased CHIKV infection. Interestingly, knockdown of other genes and regulators of the constitutive and immunoproteasome decreased CHIKV infection, indicating that proteasome components may serve opposing functions in CHIKV infection. These findings reveal new functions for the proteasome in the regulation of CHIKV.

Silencing of PSME2 enhances CHIKV infection and replication, but mechanisms of PSME2-mediated restriction are not understood. Knockdown of this gene by single siRNAs suggests that the enhancement is not a result of off-target effects. Furthermore, increased infection following inhibition of the 20S proteasome by epoxomicin suggests that a PSME2 activity may be mediated through its interactions with the 20S proteasome. Indeed, silencing PSMF1, which functions to prevent 11S activation of the proteasome, decreased CHIKV infection. In these cells, activity of the 11S regulatory subunit would not be limited by PSMF1 expression and could function to restrict CHIKV infection.

These data support a role for immunoproteasome activation in CHIKV infection. However, specific activity of the immunoproteasome will need to be determined to assess the role of this protein complex in restriction of CHIKV infection.

While evidence presented in this chapter suggests that multiple components of the proteasome influence CHIKV infection, individual proteins of the proteasome could mediate separate functions in CHIKV infection. This hypothesis is supported by the finding that silencing of PSMA2, a component of the 20S proteasome, decreases CHIKV infection. These data support opposing roles of the constitutive and immunoproteasome in CHIKV infection. The immunoproteasome is activated during infection and stress and functions in presentation of MHC Class I peptides (155, 156). Therefore, antiviral activity by the immunoproteasome and activators of the immunoproteasome would be probable. An opposite role for the constitutive proteasome in CHIKV infection seems logical given the essential role of this molecule in degradation of aberrant cellular proteins. Silencing of proteasome components may induce cell stress responses that mediate inhibition of CHIKV infection by indirect mechanisms. Alternatively, PSME2 and PSMA2 could function in CHIKV infection through proteasome-independent activities. PSME2 may interact with CHIKV proteins and modulate delivery of these proteins or peptides to the immunoproteasome for degradation. However, it is not known whether CHIKV proteins are ubiquitylated or directly interact with proteasome proteins. PSME2 also may facilitate degradation of additional host factors essential for CHIKV replication, but the identities of these factors are not known.

Understanding the host determinants and mechanisms of host cell restriction of CHIKV will provide new knowledge of CHIKV biology and may inform the design of

CHIKV-specific therapeutics. Using high-throughput, RNAi screening, I identified several antiviral gene candidates, including PSME2, critical activator of immunoproteasome activation. Knockdown of PSME2 or chemical inhibition of the proteasome enhanced CHIKV infection. In addition, I demonstrate that other components of the proteasome also contribute to CHIKV infection, suggesting that the ubiquitin-proteasome may serve a broad role in CHIKV restriction. Future studies will focus on elucidating mechanisms by which components of the cellular proteasome either augment or restrict CHIKV infection.

CHAPTER VI

SUMMARY AND FUTURE DIRECTIONS

Thesis Summary

Chikungunya virus reemerged in 2004 to cause devastating epidemics of fever, rash, and arthritis. Over the past decade CHIKV disease has been well characterized, in part, because of the rapid spread and high attack rate of this mosquito-borne virus. However, the molecular mechanisms of CHIKV pathogenesis are not known. An important determinant of viral pathogenesis is tropism for specific cells and tissues in the host. Both viral and host factors can dictate virus tropism, and these factors can vary between host species. Host restriction factors form another class of important determinants of viral pathogenesis. These factors also can influence virus tropism and are often regulated by cell-intrinsic immune responses following viral infection. The research presented in this thesis examines the viral and host determinants of CHIKV tropism and replication and how these determinants influence disease pathogenesis.

I began studies of CHIKV tropism by focusing on polymorphisms displayed by a virulent strain, AF15561, and an attenuated strain, 181/25. These strains differ at 5 synonymous and 5 nonsynonymous positions. The goal of my studies presented in Chapters II and III was to determine which of these polymorphisms are responsible for 181/25 attenuation. In Chapter II, I demonstrate that strain 181/25 consistently replicates to higher titers relative to AF15561 in mammalian cells. To identify the polymorphisms responsible for these differences in replication, I engineered and tested a panel of viruses

that vary at each of the nonsynonymous sites for the capacity to infect mammalian cells. I found that a G82R polymorphism in the E2 attachment glycoprotein mediated enhanced infectivity in these cells. However, in mosquito cells, the E2 G82R polymorphism did not enhance infectivity. Instead, introducing a glycine at this position in strain 181/25 enhanced infectivity in mosquito cells, suggesting that E2 residue 82 mediates different interactions with mammalian and mosquito cells. Moreover, additional polymorphisms in E2 and the E1 fusion protein displayed by strains AF15561 and 181/25 contributed to infection of these cells.

To understand mechanisms by which E2 residue 82 mediates enhancement of CHIKV infection, I tested the role of this residue in CHIKV attachment to host cells. Strains encoding an arginine at E2 82 more efficiently bound to host cells and exhibited a greater dependence on GAG utilization for infection compared with strains encoding a glycine at this position. These findings suggest that GAG interactions promote CHIKV infection in mammalian but not mosquito cells and that residue 82 of the E2 glycoprotein modulates these interactions.

GAGs are expressed widely in the host (158) and could serve a critical role in CHIKV tropism and virulence. To determine the role of GAG utilization in CHIKV disease, I assessed the capacity of the E2 82 reciprocal polymorphic strains to replicate, spread, and induce pathology using a mouse model of CHIKV disease. In Chapter III, I determine that E2 residue 82 contributes to CHIKV-induced pathology. Relative to the parental strain AF15561, mice inoculated with AF15561 E2 G82R gained weight more efficiently and displayed reduced swelling and muscle necrosis at the site of inoculation. However, E2 residue 82 did not strictly correlate with disease, as introduction of a

glycine at this position in strain 181/25 did not enhance virulence in mice. These data suggest that additional polymorphisms are required for full CHIKV virulence. Strains containing an arginine at E2 residue 82 replicate to equivalent titers in the hind limbs of infected mice, but display reduced titers in secondary sites of replication (e.g., spleen and serum) as compared to strains encoding a glycine at this residue. Interestingly, a glycine at E2 residue 82 was selected in the spleens of mice inoculated with AF15561 E2 G82R, suggesting a role for this residue in tissue-specific replication of CHIKV. Thus, E2 residue 82 is a critical viral determinant of CHIKV pathogenesis, likely by modulating interactions with GAGs.

To identify host factors that promote or impede CHIKV infection, I performed high-throughput chemical compound and siRNA screens in collaboration with Laurie Silva in our laboratory. In Chapter IV, I present data describing the function of the sodium-potassium ATPase in CHIKV infection in cell culture and replication *in vivo*. I demonstrate that antagonism of this ion transporter by the cardiac glycoside digoxin impairs CHIKV infection in human cells. This inhibition was not attributable to toxicity induced by digoxin treatment but, instead, occurred via on-target effects of this compound. I determined that inhibition of CHIKV infection occurred via blockade of the sodium-potassium ATPase by mimicking inhibition with a related cardiac glycoside, ouabain. Furthermore, inhibition was dependent on the relative expression of the human or murine α3 or human α1 isoforms of the sodium-potassium ATPase, which are known to be sensitive to digoxin-mediated inhibition. Transfection of digoxin-sensitive U-2 OS cells with the digoxin-resistant murine α1 isoform decreased sensitivity of these cells to digoxin inhibition of CHIKV infection. Digoxin inhibited CHIKV at both entry and post-

entry steps in the replication cycle, as determined by time-of-addition and electroporation-bypass assays. Importantly, treatment of mice with digoxin prior to inoculation with strain SL15649 decreased viral loads in musculoskeletal tissues. Passage of CHIKV in digoxin-treated cells selected several mutations, the majority of which mapped to nsP2 and nsP3, suggesting that alterations in these genes confer resistance to digoxin inhibition. These findings suggest that a functional sodium-potassium ATPase is required for CHIKV infection of cells and mice and reveal a new pathway for the development of antiviral therapeutics.

Host factors involved in the restriction of CHIKV were identified in a high-throughput siRNA screen in U-2 OS cells. In Chapter V, I provide evidence to support a role for PSME2, an interferon-regulated component of the immunoproteasome 11S regulatory complex, in CHIKV restriction. Knockdown of PSME2 by pooled or single siRNAs significantly enhanced CHIKV infection and replication in U-2 OS cells and HBMECs. Knockdown of PSME2 by siRNA resulted in a greater than 95% decrease in PSME2 protein. Inhibition of the 20S by epoxomicin treatment resulted in a dose-dependent increase in infection by CHIKV. Moreover, knockdown of additional genes involved in proteasomal degradation, PSMA2 and PSMF1, altered CHIKV infection. Of particular interest, silencing of PSMF1, an inhibitor of proteasome activation by the 11S complex, significantly decreased CHIKV infection, as would be predicted by the results obtained using PSME2 siRNA. This work implicates the proteasome in CHIKV restriction.

Collectively, findings presented in this thesis enhance an understanding of viral and host determinants of CHIKV infection and pathogenesis. Information gathered from

this work has revealed mechanisms of CHIKV attenuation and strategies for antiviral therapy.

Future Directions

Influence of other polymorphic residues on the E2 G82R polymorphism. Although the CHIKV E2 G82R polymorphism enhances infection in cell culture, the magnitude of the enhancement is dependent largely on the genetic background in which the mutations were introduced. Introducing an arginine at E2 82 in the AF15561 background resulted in nearly a 4-fold higher percentage of infected cells relative to strain 181/25, which also contains this polymorphism. These data suggest that additional polymorphisms between strains 181/25 and AF15516 influence the differences in infectivity observed for these viruses. As a first step toward understanding how additional polymorphisms between strains 181/25 and AF15561 influence the E2 G82R polymorphism, I engineered these parental strains to contain the combinatorial E2 mutations and assessed infection in Vero cells (Figure VI-1). I found that increased infection by the E2 82 G82R polymorphism predominated over the decrease in infection associated with the E2 T12I polymorphism when these polymorphisms were engineered together in the AF15561 background. In contrast, the E2 I12T polymorphism predominated over the E2 R82G polymorphism when these polymorphisms were engineered together in the 181/25 background. I conclude that viruses encoding an isoleucine at E2 residue 12 display higher infectivity following introduction of an arginine at E2 residue 82 (181/25 and AF15561 DM) but display lower infectivity with introduction of a glycine at E2 residue 82 (181/25 R82G

and AF15561 E2 T12I). These data support the hypothesis that E2 residues 12 and 82 influence each other, but the mechanism of this interplay is not known.

CHIKV E2 residues 12 and 82 reside in separate, yet neighboring domains of the E2 protein (Figure II-8) (39, 118). E2 residue 12 maps to the E2 beta ribbon, which interacts with the E2 A domain in which E2 residue 82 is found. Although these residues are physically separated, the polar and charge changes that result from these polymorphisms could alter interactions between these domains and influence the phenotypes associated with each residue. To determine whether alteration of one of these residues induces conformational changes that affect the other, crystallographic studies could be performed with recombinant forms of the wildtype and mutant E2 proteins. Furthermore, conformation-specific antibodies could be used to test whether polymorphisms at residues 12 and 82 of E2 induce alterations in the folding of the protein. In addition to structural and infectivity assays, these mutant viruses could be assessed for attachment and fusion. Such experiments would define a role for these residues at discrete steps within the replication cycle.

In mice, the E2 G82R polymorphism appears to be influenced by additional polymorphisms. I demonstrated that introduction of an arginine at E2 82 in strain AF15561 was sufficient to attenuate the virus, but introducing the reciprocal R82G substitution was not sufficient to confer virulence in attenuated strain 181/25 (Chapter III). The AF15561 E2 T12I polymorphism was shown previously to contribute to 181/25 attenuation (118), and this residue may influence the effect of E2 residue 82 in CHIKV disease as in cell culture. To determine whether residues 12 and 82 in the E2 protein cooperate to influence CHIKV disease, mice could be inoculated with the double-mutant

viruses in each reciprocal parental background. Viral loads, joint swelling, and histopathology could be assessed following inoculation with these strains. This work would provide a clearer picture of the role of E2 polymorphisms in CHIKV tropism and disease.

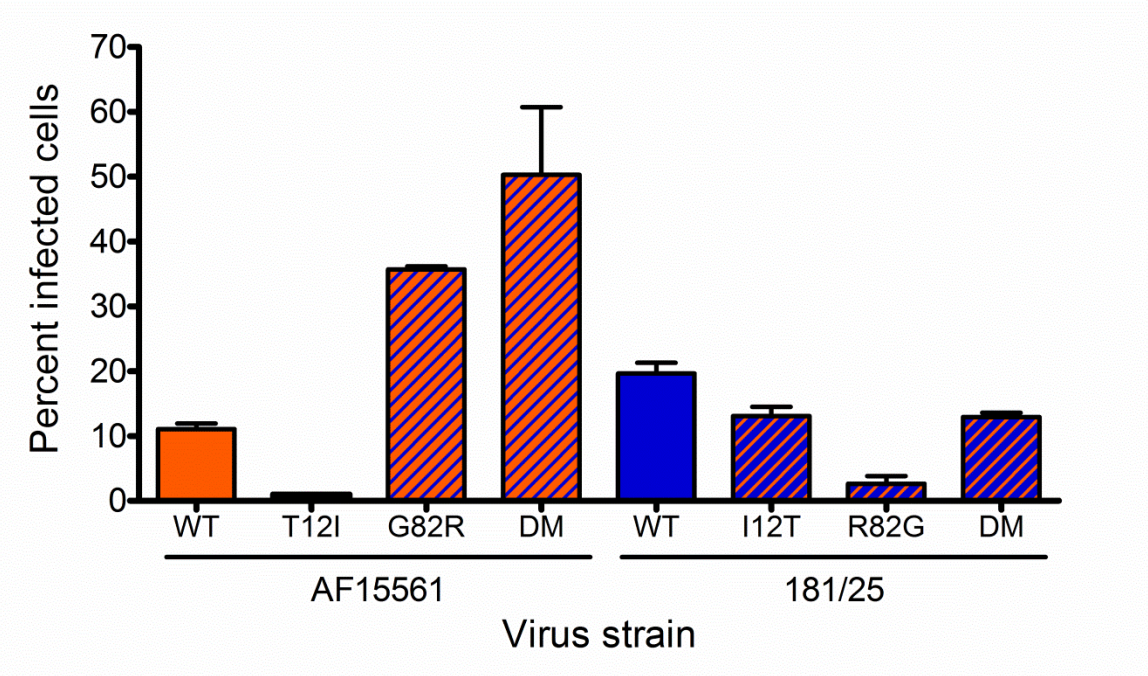

Figure VI-1. Polymorphisms at residues 12 and 82 in E2 function in concert to influence infectivity. Vero cells were adsorbed with CHIKV strains AF15561, 181/25, or the variant viruses shown at an MOI of 1 PFU/cell and incubated for 24 h. Cells were stained with CHIKV-specific antiserum and DAPI to detect nuclei and imaged by fluorescence microscopy. Results are presented as percent infected cells for triplicate wells. Error bars indicate standard deviation.

Role of polymorphisms between CHIKV strains 181/25 and AF15561 in mosquito cell infection. Studies of polymorphisms displayed by strains AF15561 and 181/25 revealed a role for E2 residue 82 in infection of mosquito cells. In contrast to mammalian cells, the E2 R82G polymorphism enhances infectivity in mosquito cells. Several possible mechanisms could contribute to the infectivity enhancement observed for this polymorphism. First, this residue may mediate interactions with host molecules on the surface of mosquito cells that are different or nonexistent in mammalian cells. The presence of a charged residue at this position may interfere with these mosquito cell-specific interactions. An alternative explanation is that the temperature at which these cells are maintained could influence protein folding. Whereas mammalian cells are grown at 37°C, mosquito cell cultures are maintained between 28 and 30°C. The E2 molecule could adopt different conformations at lower temperature as observed for DENV (159) and influence the orientation of residue 82 or adjacent residues. To assess the temperature-dependence of E2 residue 82, Vero cells were inoculated with parental viruses or the reciprocal E2 82 mutant viruses at 30°C (Figure VI-2). The E2 G82R polymorphism still enhanced infectivity in mammalian cells at the reduced temperature, but the magnitude of the difference was less striking. C6/36 cells could not be tested at 37°C as these cells were not viable at this temperature (data not shown). Additional studies, perhaps at intermediate temperatures, could be performed to determine whether phenotypes mediated by E2 residue 82 are dependent on temperature.

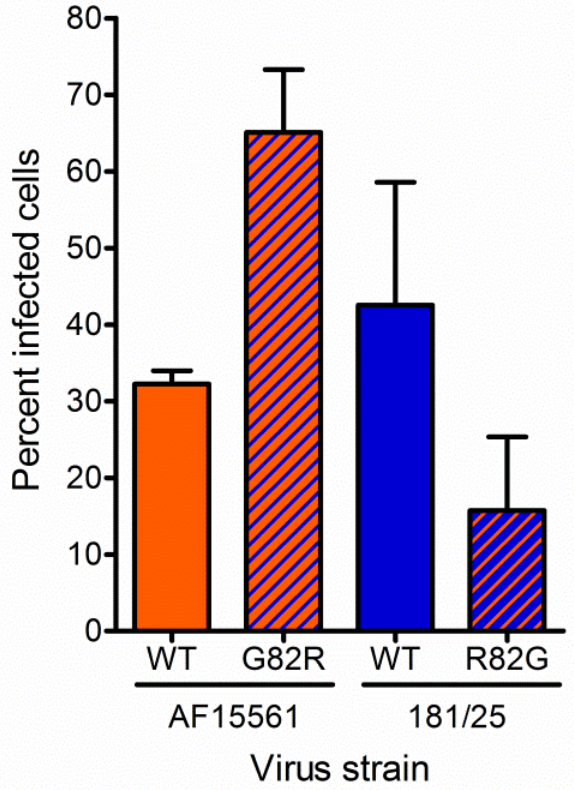

Figure VI-2. Enhancement of mammalian cell infectivity by the E2 G82R polymorphism occurs independently of temperature. Vero cells were adsorbed with CHIKV strains AF15561, 181/25, AF1561 E2 G82R, or 181/25 E2 R82G at an MOI of 1 PFU/cell and incubated at 30°C for 24 h. Cells were stained with CHIKV-specific antiserum and DAPI to detect nuclei and imaged by fluorescence microscopy. Results are presented as percent infected cells for duplicate experiments. Error bars indicate standard error of the mean.

An additional mechanism by which the E2 R82G polymorphism could enhance infection in mosquito cells is through diminished interactions with GAGs. Interactions with GAGs enhance infection in mammalian cells but may preclude interactions with a receptor required for efficient infection of mosquito cells. To understand the function of GAGs in infection of mosquito cells, I determined whether preincubation of CHIKV strains polymorphic at E2 residue 82 with soluble heparin diminished infection in mosquito cells (Figure VI-3). Heparin pretreatment significantly decreased or abolished infection of CHIKV strains in Vero cells (Figure VI-3A) but did not decrease infection in C6/36 cells. These data suggest that infection of C6/36 cells by CHIKV is not dependent on GAGs. However, it would be important to assess the level of GAG expression on these cells. Likewise, cell-surface molecules engaged by CHIKV on both mosquito and mammalian cells should be identified. E2 residue 82 may contribute critical interactions with additional receptors and attachment factors, particularly in mosquito cells in which GAGs do not appear to be used.

Although E2 residue 82 influences infectivity in mosquito cells, other polymorphisms between strains AF15561 and 181/25 also contribute to differences in infectivity in mosquito cells exhibited by these strains. In Chapter II, I show that introducing an isoleucine at E2 residue 12 in strain AF15561 significantly decreases infectivity in mosquito cells. The infectivity observed for the AF15561 E2 T12I virus was not as low as that observed for strain 181/25, but this variant was the most impaired of all viruses generated in the AF15561 background. However, exchanging this isoleucine for a threonine in strain 181/25 did not enhance infectivity in mosquito cells. These data support similar functions for E2 residue 12 in both mammalian and mosquito cells.

Because differences in infectivity did not segregate strictly with a single polymorphism, I hypothesize that these mutations function in concert to influence mosquito cell infection. To identify residues important for mosquito cell infection, AF15561 and 181/25 viruses encoding individual or multiple polymorphisms at E2 12, E2 82, and E1 404 could be tested for the capacity to infect these cells. Since these residues may influence distinct steps in the replication cycle, it is also important to assess the capacity of these viruses to bind and fuse with target cells. Virus attachment and fusion are highly synchronized events during CHIKV infection with both properties mediated by trimers of the E1/E2 heterodimer. Therefore, it is probable that residues in these proteins interact. Virus fusion could be assessed using a fusion-from-without assay (FFWA). Virus would be adsorbed to cells at 4°C to prevent internalization, and low pH medium would be added to trigger viral fusion at the plasma membrane. Media with a range of pH values could be used to determine the pH required for efficient fusion for each virus strain. Viruses that require considerably lower or higher pH to efficiently fuse with host cells may exhibit reduced infectivity and fitness.

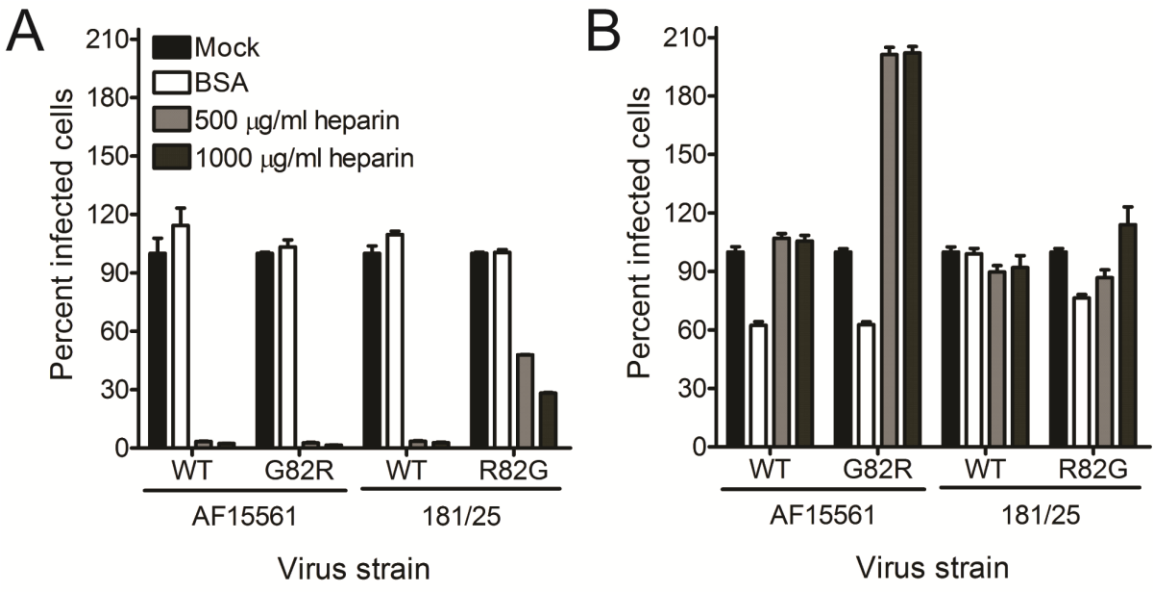

Figure VI-3. Pretreatment of CHIKV strains with soluble heparin does not diminish infection of mosquito cells. Strains AF15561, 181/25, AF1561 E2 G82R, or 181/25 E2 R82G were treated with VDB, BSA at 1000 μg/ml, or heparin at the concentrations shown for 30 min and adsorbed to (A) Vero or (B) C6/36 cells at an MOI of 2.5 PFU/cell. After incubation for 24 h, cells were stained with CHIKV-specific antiserum and DAPI to detect nuclei and imaged by fluorescence microscopy. Results are presented as percent infected cells for triplicate wells. Error bars indicate standard deviation.

Mechanisms of attenuation of GAG-dependent CHIKV strains. A correlation between GAG utilization and attenuation of alphaviruses has been reported (96, 98, 114), but the specific mechanisms are not known. GAG-dependent strains of CHIKV may disseminate less efficiently as a consequence of enhanced binding to tissues during primary replication or may be cleared more readily by the host immune response. To distinguish between these possibilities, wildtype and *Rag1*$^{-/-}$ mice can be inoculated with CHIKV strains that vary in GAG utilization, and viral titers could be determined at days 1, 3, 5, and 7 postinoculation. Because viral titers do not correlate strictly with disease, pathology could be assessed using calipers to measure swelling, and tissues could be processed for histology. The use of *Rag1*$^{-/-}$ mice will diminish clearance of CHIKV by T and B cells, which contribute importantly to clearance and persistence of CHIKV in mice (59). Therefore, decreased viral titer in the serum will be a consequence of decreased dissemination and not a result of increased clearance. Additionally, wildtype and *Rag1*$^{-/-}$ mice can be inoculated subcutaneously or intravenously to identify potential bottlenecks in CHIKV dissemination that result from enhanced GAG dependence. If failure of GAG-dependent viruses to establish serum viremia is associated with attenuation, then intravenous inoculation should bypass this dissemination block. This approach also will identify steps in CHIKV dissemination required for virulence.

Based on findings presented in Chapter III, GAG utilization may alter tissue tropism to contribute to attenuation. Only viruses containing the E2 R82G polymorphism replicated to high titers in the spleens of infected mice at early times postinoculation, suggesting that GAG utilization prevents dissemination to or replication within the spleen. Along these lines, a glycine at E2 residue 82 was selected in the majority of virus

clones isolated from this site. To assess the role of GAG utilization in tissue tropism, tissues from infected mice could be evaluated for the distribution of virus using CHIKV antigen-specific immunofluorescence and CHIKV RNA-specific fluorescence in situ hybridization (FISH).

To complement studies using viruses with altered GAG utilization, mice deficient in GAG biosynthetic enzymes can be used to define functions of specific GAG molecules in CHIKV tissue tropism and disease pathogenesis. Many such mice are viable, including those that lack xylosyltransferase 2, an initiating enzyme of GAG biosynthesis (160-162). To determine the role of tissue-specific GAGs in CHIKV infection, tissue-specific GAG knockout mice could be engineered using CRISPR/Cas9 technology. These mice could be inoculated via multiple routes to assess the roles of tissue-specific GAGs in CHIKV dissemination. These studies would elucidate functions of specific GAGs in CHIKV attenuation.

Sites targeted by CHIKV required for dissemination and pathogenesis. CHIKV replication in affected tissues of experimentally infected animals does not strictly correlate with the magnitude of disease. In Chapter III, strains attenuated for disease in mice produce similar titers at the site of inoculation but lower titers in the spleen and serum (Figure III-3). Despite comparable viral titers in the left hind limb, strain AF15561 induced more swelling in the feet of infected mice, suggesting mechanisms independent of viral load underlie CHIKV-induced pathology. Infection of mice with virulent CHIKV strains is associated with increased neutrophil recruitment to the site of inoculation and increased muscle cell necrosis relative to mice inoculated with an attenuated strain

(Figure III-2). However, the discrete cell types targeted by CHIKV in infected tissues in the host during acute and persistent phases of infection are unknown. Thus, it is essential to define the cell types responsible for tissue damage *in vivo* to understand how CHIKV causes disease.

To identify the cell types targeted by CHIKV that mediate pathology, mice can be inoculated with CHIKV strains that are restricted from replicating at discrete sites in the host. One strategy to limit virus replication in a cell type-specific manner would be to establish mice that express CHIKV-targeting miRNAs in specific tissues to ablate replication solely at those sites. Another strategy would be to generate conditionally replicative viruses by engineering virulent CHIKV strains to contain tissue-specific miRNA seed sequences. This approach has been used successfully to study coxsackievirus infection of skeletal muscle (163, 164), dengue virus infection of hematopoietic cells (165), species-specific restriction of influenza virus infection (166), and, importantly, SFV (an alphavirus) infection of the CNS (167). Potential tissue-specific miRNAs to be inserted into CHIKV include those expressed in skin or keratinocytes (miR-203 [(168)]), skeletal muscle (miR-206 [(163, 169)]), osteoblasts (miR-2861 [(170)]), endothelial cells (miR-126 [(171)]), and hematopoietic cells (miR-142-3p [(172)]). Virus strains can be engineered to encode four copies of the miRNA target sequence inserted in the nonstructural cassette using the nsP3/nsP4 protease site (Figure VII-5). Replication of engineered viruses can be compared to a control CHIKV strain encoding a scrambled miRNA target sequence to confirm that the engineered alterations do not compromise viability. Cell- and tissue-specific restriction of engineered viruses can be confirmed using single and multicycle replication experiments with

primary murine keratinocytes, muscle cells, osteoblasts, endothelial cells, and hematopoietic-derived cells or murine cell lines. C2C12 and ST2 cells are known to express the muscle and osteoblast-specific miRNAs mentioned above (170, 173) and can be used to confirm restriction of engineered viruses. Once confirmed, mice can be inoculated with these miRNA seed sequence-containing viruses to determine the cell types targeted by CHIKV for replication in the host.

CHIKV infection of specific cell types may dictate the tissues subsequently targeted or the route of dissemination. CHIKV strains encoding an arginine at E2 residue 82 displayed enhanced dependence on GAGs for infection and impaired dissemination in mice. Interactions with GAGs may contribute to altered tropism *in vivo* to prevent or misdirect virus dissemination in the host. Using virus strains encoding miRNA seed sequences, the contribution of infection of specific cells and tissues to CHIKV tropism and dissemination can be assessed by quantifying viral titers in musculoskeletal and lymphoid tissues during acute and chronic infection. In addition, joint swelling, CHIKV antigen-specific immunofluorescence or flow cytometry, and histopathology can be assessed to determine the role of tropism in CHIKV disease. Information obtained from this work will elucidate the cell types required for CHIKV dissemination and pathogenesis.

In addition to the sites of virus replication in the host, the cellular targets that influence immune responses during infection remain undefined. In humans, CHIKV infection induces the production of a multitude of proinflammatory cytokines, including IL-1β, IL-6, MCP-1, MIG, IP-10, MIF, and RANTES. High levels of these cytokines are associated with increased disease severity and a greater predisposition for persistence of

clinical symptoms (61-65). Proinflammatory cytokines recruit immune cells to sites of CHIKV infection to exacerbate tissue injury and disease. To define the specific cell types targeted by CHIKV to elicit inflammatory responses, mice can be inoculated with miRNA seed sequence-containing viruses, and levels of these proinflammatory cytokines could be quantified using ELISA and qRT-PCR. These cytokines could be assessed in the serum and at sites of tissue injury. Additionally, specific cell populations from CHIKV-infected tissues could be isolated, stained for cell-specific markers, and quantified by flow cytometry. Sections from CHIKV-infected mice also could be stained for cell-specific markers to better assess localization of specific inflammatory infiltrates. This work will allow us to define the CHIKV target cells that initiate the inflammatory processes that contribute to tissue injury and disease. These experiments also would discriminate molecules that merely correlate with CHIKV infection from molecules that contribute to CHIKV disease.

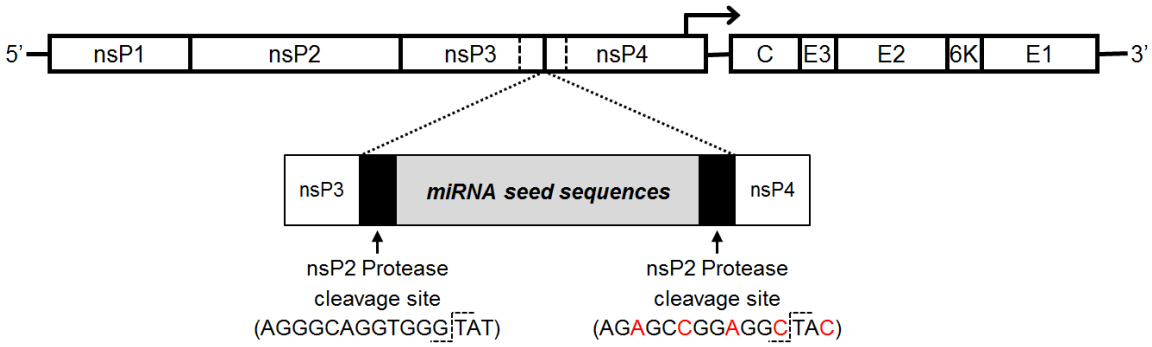

Figure VI-4. Insertion of tissue-specific miRNA seed sequences in the CHIKV SL15649 infectious clone. Four copies of miRNA seed sequences will be inserted between endogenous and duplicated nsP3/nsP4 protease cleavage sites (black boxes). The inserted sequence element will be flanked by unique restriction sites generated by silent mutations to facilitate introduction into the cDNA clone. Sequences encoding nsP3/nsP4 protease cleavage sites will be altered at synonymous positions (indicated in red) to diminish the possibility of recombination and seed sequence excision.

Mechanisms of digoxin-mediated inhibition of CHIKV. The effects of digoxin antagonism of the sodium-potassium ATPase have been well characterized. However, mechanisms by which digoxin inhibits CHIKV remain to be determined. Evidence presented in Chapter IV does not support a direct interaction with digoxin and the virus. Therefore, I hypothesize that effects induced by sodium-potassium ATPase antagonism mediate inhibition of CHIKV. A major consequence of disrupted sodium transport is an increase in intracellular calcium levels. To determine whether altered calcium levels or signaling pathways contribute to CHIKV inhibition by digoxin, intracellular calcium levels could be assessed in CHIKV-infected cells treated with DMSO as a control or digoxin. Cells can be incubated with Fura-2, a fluorescent dye that binds free intracellular calcium, and cells could be imaged by fluorescence microscopy. In addition, chemical compounds that induce calcium release, such as thapsigargin, could be tested for anti-CHIKV activity. To complement these studies, the cell-permeable calcium chelator, BAPTA-AM, could be tested for the capacity to reverse inhibition of CHIKV infection by decreasing intracellular calcium concentrations.

Another byproduct of blockade of the sodium-potassium ATPase is increased acidification of endocytic vesicles. Trafficking of CHIKV particles to endocytic vesicles with lower pH may impair viral fusion and release of the genome into the cytoplasm. The pH of the endocytic compartment could be measured following treatment of cells with DMSO or digoxin. To assess pH changes induced by digoxin treatment, CHIKV virions could be labeled with a pH-sensitive dye such as pHrodo, and internalization of CHIKV particles could be visualized using confocal microscopy. Upon encountering low pH, pHrodo becomes fluorescent and can be visualized by fluorescence microscopy. Altered

endocytic pH may also affect the development of endosomes. As such, the distribution of specific markers for early and late endosomes could be assessed using confocal microscopy of digoxin-treated, infected cells. Cells could be stained with antibodies specific for Rab5 and early endosome antigen 1 (EEA1) to detect early endosomes and Rab7, Rab9, and LAMP1 to detect late endosomes and lysosomes. Decreases in endocytic pH following digoxin treatment might reduce the number of Rab5- and EEA1-positive cells.

If digoxin treatment decreases endocytic pH, the effect of decreased pH on CHIKV infection could be investigated. A FFWA could be used to determine whether fusion at the plasma membrane bypasses the inhibitory effect in the endocytic compartment. FFWA might not provide sufficient bypass if pH changes affect multiple steps in the CHIKV replication cycle. In this case, viral transcription could be assessed by qRT-PCR and formation of replication complexes could be monitored by indirect immunofluorescence microscopy using antibodies specific for nonstructural proteins with and without digoxin treatment. Furthermore, chemical compounds that increase endocytic pH, such as bafilomycin A and NH_4Cl, could be used in combination with digoxin to test the capacity of these compounds to restore CHIKV infectivity in cells.

Passage of CHIKV in cells treated with digoxin selected several mutations, particularly in the nonstructural cassette (Table IV-1). However, the extent to which these polymorphisms contribute to digoxin-resistance is not known. To elucidate mechanisms of CHIKV resistance to digoxin, these mutations could be introduced individually or in combination into the CHIKV SL15649 background. Variant viruses could be tested for the capacity to infect digoxin-treated cells. Confirmed digoxin-resistant viruses could be

assessed for attachment, kinetics of internalization and replication, and subcellular localization to gain insights into mechanisms of digoxin-resistance. If digoxin-resistant mutant viruses display altered replication relative to wildtype strains, these strains could be used to infect mice. Studies of these viruses *in vivo* would test functions of these digoxin-resistant mutations in CHIKV dissemination and disease. This work would reveal host processes used by CHIKV to infect and replicate in its host.

Functions of the constitutive and immunoproteasome in CHIKV infection. Data presented in Chapter V demonstrate a role for PSME2 and other proteasome components in CHIKV infection. However, these studies were performed primarily using siRNA-based techniques. Although single siRNAs are less likely to exhibit off-target effects relative to pooled siRNAs, off-target knockdown can still occur. To validate a role for PSME2 in CHIKV infection, CHIKV infection and replication could be assessed in PSME2-deficient cells obtained from knockout animals or engineered using CRISPR/Cas9 technology. PSME1/PSME2$^{-/-}$ (PA28α/β$^{-/-}$) mice have been established and are viable. Wildtype and knockout mice could be inoculated with CHIKV, and viral loads could be quantified in musculoskeletal and lymphoid tissues. In addition, joint pathology and persistence could be assessed in these animals to determine whether PSME2 antagonizes CHIKV disease.

Once PSME2 is validated using these approaches, specific functions of PSME2 that mediate restriction of CHIKV could be investigated. To determine whether PSME2 limits CHIKV infection via the immunoproteasome, inhibitors (e.g., IPS1-001) or siRNAs specific to immunoproteasome subunits (β1i, β2i, and β5i) could be tested for the

capacity to enhance CHIKV infection. Enhancement of CHIKV would suggest that immunoproteasome activity restricts CHIKV infection.

To determine whether PSME2 interacts directly with CHIKV, I infected U-2 OS cells with CHIKV strain 181/25, stained cells for CHIKV antigen and PSME2, and visualized cells by confocal microscopy (Figure VI-5). In CHIKV-infected cells, the distribution of PSME2 (green) was considerably less diffuse than in uninfected cells. Instead, PSME2 localized to a perinuclear site in CHIKV-infected cells, most likely the ER. To determine whether PSME2 localizes to the ER during CHIKV infection, CHIKV cells infected could be stained with antibodies specific for PSME2 and an ER marker, such as protein disulfide isomerase (PDI) or ER tracker. Colocalization could be determined using confocal microscopy or higher-resolution techniques like structured illumination microscopy (SIM). If these techniques reveal colocalization of PSME2 with CHIKV proteins, PSME2 and individual CHIKV proteins could be co-immunoprecipitated to assess whether these proteins directly interact. If PSME2 co-immunoprecipitates CHIKV proteins, mutant constructs of PSME2 and CHIKV proteins could be expressed in cells to determine sequences required for these interactions.

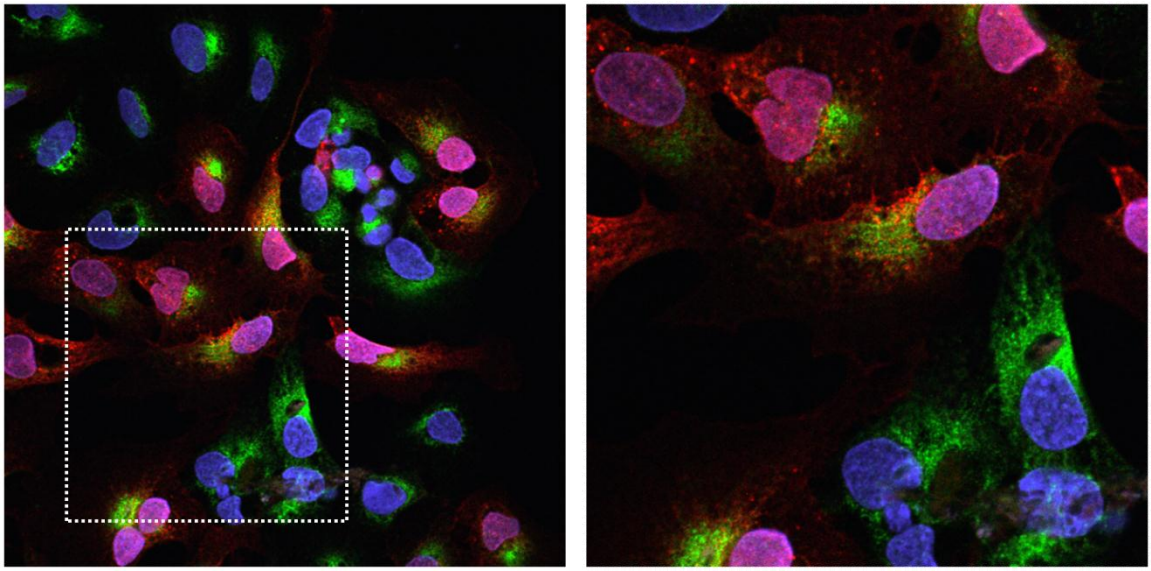

Figure VI-5. Localization of PSME2 is altered in CHIKV-infected cells. U-2 OS cells were adsorbed with CHIKV strain 181/25 at an MOI of 1 PFU/cell for 1 h at 37°C. At 6 h postinfection, cells were fixed in formalin and stained for CHIKV (red) and PSME2 (green). Nuclei were detected with TOPRO (blue). Cells were imaged by confocal microscopy. Single images from a Z-stack are shown. Inset depicts enlarged area from boxed region.

Conclusions

The findings described in this thesis identify viral and host determinants of CHIKV infection and disease in the host. The future studies presented in this chapter will elucidate the molecular mechanisms by which these determinants modulate CHIKV infection in mammalian and mosquito cell culture and *in vivo*. Elucidation of these mechanisms will enhance an understanding of CHIKV pathobiology and unveil new approaches for mitigating CHIKV disease.

CHAPTER VII

MATERIALS AND METHODS

Cells, Chemical Inhibitors, Antibodies, Plasmids, and siRNAs

Vero cells (ATCC CCL-81) and baby hamster kidney cells (BHK-21; ATCC CCL-10) were maintained in alpha-minimal essential medium (αMEM; Gibco) supplemented to contain either 5% fetal bovine serum (FBS; Gibco) or 10% FBS and 10% tryptose phosphate (TP; Sigma), respectively. MRC-5 cells (ATCC CCL-171) were maintained in αMEM supplemented to contain 10% FBS. HeLa cells were maintained in Dulbecco's modified Eagle's medium (DMEM) supplemented to contain 10% FBS. Human brain microvascular endothelial cells (HBMECs) were provided by Kwang Sik Kim (Johns Hopkins University) and maintained in RPMI 1640 medium supplemented to contain 10% FBS, 10% NuSerum (BD Biosciences), nonessential amino acids (Sigma), 1 mM sodium pyruvate, and MEM vitamins (Mediatech). L929 cells were maintained in Joklik's minimum essential medium supplemented to contain 10% FBS. NIH 3T3 cells were provided by John V. Williams (Vanderbilt University) and maintained in DMEM supplemented to contain 10% FBS. *Aedes albopictus* clone C6/36 cells (ATCC CRL-1660) were maintained in Leibovitz's L-15 medium (Gibco) supplemented to contain 10% FBS and 10% TP. CHO-K1 and CHO-pgsA745 cells (174) were provided by Benhur Lee (Mount Sinai School of Medicine) and maintained in F-12 Nutrient Mixture (Gibco) supplemented to contain 10% FBS. U-2 OS cells (ATCC HTB-96) were maintained in McCoy's 5A medium (Gibco) supplemented to contain 10% FBS. Primary

human synovial fibroblasts (HSFs) were provided by James W. Thomas (Vanderbilt University) and maintained in RPMI 1640 medium with 25 mM HEPES (Gibco) supplemented to contain 20% FBS (175). ST2 cells were provided by Julie A. Sterling (Vanderbilt University) and maintained in RPMI 1640 medium with 25 mM HEPES supplemented to contain 10% FBS. C2C12 cells were provided by David M. Bader (Vanderbilt University) and maintained in DMEM supplemented to contain 10% FBS. All media for cell maintenance were supplemented to contain 2 mM L-glutamine (Gibco), 100 U/ml of penicillin, 100 µg/ml of streptomycin (Gibco), and 25 ng/ml of amphotericin B (Sigma).

Bafilomycin A1 (Sigma), digoxin (Sigma), 5-nonyloxytryptamine oxalate (5-NT; Tocris), ouabain octahydrate (Ouabain; Sigma), and staurosporine (STS; Cell Signaling Technology) were resuspended in DMSO. Polyclonal antisera obtained from ATCC were used for CHIKV (VR-1241AF), RRV (VR-1246AF), and SINV (VR-1248AF) infectivity assays. CHIKV E2-specific monoclonal antibodies (mAbs) CHK-152 and CHK 48-G8 were provided by Michael Diamond (Washington University) and used for CHIKV binding assays. Reovirus-specific polyclonal antiserum (176) was used for reovirus infectivity assays. PSME2-specific mAb (Abcam) and β-actin-specific polyclonal antibody (Santa Cruz) were used for indirect immunofluorescence and immunoblot analysis. Human and murine ATP1A1 and ATP1A3 plasmids encoding the α1 and α3 isoforms of the sodium-potassium ATPase were provided by David Cortez (Vanderbilt University). $6V_0C$, Allstars, luciferase, STAT1, and individual PSME2 siRNAs were obtained from Qiagen. PSMA2, PSME2, and PSMF1 pooled siRNAs were obtained from

the Dharmacon siGENOME® SMARTpool® Human siRNA Library (GE Healthcare Life Sciences).

Generation of CHIKV Infectious Clone Plasmids

CHIKV strain 181/25 was provided by Robert Tesh (University of Texas Medical Branch). Viral RNA was isolated from a plaque-purified isolate, and cDNA was generated using reverse transcriptase-polymerase chain reaction (RT-PCR) with random hexamers. Overlapping fragments were amplified, cloned into pCR2.1 TOPO (Invitrogen), and sequenced. The 5′ untranslated region was sequenced using 5′ rapid amplification of cDNA ends. Using the sequence data obtained, along with the 3' untranslated region (UTR) sequence determined previously (Ann Powers, personal communication), and the polyA sequence from strain SL15649, the infectious clone (181/25ic, Figure VII-1) was synthesized by GenScript (Piscataway, NJ) in four fragments (CHIKV vaccine strain [CV/VS] 1-4). Each fragment was synthesized in the same parental plasmid (pUC57) and assembled using endogenous restriction sites unique to the CHIKV genome. The assembled genome was subcloned into a low-copy-number plasmid (pSinRep5) to maintain genome stability in bacteria. The CHIKV strain SL15649 infectious clone was provided by Mark Heise (University of North Carolina at Chapel Hill) (57).

Site-Directed Mutagenesis

Amino acid substitutions (nsP1 I301T, E2 I12T, E2 R82G, 6K P42C, and E1 V404A) were engineered individually or in combination by site-directed mutagenesis of

the 181/25 infectious clone plasmid using KOD Hot Start DNA Polymerase (Novagen). All five amino acid substitutions were introduced into the 181/25 plasmid to generate the AF15561 infectious clone plasmid. Reciprocal amino acid substitutions (nsP1 T301I, E2 T12I, E2 G82R, 6K C42P, and E1 A404V) also were generated individually or in combination in the AF15561 infectious clone plasmid. cDNA from each clone was sequenced to verify that only the desired mutations were introduced.

Biosafety

Experiments involving the generation and testing of CHIKV SL15649 replicon particles and replication-competent CHIKV were conducted in a certified biological safety level 3 (BSL3) facility in biological safety cabinets with protocols approved by the Vanderbilt University Department of Environment, Health, and Safety and the Vanderbilt Institutional Safety Committee.

Generation of CHIKV Stocks

Infectious clone plasmids were linearized with NotI restriction enzyme and transcribed *in vitro* using mMessage mMachine SP6 transcription kits (Ambion). BHK-21 cells were electroporated with viral RNA and incubated at 37°C for 24 h. Supernatants containing progeny virus were collected from electroporated cells and stored at -80°C. In some cases, viral particles were purified by ultracentrifugation of supernatants through a 20% sucrose cushion in TNE buffer (50 mM Tris-HCl [pH 7.2], 0.1 M NaCl, and 1 mM EDTA) at ~115,000 × *g* in a Beckman 32Ti rotor. Virus pellets were resuspended in

virus diluent buffer (VDB; RPMI medium with 25 mM HEPES and 1% FBS) and stored at -80°C. Viral titers were determined by plaque assay using Vero cells.

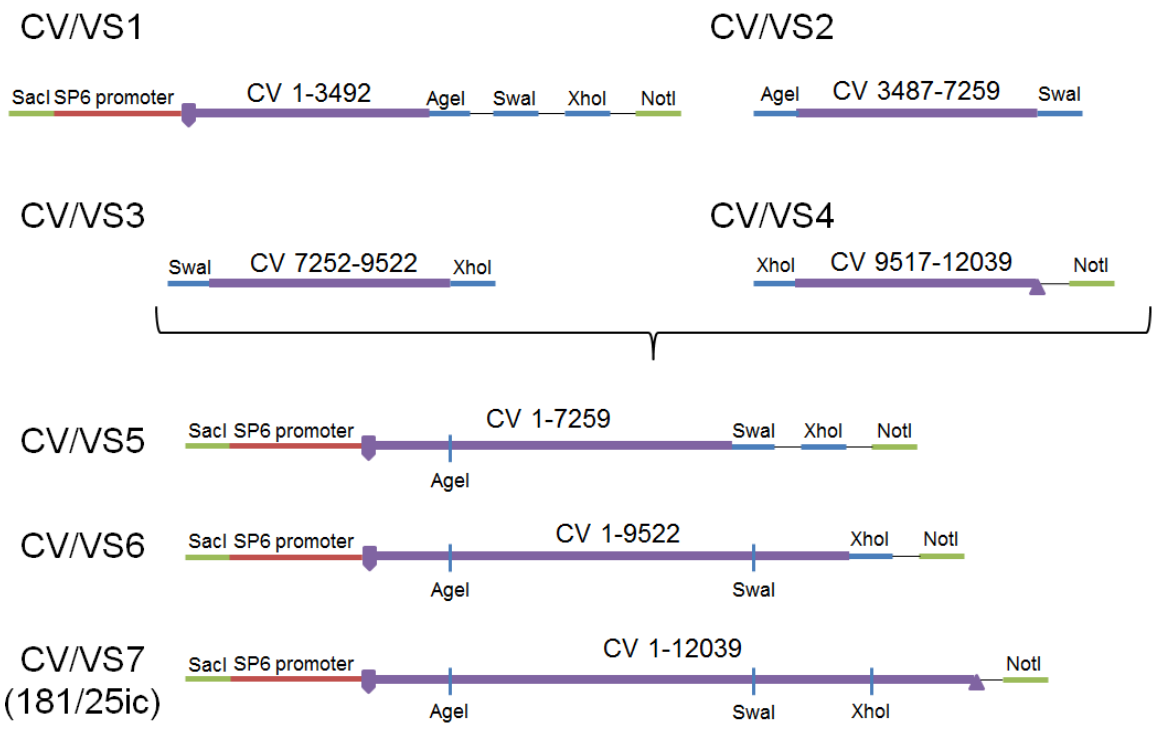

Figure VII-1. Schematic of CHIKV 181/25 infectious cDNA clone and cloning strategy. The genome of strain 181/25 was synthesized in fragments within the same parental vector (pUC57). Endogenous restriction sites flank each genome fragment and facilitate the generation of the intact infectious cDNA clone. The NotI site allows linearization of the 181/25ic plasmid encoding the full-length genome for *in vitro* transcription.

CHIKV Infectivity Assay

Vero, C6/36, CHO-K1, or CHO-pgsA745 cells seeded onto no. 2 glass coverslips (VWR) in 24-well or 96-well plates (Costar) were adsorbed with CHIKV strains in VDB at a multiplicity of infection (MOI) of 1 (Vero and C6/36) or 10 (CHO-K1 and CHO-pgsA745) plaque forming units (PFU)/cell at 37°C (Vero, CHO-K1, and CHO-pgsA745) or 28°C (C6/36) for 1 h. The inoculum was removed, complete medium was added, and cells were incubated at 37°C or 30°C for an additional hour. Medium was then supplemented to contain 20 mM ammonium chloride to prevent subsequent cycles of infection. After 24 h, cells were fixed with ice-cold 100% methanol, washed with phosphate-buffered saline (PBS), and incubated with PBS containing 5% FBS and 0.1% Triton X-100 (TX) at room temperature for 1 h. Cells were incubated with CHIKV-specific polyclonal antiserum (1:1500) in PBS with FBS and TX at 4°C overnight. Cells were washed three times with PBS and incubated with Alexa Fluor 488-labeled anti-mouse IgG (1:1000) in PBS with FBS and TX at room temperature for 2 h. Cells also were incubated with 4′,6-diamidino-2-phenylindole (DAPI; Invitrogen) to stain nuclei. Cells and nuclei were visualized by indirect immunofluorescence using an Axiovert 200 fluorescence microscope (Zeiss). CHIKV-positive cells were enumerated in three fields of view containing at least 100 cells per field of view for triplicate samples. For some experiments, cells were visualized using an ImageXpress Micro XL imaging system (Molecular Devices) at the Vanderbilt High-Throughput Screening Facility. Total and CHIKV-infected cells were quantified using MetaXpress software (Molecular Devices) in four fields of view containing at least 100 cells per field of view for triplicate samples.

Percent infectivity was determined by dividing the number of CHIKV-infected cells by the total number of cells per field.

For testing of chemical inhibitors, U-2 OS, HSF, ST2, and C6/36 cells seeded in 96-well plates (Costar) were adsorbed with CHIKV strains in VDB at an MOI of 5 PFU/cell at 37°C (U-2 OS, HSF, and ST2) or 28°C (C6/36) for 1 h. The inoculum was removed, complete medium containing DMSO or inhibitor was added, and cells were incubated at 37°C or 28°C for an additional 5 h. After incubation, cells were fixed, and CHIKV-infected cells were detected by indirect immunofluorescence using an ImageXpress Micro XL imaging system. Total and CHIKV-infected cells were quantified using MetaXpress software in four fields of view containing at least 100 cells per field of view for triplicate samples. Percent infectivity was determined by dividing the number of CHIKV-infected cells by the total number of cells per field.

Assessment of CHIKV Replication by Plaque Assay

Vero or C6/36 cells were adsorbed with CHIKV strains in VDB at an MOI of 0.01 PFU/cell at 37°C (Vero) or 28°C (C6/36) for 1 h. The inoculum was removed, cells were washed with PBS, and complete medium was added. After incubation at 37°C or 28°C for various intervals, 10% of the cell supernatant was collected and replaced with fresh medium. Viral titers in culture supernatants were determined by plaque assay using Vero cells.

Real-Time Quantitative RT-PCR

RNA was isolated using a PureLink RNA minikit (Life Technologies). The number of viral genomes/ml for each virus stock was quantified using the qScript XLT One-step RT-qPCR ToughMix kit (Quanta Biosciences) as described (99). CHIKV sequence-specific forward (CHIKVfor: 874 5'-AAAGGGCAAGCTTAGCTTCAC-3') and reverse (CHIKVrev: 961 5' GCCTGGGCTCATCGTTATTC-3') primers were used with an internal fluorogenic probe (CHIKVprobe: 899 5′-6-carboxyfluorescein [dFAM]-CGCTGTGATACAGTGGTTTCGTGTG-black hole quencher [BHQ]-3′; Biosearch Technologies). To relate *Ct* values to copies of genomic RNA, standard curves were generated from ten-fold dilutions, from 10 to 10^{10} copies, of *in vitro*-transcribed genomic 181/25 RNA.

CHIKV Binding Assay

Vero cells were adsorbed in suspension with 3 x 10^{10} genomes of various virus strains in VDB at 4°C for 30 min. Cells were washed with incomplete medium and PBS and fixed in PBS with 1% electron microscopy (EM)-grade paraformaldehyde (Electron Microscopy Sciences). Cells were washed with fluorescence-activated cell sorting (FACS) buffer (PBS with 2% FBS) and incubated with CHIKV E2-specific mAb CHK-152 (1:1000) in FACS buffer at 4°C for 30 min. Cells were incubated with Alexa Fluor 488-labeled anti-mouse IgG (1:1000) in FACS buffer at 4°C for 30 min and analyzed using a BD LSRII flow cytometer. Cell staining was quantified using FlowJo software (Tree Star).

Inhibition of CHIKV Infection with Soluble Glycosaminoglycans

Virus was pretreated with soluble heparin (Sigma) or bovine serum albumin (BSA; Sigma) at 4°C for 30 min. Vero cells were adsorbed with pretreated virus strains at an MOI of 1 PFU/cell at 37°C for 2 h. The inoculum was removed, and complete medium supplemented to contain 20 mM ammonium chloride was added to prevent subsequent cycles of infection. After incubation at 37°C for 24 h, cells were fixed and incubated with CHIKV-specific polyclonal antiserum and DAPI to detect nuclei. Infection was scored by indirect immunofluorescence. CHIKV-positive cells were enumerated in three fields of view containing at least 100 cells per field of view for triplicate samples and normalized to total cells per field.

Heparin-Agarose Binding Assay

Heparin-conjugated or unconjugated agarose beads were incubated with 5×10^9 genomes of various virus strains at 4°C for 30 min as described (99). Beads were washed with VDB containing 0.02% Tween 20, and beads or input virus were resuspended in sample buffer (50 mM Tris-HCl [pH 6.8], 2% [wt/vol] sodium dodecyl sulfate [SDS], 1% β-mercaptoethanol, 10% [vol/vol] glycerol, 0.04% [wt/vol] bromophenol blue) and boiled for 10 min. Samples were resolved by SDS-polyacrylamide gel electrophoresis (PAGE) in 10% polyacrylamide gels (Bio-Rad) and transferred to an Immun-Blot polyvinylidene difluoride (PVDF) membrane (Bio-Rad). Membranes were incubated with Tris-buffered saline (TBS) containing 5% milk at room temperature for 1 h followed by incubation with CHIKV-specific mAb CHK 48-G8 (1:2000) in TBS with 0.1% Tween 20 (TBS-T) at 4°C overnight. Membranes were washed three times with TBS-T and incubated with

IRDye 750 CW-labeled goat anti-mouse IgG (1:5000; LI-COR) in TBS-T at room temperature for 2 h. Membranes were washed three times with TBS-T and once with TBS. CHIKV-specific signal was detected using an Odyssey imaging system (LI-COR).

Infection of Mice

C57BL/6J mice were obtained from The Jackson Laboratory to establish breeding colonies. Mice (20-22 day old) were inoculated in the left rear footpad with 10^3 PFU of virus in PBS containing 1% bovine calf serum (BCS) in a 10 µl volume. Mock-infected animals received diluent alone. Mice were monitored for clinical signs of disease and weighed at 24-h intervals. At various intervals following infection, mice were euthanized by isoflurane overdose, blood was collected by cardiac puncture, and mice were perfused by intracardiac injection of PBS. Swelling of the feet was quantified using calipers. For analysis of viral replication, tissues were collected in PBS containing BCS, weighed, homogenized with a MagNA Lyser (Roche), and stored at -80°C. Viral titers in tissue homogenates were determined by plaque assay using BHK-21 cells. For RNA analysis, tissues were collected and homogenized in TRIzol Reagent (Life Technologies).

In Chapter IV, mice were inoculated subcutaneously in the left rear footpad with 10^3 PFU of SL15649 and treated on the day prior to infection and thereafter for 2 days with 40 µg of digoxin diluted in PBS containing 1% BCS by intraperitoneal injection. Tissues were harvested at 2 days postinoculation, and viral titers were determined by plaque assay using BHK-21 cells.

Animal husbandry and experiments were performed in accordance with all University of Colorado School of Medicine Institutional Animal Care and Use Committee guidelines. All mouse studies were performed using BSL3 conditions.

Histological Analysis

At day 7 postinoculation, mice were euthanized and perfused by intracardiac injection of 4% paraformaldehyde (PFA, pH 7.3). Tissues were resected and incubated in PFA at 4°C for at least 72 h. Fixed tissues were embedded in paraffin, and 5-μm sections were stained with hematoxylin and eosin (H&E) to assess histopathologic changes. Tissues were scored by an observer blinded to the conditions of the experiments for the presence, distribution, and severity of histologic lesions. For all tissue changes, the following scoring system was used: 0, no lesions; 1, minimal, 0-24% of tissue affected; 2, mild, 25-49% of tissue affected; 3, moderate, 50-75% of tissue affected; 4, marked, >75% of tissue affected.

Analysis of Sequence Reversion

RNA was isolated using a PureLink RNA minikit (Life Technologies). cDNA was generated using the SuperscriptIII First Strand kit (Life Technologies) with random hexamers and used for PCR amplification by KOD polymerase (Novagen) with CHIKV E2 sequence-specific forward (CHIKVE2for: 8336 5'-GGGCCGAAGAGTGGAGTCTT-3') and reverse (CHIKVE2rev: 9089 5' GACACCCCTGATCGCACATT-3') primers. Amplicons were cloned into pCR2.1

TOPO (Life Technologies) and sequenced over the mutagenized region of the E2 open-reading frame.

Generation of CHIKV Replicon Particles

A three-plasmid replicon system was used to generate CHIKV SL15649 replicon particles. Plasmids encoding CHIKV nonstructural proteins and eGFP, capsid protein, and the envelope glycoproteins (E3-E1) were linearized and transcribed *in vitro* using mMessage mMachine SP6 transcription kits (Ambion). BHK-21 cells were electroporated with viral RNAs generated from the three plasmids and incubated at 37°C for 24 h. Supernatants containing replicon particles were collected from electroporated cells, clarified by centrifugation, and stored at -80°C. Replicon particles were tested for propagation-competent recombinant virus by serial passage of replicon stocks on monolayers of Vero cells. Stocks were removed from the BSL3 laboratory only if cytopathic effect (CPE) was not detected 72 h after the second passage.

High-Throughput Screening of NIH Clinical Collection

U-2 OS cells seeded in 384-well plates were treated DMSO, 100 nM bafilomycin A1, or compounds from the NIH Clinical Collection (NCC) at a concentration of 1 μM using a Bravo Automated Liquid Handling Platform (Velocity 11/Agilent) and incubated at 37°C for 1 h. CHIKV SL15649 eGFP-expressing replicon particles were inoculated into wells at an MOI of 5 infectious units (IU)/cell and incubated at 37°C for 20-24 h. Medium was aspirated using an ELx405® Microplate Washer (Biotek), and cells were stained with Hoechst dye using a Multidrop® Combi Reagent Dispenser to stain nuclei.

Cells and nuclei were visualized by indirect immunofluorescence using an ImageXpress Micro XL imaging system. Total cells, infected cells, and GFP intensity were quantified using MetaXpress software in two fields of view per compound. The plate median and median absolute deviation (MAD) were calculated for each well and used to calculate robust *Z* scores with the following equation: *Z* score = ($\log_2$[percent infection]-$\log_2$[median])/($\log_2$[MAD] x 1.486). Candidates were considered positive if the robust *Z* score was $\leq$ -2 or $\geq$ 2 in at least two of three independent replicates.

Assessment of Cell Viability

U-2 OS cells seeded in 60-mm dishes were incubated with DMSO, STS as an inducer of apoptosis, or digoxin at increasing concentrations at 37°C for 6 h. Cells were washed with FACS buffer and stained with propidium iodide (PI; Sigma). Cell staining was quantified using a BD LSRII flow cytometer and FlowJo software (Tree Star). Alternatively, U-2 OS cells, HSFs, and Vero cells seeded in 96-well plates were incubated with DMSO, STS, or digoxin at increasing concentrations at 37°C for 6 h. PrestoBlue® reagent (Molecular Probes) was added to supernatants of compound-treated cells, and cells were incubated at 37°C for 30 min. Fluorescence as a surrogate for cell viability was quantified using a Synergy H1 plate reader (BioTek).

Generation of RRV and SINV Stocks

Plasmids containing the full-length cDNA sequences of RRV strain T48 (pRR64) and SINV strain AR339 (pTRSB) were provided by Richard Kuhn (Kuhn et al, *Virology*, 1991) and Robert Johnson (Polo et al, *J. Virol.,* 1988), respectively, and were generated

as described (177, 178). RRV and SINV infectious clone plasmids were linearized with SacI and XhoI restriction enzymes, respectively, and transcribed *in vitro* using mMessage mMachine SP6 transcription kits. BHK-21 cells were electroporated with viral RNA and incubated at 37°C for 24 h. Supernatants containing progeny virus were collected from electroporated cells, clarified by centrifugation, and stored at -80°C.

RRV and SINV Infectivity Assay

Vehicle or compound-treated U-2 OS cells seeded in 96-well plates (Costar) were adsorbed with RRV or SINV in VDB at an MOI of 10 or 5 PFU/cell, respectively, at 37°C for 1 h. The inoculum was removed, complete medium containing DMSO or compound was added, and cells were incubated at 37°C for an additional 5 h. Cells were fixed with ice-cold 100% methanol, washed with PBS, and incubated with PBS containing 5% FBS and 0.1% TX at room temperature for 1 h. Cells were incubated with RRV or SINV-specific polyclonal antiserum (1:1500) in PBS with FBS and TX at 4°C overnight. Cells were washed three times with PBS and incubated with Alexa Fluor 488-labeled anti-mouse IgG (1:1000) in PBS with FBS and TX at room temperature for 2 h. Cells also were incubated with DAPI to stain nuclei. Cells and nuclei were visualized by indirect immunofluorescence using an ImageXpress Micro XL imaging system. Percent infectivity was determined by dividing the number of virus-infected cells by the total number of cells per field.

Generation of Reovirus Virions and ISVPs

Reovirus strain T1L M1 P208S (179) was generated using plasmid-based reverse genetics (180). Purified virions were prepared as described (181). Reovirus particle concentration was determined from the equivalence of 1 unit of optical density at 260 nm to 2.1×10^{12} particles (182). Viral titers were determined by plaque assay using L929 cells (180). ISVPs were generated by treating particles with α-chymotrypsin (Sigma) as described (183).

Reovirus Infectivity Assay

Vehicle or compound-treated HBMECs seeded in 96-well plates (Costar) were adsorbed with reovirus virions or ISVPs at an MOI of 1500 particles/cell at room temperature for 1 h. The inoculum was removed, and cells were washed with PBS and incubated with medium containing DMSO or compound at 37°C for 20 h. After incubation, cells were fixed with ice-cold 100% methanol, washed with PBS, and incubated with PBS containing 5% BSA at room temperature for 15 min. Cells were incubated with reovirus-specific polyclonal antiserum (1:1000) in PBS with 0.5% TX at 37°C for 30 min. Cells were washed three times with PBS and incubated with Alexa Fluor 488-labeled anti-rabbit IgG (1:1000) in PBS with 0.5% TX at 37°C for 30 min. Cells also were incubated with DAPI to stain nuclei. Cells and nuclei were visualized by indirect immunofluorescence using an ImageXpress Micro XL imaging system. Percent infectivity was determined by dividing the number of virus-infected cells by the total number of cells per field.

RNA Electroporation Bypass of Virus Entry

U-2 OS cells pretreated with DMSO or inhibitor were removed from the culture dish, washed with PBS, and resuspended to a final concentration of 10^7 cells/ml. Cells were incubated with CHIKV SL15649 at an MOI of 0.01 PFU/cell at 37°C or electroporated with SL15649 RNA generated in vitro. Infected or electroporated cells were seeded into 24-well plates in complete medium or in medium containing DMSO or inhibitor. After incubation at 37°C for various intervals, 10% of the cell supernatant was collected and replaced with fresh medium. Viral titers in culture supernatants were determined by plaque assay using Vero cells.

Transient Transfections

In Chapter IV, U-2 OS cells seeded in 96-well plates were transfected with plasmids encoding human and murine α1 and α3 isoforms of the sodium-potassium ATPase using FuGENE 6 transfection reagent (Roche) according to the manufacturer's instructions. At 24 h post-transfection, cells were adsorbed with CHIKV strain 181/25 and infection was quantified by indirect immunofluorescence.

In Chapter V, U-2 OS cells or HBMECs were transfected with 10 nM nonspecific siRNA, $6V_0C$-specific siRNA, or PSME2-specific single or pooled siRNAs using Lipofectamine RNAi Max transfection reagent (Invitrogen) according to the manufacturer's instructions. At 48 h post-transfection, cells were harvested for determination of mRNA and protein levels or adsorbed with CHIKV strains. Infection was quantified by indirect immunofluorescence, and production of progeny virus was quantified by plaque assay.

Expression of Gene Transcripts by RT-PCR

In Chapter IV, RNA was isolated from U-2 OS and ST2 cells treated with 1 μM digoxin or infected with CHIKV 181/25 at an MOI of 5 PFU/cell for various intervals using a PureLink RNA minikit. cDNA was generated using the SuperscriptIII First Strand kit with random hexamers and used for PCR amplification by KOD polymerase with primers specific for the α1 and α3 isoforms of the sodium-potassium ATPase and GAPDH (Table VII-1). Reaction products were resolved by electrophoresis in 1% agarose gels (Life Technologies).

In Chapter V, RNA was isolated from U-2 OS cells and HBMECs that were untransfected or transfected with nonspecific (luciferase) siRNA or siRNAs specific for PSMA2, PSME2, or PSMF1. cDNA was generated and used for PCR amplification with primers specific for GAPDH, PSMA2, PSME2, and PSMF1 (Table VII-1).

Table VII-1. Primer sequences used to detect expression of gene transcripts.

Gene	Species	Forward Primer	Reverse Primer
ATP1A1	Human	CTG TGG ATT GGA GCG ATT CTT	ACC AGT GAG CGA GGA GTT AT
ATP1A1	Mouse	CCT GGA TGA ACT CCA TCG TAA A	TAGCACTTCGGATGCCAT AAG
ATP1A3	Human	GAG GTC TGC CGG AAA TAC AA	GAG AAG CAG CCA GTG ATG AT
ATP1A3	Mouse	CAG GGT CTG ACA CAC AGT AAA G	CAC TAT GCC CAG GTA CAG ATT G
GAPDH	Human/ mouse	CCC ATC ACC ATC TTC CAG	ATG ACC TTG CCC ACA GCC
PSMA2	Human	TGT GTA CCA AGA ACC CAT TCC	CCT CTG TCA TTT GCC CTT CA
PSME2	Human	GCA AGA GGA CTC CCT CAA TGT	CTT CTG GCT TAA CCA GGG CA
PSMF1	Human	GTG GTG ACA CAC GGT TAC TT	GAA GCT CCT CAC TGT TCT TGT

Identification of Digoxin-Resistant Mutations

CHIKV strains SL15649 and 181/25 were passaged serially in U-2 OS cells in the presence of DMSO or digoxin to select drug-resistant mutant viruses. U-2 OS cells seeded in T25 flasks were adsorbed with CHIKV SL15649 or 181/25 at an MOI of 0.01 PFU/cell in VDB at 37°C for 1 h. Virus was removed, and complete medium containing either DMSO or 100 nM digoxin was added to cells. Cells were incubated at 37°C for 48-72 h or until CPE was comparable between DMSO- and digoxin-treated cells. Cell culture supernatants were harvested, and 20% was used to inoculate a fresh flask of U-2 OS cells. The remaining supernatant was stored at -80°C. The digoxin concentration was increased when CPE developed with similar kinetics between DMSO- and digoxin-treated cells. Viruses were passaged in this manner until the digoxin concentration required to inhibit CPE production was 5 times the EC_{50} for the drug in U-2 OS cells. Titers of cell-culture supernatants at each passage were determined by plaque assay using Vero cells. Cell-culture supernatants were tested for infection in digoxin-treated U-2 OS cells. RNA was isolated from cell-culture supernatants using a PureLink RNA minikit. cDNA was generated using the SuperscriptIII First Strand kit with random hexamers and subjected to PCR amplification using KOD polymerase with CHIKV-specific primer sets to enable amplification of the entire viral genome (Table VII-2). Amplicons were cloned into pCR2.1 TOPO and sequenced. Candidate mutations for digoxin-resistance were identified as polymorphic residues in virus stocks passaged in the presence of digoxin compared with those passaged in the presence of DMSO.

Table VII-2. Primers used for sequencing of CHIKV strain SL15649.

Genome Region (Approximate)	Forward Primer	Reverse Primer
1-809	GTG AGA CAC ACG TAG CCT ACC	TTC CGT CAG GTC TGT TGA AC
455-1300	AGA CAG AGA GCA GAC GTC GC	CTT ACT GAA GGC TTG GGC G
1032-1900	ATG ACC GGC ATC CTT GCT AC	ACG TCT TCA CTT GCT CCG CT
1539-2518	ACT GCC CAA CTA ACA GAC CAC GTC G	CGG TGC TGA TTT CTT GGC AGT TTT C
2239-3104	GCG GAA AGA AAG AAA ACT GC	TCC ACC TCC CAC TCC TTA AT
2827-3700	TCA GAG CAC GTC AAC GTA CT	TTA GTA GGC AGT GCA AGG TT
3442-4307	CAC ACT CAT TAG TGG CCG AA	TTT GCG GTT CCT ACT GGT GT
4028-4956	GTT ACC GGG TGA CGG TGT T	TGC ATC ATC CAC CGG GCA TT
4655-5545	ACA GAG GCC AAT GAG CAA GT	GTA CTC GGT GGT GCC TGA AG
5247-6100	AAC CTG ACT GTG ACA TGT GAC	ACT CAT TAC ATG CTG CCA CT
5840-6760	CGG ACT ACA TAT CCG GCG	CCC ACA TAG GTA TGC TGT CG
6424-7300	CAG GAT GTA CCA ATG GAT AGG	CAA GCT GTT CCT GTC ACA GT
7094-7921	TGG ATG AAC ATG GAA GTG AAG	CGA TTT TCA TGC ACA TCC TC
7656-8530	CGG TAC CCC AAC AGA AGC CA	CGT AGG GTT TCC TCC GGT TC
8280-9136	GGG CCG AAG AGT GGA GTC TT	AAT GTG CGA TCA GGG GTG TC
8894-9720	CAC CCA TTT CAC CAC GAC CC	CCA TAC CCA CCA TCG ACA GG
9452-10320	GAG GTC ACG TGG GGC AAC AA	ATG GGT AGA CGC CGG TGA AG
10093-10920	TCG CTT GAT TAC ATC ACG TG	CGA CAT GTC CGT TAA AGA GG
10601-11520	TGG CTA AAA GAA CGC GGG GC	GGT TGC GTA GCC CTT TGA TC
11239-12039	AAT TAA GTA TGA AGG TAT ATG TG	GCG CGC TTT TTT TTT TTT TTT TTT TTT TTG

High-Throughput RNAi Screening

Lipofectamine® RNAiMAX (Life Technologies) was incubated in McCoy's 5A medium at room temperature for 5 min and dispensed into 384-well plates containing either nonspecific (Luciferase), control ($6V_0C$, or STAT1), or pooled siRNAs from the Dharmacon ON-TARGETplus® SMARTpool® Human siRNA Library (GE Healthcare Life Sciences). After 15 min, U-2 OS cells were added to wells and incubated at 37ºC for 48 h. Transfection reagent and cells were dispensed using a MultiFlo Microplate Dispenser (Biotek). Medium was removed using a Bravo Automated Liquid Handling Platform, and CHIKV SL15649 eGFP-expressing replicon particles were inoculated into wells at an MOI of 5 IU/cell using a Multidrop® Combi Reagent Dispenser (Thermo Scientific) and incubated at 37ºC for 18-24 h. Medium was aspirated using an ELx405® Microplate Washer (Biotek), and cells were stained with Hoechst dye using a Multidrop® Combi Reagent Dispenser to stain nuclei. Cells and nuclei were visualized by indirect immunofluorescence using an ImageXpress Micro XL imaging system. Total cells, infected cells, and GFP intensity were quantified using MetaXpress software in two fields of view per siRNA pool. The plate median and median absolute deviation (MAD) were calculated for each well and used to calculate robust *Z* scores with the following equation: *Z* score = ($\log_2$[percent infection]-$\log_2$[median])/($\log_2$[MAD] x 1.486).

Immunoblotting for PSME2

Total cell lysates of U-2 OS cells transfected with nonspecific or PSME2-specific siRNAs were resolved by SDS-PAGE in 10% polyacrylamide gels and transferred to an Immun-Blot PVDF membrane. Membranes were incubated with TBS containing 5%

milk at room temperature for 1 h followed by incubation with PSME2-specific mAb (1:2000) in TBS with 0.1% Tween 20 (TBS-T) at 4°C overnight. Membranes were washed three times with TBS-T and incubated with IRDye 750 CW-labeled goat anti-mouse IgG (1:5000; LI-COR) in TBS-T at room temperature for 2 h. Membranes were washed three times with TBS-T and once with TBS, and CHIKV-specific signal was detected using an Odyssey imaging system (LI-COR).

Confocal Microscopy of CHIKV-Infected Cells

U-2 OS cells seeded onto no. 2 glass coverslips (VWR) in 24-well plates were adsorbed with CHIKV strain 181/25 in VDB at an MOI of 1 PFU/cell at 37°C for 1 h. Virus was removed, and cells were incubated in complete medium for 5 h. Cells were washed with PBS, fixed with 10% formalin, and quenched with 0.1 M glycine. Cells were incubated with 1% TX for 5 min and PBS-BGT (PBS, 0.5% BSA, 0.1% glycine, 0.05% Tween 20) for 10 min. Cells were incubated with PSME2-specific monoclonal antiserum (1:500) and CHIKV-specific polyclonal antiserum (1:1500) in PBS-BGT for 1 h, washed with PBS-BGT, and incubated with Alexa Fluor 488 IgG and Alexa Fluor 546 IgG (1:1000) in PBS-BGT for 1 h. Nuclei were visualized by incubating cells with TO-PRO-3 stain (Invitrogen) conjugated to Alexa Fluor 642 (1:1000) in PBS-BGT for 20 min. Cells were washed with PBS-BGT, and coverslips were placed on slides using Aqua-Poly/Mount mounting medium (Polysciences, Inc.). Images were captured using a Zeiss LSM 510 Meta laser scanning confocal microscope.

Statistical Analysis

Mean values for at least duplicate experiments were compared using an unpaired Student's *t* test, one-way analysis of variance (ANOVA) followed by Bonferroni or Tukey *post hoc* test, or Kruskal-Wallis followed by Dunn's *post hoc* test (GraphPad Prism). *P* values of < 0.05 were considered to be statistically significant.

REFERENCES

1. **Griffin, DE.** 2001. Alphaviruses, p. 917-962. *In* D. M. Knipe and P. M. Howley (ed.), Fields Virology, Fourth ed. Lippincott-Raven Press, Philadelphia.

2. **Robinson, MC.** 1955. An epidemic of virus disease in Southern Province, Tanganyika Territory, in 1952-53. I. Clinical features. Transactions of the Royal Society of Tropical Medicine and Hygiene **49:**28-32.

3. **Carey, DE.** 1971. Chikungunya and dengue: a case of mistaken identity? J Hist Med Allied Sci **26:**243-262.

4. **Simizu, B, Yamamoto, K, Hashimoto, K, and Ogata, T.** 1984. Structural proteins of Chikungunya virus. J Virol **51:**254-258.

5. **Powers, AM, and Logue, CH.** 2007. Changing patterns of chikungunya virus: re-emergence of a zoonotic arbovirus. Journal of General Virology **88:**2363-2377.

6. **Sergon, K, Njuguna, C, Kalani, R, Ofula, V, Onyango, C, Konongoi, LS, Bedno, S, Burke, H, Dumilla, AM, Konde, J, Njenga, MK, Sang, R, and Breiman, RF.** 2008. Seroprevalence of Chikungunya virus (CHIKV) infection on Lamu Island, Kenya, October 2004. Am J Trop Med Hyg **78:**333-337.

7. **Renault, P, Solet, JL, Sissoko, D, Balleydier, E, Larrieu, S, Filleul, L, Lassalle, C, Thiria, J, Rachou, E, de Valk, H, Ilef, D, Ledrans, M, Quatresous, I, Quenel, P, and Pierre, V.** 2007. A major epidemic of chikungunya virus infection on Reunion Island, France, 2005-2006. American Journal of Tropical Medicine and Hygiene **77:**727-731.

8. **Arankalle, VA, Shrivastava, S, Cherian, S, Gunjikar, RS, Walimbe, AM, Jadhav, SM, Sudeep, AB, and Mishra, AC.** 2007. Genetic divergence of Chikungunya viruses in India (1963-2006) with special reference to the 2005-2006 explosive epidemic. Journal of General Virology **88:**1967-1976.

9. **Johnson, DF, Druce, JD, Chapman, S, Swaminathan, A, Wolf, J, Richards, JS, Korman, T, Birch, C, and Richards, MJ.** 2008. Chikungunya virus infection in travellers to Australia. Medical Journal of Australia **188:**41-43.

10. **Rezza, G, Nicoletti, L, Angelini, R, Romi, R, Finarelli, AC, Panning, M, Cordioli, P, Fortuna, C, Boros, S, Magurano, F, Silvi, G, Angelini, P, Dottori, M, Ciufolini, MG, Majori, GC, Cassone, A, and group, Cs.** 2007. Infection with chikungunya virus in Italy: an outbreak in a temperate region. Lancet **370:**1840-1846.

11. **Simon, F, Parola, P, Grandadam, M, Fourcade, S, Oliver, M, Brouqui, P, Hance, P, Kraemer, P, Ali Mohamed, A, de Lamballerie, X, Charrel, R, and Tolou, H.** 2007. Chikungunya infection: an emerging rheumatism among

travelers returned from Indian Ocean islands. Report of 47 cases. Medicine (Baltimore) **86:**123-137.

12. **Grandadam, M, Caro, V, Plumet, S, Thiberge, JM, Souares, Y, Failloux, AB, Tolou, HJ, Budelot, M, Cosserat, D, Leparc-Goffart, I, and Despres, P.** 2011. Chikungunya virus, southeastern France. Emerg Infect Dis **17:**910-913.

13. **Gibney, KB, Fischer, M, Prince, HE, Kramer, LD, St George, K, Kosoy, OL, Laven, JJ, and Staples, JE.** 2011. Chikungunya fever in the United States: a fifteen year review of cases. Clin Infect Dis **52:**e121-126.

14. **Schuffenecker, I, Iteman, I, Michault, A, Murri, S, Frangeul, L, Vaney, MC, Lavenir, R, Pardigon, N, Reynes, JM, Pettinelli, F, Biscornet, L, Diancourt, L, Michel, S, Duquerroy, S, Guigon, G, Frenkiel, MP, Brehin, AC, Cubito, N, Despres, P, Kunst, F, Rey, FA, Zeller, H, and Brisse, S.** 2006. Genome microevolution of chikungunya viruses causing the Indian Ocean outbreak. PLoS Med **3:**e263.

15. **Cassadou, S, Boucau, S, Petit-Sinturel, M, Huc, P, Leparc-Goffart, I, and Ledrans, M.** 2014. Emergence of chikungunya fever on the French side of Saint Martin island, October to December 2013. Euro Surveill. **19**.

16. **Leparc-Goffart, I, Nougairede, A, Cassadou, S, Prat, C, and de Lamballerie, X.** 2014. Chikungunya in the Americas. Lancet **383:**514.

17. **Lanciotti, RS, and Valadere, AM.** 2014. Transcontinental movement of Asian genotype chikungunya virus. Emerging Infectious Diseases **20:**1400-1402.

18. **Marchette, NJ, Rudnick, A, Garcia, R, and MacVean, DW.** 1978. Alphaviruses in Peninusular Malaysia: I. Virus isolations and animal serology. Southeast Asian Journal of Tropical Medicine and Public Health **9:**317-329.

19. **Nakgoi, K, Nitatpattana, N, Wajjwalku, W, Pongsopawijit, P, Kaewchot, S, Yoksan, S, Siripolwat, V, Souris, M, and Gonzalez, JP.** Dengue, Japanese encephalitis and Chikungunya virus antibody prevalence among captive monkey (Macaca nemestrina) colonies of Northern Thailand. American Journal of Primatology **76:**97-102.

20. **Singh, SK, and Unni, SK.** Chikungunya virus: host pathogen interaction. Rev Med Virol **21:**78-88.

21. **Tsetsarkin, KA, Vanlandingham, DL, McGee, CE, and Higgs, S.** 2007. A single mutation in chikungunya virus affects vector specificity and epidemic potential. PLoS Pathog **3:**e201.

22. **Tsetsarkin, KA, McGee, CE, Volk, SM, Vanlandingham, DL, Weaver, SC, and Higgs, S.** 2009. Epistatic roles of E2 glycoprotein mutations in adaption of chikungunya virus to Aedes albopictus and Ae. aegypti mosquitoes. PLoS One **4:**e6835.

23. **Her, Z, Kam, YW, Lin, RT, and Ng, LF.** 2009. Chikungunya: a bending reality. Microbes Infect **11:**1165-1176.

24. **Tsetsarkin, KA, Chen, R, Leal, G, Forrester, N, Higgs, S, Huang, J, and Weaver, SC.** 2011. Chikungunya virus emergence is constrained in Asia by lineage-specific adaptive landscapes. Proceedings of the National Academy of Sciences of the United States of America **108:**7872-7877.

25. **Sissoko, D, Moendandze, A, Malvy, D, Giry, C, Ezzedine, K, Solet, JL, and Pierre, V.** 2008. Seroprevalence and risk factors of chikungunya virus infection in Mayotte, Indian Ocean, 2005-2006: a population-based survey. PLoS One **3:**e3066.

26. **Queyriaux, B, Simon, F, Grandadam, M, Michel, R, Tolou, H, and Boutin, JP.** 2008. Clinical burden of chikungunya virus infection. Lancet Infect Dis **8:**2-3.

27. **Borgherini, G, Poubeau, P, Jossaume, A, Gouix, A, Cotte, L, Michault, A, Arvin-Berod, C, and Paganin, F.** 2008. Persistent arthralgia associated with chikungunya virus: a study of 88 adult patients on reunion island. Clinical Infectious Diseases **47:**469-475.

28. **Suhrbier, A, Jaffar-Bandjee, MC, and Gasque, P.** 2012. Arthritogenic alphaviruses--an overview. Nat. Rev. Rheumatol. **8:**420-429.

29. **Economopoulou, A, Dominguez, M, Helynck, B, Sissoko, D, Wichmann, O, Quenel, P, Germonneau, P, and Quatresous, I.** 2009. Atypical Chikungunya virus infections: clinical manifestations, mortality and risk factors for severe disease during the 2005-2006 outbreak on Reunion. Epidemiol Infect **137:**534-541.

30. **Borgherini, G, Poubeau, P, Staikowsky, F, Lory, M, Le Moullec, N, Becquart, JP, Wengling, C, Michault, A, and Paganin, F.** 2007. Outbreak of chikungunya on Reunion Island: early clinical and laboratory features in 157 adult patients. Clin Infect Dis **44:**1401-1407.

31. **Tandale, BV, Sathe, PS, Arankalle, VA, Wadia, RS, Kulkarni, R, Shah, SV, Shah, SK, Sheth, JK, Sudeep, AB, Tripathy, AS, and Mishra, AC.** 2009. Systemic involvements and fatalities during Chikungunya epidemic in India, 2006. J Clin Virol **46:**145-149.

32. **Gerardin, P, Barau, G, Michault, A, Bintner, M, Randrianaivo, H, Choker, G, Lenglet, Y, Touret, Y, Bouveret, A, Grivard, P, Le Roux, K, Blanc, S, Schuffenecker, I, Couderc, T, Arenzana-Seisdedos, F, Lecuit, M, and Robillard, PY.** 2008. Multidisciplinary prospective study of mother-to-child chikungunya virus infections on the island of La Reunion. PLoS Medicine **5:**e60.

33. **Gerardin, P, Samperiz, S, Ramful, D, Boumahni, B, Bintner, M, Alessandri, JL, Carbonnier, M, Tiran-Rajaoefera, I, Beullier, G, Boya, I, Noormahomed, T, Okoi, J, Rollot, O, Cotte, L, Jaffar-Bandjee, MC, Michault, A, Favier, F,**

Kaminski, M, Fourmaintraux, A, and Fritel, X. 2014. Neurocognitive outcome of children exposed to perinatal mother-to-child Chikungunya virus infection: the CHIMERE cohort study on Reunion Island. PLoS Negl. Trop. Dis. **8:**e2996.

34. **Robin, S, Ramful, D, Le Seach, F, Jaffar-Bandjee, MC, Rigou, G, and Alessandri, JL.** 2008. Neurologic manifestations of pediatric chikungunya infection. Journal of Child Neurology **23:**1028-1035.

35. **de Andrade, DC, Jean, S, Clavelou, P, Dallel, R, and Bouhassira, D.** 2010. Chronic pain associated with the Chikungunya Fever: long lasting burden of an acute illness. BMC Infect Dis **10:**31.

36. **Soumahoro, MK, Gerardin, P, Boelle, PY, Perrau, J, Fianu, A, Pouchot, J, Malvy, D, Flahault, A, Favier, F, and Hanslik, T.** 2009. Impact of Chikungunya virus infection on health status and quality of life: a retrospective cohort study. PLoS One **4:**e7800.

37. **Nakaya, HI, Gardner, J, Poo, YS, Major, L, Pulendran, B, and Suhrbier, A.** Gene profiling of Chikungunya virus arthritis in a mouse model reveals significant overlap with rheumatoid arthritis. Arthritis and Rheumatism **64:**3553-3563.

38. **Bernard, E, Solignat, M, Gay, B, Chazal, N, Higgs, S, Devaux, C, and Briant, L.** 2010. Endocytosis of chikungunya virus into mammalian cells: role of clathrin and early endosomal compartments. PLoS One **5:**e11479.

39. **Voss, JE, Vaney, MC, Duquerroy, S, Vonrhein, C, Girard-Blanc, C, Crublet, E, Thompson, A, Bricogne, G, and Rey, FA.** 2010. Glycoprotein organization of Chikungunya virus particles revealed by X-ray crystallography. Nature **468:**709-712.

40. **Fields, BN, Knipe, DM, and Howley, PM.** 2007. Fields' virology, 5th ed. Wolters Kluwer Health/Lippincott Williams & Wilkins, Philadelphia.

41. **Sourisseau, M, Schilte, C, Casartelli, N, Trouillet, C, Guivel-Benhassine, F, Rudnicka, D, Sol-Foulon, N, Le Roux, K, Prevost, MC, Fsihi, H, Frenkiel, MP, Blanchet, F, Afonso, PV, Ceccaldi, PE, Ozden, S, Gessain, A, Schuffenecker, I, Verhasselt, B, Zamborlini, A, Saib, A, Rey, FA, Arenzana-Seisdedos, F, Despres, P, Michault, A, Albert, ML, and Schwartz, O.** 2007. Characterization of reemerging chikungunya virus. PLoS Pathog **3:**e89.

42. **Sanchez-San Martin, C, Liu, CY, and Kielian, M.** 2009. Dealing with low pH: entry and exit of alphaviruses and flaviviruses. Trends Microbiol **17:**514-521.

43. **Li, L, Jose, J, Xiang, Y, Kuhn, RJ, and Rossmann, MG.** 2010. Structural changes of envelope proteins during alphavirus fusion. Nature **468:**705-708.

44. **Khan, AH, Morita, K, Parquet Md Mdel, C, Hasebe, F, Mathenge, EG, and Igarashi, A.** 2002. Complete nucleotide sequence of chikungunya virus and

evidence for an internal polyadenylation site. Journal of General Virology **83:**3075-3084.

45. **Solignat, M, Gay, B, Higgs, S, Briant, L, and Devaux, C.** 2009. Replication cycle of chikungunya: a re-emerging arbovirus. Virology **393:**183-197.

46. **Firth, AE, Chung, BY, Fleeton, MN, and Atkins, JF.** 2008. Discovery of frameshifting in alphavirus 6K resolves a 20-year enigma. Virol. J. **5:**108.

47. **Snyder, JE, Kulcsar, KA, Schultz, KL, Riley, CP, Neary, JT, Marr, S, Jose, J, Griffin, DE, and Kuhn, RJ.** 2013. Functional characterization of the alphavirus TF protein. J Virol **87:**8511-8523.

48. **Strauss, JH, and Strauss, EG.** 1994. The alphaviruses: gene expression, replication, and evolution. Microbiol. Rev. **58:**491-562.

49. **Konishi, E, and Hotta, S.** 1980. Studies on structural proteins of Chikungunya Virus. I. Separation of three species of proteins and their preliminary characterization. Microbiology and Immunology **24:**419-428.

50. **de Curtis, I, and Simons, K.** 1988. Dissection of Semliki Forest virus glycoprotein delivery from the trans-Golgi network to the cell surface in permeabilized BHK cells. Proceedings of the National Academy of Sciences of the United States of America **85:**8052-8056.

51. **Ozden, S, Lucas-Hourani, M, Ceccaldi, PE, Basak, A, Valentine, M, Benjannet, S, Hamelin, J, Jacob, Y, Mamchaoui, K, Mouly, V, Despres, P, Gessain, A, Butler-Browne, G, Chretien, M, Tangy, F, Vidalain, PO, and Seidah, NG.** 2008. Inhibition of Chikungunya virus infection in cultured human muscle cells by furin inhibitors: impairment of the maturation of the E2 surface glycoprotein. Journal of Biological Chemistry **283:**21899-21908.

52. **Jose, J, Snyder, JE, and Kuhn, RJ.** 2009. A structural and functional perspective of alphavirus replication and assembly. Future Microbiol **4:**837-856.

53. **Couderc, T, Chretien, F, Schilte, C, Disson, O, Brigitte, M, Guivel-Benhassine, F, Touret, Y, Barau, G, Cayet, N, Schuffenecker, I, Despres, P, Arenzana-Seisdedos, F, Michault, A, Albert, ML, and Lecuit, M.** 2008. A mouse model for Chikungunya: young age and inefficient type-I interferon signaling are risk factors for severe disease. PLoS Pathogens **4:**e29.

54. **Ziegler, SA, Lu, L, da Rosa, AP, Xiao, SY, and Tesh, RB.** 2008. An animal model for studying the pathogenesis of chikungunya virus infection. American Journal of Tropical Medicine and Hygiene **79:**133-139.

55. **Gardner, J, Anraku, I, Le, TT, Larcher, T, Major, L, Roques, P, Schroder, WA, Higgs, S, and Suhrbier, A.** 2010. Chikungunya virus arthritis in adult wild-type mice. J Virol **84:**8021-8032.

56. **Schilte, C, Couderc, T, Chretien, F, Sourisseau, M, Gangneux, N, Guivel-Benhassine, F, Kraxner, A, Tschopp, J, Higgs, S, Michault, A, Arenzana-Seisdedos, F, Colonna, M, Peduto, L, Schwartz, O, Lecuit, M, and Albert, ML.** 2010. Type I IFN controls chikungunya virus via its action on nonhematopoietic cells. Journal of Experimental Medicine **207:**429-442.

57. **Morrison, TE, Oko, L, Montgomery, SA, Whitmore, AC, Lotstein, AR, Gunn, BM, Elmore, SA, and Heise, MT.** 2011. A mouse model of chikungunya virus-induced musculoskeletal inflammatory disease: evidence of arthritis, tenosynovitis, myositis, and persistence. American Journal of Pathology **178:**32-40.

58. **Werneke, SW, Schilte, C, Rohatgi, A, Monte, KJ, Michault, A, Arenzana-Seisdedos, F, Vanlandingham, DL, Higgs, S, Fontanet, A, Albert, ML, and Lenschow, DJ.** 2011. ISG15 is critical in the control of Chikungunya virus infection independent of UbE1L mediated conjugation. PLoS Pathogens **7:**e1002322.

59. **Hawman, DW, Stoermer, KA, Montgomery, SA, Pal, P, Oko, L, Diamond, MS, and Morrison, TE.** 2013. Chronic joint disease caused by persistent Chikungunya virus infection is controlled by the adaptive immune response. Journal of Virology **87:**13878-13888.

60. **Poo, YS, Rudd, PA, Gardner, J, Wilson, JA, Larcher, T, Colle, MA, Le, TT, Nakaya, HI, Warrilow, D, Allcock, R, Bielefeldt-Ohmann, H, Schroder, WA, Khromykh, AA, Lopez, JA, and Suhrbier, A.** 2014. Multiple immune factors are involved in controlling acute and chronic chikungunya virus infection. PLoS Negl. Trop. Dis. **8:**e3354.

61. **Ng, LF, Chow, A, Sun, YJ, Kwek, DJ, Lim, PL, Dimatatac, F, Ng, LC, Ooi, EE, Choo, KH, Her, Z, Kourilsky, P, and Leo, YS.** 2009. IL-1beta, IL-6, and RANTES as biomarkers of Chikungunya severity. PLoS One **4:**e4261.

62. **Kelvin, AA, Banner, D, Silvi, G, Moro, ML, Spataro, N, Gaibani, P, Cavrini, F, Pierro, A, Rossini, G, Cameron, MJ, Bermejo-Martin, JF, Paquette, SG, Xu, L, Danesh, A, Farooqui, A, Borghetto, I, Kelvin, DJ, Sambri, V, and Rubino, S.** 2011. Inflammatory cytokine expression is associated with chikungunya virus resolution and symptom severity. PLoS Negl. Trop. Dis. **5:**e1279.

63. **Lohachanakul, J, Phuklia, W, Thannagith, M, Thonsakulprasert, T, and Ubol, S.** 2012. High concentrations of circulating interleukin-6 and monocyte chemotactic protein-1 with low concentrations of interleukin-8 were associated with severe chikungunya fever during the 2009-2010 outbreak in Thailand. Microbiology and Immunology **56:**134-138.

64. **Herrero, LJ, Sheng, KC, Jian, P, Taylor, A, Her, Z, Herring, BL, Chow, A, Leo, YS, Hickey, MJ, Morand, EF, Ng, LF, Bucala, R, and Mahalingam, S.** 2013. Macrophage migration inhibitory factor receptor CD74 mediates

alphavirus-induced arthritis and myositis in murine models of alphavirus infection. Arthritis & Rheumatism **65:**2724-2736.

65. **Venugopalan, A, Ghorpade, RP, and Chopra, A.** 2014. Cytokines in acute chikungunya. PLoS One **9:**e111305.

66. **Gardner, CL, Hritz, J, Sun, C, Vanlandingham, DL, Song, TY, Ghedin, E, Higgs, S, Klimstra, WB, and Ryman, KD.** 2014. Deliberate attenuation of chikungunya virus by adaptation to heparan sulfate-dependent infectivity: a model for rational arboviral vaccine design. PLoS Negl. Trop. Dis. **8:**e2719.

67. **Teo, TH, Lum, FM, Claser, C, Lulla, V, Lulla, A, Merits, A, Renia, L, and Ng, LF.** 2013. A pathogenic role for CD4+ T cells during Chikungunya virus infection in mice. Journal of Immunology **190:**259-269.

68. **Ozden, S, Huerre, M, Riviere, JP, Coffey, LL, Afonso, PV, Mouly, V, de Monredon, J, Roger, JC, El Amrani, M, Yvin, JL, Jaffar, MC, Frenkiel, MP, Sourisseau, M, Schwartz, O, Butler-Browne, G, Despres, P, Gessain, A, and Ceccaldi, PE.** 2007. Human muscle satellite cells as targets of Chikungunya virus infection. PLoS One **2:**e527.

69. **Hoarau, JJ, Jaffar Bandjee, MC, Krejbich Trotot, P, Das, T, Li-Pat-Yuen, G, Dassa, B, Denizot, M, Guichard, E, Ribera, A, Henni, T, Tallet, F, Moiton, MP, Gauzere, BA, Bruniquet, S, Jaffar Bandjee, Z, Morbidelli, P, Martigny, G, Jolivet, M, Gay, F, Grandadam, M, Tolou, H, Vieillard, V, Debre, P, Autran, B, and Gasque, P.** 2010. Persistent chronic inflammation and infection by Chikungunya arthritogenic alphavirus in spite of a robust host immune response. Journal of Immunology **184:**5914-5927.

70. **Powers, AM.** 2010. Chikungunya. Clin Lab Med **30:**209-219.

71. **Delogu, I, and de Lamballerie, X.** Chikungunya disease and chloroquine treatment. Journal of Medical Virology **83:**1058-1059.

72. **Chopra, A, Saluja, M, and Venugopalan, A.** 2014. Effectiveness of chloroquine and inflammatory cytokine response in patients with early persistent musculoskeletal pain and arthritis following chikungunya virus infection. Arthritis Rheumatol **66:**319-326.

73. **Ganu, MA, and Ganu, AS.** 2011. Post-chikungunya chronic arthritis--our experience with DMARDs over two year follow up. Journal of the Association of Physicians of India **59:**83-86.

74. **Taylor, A, Sheng, KC, Herrero, LJ, Chen, W, Rulli, NE, and Mahalingam, S.** 2013. Methotrexate treatment causes early onset of disease in a mouse model of Ross River virus-induced inflammatory disease through increased monocyte production. PLoS One **8:**e71146.

75. **Rulli, NE, Rolph, MS, Srikiatkhachorn, A, Anantapreecha, S, Guglielmotti, A, and Mahalingam, S.** 2011. Protection from arthritis and myositis in a mouse model of acute chikungunya virus disease by bindarit, an inhibitor of monocyte chemotactic protein-1 synthesis. Journal of Infectious Diseases **204:**1026-1030.

76. **Kaur, P, Thiruchelvan, M, Lee, RC, Chen, H, Chen, KC, Ng, ML, and Chu, JJ.** 2013. Inhibition of chikungunya virus replication by harringtonine, a novel antiviral that suppresses viral protein expression. Antimicrobial Agents and Chemotherapy **57:**155-167.

77. **Teng, TS, Foo, SS, Simamarta, D, Lum, FM, Teo, TH, Lulla, A, Yeo, NK, Koh, EG, Chow, A, Leo, YS, Merits, A, Chin, KC, and Ng, LF.** Viperin restricts chikungunya virus replication and pathology. Journal of Clinical Investigation **122:**4447-4460.

78. **Harrison, VR, Eckels, KH, Bartelloni, PJ, and Hampton, C.** 1971. Production and evaluation of a formalin-killed Chikungunya vaccine. J Immunol **107:**643-647.

79. **Levitt, NH, Ramsburg, HH, Hasty, SE, Repik, PM, Cole, FE, Jr., and Lupton, HW.** 1986. Development of an attenuated strain of chikungunya virus for use in vaccine production. Vaccine **4:**157-162.

80. **Edelman, R, Tacket, CO, Wasserman, SS, Bodison, SA, Perry, JG, and Mangiafico, JA.** 2000. Phase II safety and immunogenicity study of live chikungunya virus vaccine TSI-GSD-218. Am J Trop Med Hyg **62:**681-685.

81. **Akahata, W, Yang, ZY, Andersen, H, Sun, S, Holdaway, HA, Kong, WP, Lewis, MG, Higgs, S, Rossmann, MG, Rao, S, and Nabel, GJ.** 2010. A virus-like particle vaccine for epidemic Chikungunya virus protects nonhuman primates against infection. Nat Med **16:**334-338.

82. **Chu, H, Das, SC, Fuchs, JF, Suresh, M, Weaver, SC, Stinchcomb, DT, Partidos, CD, and Osorio, JE.** 2013. Deciphering the protective role of adaptive immunity to CHIKV/IRES a novel candidate vaccine against Chikungunya in the A129 mouse model. Vaccine **31:**3353-3360.

83. **Roy, CJ, Adams, AP, Wang, E, Plante, K, Gorchakov, R, Seymour, RL, Vinet-Oliphant, H, and Weaver, SC.** 2014. Chikungunya vaccine candidate is highly attenuated and protects nonhuman primates against telemetrically monitored disease following a single dose. Journal of Infectious Diseases **209:**1891-1899.

84. **Chattopadhyay, A, Wang, E, Seymour, R, Weaver, SC, and Rose, JK.** 2013. A chimeric vesiculo/alphavirus is an effective alphavirus vaccine. Journal of Virology **87:**395-402.

85. **Thiboutot, MM, Kannan, S, Kawalekar, OU, Shedlock, DJ, Khan, AS, Sarangan, G, Srikanth, P, Weiner, DB, and Muthumani, K.** 2010. Chikungunya: a potentially emerging epidemic? PLoS Negl Trop Dis **4:**e623.

86. **Renault, P, Solet, JL, Sissoko, D, Balleydier, E, Larrieu, S, Filleul, L, Lassalle, C, Thiria, J, Rachou, E, de Valk, H, Ilef, D, Ledrans, M, Quatresous, I, Quenel, P, and Pierre, V.** 2007. A major epidemic of chikungunya virus infection on Reunion Island, France, 2005-2006. Am J Trop Med Hyg **77:**727-731.

87. **Rezza, G, Nicoletti, L, Angelini, R, Romi, R, Finarelli, AC, Panning, M, Cordioli, P, Fortuna, C, Boros, S, Magurano, F, Silvi, G, Angelini, P, Dottori, M, Ciufolini, MG, Majori, GC, and Cassone, A.** 2007. Infection with chikungunya virus in Italy: an outbreak in a temperate region. Lancet **370:**1840-1846.

88. **Coffey, LL, and Vignuzzi, M.** 2011. Host alternation of chikungunya virus increases fitness while restricting population diversity and adaptability to novel selective pressures. J Virol **85:**1025-1035.

89. **Weaver, SC, Brault, AC, Kang, W, and Holland, JJ.** 1999. Genetic and fitness changes accompanying adaptation of an arbovirus to vertebrate and invertebrate cells. J Virol **73:**4316-4326.

90. **Krieger, N, Lohmann, V, and Bartenschlager, R.** 2001. Enhancement of hepatitis C virus RNA replication by cell culture-adaptive mutations. J Virol **75:**4614-4624.

91. **Blaney, JE, Jr., Manipon, GG, Firestone, CY, Johnson, DH, Hanson, CT, Murphy, BR, and Whitehead, SS.** 2003. Mutations which enhance the replication of dengue virus type 4 and an antigenic chimeric dengue virus type 2/4 vaccine candidate in Vero cells. Vaccine **21:**4317-4327.

92. **Greene, IP, Wang, E, Deardorff, ER, Milleron, R, Domingo, E, and Weaver, SC.** 2005. Effect of alternating passage on adaptation of sindbis virus to vertebrate and invertebrate cells. J Virol **79:**14253-14260.

93. **Volchkova, VA, Dolnik, O, Martinez, MJ, Reynard, O, and Volchkov, VE.** 2011. Genomic RNA editing and its impact on Ebola virus adaptation during serial passages in cell culture and infection of guinea pigs. J Infect Dis **204 Suppl 3:**S941-946.

94. **Klimstra, WB, Ryman, KD, and Johnston, RE.** 1998. Adaptation of Sindbis virus to BHK cells selects for use of heparan sulfate as an attachment receptor. J Virol **72:**7357-7366.

95. **Byrnes, AP, and Griffin, DE.** 1998. Binding of Sindbis virus to cell surface heparan sulfate. J Virol **72:**7349-7356.

96. **Bernard, KA, Klimstra, WB, and Johnston, RE.** 2000. Mutations in the E2 glycoprotein of Venezuelan equine encephalitis virus confer heparan sulfate interaction, low morbidity, and rapid clearance from blood of mice. Virology **276:**93-103.

97. **Heil, ML, Albee, A, Strauss, JH, and Kuhn, RJ.** 2001. An amino acid substitution in the coding region of the E2 glycoprotein adapts Ross River virus to utilize heparan sulfate as an attachment moiety. J Virol **75:**6303-6309.

98. **Smit, JM, Waarts, BL, Kimata, K, Klimstra, WB, Bittman, R, and Wilschut, J.** 2002. Adaptation of alphaviruses to heparan sulfate: interaction of Sindbis and Semliki forest viruses with liposomes containing lipid-conjugated heparin. J Virol **76:**10128-10137.

99. **Silva, LA, Khomandiak, S, Ashbrook, AW, Weller, R, Heise, MT, Morrison, TE, and Dermody, TS.** 2014. A single-amino-acid polymorphism in Chikungunya virus E2 glycoprotein influences glycosaminoglycan utilization. J Virol **88:**2385-2397.

100. **Gardner, CL, Burke, CW, Higgs, ST, Klimstra, WB, and Ryman, KD.** 2012. Interferon-alpha/beta deficiency greatly exacerbates arthritogenic disease in mice infected with wild-type chikungunya virus but not with the cell culture-adapted live-attenuated 181/25 vaccine candidate. Virology **425:**103-112.

101. **Sinnis, P, Coppi, A, Toida, T, Toyoda, H, Kinoshita-Toyoda, A, Xie, J, Kemp, MM, and Linhardt, RJ.** 2007. Mosquito heparan sulfate and its potential role in malaria infection and transmission. J Biol Chem **282:**25376-25384.

102. **Dinglasan, RR, Alaganan, A, Ghosh, AK, Saito, A, van Kuppevelt, TH, and Jacobs-Lorena, M.** 2007. Plasmodium falciparum ookinetes require mosquito midgut chondroitin sulfate proteoglycans for cell invasion. Proc Natl Acad Sci U S A **104:**15882-15887.

103. **Gidwitz, S, Polo, JM, Davis, NL, and Johnston, RE.** 1988. Differences in virion stability among Sindbis virus pathogenesis mutants. Virus Res **10:**225-239.

104. **Snyder, AJ, Sokoloski, KJ, and Mukhopadhyay, S.** 2012. Mutating conserved cysteines in the alphavirus e2 glycoprotein causes virus-specific assembly defects. J Virol **86:**3100-3111.

105. **Fields, W, and Kielian, M.** 2013. A key interaction between the alphavirus envelope proteins responsible for initial dimer dissociation during fusion. J Virol **87:**3774-3781.

106. **Cutler, DF, Melancon, P, and Garoff, H.** 1986. Mutants of the membrane-binding region of Semliki Forest virus E2 protein. II. Topology and membrane binding. J Cell Biol **102:**902-910.

107. **Lopez, S, Yao, JS, Kuhn, RJ, Strauss, EG, and Strauss, JH.** 1994. Nucleocapsid-glycoprotein interactions required for assembly of alphaviruses. J Virol **68:**1316-1323.

108. **Ryman, KD, Klimstra, WB, and Johnston, RE.** 2004. Attenuation of Sindbis virus variants incorporating uncleaved PE2 glycoprotein is correlated with attachment to cell-surface heparan sulfate. Virology **322:**1-12.

109. **Bear, JS, Byrnes, AP, and Griffin, DE.** 2006. Heparin-binding and patterns of virulence for two recombinant strains of Sindbis virus. Virology **347:**183-190.

110. **Ryman, KD, Gardner, CL, Burke, CW, Meier, KC, Thompson, JM, and Klimstra, WB.** 2007. Heparan sulfate binding can contribute to the neurovirulence of neuroadapted and nonneuroadapted Sindbis viruses. J Virol **81:**3563-3573.

111. **Lee, E, Wright, PJ, Davidson, A, and Lobigs, M.** 2006. Virulence attenuation of Dengue virus due to augmented glycosaminoglycan-binding affinity and restriction in extraneural dissemination. J Gen Virol **87:**2791-2801.

112. **Gardner, CL, Ebel, GD, Ryman, KD, and Klimstra, WB.** 2011. Heparan sulfate binding by natural eastern equine encephalitis viruses promotes neurovirulence. Proc Natl Acad Sci U S A **108:**16026-16031.

113. **Gardner, CL, Choi-Nurvitadhi, J, Sun, C, Bayer, A, Hritz, J, Ryman, KD, and Klimstra, WB.** 2013. Natural variation in the heparan sulfate binding domain of the eastern equine encephalitis virus E2 glycoprotein alters interactions with cell surfaces and virulence in mice. J Virol **87:**8582-8590.

114. **Ferguson, MC, Saul, S, Fragkoudis, R, Weisheit, S, Cox, J, Patabendige, A, Sherwood, K, Watson, M, Merits, A, and Fazakerley, JK.** 2015. The ability of the encephalitic arbovirus Semliki Forest virus to cross the blood brain barrier is determined by the charge of the E2 glycoprotein. Journal of Virology.

115. **Drake, JW, and Holland, JJ.** 1999. Mutation rates among RNA viruses. Proc Natl Acad Sci U S A **96:**13910-13913.

116. **Crotty, S, Maag, D, Arnold, JJ, Zhong, W, Lau, JY, Hong, Z, Andino, R, and Cameron, CE.** 2000. The broad-spectrum antiviral ribonucleoside ribavirin is an RNA virus mutagen. Nat Med **6:**1375-1379.

117. **Burt, FJ, Rolph, MS, Rulli, NE, Mahalingam, S, and Heise, MT.** 2012. Chikungunya: a re-emerging virus. Lancet **379:**662-671.

118. **Gorchakov, R, Wang, E, Leal, G, Forrester, NL, Plante, K, Rossi, SL, Partidos, CD, Adams, AP, Seymour, RL, Weger, J, Borland, EM, Sherman, MB, Powers, AM, Osorio, JE, and Weaver, SC.** 2012. Attenuation of Chikungunya virus vaccine strain 181/clone 25 is determined by two amino acid substitutions in the E2 envelope glycoprotein. J Virol **86:**6084-6096.

119. **Klimstra, WB, Ryman, KD, Bernard, KA, Nguyen, KB, Biron, CA, and Johnston, RE.** 1999. Infection of neonatal mice with sindbis virus results in a systemic inflammatory response syndrome. J Virol **73:**10387-10398.

120. **Byrnes, AP, and Griffin, DE.** 2000. Large-plaque mutants of Sindbis virus show reduced binding to heparan sulfate, heightened viremia, and slower clearance from the circulation. J Virol **74:**644-651.

121. **Gupta, RS, Chopra, A, and Stetsko, DK.** 1986. Cellular basis for the species differences in sensitivity to cardiac glycosides (digitalis). Journal of Cellular Physiology **127:**197-206.

122. **Kent, RB, Emanuel, JR, Ben Neriah, Y, Levenson, R, and Housman, DE.** 1987. Ouabain resistance conferred by expression of the cDNA for a murine Na+, K+-ATPase alpha subunit. Science **237:**901-903.

123. **Lin, Y, Dubinsky, WP, Ho, DH, Felix, E, and Newman, RA.** 2008. Determinants of human and mouse melanoma cell sensitivities to oleandrin. Journal of Experimental Therapeutics and Oncology **7:**195-205.

124. **Schoner, W, and Scheiner-Bobis, G.** 2007. Endogenous and exogenous cardiac glycosides and their mechanisms of action. Am J Cardiovasc Drugs **7:**173-189.

125. **Smith, TW.** 1988. Digitalis. Mechanisms of action and clinical use. New England Journal of Medicine **318:**358-365.

126. **Aizman, O, Uhlen, P, Lal, M, Brismar, H, and Aperia, A.** 2001. Ouabain, a steroid hormone that signals with slow calcium oscillations. Proceedings of the National Academy of Sciences of the United States of America **98:**13420-13424.

127. **Li, J, Zelenin, S, Aperia, A, and Aizman, O.** 2006. Low doses of ouabain protect from serum deprivation-triggered apoptosis and stimulate kidney cell proliferation via activation of NF-kappaB. Journal of the American Society of Nephrology **17:**1848-1857.

128. **Takeuchi, O, and Akira, S.** Pattern recognition receptors and inflammation. Cell **140:**805-820.

129. **Selvamani, SP, Mishra, R, and Singh, SK.** 2014. Chikungunya virus exploits miR-146a to regulate NF-kappaB pathway in human synovial fibroblasts. PLoS One **9:**e103624.

130. **Fontana, JM, Burlaka, I, Khodus, G, Brismar, H, and Aperia, A.** 2013. Calcium oscillations triggered by cardiotonic steroids. FEBS J **280:**5450-5455.

131. **Cain, CC, Sipe, DM, and Murphy, RF.** 1989. Regulation of endocytic pH by the Na+,K+-ATPase in living cells. Proceedings of the National Academy of Sciences of the United States of America **86:**544-548.

132. **Feldmann, T, Glukmann, V, Medvenev, E, Shpolansky, U, Galili, D, Lichtstein, D, and Rosen, H.** 2007. Role of endosomal Na+-K+-ATPase and cardiac steroids in the regulation of endocytosis. Am J Physiol Cell Physiol **293:**C885-896.

133. **Sanchez-San Martin, C, Nanda, S, Zheng, Y, Fields, W, and Kielian, M.** 2013. Cross-inhibition of chikungunya virus fusion and infection by alphavirus E1 domain III proteins. Journal of Virology **87:**7680-7687.

134. **Barton, ES, Forrest, JC, Connolly, JL, Chappell, JD, Liu, Y, Schnell, F, Nusrat, A, Parkos, CA, and Dermody, TS.** 2001. Junction adhesion molecule is a receptor for reovirus. Cell **104:**441-451.

135. **Sturzenbecker, LJ, Nibert, ML, Furlong, DB, and Fields, BN.** 1987. Intracellular digestion of reovirus particles requires a low pH and is an essential step in the viral infectious cycle. Journal of Virology **61:**2351-2361.

136. **Borsa, J, Morash, BD, Sargent, MD, Copps, TP, Lievaart, PA, and Szekely, JG.** 1979. Two modes of entry of reovirus particles into L cells. Journal of General Virology **45:**161-170.

137. **Boulant, S, Stanifer, M, Kural, C, Cureton, DK, Massol, R, Nibert, ML, and Kirchhausen, T.** 2013. Similar uptake but different trafficking and escape routes of reovirus virions and infectious subvirion particles imaged in polarized Madin-Darby canine kidney cells. Mol Biol Cell **24:**1196-1207.

138. **Thete, D, and Danthi, P.** 2015. Conformational changes required for reovirus cell entry are sensitive to pH. Virology **483:**291-301.

139. **Johansson, S, Lindholm, P, Gullbo, J, Larsson, R, Bohlin, L, and Claeson, P.** 2001. Cytotoxicity of digitoxin and related cardiac glycosides in human tumor cells. Anti-Cancer Drugs **12:**475-483.

140. **Paula, S, Tabet, MR, and Ball, WJ, Jr.** 2005. Interactions between cardiac glycosides and sodium/potassium-ATPase: three-dimensional structure-activity relationship models for ligand binding to the E2-Pi form of the enzyme versus activity inhibition. Biochemistry **44:**498-510.

141. **Nesher, M, Shpolansky, U, Rosen, H, and Lichtstein, D.** 2007. The digitalis-like steroid hormones: new mechanisms of action and biological significance. Life Sciences **80:**2093-2107.

142. **Huh, JR, Leung, MW, Huang, P, Ryan, DA, Krout, MR, Malapaka, RR, Chow, J, Manel, N, Ciofani, M, Kim, SV, Cuesta, A, Santori, FR, Lafaille, JJ, Xu, HE, Gin, DY, Rastinejad, F, and Littman, DR.** 2011. Digoxin and its derivatives suppress TH17 cell differentiation by antagonizing RORgammat activity. Nature **472:**486-490.

143. **Her, Z, Malleret, B, Chan, M, Ong, EK, Wong, SC, Kwek, DJ, Tolou, H, Lin, RT, Tambyah, PA, Renia, L, and Ng, LF.** 2010. Active infection of human blood monocytes by Chikungunya virus triggers an innate immune response. J Immunol **184:**5903-5913.

144. **Hoarau, JJ, Jaffar Bandjee, MC, Krejbich Trotot, P, Das, T, Li-Pat-Yuen, G, Dassa, B, Denizot, M, Guichard, E, Ribera, A, Henni, T, Tallet, F, Moiton, MP, Gauzere, BA, Bruniquet, S, Jaffar Bandjee, Z, Morbidelli, P, Martigny, G, Jolivet, M, Gay, F, Grandadam, M, Tolou, H, Vieillard, V, Debre, P, Autran, B, and Gasque, P.** 2010. Persistent chronic inflammation and infection by Chikungunya arthritogenic alphavirus in spite of a robust host immune response. J Immunol **184:**5914-5927.

145. **Labadie, K, Larcher, T, Joubert, C, Mannioui, A, Delache, B, Brochard, P, Guigand, L, Dubreil, L, Lebon, P, Verrier, B, de Lamballerie, X, Suhrbier, A, Cherel, Y, Le Grand, R, and Roques, P.** 2010. Chikungunya disease in nonhuman primates involves long-term viral persistence in macrophages. J Clin Invest **120:**894-906.

146. **Ryman, KD, and Klimstra, WB.** 2008. Host responses to alphavirus infection. Immunol Rev **225:**27-45.

147. **Brass, AL, Dykxhoorn, DM, Benita, Y, Yan, N, Engelman, A, Xavier, RJ, Lieberman, J, and Elledge, SJ.** 2008. Identification of host proteins required for HIV infection through a functional genomic screen. Science **319:**921-926.

148. **Sessions, OM, Barrows, NJ, Souza-Neto, JA, Robinson, TJ, Hershey, CL, Rodgers, MA, Ramirez, JL, Dimopoulos, G, Yang, PL, Pearson, JL, and Garcia-Blanco, MA.** 2009. Discovery of insect and human dengue virus host factors. Nature **458:**1047-1050.

149. **Tai, AW, Benita, Y, Peng, LF, Kim, SS, Sakamoto, N, Xavier, RJ, and Chung, RT.** 2009. A functional genomic screen identifies cellular cofactors of hepatitis C virus replication. Cell Host Microbe **5:**298-307.

150. **Krishnan, MN, Ng, A, Sukumaran, B, Gilfoy, FD, Uchil, PD, Sultana, H, Brass, AL, Adametz, R, Tsui, M, Qian, F, Montgomery, RR, Lev, S, Mason, PW, Koski, RA, Elledge, SJ, Xavier, RJ, Agaisse, H, and Fikrig, E.** 2008. RNA interference screen for human genes associated with West Nile virus infection. Nature **455:**242-245.

151. **Ooi, YS, Stiles, KM, Liu, CY, Taylor, GM, and Kielian, M.** 2013. Genome-wide RNAi screen identifies novel host proteins required for alphavirus entry. PLoS Pathogens **9:**e1003835.

152. **Yasunaga, A, Hanna, SL, Li, J, Cho, H, Rose, PP, Spiridigliozzi, A, Gold, B, Diamond, MS, and Cherry, S.** 2014. Genome-wide RNAi screen identifies broadly-acting host factors that inhibit arbovirus infection. PLoS Pathog **10:**e1003914.

153. **Poenisch, M, Metz, P, Blankenburg, H, Ruggieri, A, Lee, JY, Rupp, D, Rebhan, I, Diederich, K, Kaderali, L, Domingues, FS, Albrecht, M, Lohmann, V, Erfle, H, and Bartenschlager, R.** 2015. Identification of HNRNPK as regulator of hepatitis C virus particle production. PLoS Pathog **11:**e1004573.

154. **Ciechanover, A.** 1994. The ubiquitin-proteasome proteolytic pathway. Cell **79:**13-21.

155. **Sijts, A, Sun, Y, Janek, K, Kral, S, Paschen, A, Schadendorf, D, and Kloetzel, PM.** 2002. The role of the proteasome activator PA28 in MHC class I antigen processing. Molecular Immunology **39:**165-169.

156. **Ferrington, DA, and Gregerson, DS.** 2012. Immunoproteasomes: structure, function, and antigen presentation. Prog Mol Biol Transl Sci **109:**75-112.

157. **Amaya, M, Keck, F, Lindquist, M, Voss, K, Scavone, L, Kehn-Hall, K, Roberts, B, Bailey, C, Schmaljohn, C, and Narayanan, A.** 2015. The ubiquitin proteasome system plays a role in venezuelan equine encephalitis virus infection. PLoS One **10:**e0124792.

158. **Esko, JD, Kimata, K, and Lindahl, U.** 2009. Proteoglycans and sulfated glycosaminoglycans. *In* A. Varki, R. D. Cummings, J. D. Esko, H. H. Freeze, P. Stanley, C. R. Bertozzi, G. W. Hart, and M. E. Etzler (ed.), Essentials of Glycobiology, 2nd ed, Cold Spring Harbor (NY).

159. **Fibriansah, G, Ng, TS, Kostyuchenko, VA, Lee, J, Lee, S, Wang, J, and Lok, SM.** 2013. Structural changes in dengue virus when exposed to a temperature of 37 degrees C. Journal of Virology **87:**7585-7592.

160. **Condac, E, Silasi-Mansat, R, Kosanke, S, Schoeb, T, Towner, R, Lupu, F, Cummings, RD, and Hinsdale, ME.** 2007. Polycystic disease caused by deficiency in xylosyltransferase 2, an initiating enzyme of glycosaminoglycan biosynthesis. Proceedings of the National Academy of Sciences of the United States of America **104:**9416-9421.

161. **Gotting, C, Kuhn, J, Zahn, R, Brinkmann, T, and Kleesiek, K.** 2000. Molecular cloning and expression of human UDP-d-Xylose:proteoglycan core protein beta-d-xylosyltransferase and its first isoform XT-II. Journal of Molecular Biology **304:**517-528.

162. **Ponighaus, C, Ambrosius, M, Casanova, JC, Prante, C, Kuhn, J, Esko, JD, Kleesiek, K, and Gotting, C.** 2007. Human xylosyltransferase II is involved in the biosynthesis of the uniform tetrasaccharide linkage region in chondroitin sulfate and heparan sulfate proteoglycans. Journal of Biological Chemistry **282:**5201-5206.

163. **Kelly, EJ, Hadac, EM, Greiner, S, and Russell, SJ.** 2008. Engineering microRNA responsiveness to decrease virus pathogenicity. Nature Medicine **14:**1278-1283.

164. **He, F, Yao, H, Wang, J, Xiao, Z, Xin, L, Liu, Z, Ma, X, Sun, J, Jin, Q, and Liu, Z.** 2015. Coxsackievirus B3 engineered to contain microRNA targets for muscle-specific microRNAs displays attenuated cardiotropic virulence in mice. Journal of Virology **89:**908-916.

165. **Pham, AM, Langlois, RA, and TenOever, BR.** 2012. Replication in cells of hematopoietic origin is necessary for Dengue virus dissemination. PLoS Pathogens **8:**e1002465.

166. **Langlois, RA, Albrecht, RA, Kimble, B, Sutton, T, Shapiro, JS, Finch, C, Angel, M, Chua, MA, Gonzalez-Reiche, AS, Xu, K, Perez, D, Garcia-Sastre, A, and tenOever, BR.** 2013. MicroRNA-based strategy to mitigate the risk of gain-of-function influenza studies. Nature Biotechnology **31:**844-847.

167. **Ylosmaki, E, Martikainen, M, Hinkkanen, A, and Saksela, K.** 2013. Attenuation of Semliki Forest virus neurovirulence by microRNA-mediated detargeting. Journal of Virology **87:**335-344.

168. **Sonkoly, E, Wei, T, Janson, PC, Saaf, A, Lundeberg, L, Tengvall-Linder, M, Norstedt, G, Alenius, H, Homey, B, Scheynius, A, Stahle, M, and Pivarcsi, A.** 2007. MicroRNAs: novel regulators involved in the pathogenesis of psoriasis? PLoS One **2:**e610.

169. **Guo, Z, Maki, M, Ding, R, Yang, Y, Zhang, B, and Xiong, L.** 2014. Genome-wide survey of tissue-specific microRNA and transcription factor regulatory networks in 12 tissues. Sci. Rep. **4:**5150.

170. **Li, H, Xie, H, Liu, W, Hu, R, Huang, B, Tan, YF, Xu, K, Sheng, ZF, Zhou, HD, Wu, XP, and Luo, XH.** 2009. A novel microRNA targeting HDAC5 regulates osteoblast differentiation in mice and contributes to primary osteoporosis in humans. Journal of Clinical Investigation **119:**3666-3677.

171. **Wang, S, Aurora, AB, Johnson, BA, Qi, X, McAnally, J, Hill, JA, Richardson, JA, Bassel-Duby, R, and Olson, EN.** 2008. The endothelial-specific microRNA miR-126 governs vascular integrity and angiogenesis. Developmental Cell **15:**261-271.

172. **Landgraf, P, Rusu, M, Sheridan, R, Sewer, A, Iovino, N, Aravin, A, Pfeffer, S, Rice, A, Kamphorst, AO, Landthaler, M, Lin, C, Socci, ND, Hermida, L, Fulci, V, Chiaretti, S, Foa, R, Schliwka, J, Fuchs, U, Novosel, A, Muller, RU, Schermer, B, Bissels, U, Inman, J, Phan, Q, Chien, M, Weir, DB, Choksi, R, De Vita, G, Frezzetti, D, Trompeter, HI, Hornung, V, Teng, G, Hartmann, G, Palkovits, M, Di Lauro, R, Wernet, P, Macino, G, Rogler, CE, Nagle, JW, Ju, J, Papavasiliou, FN, Benzing, T, Lichter, P, Tam, W, Brownstein, MJ, Bosio, A, Borkhardt, A, Russo, JJ, Sander, C, Zavolan, M, and Tuschl, T.** 2007. A

mammalian microRNA expression atlas based on small RNA library sequencing. Cell **129:**1401-1414.

173. **Anderson, C, Catoe, H, and Werner, R.** 2006. MIR-206 regulates connexin43 expression during skeletal muscle development. Nucleic Acids Research **34:**5863-5871.

174. **Esko, JD, Stewart, TE, and Taylor, WH.** 1985. Animal cell mutants defective in glycosaminoglycan biosynthesis. Proceedings of the National Academy of Sciences of the United States of America **82:**3197-3201.

175. **Thomas, JW, Thieu, TH, Byrd, VM, and Miller, GG.** 2000. Acidic fibroblast growth factor in synovial cells. Arthritis and Rheumatism **43:**2152-2159.

176. **Barton, ES, Connolly, JL, Forrest, JC, Chappell, JD, and Dermody, TS.** 2001. Utilization of sialic acid as a coreceptor enhances reovirus attachment by multistep adhesion strengthening. Journal of Biological Chemistry **276:**2200-2211.

177. **Polo, JM, Davis, NL, Rice, CM, Huang, HV, and Johnston, RE.** 1988. Molecular analysis of Sindbis virus pathogenesis in neonatal mice by using virus recombinants constructed in vitro. Journal of Virology **62:**2124-2133.

178. **Kuhn, RJ, Niesters, HG, Hong, Z, and Strauss, JH.** 1991. Infectious RNA transcripts from Ross River virus cDNA clones and the construction and characterization of defined chimeras with Sindbis virus. Virology **182:**430-441.

179. **Kobayashi, T, Ooms, LS, Chappell, JD, and Dermody, TS.** 2009. Identification of functional domains in reovirus replication proteins mNS and m2. J Virol **83:**2892-2906.

180. **Virgin, HW, IV, Bassel-Duby, R, Fields, BN, and Tyler, KL.** 1988. Antibody protects against lethal infection with the neurally spreading reovirus type 3 (Dearing). Journal of Virology **62:**4594-4604.

181. **Furlong, DB, Nibert, ML, and Fields, BN.** 1988. Sigma 1 protein of mammalian reoviruses extends from the surfaces of viral particles. Journal of Virology **62:**246-256.

182. **Smith, RE, Zweerink, HJ, and Joklik, WK.** 1969. Polypeptide components of virions, top component and cores of reovirus type 3. Virology **39:**791-810.

183. **Mainou, BA, and Dermody, TS.** 2011. Src kinase mediates productive endocytic sorting of reovirus during cell entry. Journal of Virology **85:**3203-3213.

RESEARCH ARTICLE

Reovirus Cell Entry Requires Functional Microtubules

Bernardo A. Mainou,[a,b] Paula F. Zamora,[b,c] Alison W. Ashbrook,[b,c] Daniel C. Dorset,[d] Kwang S. Kim,[e] Terence S. Dermody[a,b,c]

Departments of Pediatrics,[a] Pathology, Microbiology, and Immunology,[c] Elizabeth B. Lamb Center for Pediatric Research,[b] and Vanderbilt Technologies for Advanced Genomics,[d] Vanderbilt University School of Medicine, Nashville, Tennessee, USA; Division of Pediatric Infectious Diseases, Johns Hopkins School of Medicine, Baltimore, Maryland, USA[e]

ABSTRACT Mammalian reovirus binds to cell-surface glycans and junctional adhesion molecule A and enters cells by receptor-mediated endocytosis in a process dependent on β1 integrin. Within the endocytic compartment, reovirus undergoes stepwise disassembly, allowing release of the transcriptionally active viral core into the cytoplasm. To identify cellular mediators of reovirus infectivity, we screened a library of small-molecule inhibitors for the capacity to block virus-induced cytotoxicity. In this screen, reovirus-induced cell killing was dampened by several compounds known to impair microtubule dynamics. Microtubule inhibitors were assessed for blockade of various stages of the reovirus life cycle. While these drugs did not alter reovirus cell attachment or internalization, microtubule inhibitors diminished viral disassembly kinetics with a concomitant decrease in infectivity. Reovirus virions colocalize with microtubules and microtubule motor dynein 1 during cell entry, and depolymerization of microtubules results in intracellular aggregation of viral particles. These data indicate that functional microtubules are required for proper sorting of reovirus virions following internalization and point to a new drug target for pathogens that use the endocytic pathway to invade host cells.

IMPORTANCE Screening libraries of well-characterized drugs for antiviral activity enables the rapid characterization of host processes required for viral infectivity and provides new therapeutic applications for established pharmaceuticals. Our finding that microtubule-inhibiting drugs impair reovirus infection identifies a new cell-based antiviral target.

Received 30 May 2013 **Accepted** 10 June 2013 **Published** 2 July 2013

Citation Mainou BA, Zamora PF, Ashbrook AW, Dorset DC, Kim KS, Dermody TS. 2013. Reovirus cell entry requires functional microtubules. mBio 4(4):e00405-13. doi:10.1128/mBio.00405-13.

Editor Anne Moscona, Weill Medical College—Cornell

Address correspondence to Terence S. Dermody, terry.dermody@vanderbilt.edu.

The interplay between viruses and host cells regulates each step of the virus-host encounter. Viral tropism is restricted by the availability of cell-surface receptors and host molecules that promote viral internalization, replication, assembly, and release. Understanding the cellular components that underlie productive viral infection can illuminate new targets for development of antiviral therapies, improve viral vector design, and enhance an understanding of cellular processes at the pathogen-host interface.

Mammalian orthoreovirus (called reoviruses here) are nonenveloped, double-stranded RNA viruses that are formed from two concentric protein shells (1). Reoviruses infect most mammalian species, and although most humans are exposed during childhood, infection seldom results in disease (1, 2). The reovirus genome can now be engineered using reverse genetics, leading to the recovery of viable viruses with targeted alterations (3). Coupled with the capacity to elicit mucosal immune responses (1, 4) and natural attenuation in humans (1), this technology provides an opportunity to develop reovirus as a vaccine vector. Moreover, reovirus is currently being tested in clinical trials for efficacy as an oncolytic agent against a variety of cancers (5).

Reovirus attaches to host cells via interactions with cell-surface glycans (6, 7) and junctional adhesion molecule A (JAM-A) (8–10). Following attachment to JAM-A, reovirus is internalized in a β1 integrin-dependent manner via receptor-mediated endocytosis (11). Following internalization, reovirus activates Src kinase (12) and traverses through early and late endosomes (13). In late endosomes, virions undergo stepwise acid-dependent proteolytic disassembly catalyzed by cysteine cathepsin proteases to form infectious subvirion particles (ISVPs). ISVPs are characterized by the loss of outer-capsid protein σ3 and cleavage of outer-capsid protein μ1. The μ1 cleavage fragments mediate endosomal membrane penetration and release of the transcriptionally active viral core into the cytoplasm (14–16). ISVPs also can be generated *in vitro* by treatment of virions with a variety of proteases (14, 16). These particles bind JAM-A to initiate infection but are thought to penetrate at or near the cell surface (8, 17, 18), bypassing a requirement for acid-dependent proteolytic disassembly (16, 18). Host factors that mediate internalization and endosomal transport of reovirus virions are not completely understood.

Microtubules are long, filamentous protein polymers composed of α-tubulin and β-tubulin heterodimers (19). These structures regulate a wide variety of cellular functions, including mitosis, maintenance of cell shape, and intracellular transport (19). Posttranslational modifications of tubulin subunits and the interaction of microtubule-associated proteins with microtubules regulate polymerization dynamics (20). Because of the essential role in cell division, microtubules are targets for several anticancer chemotherapeutic agents (20, 21). For example, paclitaxel was originally developed for use against ovarian cancer but also is used

to treat other cancers, including metastatic breast cancer (20–22). Vinca alkaloids, including vindesine sulfate, are used to treat non-small-cell lung cancer, leukemia, lymphoma, and breast cancer (20, 21, 23). Microtubule-inhibiting compounds are classified into two groups based on whether the drug stabilizes or destabilizes microtubules. Stabilizing agents, such as taxanes, enhance microtubule polymerization, whereas destabilizing agents, such as vinca alkaloids and colchicine, inhibit microtubule polymerization by directly binding to microtubule subunits (20). Microtubule motors are used for bidirectional transport of cargo (24). Minus-end motors (dyneins) transport cargo toward the cell interior, whereas plus-end motors (kinesins) move cargo toward the cell periphery (24). It is not known whether microtubules or microtubule motors are required for reovirus entry.

In this study, we identified microtubule inhibitors in a high-throughput screen of small molecules for blockade of reovirus-mediated cell death. These drugs do not impede reovirus attachment or internalization but delay the intracellular transport of incoming virions, with a concomitant decrease in viral infectivity. Diminished expression of the dynein 1 heavy chain by RNA interference (RNAi) decreases reovirus infection. These findings indicate that reovirus uses microtubules and dynein 1 to efficiently enter and infect host cells, providing a potential new therapeutic option for viruses that penetrate deep into the endocytic pathway to establish infection.

RESULTS

Identification of microtubule inhibitors using a high-throughput small-molecule screen. To identify cellular factors required for reovirus cytotoxicity, we performed a high-throughput screen using small molecules from the NIH Clinical Collection (NCC), a library that contains 446 compounds that have been used in phase I, II, and III clinical trials in humans (see Fig. S1A in the supplemental material). Small molecules in the NCC were initially developed for use against a variety of diseases, including central nervous system, cardiovascular, and gastrointestinal malignancies, as well as numerous anti-infectives. HeLa S3 cells, which undergo cell death following reovirus infection (25), were incubated with dimethyl sulfoxide (DMSO) (vehicle control), 10 μM cysteine-protease inhibitor E64-d as a positive control (26), or a 10 μM concentration of each of the compounds in the NCC, adsorbed with cytopathic reovirus strain T3SA+ (6, 27), and incubated for 48 h. Cellular ATP levels were assessed as a proxy for cell viability. *Z* scores were calculated to identify compounds that significantly diminished reovirus-induced cell death (see Table S1 in the supplemental material). Eleven compounds had *Z* scores of greater than 2.0, with *Z* scores in this group ranging from 2.758 to 8.444 (Fig. S1B). Interestingly, 5 of the 11 compounds identified are drugs that influence microtubule stability and function (20) (Fig. S1C). Microtubule-inhibiting compounds constitute <1% of the total number of small molecules in the NCC, suggesting that the large number of microtubule inhibitors identified does not reflect bias within the screen. Thus, these data suggest that functional microtubules are required for reovirus-induced cytotoxicity.

Microtubule inhibitors diminish reovirus-mediated cell death and infectivity. To verify that microtubule-inhibiting drugs block cytotoxicity induced by reovirus, HeLa S3 cells were incubated with DMSO, E64-d, or NH_4Cl as positive controls, or increasing concentrations of microtubule-inhibiting drugs for 1 h prior to reovirus adsorption. Cell viability was assessed by quantifying cellular ATP levels 48 h after adsorption (Fig. 1A). Similar to the observations made using the NCC screen, we observed a dose-dependent decrease in reovirus-mediated cytotoxicity with increasing concentrations of microtubule-inhibiting compounds, E64-d, or NH_4Cl. The observed inhibition was statistically significant at concentrations of 0.1 to 1.0 μM for all compounds tested except for flubendazole, which inhibited at concentrations of 1.0 and 10 μM. These data confirm findings obtained from the small-molecule screen and provide further evidence that microtubule function is required for reovirus-induced cell death.

To determine whether microtubule function is required for reovirus infectivity in epithelial and endothelial cells, we tested the effect of microtubule-inhibiting compounds on reovirus infection of CCL2 HeLa cells, HeLa S3 cells, and human brain microvascular endothelial cells (HBMECs). Both CCL2 and S3 HeLa cells are highly susceptible to reovirus infection and have been used in studies to understand cellular mediators of reovirus cell entry (12, 13). HBMECs are highly transfectable and provide a tractable model cell line for studies of virus replication in endothelial cells (28). Cells were treated with DMSO, E64-d, NH_4Cl, or increasing concentrations of microtubule inhibitors for 1 h prior to adsorption with reovirus T3SA+, incubated in the presence of inhibitors, and scored for infection by indirect immunofluorescence (Fig. 1B). For all cell lines tested, treatment with vindesine sulfate yielded a statistically significant decrease in infectivity. While colchicine and docetaxel also decreased infectivity in the cell types tested, the effects were not as pronounced as those observed with vindesine sulfate. Interestingly, among the compounds from the NCC, we identified three vinca alkaloid compounds, vindesine sulfate, vincristine sulfate, and vinorelbine bitartrate, that impaired reovirus-mediated cytotoxicity. These data suggest that vinca alkaloids are more potent as anti-infectives against reovirus than other microtubule-inhibiting agents. Together, these data indicate that microtubule function is required for maximal reovirus infectivity and reovirus-mediated cell killing.

Vindesine sulfate blocks reovirus replication at early times of infection. To define the temporal window in which microtubule inhibitors act to impair reovirus infection, CCL2 HeLa cells were treated with DMSO, NH_4Cl, or 1 μM vindesine sulfate for 1 h prior to reovirus adsorption or in 1-h increments up to 2 h post-adsorption. Cells were then incubated in the presence or absence of inhibitors and scored for infection by indirect immunofluorescence 20 h after adsorption (Fig. 2A). Since microtubules depolymerize at cold temperatures (29), virus was adsorbed at room temperature to prevent microtubule depolymerization while also allowing sufficient time for reovirus to attach to cells. For the remainder of the descriptions of our studies, 0 min represents the initiation of infection following adsorption at room temperature. Vindesine sulfate treatment 1 h prior to or immediately following adsorption substantially decreased reovirus infection. However, addition of vindesine sulfate 1 h or more after adsorption decreased reovirus infection much less efficiently. These data indicate that vindesine sulfate is most potent in diminishing reovirus infection during the first hour of the infectious cycle, suggesting that reovirus requires microtubule function during the interval required for viral entry and uncoating. In addition, these findings demonstrate that impairment of reovirus infection by vindesine sulfate is not attributable to toxicity of the compound.

To determine whether vindesine sulfate impairs infection by

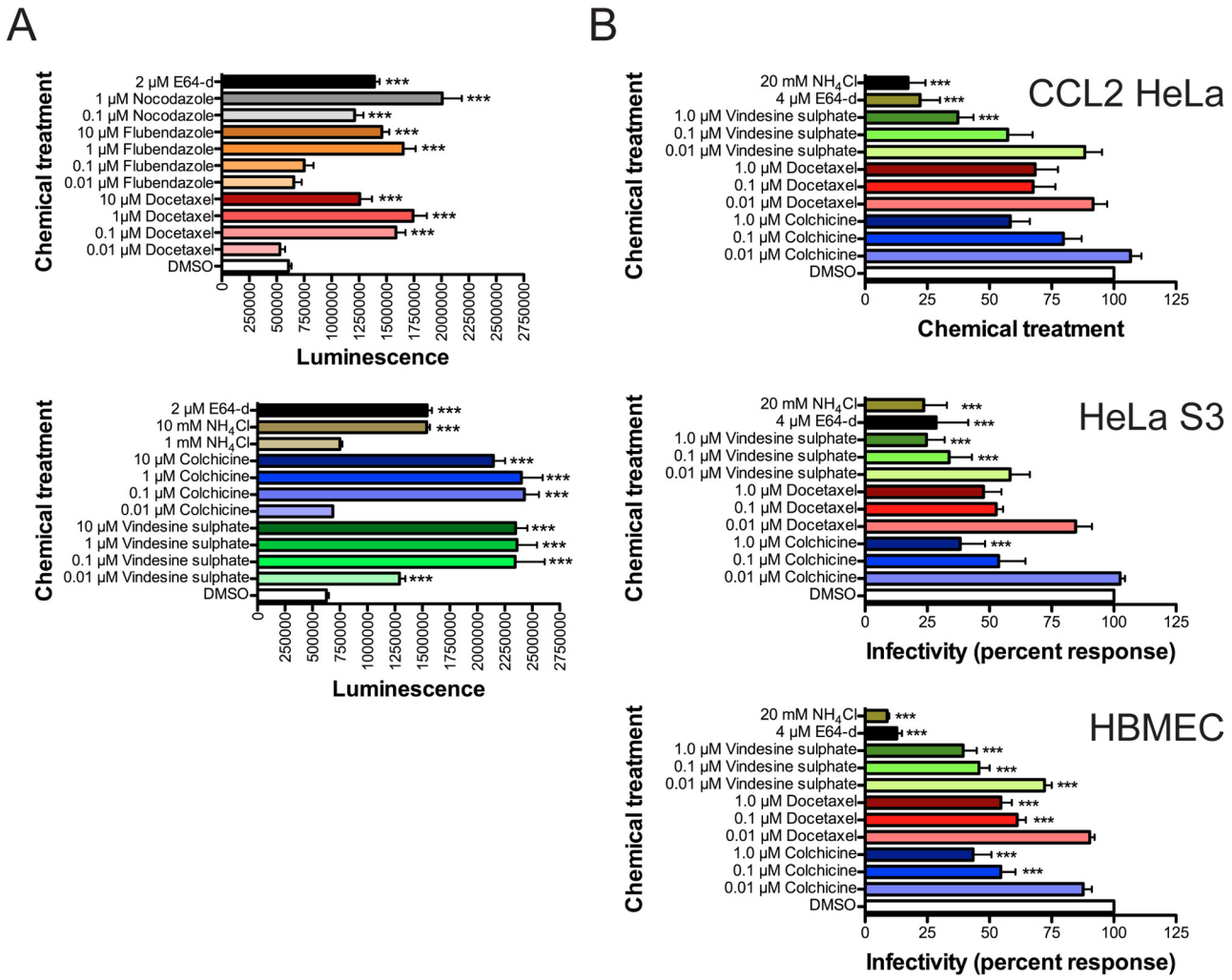

FIG 1 Microtubule-inhibiting compounds diminish reovirus-mediated cytotoxicity and inhibit reovirus infectivity. (A) HeLa S3 cells were incubated with DMSO, increasing concentrations of docetaxel, flubendazole, nocodazole, vindesine sulfate, colchicine, or NH_4Cl, or 2 μM E64-d, adsorbed with T3SA+, and incubated for 48 h. Cell viability was quantified using an ATP-dependent luminescence assay. Results are presented as total luminescence intensity values from experiments performed in quadruplicate. Error bars indicate standard deviations. (B) CCL2 HeLa cells, HeLa S3 cells, or HBMECs were incubated with DMSO or increasing concentrations of colchicine, docetaxel, vindesine sulfate, E64-d, or NH_4Cl and adsorbed with T3SA+ at an MOI of either 5 PFU/cell for HeLa S3 cells and HBMECs or 1 PFU/cell for CCL2 HeLa cells. Cells were incubated in the presence of inhibitors for 20 h and scored for infection by indirect immunofluorescence. Results are presented as percent mean fluorescence intensity compared with DMSO, normalized to cell number and background fluorescence, for quadruplicate experiments with CCL2 HeLa cells and triplicate experiments with HeLa S3 cells and HBMECs. Error bars indicate standard errors of the mean. ***, $P < 0.05$ in comparison to DMSO by one-way ANOVA with Dunnett's multiple-comparison test.

ISVPs, which bind JAM-A at the cell surface but do not require intracellular transport for infection (8, 16–18), CCL2 HeLa cells were treated with DMSO, 20 mM NH_4Cl, or increasing concentrations of vindesine sulfate for 1 h, adsorbed with reovirus virions or ISVPs, and scored for infection by indirect immunofluorescence 20 h after adsorption (Fig. 2B). As observed previously, treatment of cells with NH_4Cl or vindesine sulfate diminished infection following adsorption with virions. In contrast, treatment of cells with NH_4Cl or vindesine sulfate did not significantly alter infection following adsorption with ISVPs. These data indicate that vindesine sulfate blocks a step in reovirus replication following attachment to JAM-A but prior to viral protein synthesis.

Microtubules are required for endocytic sorting of reovirus during cell entry. To determine whether reovirus uses microtubule tracks during cell entry, CCL2 HeLa cells were treated with DMSO or 1 μM vindesine sulfate for 1 h, adsorbed with reovirus, and incubated for 0, 20, or 120 min. Cells were stained for reovirus and α-tubulin and imaged using confocal microscopy (Fig. 3). In DMSO-treated cells, virions were detected on microtubule tracks at 0, 20, and 120 min, with an increasing number of particles observed in the perinuclear area at 120 min. The perinuclear distribution of reovirus virions is consistent with access to late endosomes for disassembly by cathepsin proteases to allow productive infection (13). In vindesine sulfate-treated cells, virions were associated with depolymerized microtubules at 0 and 20 min, but by 120 min, particles appeared to form clusters in the cytoplasm. Treatment of HBMECs with vindesine sulfate also resulted in aggregation of viral particles at 120 min postadsorption, although the clusters were not as prominent as those observed in vindesine

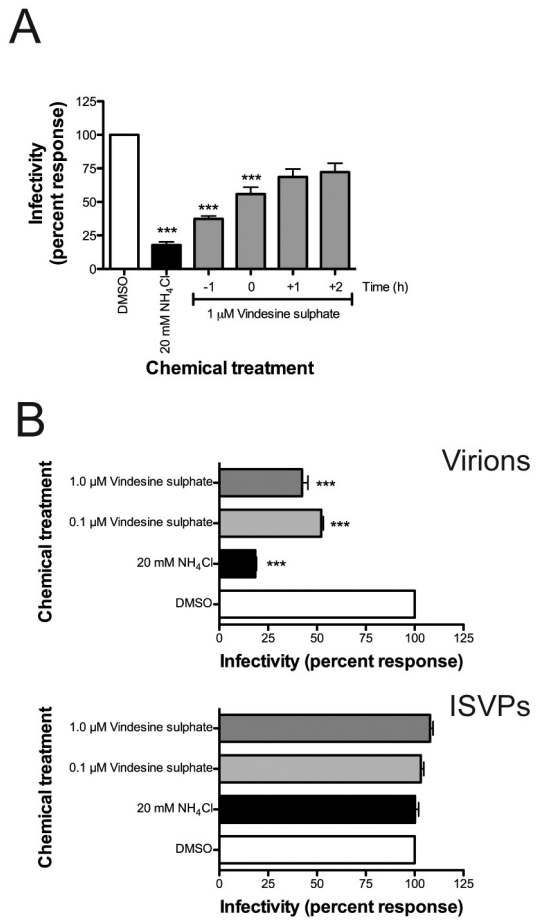

FIG 2 Vindesine sulfate blocks reovirus replication at early times of infection. (A) CCL2 HeLa cells were incubated with DMSO, 20 mM NH_4Cl, or 1 μM vindesine sulfate, adsorbed with T3SA+ at an MOI of 5 PFU/cell, and incubated in the presence of inhibitors for 20 h. Alternatively, cells were incubated with 1 μM vindesine sulfate immediately following adsorption or at 1-h intervals after adsorption. Cells were scored for infection by indirect immunofluorescence. (B) CCL2 HeLa cells were incubated with DMSO, NH_4Cl, or vindesine sulfate, adsorbed with T3SA+ virions or ISVPs at an MOI of 1.63×10^3 particles/cell, and incubated in the presence of inhibitors for 20 h. Cells were scored for infection by indirect immunofluorescence. Results are presented as percent mean fluorescence intensity compared with DMSO, normalized to cell number and background fluorescence, for triplicate experiments. ***, $P < 0.05$ in comparison to DMSO by one-way ANOVA with Dunnett's multiple-comparison test.

sulfate-treated CCL2 HeLa cells (data not shown). These observations suggest that depolymerization of microtubules by vindesine sulfate leads to missorting of reovirus virions during cell entry.

Vindesine sulfate does not affect internalization of reovirus into cells. Since depolymerization of microtubules impairs reovirus intracellular transport and infectivity, we sought to determine whether vindesine sulfate inhibits internalization of viral particles from the cell surface. CCL2 HeLa cells were treated with DMSO or 1 μM vindesine sulfate for 1 h, adsorbed with Alexa 546-labeled reovirus, and incubated for 0, 60, or 120 min. Cells were stained for extracellular virus using reovirus-specific antiserum under nonpermeabilizing conditions, and the ratio of extracellular to internalized reovirus particles was quantified by flow cytometry (Fig. 4A). Over the course of the infection, we observed a decrease in extracellular virus in the presence and absence of vindesine sulfate. These results suggest that vindesine sulfate does not significantly impede internalization of reovirus, at least up to 120 min after adsorption. Consistent with this finding, vindesine sulfate treatment did not diminish cell-surface expression of JAM-A or β1 integrin (data not shown). These results suggest that microtubule function is not required for reovirus attachment or internalization.

Vindesine sulfate impairs reovirus access to intracellular acidified compartments. To determine whether vindesine sulfate alters transport of reovirus to acidified compartments during cell entry, CCL2 HeLa cells were treated with DMSO or 1 μM vindesine sulfate for 1 h, adsorbed with reovirus labeled with a pH-sensitive dye (pHrodo), and incubated for 0, 60, or 120 min. The fluorescence intensity of intracellular virus was quantified by flow cytometry (Fig. 4B). In DMSO-treated cells, mean fluorescence intensity increased over time, indicating that virions gain access to an acidified compartment between 60 and 120 min after adsorption, consistent with prior studies of the kinetics of reovirus delivery to acidified endosomes (13, 30). In contrast, mean fluorescence intensity was dampened during the interval of reovirus entry into vindesine sulfate-treated cells. Importantly, microtubule-inhibiting drugs do not affect the intraluminal pH of endosomes (31). These data suggest that vindesine sulfate impairs reovirus infection by impeding transport of virions to acidified intracellular organelles.

During cell entry, reovirus traverses through Rab5-marked early endosomes en route to Rab7- and Rab9-marked late endosomes for proteolytic disassembly (12). To determine whether vindesine sulfate treatment leads to retention of reovirus particles in early endosomes, CCL2 HeLa cells were transfected with enhanced green fluorescent protein (EGFP)-Rab5A, incubated with DMSO or 1 μM vindesine sulfate for 1 h, adsorbed with Alexa-labeled reovirus, incubated for 120 min, and imaged by confocal microscopy. Analysis of the spectral overlap of fluorescently labeled virions and Rab5A-positive compartments showed no statistically significant difference in the percentages of virions in early endosomes in cells treated with either DMSO or vindesine sulfate (Fig. 4C). These data suggest that inhibition of microtubule function by vindesine sulfate does not lead to an accumulation of reovirus particles in early endosomes.

In a complementary experiment, CCL2 HeLa cells were incubated with DMSO or 1 μM vindesine sulfate for 1 h, adsorbed with Alexa-labeled reovirus, and incubated for 60 or 120 min. Cells were stained for lysosomal-associated membrane protein 1 (LAMP1) to identify late endosomes and lysosomes (Fig. 4D). Analysis of the spectral overlap of fluorescently labeled virions and LAMP1-positive compartments revealed a higher percentage of viral particles distributed to LAMP1-positive endosomes in control-treated cells than in those treated with vindesine sulfate (Fig. 4E). Concordant with these observations, vindesine sulfate decreased reovirus colocalization with Rab7-marked endosomes compared to that seen with control-treated cells (data not shown). Together, these data indicate that although vindesine sulfate does not inhibit reovirus internalization or lead to retention of virus in early endosomes, the drug impedes efficient transport of virions to acidified intracellular compartments where viral disassembly takes place.

Reovirus requires dynein 1 to efficiently infect cells. To determine whether reovirus uses minus-end microtubule motor dy-

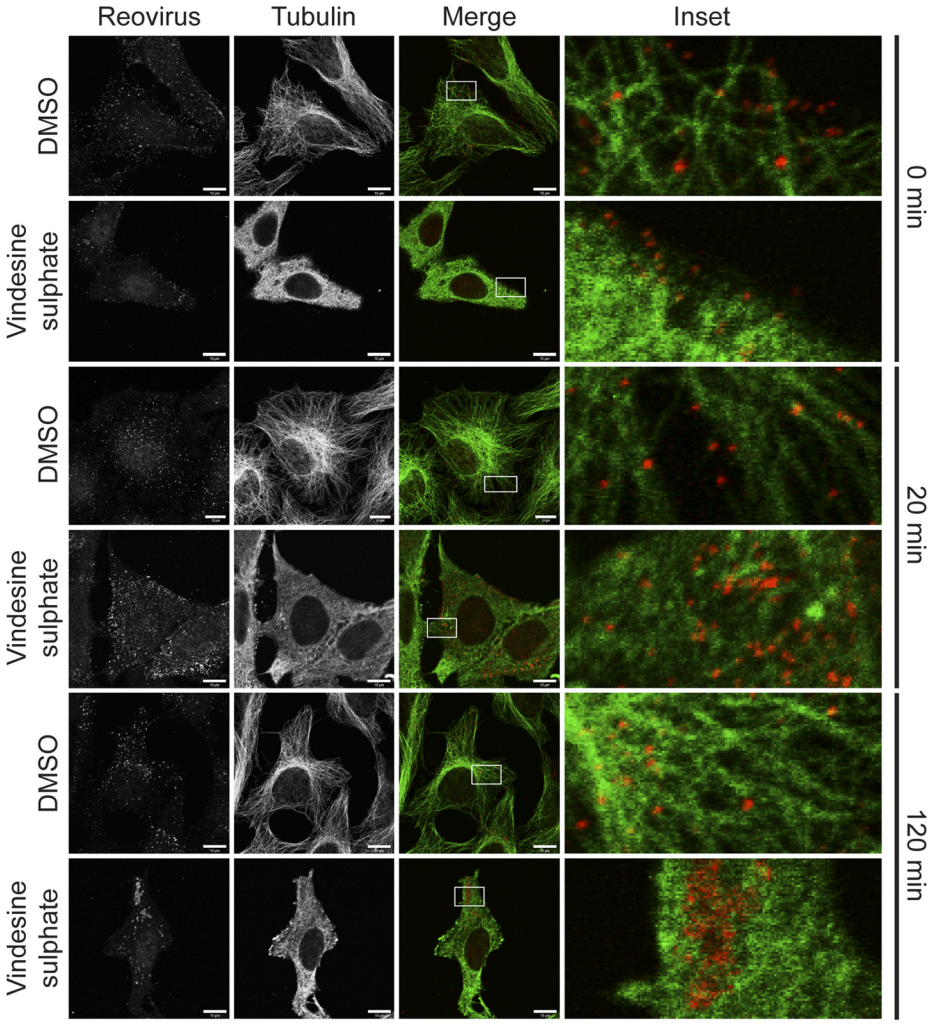

FIG 3 Reovirus uses microtubules to enter cells. CCL2 HeLa cells were adsorbed with T3SA+ at an MOI of 2×10^4 particles/cell at room temperature and incubated at 37°C for 0, 20, or 120 min. Cells were fixed in methanol, stained for reovirus (red) or α-tubulin (green), and imaged by confocal microscopy. Single sections from a Z-stack as well as a merged image are shown for each stain. Insets depict enlarged areas from boxed regions. Scale bars, 10 μm.

nein 1 for transport into the cell interior, HBMECs were transfected with small interfering RNAs (siRNAs) specific for the dynein 1 heavy chain, adsorbed with reovirus strains type 1 Lang (T1L) or type 3 Dearing (T3D), incubated for 48 h, and scored for infection by indirect immunofluorescence (Fig. 5A). Of the cell lines used in this study, diminished expression of dynein 1 caused by RNAi treatment is most efficient in HBMECs (data not shown). Consistent with a requirement for microtubule function for efficient reovirus infection, diminished dynein 1 heavy chain expression caused by RNAi treatment decreased infection by both T1L and T3D. To further define the role of dynein 1 in reovirus cell entry, cells were adsorbed with T1L, incubated for 20 min, stained for reovirus and dynein 1 heavy chain, and imaged by confocal microscopy. Virions were observed in close proximity to dynein 1 in both HBMECs (Fig. 5B) and CCL2 HeLa cells (Fig. 5C), suggesting that reovirus uses dynein 1 to promote cell entry. Together, these data indicate that reovirus requires the microtubule minus-end motor dynein 1 to efficiently infect cells.

CHKV does not require microtubules to infect cells. Chikungunya virus (CHKV), a mosquito-transmitted alphavirus that causes epidemics of arthritis (32), requires acidification to efficiently enter cells, but unlike reovirus, CHKV does not require access to late endosomes (33). To determine whether vindesine sulfate inhibits CHKV infection, BHK-21 cells, which are susceptible to CHKV, were treated with DMSO or 1 μM vindesine sulfate for 1 h, adsorbed with CHKV vaccine strain 181/25 or virulent strain SL15649, incubated for 10 h, and scored for infection by indirect immunofluorescence (Fig. 6A and B). In contrast to findings made in our studies of reovirus, vindesine sulfate did not impair CHKV infection, suggesting that CHKV does not require microtubule function to efficiently enter cells. These results are in agreement with a requirement for microtubules in the maturation of early to late endosomes (34) and provide additional evidence that the drug does not impair reovirus infection by nonspecific cytotoxic effects.

Vindesine sulfate alters reovirus disassembly kinetics. As a final experiment to define the step in reovirus replication blocked by microtubule inhibitors, we tested whether inhibition of microtubule function alters the kinetics of reovirus disassembly. CCL2 HeLa cells were treated with DMSO or 1 μM vindesine sulfate for

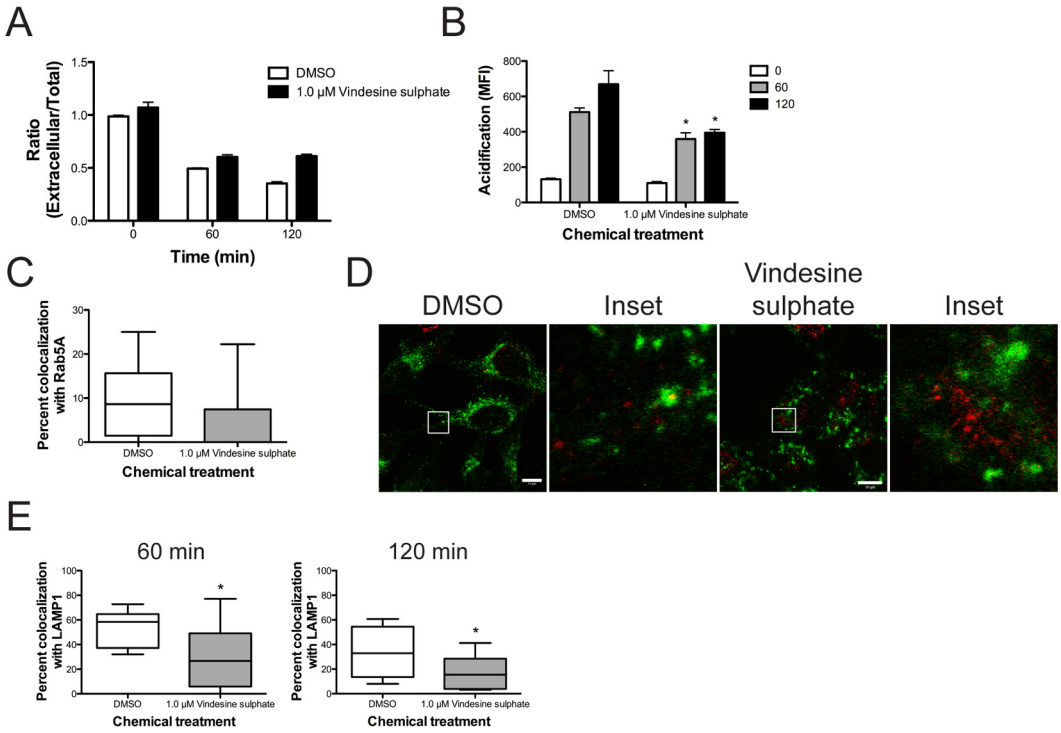

FIG 4 Vindesine sulfate impairs transport of reovirus in the endocytic pathway. (A) CCL2 HeLa cells were incubated with DMSO or 1 μM vindesine sulfate, adsorbed with A546-labeled T3SA+ at an MOI of 5×10^3 particles/cell, and incubated with DMSO or 1 μM vindesine sulfate for the times shown. Cells were stained with reovirus-specific antiserum using nonpermeabilizing conditions. Mean fluorescence intensity (MFI) was assessed by flow cytometry. Results are presented as a ratio of extracellular to total mean fluorescence intensity for triplicate samples. Error bars indicate standard deviations. (B) CCL2 HeLa cells were incubated with DMSO or 1 μM vindesine sulfate, adsorbed with pHrodo-labeled T3SA+ at an MOI of 5×10^3 particles/cell, and incubated with DMSO or 1 μM vindesine sulfate for the times shown. MFI was assessed by flow cytometry. Error bars indicate standard deviations. (C) CCL2 HeLa cells were transfected with EGFP-Rab5A, incubated with DMSO or 1 μM vindesine sulfate, adsorbed with A546-labeled T3SA+ at an MOI of 10^4 particles/cell, and incubated with DMSO or 1 μM vindesine for 120 min. Cells were fixed and imaged by confocal microscopy. Results are expressed as percent colocalization of reovirus particles with Rab5A-positive endosomes ($n = 8$ cells per condition). Error bars indicate minimum and maximum values. (D) CCL2 HeLa cells were incubated with DMSO or 1 μM vindesine sulfate, adsorbed with A546-labeled T3SA+ (red) at an MOI of 10^4 particles/cell, and incubated with DMSO or 1 μM vindesine sulfate for 60 or 120 min. Cells were fixed, stained with a LAMP1-specific antibody (green), and imaged by confocal microscopy. Representative images from 120 min shown. Insets depict enlarged areas of boxed regions. Scale bars, 10 μm. (E) Percent colocalization of reovirus particles with LAMP-1-positive endosomes ($n = 10$ cells per condition). Error bars indicate minimum and maximum values. *, $P < 0.05$ in comparison to DMSO by Student's t test.

1 h, adsorbed with reovirus, and incubated from 0 to 120 min. Whole-cell lysates were resolved by SDS-PAGE and immunoblotted using a reovirus-specific antiserum to detect viral capsid protein μ1 and its major cleavage fragment, δ (Fig. 6C). In control-treated cells, δ was detected by 20 min, with increasing band intensity noted over the experimental time course. In vindesine sulfate-treated cells, δ was not detected until 60 min after adsorption. Densitometric analysis of three independent experiments showed delayed μ1-to-δ conversion at all times tested in vindesine sulfate-treated cells in comparison to control cells (Fig. 6D). We conclude that inhibition of microtubule function leads to inefficient access to acidified endosomal compartments, which in turn delays the disassembly of internalized virions.

DISCUSSION

In this study, we found that reovirus colocalizes with microtubule tracks during cell entry and requires microtubule function and microtubule motor dynein 1 to efficiently traverse the endocytic pathway. Microtubule function is not required for internalization of reovirus virions but rather facilitates targeting of reovirus to acidified endosomes for viral disassembly. Treatment of cells with microtubule inhibitors blocks reovirus infection in a temporal window in which the virus transits from early to late endosomes. These results highlight a new function for microtubules in reovirus replication and suggest that impairment of microtubule activity might diminish infection by viruses that require access to late endosomes to establish productive infection.

Endocytic uptake of macromolecular cargo requires the coordinated action of several host factors, including receptors, Rab GTPases, and enzymes that regulate endocytic transport by modifying targets at specific intracellular sites. For some cargo, microtubules and microtubule-associated motors are required for transport to and from the cell surface. Importantly, the maturation of early to late endosomes is dependent on microtubule function (34). Rab-interacting lysosomal protein (RILP), a Rab7 adapter, recruits dynactin and dynein to late endosomes, promoting late endosome movement toward the cell interior (35). Reovirus is transported to Rab7-marked endosomes during cell entry (13), and expression of dominant-negative RILP inhibits reovirus infection (13). Thus, disruption of microtubule function appears to delay reovirus disassembly by slowing the maturation of the reovirus-containing endosomal fraction. This model is supported by the observed decrease in colocalization of reovirus with LAMP1-marked endosomes. Additional support comes from the

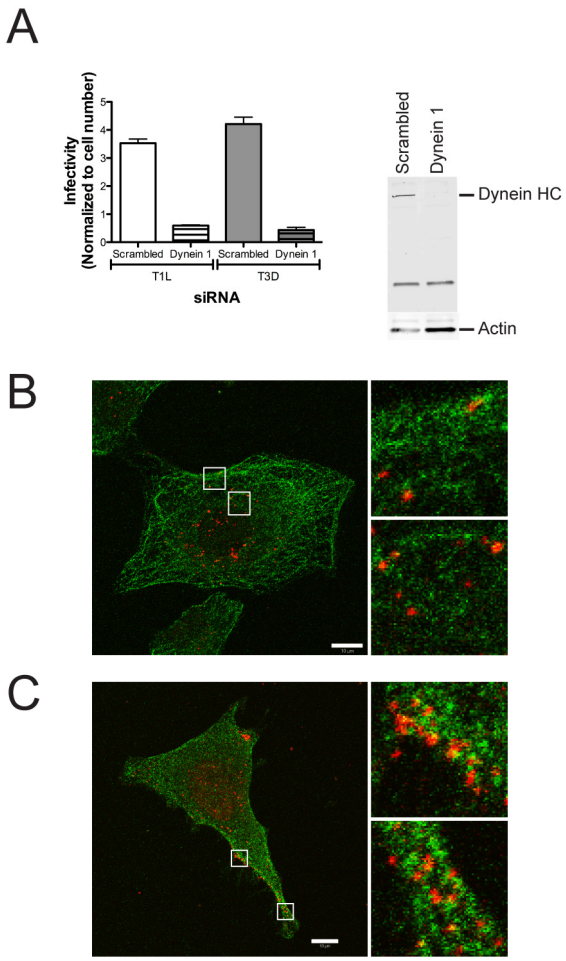

FIG 5 Reovirus uses microtubule motor dynein 1 to efficiently infect cells. (A) (Left panel) HBMECs were transfected with a nonspecific siRNA (scrambled) or an siRNA specific for dynein 1 heavy chain (dynein 1), adsorbed with reovirus strains T1L or T3D at an MOI of 15 PFU/cell, and incubated for 24 h. Cells were scored for infection by indirect immunofluorescence. Results are presented as mean fluorescence intensity normalized to cell number and background fluorescence for triplicate wells. Error bars indicate standard deviations. (Right panel) Whole-cell lysates of HBMECs transfected with nonspecific or dynein 1-specific siRNAs were analyzed by immunoblotting using dynein 1 heavy chain (HC)-specific or actin-specific antibodies. (B and C) HBMECs (B) or CCL2 HeLa cells (C) were adsorbed with T1L at an MOI of 10^4 particles/cell and incubated for 20 min. Cells were stained for reovirus (red) and dynein 1 heavy chain (green) and imaged by confocal microscopy. A single section from a Z-stack is shown. Insets depict enlarged areas from boxed regions. Scale bars, 10 μm.

observation that vindesine sulfate does not diminish infection after adsorption of ISVPs, which are uncoated *in vitro* and thus do not require access to cathepsin-containing organelles to establish infection (16–18). As an important control, vindesine sulfate does not inhibit infection by CHKV, which uncoats in early endosomes (33). Impairment of endosomal maturation might be responsible for the aggregates of reovirus particles observed in vindesine sulfate-treated cells. Interestingly, reovirus virions do not accumulate in early endosomes in cells treated with vindesine sulfate (Fig. 4C). Instead, viral particles in vindesine sulfate-treated cells aggregate in clusters in the cytoplasm. These observations suggest that in the absence of microtubule function, viral particles are missorted during cell entry and not trapped in early endosomes.

Our report highlights the potential for drugs that inhibit endosomal maturation for use as broadly active anti-infectives. Such drugs could inhibit viruses, bacteria, bacterial toxins, and parasites that require access to late endosomes and lysosomes to mediate pathological effects. Avian reovirus, a fusogenic reovirus that, unlike mammalian reovirus, enters cells via caveolin-1 and causes infected cells to form syncytia (36, 37), also uses microtubules to enter cells (36). This finding suggests that employment of microtubules by fusogenic and nonfusogenic reoviruses is a conserved cell entry mechanism despite the use of different endocytic uptake pathways. Adenovirus (38) and Borna disease virus (39) also use microtubules and microtubule motors during cell entry (40). *Enterococcus faecalis* requires microtubules for efficient internalization into cells (41). Cytotoxic necrotizing factor 1 (CNF1), a toxin produced by some pathogenic *Escherichia coli* strains, requires microtubule function to access late endosomes for the processing required for cytotoxicity (42). Flubendazole, a compound identified in our screen as impairing reovirus cytotoxicity, inhibits infection by nematodes (43). While currently available microtubule-inhibiting compounds are associated with significant adverse effects (21), it is possible that safer agents could be developed for anti-infective therapies that transiently inhibit endosomal maturation.

Reovirus strain T3D, which has been trademarked as Reolysin, is being evaluated in clinical trials for efficacy as an oncolytic agent in combination with various chemotherapeutic drugs, including the microtubule inhibitor docetaxel (5). Our findings suggest that pairing reovirus with microtubule-inhibiting agents during oncolytic therapy may limit virus-induced cell killing. Cancer treatment regimens that use reovirus and microtubule-inhibiting drugs may be more efficacious if the administration of virus and chemotherapeutic is not simultaneous. We found that addition of vindesine sulfate to reovirus-infected cells at up to 1 h after infection fails to significantly diminish infection. Thus, we think it important to assess the effects of pharmacological agents on viral infectivity when these treatments are used in combination.

The NCC screen yielded six candidate compounds that do not target microtubules. Procarbazine, which promotes DNA damage (44), and 6-azauridine, which inhibits pyrimidine synthesis (45), likely impair reovirus replication by affecting viral transcription or genome replication. The identification of nicotinic acetylcholine receptor and serotonin receptor agonists as drugs that impair reovirus-induced cytotoxicity points to interesting cellular targets. The nicotinic acetylcholine receptor is expressed in the brain (46), and serotonin receptors are expressed in both the brain and gastrointestinal tract (47). Both of these organs are sites for reovirus replication in the infected host (1). Finally, the identification of indomethacin, which inhibits cyclooxygenase 1 and 2 (48), suggests a yet-uncharacterized function for cyclooxygenases in reovirus replication. Further studies are required to determine whether these drugs inhibit reovirus replication and to define the antiviral mechanisms by which they act.

The identification of host molecules that regulate steps in viral replication enhances an understanding of how viruses use basic cellular processes to propagate and disseminate. These studies also yield new knowledge about cellular functions and illuminate new targets for antiviral drug development. In this study, we used a high-throughput screening approach to identify microtubules and microtubule motor dynein 1 as host factors required for reovirus cell entry, initiation of infection, and consequent cell death.

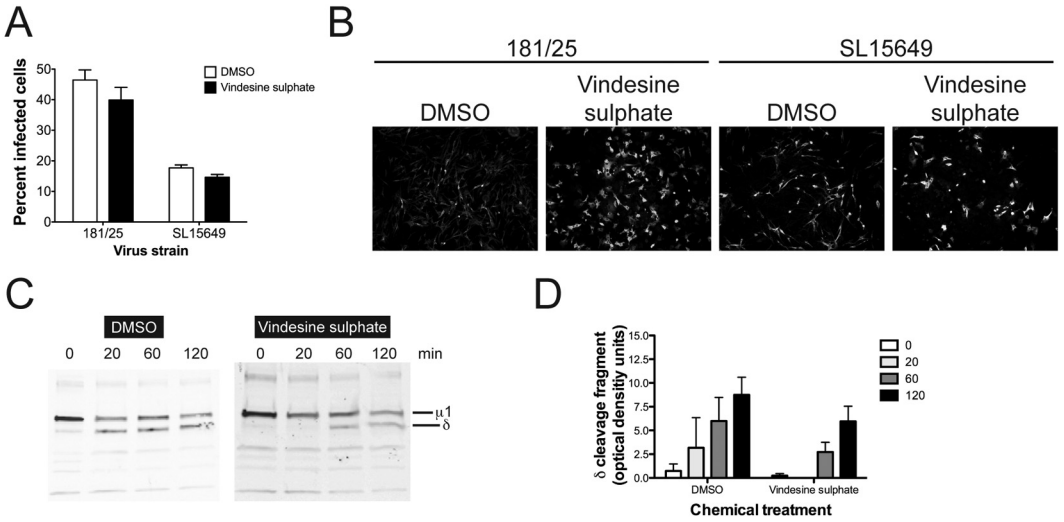

FIG 6 Vindesine sulfate does not affect CHKV infection but alters reovirus disassembly kinetics. (A) BHK-21 cells were incubated with DMSO or 1 μM vindesine sulfate, adsorbed with CHKV strain 181/25 or SL15649 at an MOI of 1 PFU/cell, and incubated with DMSO or vindesine sulfate for 10 h. Cells were stained with CHKV-specific antiserum and DAPI to detect nuclei. Infection was quantified by indirect immunofluorescence. Results are presented as percent infected cells from triplicate wells. Error bars indicate standard deviations. (B) Images of DMSO- or vindesine sulfate-treated BHK-21 cells infected with CHKV strain 181/25 or SL15659 and stained with CHKV-specific antiserum. (C) CCL2 HeLa cells were incubated with DMSO or 1 μM vindesine sulfate, adsorbed with T3SA+ at an MOI of 10 PFU/cell, and incubated with DMSO or 1 μM vindesine sulfate for the times shown. Whole-cell lysates were immunoblotted using reovirus-specific antiserum. (D) Densitometric analysis of the δ cleavage fragment of reovirus μ1 protein from triplicate experiments. Error bars indicate standard errors of the mean. The key indicates times in minutes.

Findings made in this study should contribute to the development of improved strategies for use of reovirus as an oncolytic and establish a platform for testing microtubule inhibitors as antiinfective agents.

MATERIALS AND METHODS

Cells, viruses, chemical inhibitors, and antibodies. Spinner-adapted murine L929 cells, CCL2 HeLa cells, HeLa S3 cells, and HBMECs were cultivated as previously described (13, 28). BHK-21 and Vero81 cells were cultivated in Alpha minimal essential medium (MEM) (Sigma) supplemented to contain 5% fetal bovine serum (FBS) (Vero81) or 10% FBS (BHK-21) and L-glutamine. Medium for all cells was supplemented with penicillin-streptomycin (Invitrogen) and amphotericin B (Sigma).

Purified virions of reovirus strains T1L, T3D, and T3SA+ were prepared by plaque purification and passage using L929 cells as previously described (12, 13, 28). ISVPs were generated by treating particles with α-chymotrypsin (Sigma) as previously described (12). Reovirus virions were labeled with succinimidyl ester Alexa Fluor 546 (A546) or pHrodo SE (pHrodo) (Invitrogen) as previously described (13).

CHKV strain 181/25 was provided by Robert Tesh (University of Texas Medical Branch). Viral RNA was isolated from a plaque-purified isolate, and cDNA was generated using random hexamers. Overlapping fragments were amplified, cloned into pCR2.1 TOPO (Invitrogen), and sequenced. The 5′ untranslated region was sequenced using 5′ rapid amplification of cDNA ends. An infectious clone was synthesized by GenScript (Piscataway, NJ) in four fragments. Genome fragments were assembled and subcloned into pSinRep5 low-copy-number plasmid. The CHKV strain SL15649 infectious clone was provided by Mark Heise (University of North Carolina at Chapel Hill) (49). Infectious clone plasmids for 181/25 and SL15649 were linearized and transcribed *in vitro* using an mMessage mMachine SP6 transcription kit (Ambion). BHK-21 cells were electroporated with viral RNA and incubated at 37°C for 24 h. Supernatants containing progeny virus were harvested from electroporated cells and stored at −80°C. All experiments using SL15649 were performed using biosafety level 3 conditions.

Ammonium chloride (NH_4Cl; Gibco) was resuspended in water. E64-d, colchicine, nocodazole (Sigma), docetaxel, flubendazole, and vindesine sulfate (Sequoia Research Products) were resuspended in DMSO. The immunoglobulin G (IgG) fraction of a rabbit antiserum raised against T1L or T3D was purified as previously described (6). LAMP1-specific and dynein heavy chain-specific monoclonal antibodies (Abcam), α-tubulin-specific monoclonal antibody (Cell Signaling Technology), actin-specific polyclonal antiserum (Santa Cruz Biotechnology), and CHKV-specific antiserum (ATCC) were used for indirect immunofluorescence experiments, infectivity assays, and immunoblot analyses. Alexa Fluor-conjugated antibodies (Invitrogen) were used as secondary antibodies.

Cell viability assay. HeLa S3 cells were incubated with OMEM-1 (Invitrogen) medium containing DMSO, E64-d, NH_4Cl, or microtubule inhibitors at 37°C for 1 h and adsorbed with T3SA+ at a multiplicity of infection (MOI) of 200 PFU/cell in the presence of DMSO, E64-d, NH_4Cl, or microtubule inhibitors in OMEM-I medium at 37°C for 48 h. Cell viability was quantified using the Cell Titer Glo assay.

Quantification of reovirus infectivity. Reovirus infectivity was assessed by indirect immunofluorescence (50). Cells were incubated with complete medium containing DMSO or chemical inhibitors at 37°C for 1 h, adsorbed with reovirus at room temperature for 1 h, and incubated with complete medium containing DMSO or chemical inhibitors at 37°C for 20 h. Cells were fixed and stained with reovirus-specific antiserum and goat anti-rabbit IRDye 800 (Li-COR), DRAQ5 (Cell Signaling), and Sapphire700 (Li-COR). Immunofluorescence was detected using a Li-COR Odyssey infrared imaging system (Li-COR). Infectivity was quantified using the In-Cell Western feature of the Odyssey software suite.

Confocal microscopy of reovirus-infected cells. Confocal microscopy of reovirus-infected cells was performed as previously described (12, 13). HeLa CCL2 cells were incubated with complete medium containing DMSO or vindesine sulfate at 37°C for 1 h. Cells were adsorbed with reovirus at an MOI of 2×10^4 particles/cell and either fixed with ice-cold methanol or incubated in complete medium containing DMSO or vindesine sulfate at 37°C for 120 min followed by fixation with ice-cold methanol. Cells were incubated with reovirus-specific polyclonal and α-tubulin-specific antiserum followed by Alexa Fluor IgG A488 or A546.

Coverslips were placed on slides using aqua-Poly/Mount mounting medium (Polysciences, Inc.).

Colocalization of reovirus particles with Rab5A-positive endosomes was assessed by transfecting CCL2 HeLa cells with EGFP-Rab5A (13) using Fugene 6 (Roche). Cells were incubated at 37°C for 24 h, incubated with medium containing DMSO or vindesine sulfate at 37°C for 1 h, adsorbed with A546-labeled reovirus at an MOI of 10^4 particles/cell, incubated with complete medium containing DMSO or vindesine sulfate for 120 min, fixed for 20 min with 10% formalin, quenched with 0.1 M glycine, washed with phosphate-buffered saline (PBS), and placed on slides using aqua-Poly/Mount mounting medium.

Colocalization of reovirus particles with LAMP1-positive endosomes was determined by incubating CCL2 HeLa cells with complete medium containing DMSO or vindesine sulfate at 37°C for 1 h followed by adsorption with A546-labeled reovirus at an MOI of 10^4 particles/cell and incubation with complete medium containing DMSO or vindesine sulfate for various intervals, after which the cells were fixed and stained with LAMP1-specific antibody. Colocalization of reovirus particles with dynein 1 was determined by adsorbing HBMECs or CCL2 HeLa cells with reovirus at an MOI of 10^4 particles/cell, after which the cells were incubated with complete medium for 20 min, fixed in methanol, and stained with reovirus-specific antiserum and dynein heavy chain-specific antibody.

Images were captured using a Zeiss LSM 510 Meta laser scanning confocal microscope and a 63×/1.40 numerical aperture (NA) Plan-Apochromat oil objective. Pinhole sizes were identical for all fluors. Images were normalized for pixel intensity, brightness, and contrast. Single sections of 0.39 μM thickness from a Z-stack are presented. Colocalization was determined using the Profile function of LSM Image software (Zeiss) (12, 13).

Flow cytometric analysis of reovirus internalization. CCL2 HeLa cells were treated with DMSO or vindesine sulfate in complete medium at 37°C for 1 h and adsorbed with A546-labeled reovirus at an MOI of 5×10^3 particles/cell at room temperature for 1 h. The inoculum was removed, and cells were incubated with complete medium containing DMSO or vindesine sulfate for various intervals. Cells were detached with Cellstripper (Cellgro) at 37°C for 15 min, quenched with fluorescence-activated cell sorter (FACS) buffer (PBS with 2% FBS), and stained with reovirus-specific polyclonal antiserum in FACS buffer at 4°C for 30 min. Cells were washed with FACS buffer, stained with Alexa Fluor-conjugated antibodies in FACS buffer at 4°C for 30 min, and fixed in PBS with 1% electron microscopy (EM)-grade paraformaldehyde (FACS Fix; Electron Microscopy Sciences).

Flow cytometric analysis of reovirus acidification was performed as previously described (13). Cells were treated with DMSO or vindesine sulfate in complete medium at 37°C for 1 h, adsorbed with pHrodo-labeled reovirus at an MOI of 5×10^3 particles/cell, incubated in complete medium containing DMSO or vindesine sulfate for various intervals, and fixed in FACS Fix. Cell staining was assessed using a BD LSRII flow cytometer and quantified using FlowJo software.

Knockdown of dynein 1 heavy chain by RNAi. HBMECs were transfected with 10 nM nonspecific siRNA or an siRNA specific for the dynein 1 heavy chain using Lipofectamine RNAi Max (Invitrogen) according to the manufacturer's instructions. Cells were incubated at 37°C for 48 h, adsorbed with reovirus at an MOI of 15 PFU/cell at room temperature for 1 h, and incubated at 37°C for 24 h. Cells were fixed with methanol and scored for infection by indirect immunofluorescence.

Immunoblotting for dynein 1 heavy chain. Immunoblot analysis of cell lysates was performed as previously described (12). Total cell lysates of HBMECs transfected with nonspecific or dynein 1 heavy chain-specific siRNAs were resolved by SDS-PAGE and immunoblotted with primary antibodies specific for dynein 1 heavy chain and actin. Membranes were scanned using an Odyssey imaging system, and band intensity was quantified using the Odyssey software suite.

CHKV infectivity assay. BHK-21 cells were incubated with DMSO or vindesine sulfate in complete medium at 37°C for 1 h and adsorbed with CHKV strain 181/25 or SL15649 at an MOI of 1 PFU/cell in the presence of DMSO or vindesine sulfate at 37°C for 1 h. The inoculum was removed, and cells were incubated with complete medium containing DMSO or vindesine sulfate at 37°C for 10 h. Cells were fixed with ice-cold methanol and incubated with CHKV-specific polyclonal antiserum, A488-labeled IgG, and 4′,6-diamidino-2-phenylindole (DAPI; Invitrogen). Cells were visualized using an Axiovert 200 fluorescence microscope (Zeiss). CHKV-positive cells were enumerated in three fields of view for triplicate samples and normalized to total cells per field.

Assessment of reovirus disassembly kinetics. CCL2 HeLa cells were treated with DMSO or vindesine sulfate in complete medium at 37°C for 1 h, adsorbed with reovirus at an MOI of 10 PFU/cell at room temperature for 1 h, and incubated in complete medium with DMSO or vindesine sulfate for various intervals. Total cell lysates were resolved by SDS-PAGE and immunoblotted with reovirus-specific polyclonal antiserum. Immunoblots were quantified by densitometry analysis using Odyssey software.

Statistical analysis. Mean values for at least triplicate experiments were compared using one-way analysis of variance (ANOVA) with Dunnett's multiple-comparison test (Graph Pad Prism). P values of <0.05 were considered to be statistically significant. Alternatively, samples were compared using an unpaired Student's t test (Graph Pad Prism). P values of <0.05 were considered to be statistically significant.

SUPPLEMENTAL MATERIAL

Supplemental material for this article may be found at http://mbio.asm.org/lookup/suppl/doi:10.1128/mBio.00405-13/-/DCSupplemental.

Text S1, DOCX file, 0.1 MB.
Figure S1, TIF file, 8.9 MB.
Table S1, PDF file, 0.1 MB.

ACKNOWLEDGMENTS

We thank Jennifer Konopka and Caroline Lai for critical review of the manuscript. We are grateful to members of the Dermody laboratory for useful suggestions during the course of this study. Small-molecule screening was conducted with assistance from the Vanderbilt High-Throughput Screening Facility. Confocal microscopy experiments were conducted in the Vanderbilt Cell Imaging Shared Resource. Flow cytometry experiments were performed in the Vanderbilt Cytometry Shared Resource.

This work was supported by Public Health Service awards T32 HL07751 (B.A.M. and A.W.A.), F32 A1801082 (B.A.M.), R01 AI32539 (T.S.D.), and U54 AI057157 (T.S.D.) and by the Elizabeth B. Lamb Center for Pediatric Research. Additional support was provided by Public Health Service awards P30 CA68485 for the Vanderbilt-Ingram Cancer Center and P60 DK20593 for the Vanderbilt Diabetes Research and Training Center.

REFERENCES

1. **Dermody TS, Parker J, Sherry B.** 2013. Orthoreoviruses. pp. 1304–1346. *In* Knipe DM, Howley PM (ed.), Fields virology, vol. 2, 6th ed., Lippincott Williams & Wilkins, Philadelphia, PA.
2. **Ouattara LA, Barin F, Barthez MA, Bonnaud B, Roingeard P, Goudeau A, Castelnau P, Vernet G, Paranhos-Baccalà G, Komurian-Pradel F.** 2011. Novel human reovirus isolated from children with acute necrotizing encephalopathy. Emerg. Infect. Dis. **17:**1436–1444.
3. **Kobayashi T, Antar AA, Boehme KW, Danthi P, Eby EA, Guglielmi KM, Holm GH, Johnson EM, Maginnis MS, Naik S, Skelton WB, Wetzel JD, Wilson GJ, Chappell JD, Dermody TS.** 2007. A plasmid-based reverse genetics system for animal double-stranded RNA viruses. Cell Host Microbe **1:**147–157.
4. **London SD, Cebra-Thomas JA, Rubin DH, Cebra JJ.** 1990. CD8 lymphocyte subpopulations in Peyer's patches induced by reovirus serotype 1 infection. J. Immunol. **144:**3187–3194.
5. **Maitra R, Ghalib MH, Goel S.** 2012. Reovirus: a targeted therapeutic—progress and potential. Mol. Cancer Res. **10:**1514–1525.
6. **Barton ES, Connolly JL, Forrest JC, Chappell JD, Dermody TS.** 2001.

Utilization of sialic acid as a coreceptor enhances reovirus attachment by multistep adhesion strengthening. J. Biol. Chem. **276:**2200–2211.
7. **Reiss K, Stencel JE, Liu Y, Blaum BS, Reiter DM, Feizi T, Dermody TS, Stehle T.** 2012. The GM2 glycan serves as a functional coreceptor for serotype 1 reovirus. PLoS Pathog. **8:**e1003078. doi: 10.1371/journal.ppat.1003078.
8. **Barton ES, Forrest JC, Connolly JL, Chappell JD, Liu Y, Schnell FJ, Nusrat A, Parkos CA, Dermody TS.** 2001. Junction adhesion molecule is a receptor for reovirus. Cell **104:**441–451.
9. **Campbell JA, Schelling P, Wetzel JD, Johnson EM, Wilson GA, Forrest JC, Aurrand-Lions M, Imhof BA, Stehle T, Dermody TS.** 2005. Junctional adhesion molecule-A serves as a receptor for prototype and field-isolate strains of mammalian reovirus. J. Virol. **79:**7967–7978.
10. **Forrest JC, Campbell JA, Schelling P, Stehle T, Dermody TS.** 2003. Structure-function analysis of reovirus binding to junctional adhesion molecule 1. Implications for the mechanism of reovirus attachment. J. Biol. Chem. **278:**48434–48444.
11. **Maginnis MS, Forrest JC, Kopecky-Bromberg SA, Dickeson SK, Santoro SA, Zutter MM, Nemerow GR, Bergelson JM, Dermody TS.** 2006. Beta1 integrin mediates internalization of mammalian reovirus. J. Virol. **80:**2760–2770.
12. **Mainou BA, Dermody TS.** 2011. Src kinase mediates productive endocytic sorting of reovirus during cell entry. J. Virol. **85:**3203–3213.
13. **Mainou BA, Dermody TS.** 2012. Transport to late endosomes is required for efficient reovirus infection. J. Virol. **86:**8346–8358.
14. **Ebert DH, Deussing J, Peters C, Dermody TS.** 2002. Cathepsin L and cathepsin B mediate reovirus disassembly in murine fibroblast cells. J. Biol. Chem. **277:**24609–24617.
15. **Maratos-Flier E, Goodman MJ, Murray AH, Kahn CR.** 1986. Ammonium inhibits processing and cytotoxicity of reovirus, a nonenveloped virus. J. Clin. Invest. **78:**1003–1007.
16. **Sturzenbecker LJ, Nibert M, Furlong D, Fields BN.** 1987. Intracellular digestion of reovirus particles requires a low pH and is an essential step in the viral infectious cycle. J. Virol. **61:**2351–2361.
17. **Borsa J, Morash BD, Sargent MD, Copps TP, Lievaart PA, Szekely JG.** 1979. Two modes of entry of reovirus particles into L cells. J. Gen. Virol. **45:**161–170.
18. **Boulant S, Stanifer M, Kural C, Cureton DK, Massol R, Nibert ML, Kirchhausen T.** 2013. Similar uptake but different trafficking and escape routes of reovirus virions and ISVPs imaged in polarized MDCK cells. Mol. Biol. Cell, **24:**1196–1207.
19. **Jordan MA.** 2002. Mechanism of action of antitumor drugs that interact with microtubules and tubulin. Curr. Med. Chem. Anticancer Agents **2:**1–17.
20. **Dumontet C, Jordan MA.** 2010. Microtubule-binding agents: a dynamic field of cancer therapeutics. Nat. Rev. Drug Discov. **9:**790–803.
21. **McGrogan BT, Gilmartin B, Carney DN, McCann A.** 2008. Taxanes, microtubules and chemoresistant breast cancer. Biochim. Biophys. Acta **1785:**96–132.
22. **Guéritte F.** 2001. General and recent aspects of the chemistry and structure-activity relationships of taxoids. Curr. Pharm. Des. **7:**1229–1249.
23. **Duflos A, Kruczynski A, Barret JM.** 2002. Novel aspects of natural and modified vinca alkaloids. Curr. Med. Chem. Anticancer Agents **2:**55–70.
24. **Gennerich A, Vale RD.** 2009. Walking the walk: how kinesin and dynein coordinate their steps. Curr. Opin. Cell Biol. **21:**59–67.
25. **Danthi P, Coffey CM, Parker JS, Abel TW, Dermody TS.** 2008. Independent regulation of reovirus membrane penetration and apoptosis by the mu1 phi domain. PLoS Pathog. **4:**e1000248. doi:10.1371/journal.ppat.1000248.
26. **Ebert DH, Wetzel JD, Brumbaugh DE, Chance SR, Stobie LE, Baer GS, Dermody TS.** 2001. Adaptation of reovirus to growth in the presence of protease inhibitor E64 segregates with a mutation in the carboxy terminus of viral outer-capsid protein sigma3. J. Virol. **75:**3197–3206.
27. **Connolly JL, Barton ES, Dermody TS.** 2001. Reovirus binding to cell surface sialic acid potentiates virus-induced apoptosis. J. Virol. **75:**4029–4039.
28. **Lai CM, Mainou BA, Kim KS, Dermody TS.** 2013. Directional release of reovirus from the apical surface of polarized endothelial cells. mBio **4:**e00049-13. doi: 10.1128/mBio.00049-13.
29. **Weatherbee JA, Luftig RB, Weihing RR.** 1978. In vitro polymerization of microtubules from HeLa cells. J. Cell Biol. **78:**47–57.
30. **Doyle JD, Danthi P, Kendall EA, Ooms LS, Wetzel JD, Dermody TS.** 2012. Molecular determinants of proteolytic disassembly of the reovirus outer capsid. J. Biol. Chem. **287:**8029–8038.
31. **Bayer N, Schober D, Prchl E, Murphy RF, Blaas D, Fuchs R.** 1998. Effect of bafilomycin A1 and nocodazole on endocytic transport in HeLa cells: implications for viral uncoating and infection. J. Virol. **72:**9645–9655.
32. **Pastorino B, Muyembe-Tamfum JJ, Bessaud M, Tock F, Tolou H, Durand JP, Peyrefitte CN.** 2004. Epidemic resurgence of chikungunya virus in democratic Republic of the Congo: identification of a new Central African strain. J. Med. Virol. **74:**277–282.
33. **Bernard E, Solignat M, Gay B, Chazal N, Higgs S, Devaux C, Briant L.** 2010. Endocytosis of chikungunya virus into mammalian cells: role of clathrin and early endosomal compartments. PLoS One **5:**e11479. doi: 10.1371/journal.pone.0011479.
34. **Huotari J, Helenius A.** 2011. Endosome maturation. EMBO J. **30:**3481–3500.
35. **Jordens I, Fernandez-Borja M, Marsman M, Dusseljee S, Janssen L, Calafat J, Janssen H, Wubbolts R, Neefjes J.** 2001. The Rab7 effector protein RILP controls lysosomal transport by inducing the recruitment of dynein-dynactin motors. Curr. Biol. **11:**1680–1685.
36. **Huang WR, Wang YC, Chi PI, Wang L, Wang CY, Lin CH, Liu HJ.** 2011. Cell entry of avian reovirus follows a caveolin-1-mediated and dynamin-2-dependent endocytic pathway that requires activation of p38 mitogen-activated protein kinase (MAPK) and Src signaling pathways as well as microtubules and small GTPase Rab5 protein. J. Biol. Chem. **286:**30780–30794.
37. **Salsman J, Top D, Boutilier J, Duncan R.** 2005. Extensive syncytium formation mediated by the reovirus FAST proteins triggers apoptosis-induced membrane instability. J. Virol. **79:**8090–8100.
38. **Bremner KH, Scherer J, Yi J, Vershinin M, Gross SP, Vallee RB.** 2009. Adenovirus transport via direct interaction of cytoplasmic dynein with the viral capsid hexon subunit. Cell Host Microbe **6:**523–535.
39. **Clemente R, de la Torre JC.** 2009. Cell entry of Borna disease virus follows a clathrin-mediated endocytosis pathway that requires Rab5 and microtubules. J. Virol. **83:**10406–10416.
40. **Hsieh MJ, White PJ, Pouton CW.** 2010. Interaction of viruses with host cell molecular motors. Curr. Opin. Biotechnol. **21:**633–639.
41. **Millán D, Chiriboga C, Patarroyo MA, Fontanilla MR.** 2013. Enterococcus faecalis internalization in human umbilical vein endothelial cells (HUVEC). Microb. Pathog. **57:**62–69.
42. **Contamin S, Galmiche A, Doye A, Flatau G, Benmerah A, Boquet P.** 2000. The p21 Rho-activating toxin cytotoxic necrotizing factor 1 is endocytosed by a clathrin-independent mechanism and enters the cytosol by an acidic-dependent membrane translocation step. Mol. Biol. Cell **11:**1775–1787.
43. **Hanser E, Mehlhorn H, Hoeben D, Vlaminck K.** 2003. In vitro studies on the effects of flubendazole against Toxocara canus and Ascaris suum. Parasitol. Res. **89:**63–74.
44. **Erikson JM, Tweedie DJ, Ducore JM, Prough RA.** 1989. Cytotoxicity and DNA damage caused by the azoxy metabolites of procarbazine in L1210 tumor cells. Cancer Res. **49:**127–133.
45. **Tatibana M, Kita K, Asai T.** 1982. Stimulation by 6-azauridine of carbamoyl phosphate synthesis for pyrimidine biosynthesis in mouse spleen slices. Eur. J. Biochem. **128:**625–629.
46. **Changeux JP.** 2012. The nicotinic acetylcholine receptor: the founding father of the pentameric ligand-gated ion channel superfamily. J. Biol. Chem. **287:**40207–40215.
47. **Hannon J, Hoyer D.** 2008. Molecular biology of 5-HT receptors. Behav. Brain Res. **195:**198–213.
48. **Dannhardt G, Kiefer W.** 2001. Cyclooxygenase inhibitors—current status and future prospects. Eur. J. Med. Chem. **36:**109–126.
49. **Morrison TE, Oko L, Montgomery SA, Whitmore AC, Lotstein AR, Gunn BM, Elmore SA, Heise MT.** 2011. A mouse model of chikungunya virus-induced musculoskeletal inflammatory disease: evidence of arthritis, tenosynovitis, myositis, and persistence. Am. J. Pathol. **178:**32–40.
50. **Iskarpatyoti JA, Willis JZ, Guan J, Morse EA, Ikizler M, Wetzel JD, Dermody TS, Contractor N.** 2012. A rapid, automated approach for quantitation of rotavirus and reovirus infectivity. J. Virol. Methods **184:**1–7.

JVI Journals.ASM.org

A Single-Amino-Acid Polymorphism in Chikungunya Virus E2 Glycoprotein Influences Glycosaminoglycan Utilization

Laurie A. Silva,[a,b] Solomiia Khomandiak,[a,b] Alison W. Ashbrook,[b,c] Romy Weller,[a,b]* Mark T. Heise,[d] Thomas E. Morrison,[e] Terence S. Dermody[a,b,c]

Departments of Pediatrics[a] and Pathology, Microbiology, and Immunology[c] and Elizabeth B. Lamb Center for Pediatric Research,[b] Vanderbilt University School of Medicine, Nashville, Tennessee, USA; Departments of Genetics and Microbiology and Immunology and Carolina Vaccine Institute, University of North Carolina—Chapel Hill, Chapel Hill, North Carolina, USA[d]; Departments of Microbiology and Immunology, University of Colorado School of Medicine, Aurora, Colorado, USA[e]

ABSTRACT

Chikungunya virus (CHIKV) is a reemerging arbovirus responsible for outbreaks of infection throughout Asia and Africa, causing an acute illness characterized by fever, rash, and polyarthralgia. Although CHIKV infects a broad range of host cells, little is known about how CHIKV binds and gains access to the target cell interior. In this study, we tested whether glycosaminoglycan (GAG) binding is required for efficient CHIKV replication using CHIKV vaccine strain 181/25 and clinical isolate SL15649. Preincubation of strain 181/25, but not SL15649, with soluble GAGs resulted in dose-dependent inhibition of infection. While parental Chinese hamster ovary (CHO) cells are permissive for both strains, neither strain efficiently bound to or infected mutant CHO cells devoid of GAG expression. Although GAGs appear to be required for efficient binding of both strains, they exhibit differential requirements for GAGs, as SL15649 readily infected cells that express excess chondroitin sulfate but that are devoid of heparan sulfate, whereas 181/25 did not. We generated a panel of 181/25 and SL15649 variants containing reciprocal amino acid substitutions at positions 82 and 318 in the E2 glycoprotein. Reciprocal exchange at residue 82 resulted in a phenotype switch; Gly^{82} results in efficient infection of mutant CHO cells but a decrease in heparin binding, whereas Arg^{82} results in reduced infectivity of mutant cells and an increase in heparin binding. These results suggest that E2 residue 82 is a primary determinant of GAG utilization, which likely mediates attenuation of vaccine strain 181/25.

IMPORTANCE

Chikungunya virus (CHIKV) infection causes a debilitating rheumatic disease that can persist for months to years, and yet there are no licensed vaccines or antiviral therapies. Like other alphaviruses, CHIKV displays broad tissue tropism, which is thought to be influenced by virus-receptor interactions. In this study, we determined that cell-surface glycosaminoglycans are utilized by both a vaccine strain and a clinical isolate of CHIKV to mediate virus binding. We also identified an amino acid polymorphism in the viral E2 attachment protein that influences utilization of glycosaminoglycans. These data enhance an understanding of the viral and host determinants of CHIKV cell entry, which may foster development of new antivirals that act by blocking this key step in viral infection.

Chikungunya virus (CHIKV) is a reemerging arbovirus indigenous to Africa and Asia that causes Chikungunya fever in humans (1, 2). This illness is most often characterized by rapid onset of fever, incapacitating polyarthralgia, rash, myalgia, and headache (1–3). Although viremia is usually cleared 5 to 7 days after infection, a characteristic feature of CHIKV disease is recurring polyarthritis that can persist for months or years (4–8). Several *Aedes* species of mosquitoes serve as vectors of CHIKV, including *A. aegypti* and *A. albopictus* (9–12). CHIKV caused an explosive outbreak of disease beginning in 2004 that expanded to areas beyond the historical range of the virus, including Europe and many islands in the Indian Ocean (1, 2, 13), and produced more-severe illness than previously observed (14–17). CHIKV continues to spread to new regions (18–22), and currently there are no available vaccines or treatments for this disease (23).

CHIKV is a member of the *Togaviridae* and belongs to the Old World Semliki Forest virus (SFV) group of arthritogenic alphaviruses (reviewed in reference 24). The CHIKV genome is ~11.8 kb comprising a single-stranded, message-sense RNA molecule that is capped and polyadenylated (25). Viral proteins are synthesized as two independent polyprotein precursors that undergo proteolytic cleavage by viral and cellular proteases. The virion is a 70-nm-diameter, icosahedral, enveloped particle that contains three structural proteins, a capsid protein and two glycoproteins, E1 and E2 (26–29). E1 and E2 form heterodimers that associate in trimers, which constitute spikes on the viral envelope (28, 30). E1 is a class II viral fusion protein, while E2 mediates attachment of the virus to cells and is the most likely candidate for engagement of cell-surface receptors (29). After attachment and internalization, CHIKV is thought to enter the endocytic pathway, where E1 mediates fusion of the viral and endosomal membranes (31). This process is dependent on acidification of endosomal vesicles and most likely occurs in early endosomes in both mammalian and mosquito cells (13, 31–34).

Attachment to the host cell surface is the initial step in viral

Received 25 October 2013 **Accepted** 19 December 2013
Published ahead of print 26 December 2013
Editor: D. S. Lyles
Address correspondence to Terence S. Dermody, terry.dermody@vanderbilt.edu.
* Present address: Romy Weller, Institute of Virology and Cell Biology, University of Lübeck, Lübeck, Germany.

doi:10.1128/JVI.03116-13

infection and a critical determinant of tissue tropism. Many viruses use adhesion strengthening to engage cells via low-affinity tethering to common cell-surface molecules such as carbohydrates followed by binding to less-abundant, usually proteinaceous molecules with higher affinity (35, 36). A diverse array of viral pathogens, including adenovirus (37), coxsackievirus B3 variant PD (38), dengue virus (39), enterovirus 71 (40), herpes simplex virus (41), HIV-1 (42), human papillomavirus (43), and respiratory syncytial virus (44), use glycosaminoglycans (GAGs) as attachment factors. GAGs are negatively charged, unbranched linear carbohydrate polymers consisting of repeating disaccharide units made of glucuronic acid or iduronic acid, linked to an amino sugar, glucosamine or galactosamine. Types of GAGs include heparan sulfate, keratan sulfate, chondroitin sulfate, and dermatan sulfate. GAGs are found on the surface of most mammalian cell types and in the extracellular matrix. These molecules are involved in a number of biological functions, including embryonic development, cell adhesion, proliferation, migration, wound healing, and extracellular matrix assembly, among many others (reviewed in references 45 and 46). Most GAG-protein interactions are mediated between the negatively charged polysaccharide chain or sulfate groups of the GAG and clusters of basic amino acids, which may form a conformation-specific binding site, in the protein ligand (46–49).

Certain strains of several alphaviruses, including eastern equine encephalitis virus (EEEV) (50), Ross River virus (RRV) (51), Sindbis virus (SINV) (52, 53), SFV (54), and Venezuelan equine encephalitis virus (VEEV) (55), use glycosaminoglycans as attachment receptors. During cell culture adaptation of many alphaviruses, basic amino acids in E2 glycoproteins are rapidly selected (51–53, 55, 56). Concordantly, positively charged amino acid substitutions in E2 are implicated in mediating interactions with GAGs and in most cases with heparan sulfate (50–55, 57–62). Heparan sulfate binding by alphaviruses and other viruses often correlates with attenuation of disease in animal models (50, 55–59, 63), likely due to rapid clearance of the virus from the circulation of the infected animal (55, 58). However, natural isolates of EEEV display dependence on GAGs for infection of cells in culture, which correlates with increased neurovirulence (50). In addition, several low-passage-number strains of VEEV also exhibit different degrees of GAG dependence (62). Thus, GAG binding might confer some replicative advantage during infection with EEEV or VEEV and perhaps other alphaviruses as well. The role of GAGs in replication of CHIKV clinical isolates is not clear.

In this study, we examined whether a clinical isolate (SL15649) (64) or an attenuated, vaccine strain (181/25) (65) requires cell-surface GAGs for efficient attachment to target cells and subsequent infection. Strain SL15649 was isolated from a CHIKV-infected patient in Sri Lanka in 2006, has been minimally passaged in cell culture, and is pathogenic in a mouse model of CHIKV disease (64). Strain 181/25 was derived from strain AF15661, which was isolated from a patient in Thailand in 1962. Strain 181/25 was developed as a vaccine candidate for CHIKV by adapting AF15561 to cell culture by 18 plaque-to-plaque passages in a human lung fibroblast cell line (MRC-5) (65). In both mouse (76, 80) and nonhuman primate models, 181/25 is attenuated but immunogenic (65). In addition, administration of 181/25 protects against CHIKV challenge in nonhuman primates (65). Although 181/25 (called TSI-GSD-218) was highly immunogenic in phase II clinical trials, ~8% of vaccinees developed mild, transient arthralgia, suggesting partial or unstable attenuation (66, 67). Gardner et al. previously demonstrated that 181/25 infectivity was decreased in GAG-deficient Chinese hamster ovary (CHO) cells, suggesting that this laboratory-adapted strain is dependent on GAGs for infectivity (76). Here, we expanded upon previous studies and found that several GAGs competitively inhibit infectivity of BHK-21 cells by 181/25 but not SL16549. In contrast, both 181/25 and SL15649 depend on cell-surface GAGs for binding and infection of CHO cells. Furthermore, we identified residue 82 in the E2 glycoprotein as a key determinant of GAG utilization and binding to heparin by CHIKV. Collectively, these findings indicate that vaccine strain 181/25 is more dependent on GAGs than SL15649 for infectivity and suggest a mechanism of attenuation for 181/25.

MATERIALS AND METHODS

Cells and reagents. BHK-21 cells (ATCC CCL-10) were maintained in alpha minimal essential medium (αMEM; Gibco) supplemented to contain 10% fetal bovine serum (FBS) and 10% tryptose phosphate. Vero 81 cells (ATCC CCL-81) were maintained in αMEM supplemented to contain 5% FBS. Parental CHO-K1 and mutant CHO-pgsA745, CHO-pgsB761, and CHO-pgsD677 cell lines were maintained in Ham's F-12 nutrient mixture (Gibco) supplemented to contain 10% FBS. Media for all cells were supplemented with 0.29 mg/ml L-glutamine (Gibco), 100 U/ml penicillin (Gibco), 100 μg/ml streptomycin (Gibco), and 25 ng/ml amphotericin B. Cells were maintained at 37°C in an atmosphere of 5% CO_2. Parental CHO-K1 and CHO-pgsA745 cell lines were provided by Benhur Lee (University of California, Los Angeles). CHO-pgsB761 and CHO-pgsD677 cell lines were provided by Mark Peeples (The Research Institute at Nationwide Children's Hospital) with permission from Jeffrey Esko (University of California, San Diego). All chemicals were purchased from Sigma unless otherwise noted.

Biosafety. All studies using viable SL15649 and any mutant virus were conducted in a certified biological safety level 3 facility in biological safety cabinets with protocols approved by Vanderbilt University Department of Environment, Health, and Safety and the Vanderbilt Institutional Biosafety Committee.

Viruses. Virus stocks were generated from full-length wild-type (WT) and mutant virus infectious cDNA clones as described in references 64 and 68. Plasmids containing virus cDNAs were linearized by digestion with NotI-HF (NEB). Capped, full-length RNA transcripts were generated *in vitro* using mMessage mMachine SP6 transcription kits (Ambion) and introduced into BHK-21 cells by electroporation using a Gene Pulser electroporator (Bio-Rad). Culture supernatants were harvested 24 to 48 h after electroporation and clarified by centrifugation at 855 × *g* for 20 min. Virus stocks were purified by ultracentrifugation of clarified supernatants through a 20% sucrose cushion in TNE buffer (50 mM Tris-HCl [pH 7.2], 0.1 M NaCl, and 1 mM EDTA) at ~115,000 × *g* in a Beckman 32Ti rotor. Virus pellets were resuspended in virus dilution buffer (VDB; RPMI medium containing 20 mM HEPES [Gibco] supplemented to contain 1% FBS), aliquoted, and stored at −70°C. Virus titers were determined by plaque assay using Vero cells.

Assessment of CHIKV infectivity. BHK-21 cells (~4×10^3 cells/well) or CHO cells (~8×10^3 cells/well) were seeded into wells of 48-well plates (Costar) and incubated at 37°C for 24 h. Triplicate wells were inoculated with various virus strains at a multiplicity of infection (MOI) of 2.5 (BHK-21) or 10 (CHO) PFU/cell in VDB. Following adsorption at 37°C for 2 h, the inoculum was removed, and cells were incubated at 37°C for 18 h in complete medium containing 20 mM NH_4Cl (to block subsequent rounds of viral replication). Cells were washed twice with PBS, fixed in 100% ice-cold methanol, and incubated at −20°C for at least 20 min. Infected cells were visualized using indirect immunofluorescence. Cells were incubated in blocking buffer (phosphate-buffered saline [PBS; Gibco] containing 5% FBS and 0.1% Triton X-100) at room temperature for 1 h and stained with precleared anti-CHIKV immune ascetic fluid

(ATCC VR-1241AF) diluted 1:1,500 and secondary Alexa 488 goat anti-mouse antibody diluted 1:1,000 (Invitrogen), followed by addition of DAPI (4′,6-diamidino-2-phenylindole) to visualize cell nuclei. All antibodies were diluted in blocking buffer. For some experiments, cells were visualized using an Axiovert 200 fluorescence microscope (Zeiss). Total and CHIKV-infected cells were quantified using ImageJ software (69) in two fields of view per well. For other experiments, cells were visualized using an ImageExpress Micro XL imaging system (Molecular Devices) at the Vanderbilt High-Throughput Screening Facility. Total and CHIKV-infected cells were quantified using MetaExpress software (Molecular Devices) in two fields of view per well. No background stain was noted on uninfected control monolayers.

Infectivity inhibition assays. Purified CHIKV virions were pretreated with a range of dilutions of heparin, heparan sulfate, chondroitin sulfate A, chondroitin sulfate A/C/E from shark, dermatan sulfate, or hyaluronic acid at 4°C for 30 min before inoculation of BHK-21 monolayers with virus-GAG mixtures. For some experiments, bovine serum albumin (BSA) was included as a negative control. Following incubation at 37°C for 2 h, the inoculum was removed, and cells were incubated at 37°C for 18 h in complete medium with 20 mM NH_4Cl. Infectivity was quantified using indirect immunofluorescence.

Flow cytometric analysis of virus binding to cells. The effect of soluble GAGs on CHIKV binding to BHK-21 cells was determined by preincubating virus with GAGs in VDB at various concentrations at 4°C for 30 min. BHK-21 monolayers were washed and detached using Cellstripper (Cellgro), quenched with fluorescence-activated cell-sorting (FACS) buffer (PBS supplemented to contain 2% FBS), pelleted at 600 × *g*, washed once with PBS, and pelleted a second time at 600 × *g*. Cells (~1×10^5 to 3×10^5) were adsorbed with the virus-GAG mixtures at an MOI of 5 PFU/cell and incubated at 4°C for 30 min, washed twice in VDB, pelleted, and stained in VDB containing CHIKV-specific mouse monoclonal antibody CHK-187 (provided by Michael Diamond, Washington University). Cells were washed twice in VDB, pelleted, and stained in VDB containing Alexa Fluor 488-labeled goat anti-mouse IgG (Molecular Probes) at 4°C for 30 min. Cells were washed twice in VDB, pelleted, and fixed in FACS fix (PBS supplemented to contain 1% electron microscopy [EM]-grade paraformaldehyde [Electron Microscopy Sciences]). Cell-associated fluorescence was quantified using an LSRII flow cytometer (BD Biosciences, Vanderbilt University Flow Cytometry Shared Resource). The mean fluorescence intensity (MFI) of forward- and side-scatter gated populations was determined using FACSDiva software (BD Biosciences). Binding of pretreated virus to BHK-21 cells was normalized to binding of untreated virus controls and expressed as percent bound virus. Binding assays were performed using triplicate samples with at least 5×10^3 cells analyzed for each sample.

CHO cell monolayers were washed once with PBS and detached using Cellstripper (Cellgro) at 37°C, quenched with FACS buffer, pelleted at 600 × *g*, washed once with PBS, and pelleted a second time at 600 × *g*. Cells (~1×10^5 to 3×10^5) were adsorbed with virus at an MOI of 5 PFU/cell at 4°C for 1 h. Bound virus was quantified using flow cytometry. Binding of each virus to mutant CHO cells was normalized to virus bound to parental CHO-K1 cells and expressed as percent bound virus.

Kinetic heparan sulfate protection assay. Purified virions of strain 181/25 were adsorbed to monolayers of BHK-21 cells (~10^4) at an MOI of 2.5 PFU/cell. At 10 or 30 min prior to or 5, 10, 20, 30, or 45 min after adsorption, either heparan sulfate (250 μg/ml) or BSA (250 μg/ml) was added to the virus inoculum and rapidly mixed. Following incubation at 37°C for 2 h, the inoculum was removed, and cells were incubated at 37°C for 18 h in complete medium with 20 mM NH_4Cl. Infectivity was quantified using indirect immunofluorescence.

Kinetic ammonium chloride protection assay. Monolayers of BHK-21 cells (~10^4) seeded in 48-well plates were adsorbed with virus strains at an MOI of 2.5 PFU/cell and incubated at 37°C. At various times after adsorption, the inoculum was removed, and cells were incubated in complete medium containing 20 mM NH_4Cl at 37°C for 18 h. Infectivity was quantified using indirect immunofluorescence.

Generation of mutant viruses. Reciprocal single and double amino acid substitutions in the E2 glycoprotein were introduced into plasmids containing cDNAs of either strain 181/25 (p181/25 [68]) or SL15649 (pMH56.1 [64]) by PCR using mutagenic primers. Clones containing desired mutations were identified by DNA sequencing (GenHunter and Vanderbilt Sequencing Core) and digested with restriction endonucleases (SmaI and XhoI for p181/25 and SfiI and XhoI for pMH56.1). Mutagenized fragments were subcloned into unmodified versions of p181/25 or pMH56.1. Sequences of subcloned fragments of each mutant were determined to verify the fidelity of mutagenesis. Primer sequences for mutagenesis and sequencing are available from the corresponding author by request.

Genome-to-PFU ratios. The number of CHIKV genomes/ml for each purified virus stock was determined using reverse transcription-quantitative PCR (RT-qPCR). Viral RNA was extracted from 10 μl of purified virus stocks using TRIzol reagent (Life Technologies), purified using a PureLink RNA Minikit (Life Technologies), and eluted into a final volume of 100 μl. Quantification of the number of genomes in each virus stock was performed using a qScript XLT One-step RT-qPCR ToughMix kit (Quanta Biosciences) according to the manufacturer's instructions with minor modifications. Each 20-μl reaction mixture contained 5 μl viral RNA, 450 nM forward primer (SL15649for [874 5′-AAAGGGCAAACTC AGCTTCAC-3′] or 181-25for [5′-AAAGGGCAAGCTTAGCTTCAC-3′]), 900 nM reverse transcriptase and reverse primer (CHIKVrev [961 5′-GCCTGGGCTCATCGTTATTC-3′]), and 200 nM fluorogenic probe (CHIKVprobe [899 5′-6-carboxyfluorescein {dFAM}-CGCTGTGATAC AGTGGTTTCGTGTG-black hole quencher {BHQ}-3′]; Biosearch Technologies). Standard curves relating threshold cycle (C_T) values to copies of genomic RNA were generated from *in vitro*-transcribed genomic 181/25 or SL15649 RNA as described. Ten-fold dilutions of genomic RNA, from 10^{10} to 10^5 copies, were generated by calculating the number of genomes from *in vitro*-transcribed RNA by dividing the mass (measured by spectrometry [Nanodrop; Thermo Scientific]) by the genome molecular mass. RT-qPCR was performed using an Applied Biosystems 7500 Real-Time PCR system (Life Technologies, Foster City, CA) under the following cycling conditions: 50°C for 2 min, 95°C for 10 min, 40 cycles of 95°C for 15 s, and 60°C for 60 s, with data acquisition in the FAM channel during the 60°C step. The viral RNA concentration in each sample was determined by comparing C_T values of samples to the appropriate standard curve. Genome values per ml are expressed as the means of the results from two wells for three samples. Genome/PFU ratios are expressed as the mean number of genomes/ml divided by the mean number of PFU/ml for three RNA replicates using values from three plaque assay titrations.

Heparin-agarose-binding assay. Heparin-coated agarose beads or unconjugated beads were washed twice in PBS and twice in VDB. Washed beads (0.075 ml) were mixed with ~1×10^9 genomes of each virus in VDB and incubated with gentle agitation at 4°C for 30 min. Beads were washed three times in VDB and resuspended in 35 μl of 1× sample buffer (50 mM Tris-HCl [pH 6.8], 2% [wt/vol] sodium dodecyl sulfate [SDS], 1% β-mercaptoethanol, 6% [vol/vol] glycerol, 0.004% [wt/vol] bromophenol blue). Samples containing 12.5% of the input virus in 20 μl VDB were incubated with an equivalent volume of 2× sample buffer. All samples were boiled for 10 min, removed from the biosafety level 3 (BSL3) laboratory after disinfection, and stored at −70°C. Samples were resolved by SDS-polyacrylamide gel electrophoresis (PAGE) in 10% polyacrylamide gels (Bio-Rad) and transferred to an Immun-Blot polyvinylidene difluoride (PVDF) membrane (Bio-Rad). Membranes were incubated at room temperature for 1 h in blocking buffer (Tris-buffered saline [TBS] with 5% powdered milk), followed by incubation with mouse monoclonal antibody specific for CHIKV E2 (CHK 48-G8; provided by Michael Diamond, Washington University) diluted in TBS-T (TBS with 0.1% Tween 20) at 4°C overnight with gentle agitation. Membranes were washed with TBS-T three times for 5 min each time and incubated for 1 to 2 h with goat

anti-mouse secondary antibody conjugated to IRDye 800CW (Li-COR) dye diluted 1:2,000 in TBS-T at room temperature. Following three 5-min washes with TBS-T, membranes were rinsed twice with double-distilled water and scanned using an Odyssey imaging system (Li-COR).

Structural and sequence analysis. The crystallographic structure of the CHIKV E1/E2 trimer placed into the Sindbis virus cryo-EM map (Protein Data Base [PDB] accession no. 2XFB [30]) was used as a template to model the electrostatic surface potential of the E1/E2 trimers of SL15649 and 181/25. Coot (70) was used to alter 12 of the 16 amino acids within E2 that are located in the crystal structure from SL15649 to 181/25 residues using the lowest free-energy rotamers. Electrostatic surface potentials for 181/25 and SL15649 were generated with the Adaptive Poisson-Boltzmann Solver (APBS) (71) using the PyMOL plug-in as implemented in PyMOL under dielectric constants of 2.0 and 80.0 for protein and solvent regions, respectively, and contoured at levels of ± 2.5 kT.

Amino acid sequences of the E2 protein from 158 CHIKV strains were aligned using data obtained from the NIAID Virus Pathogen Database and Analysis Resource (ViPR) (72) online through the web site at http://www.viprbrc.org.

Statistical analysis. Statistical analysis was performed using GraphPad Prism (Graphpad). Soluble-GAG competition assays and time course assays were evaluated for statistically significant differences by one-way analysis of variance (ANOVA) followed by Dunnett's *post hoc* test. Calculation of 50% inhibitory concentration (IC_{50}) values with 95% confidence intervals was facilitated using GraphPad Prism. Binding and infectivity assays with CHO cells and infectivity assays with mutant viruses were evaluated for statistically significant differences by one-way ANOVA followed by Tukey's multiple-comparison test. *P* values of <0.05 were considered to be statistically significant. All differences not specifically indicated to be significant were not significant ($P > 0.05$). All experiments were performed in triplicate at least twice.

RESULTS

Inhibition of strain 181/25 infectivity by soluble GAGs. We hypothesized that CHIKV vaccine strain 181/25 might have become adapted to use GAGs as attachment receptors during passage in cell culture, as has been demonstrated for other alphaviruses (51–53, 55). We also thought it possible that a clinical isolate of CHIKV could use GAGs for infectivity, as has been noted for natural isolates of EEEV and VEEV (50, 62). To assess whether soluble GAGs act as competitive agonists and block infectivity of CHIKV strains 181/25 and SL15649, we performed competition assays using increasing concentrations of different GAGs. Purified 181/25 or SL16549 virions were preincubated with heparin, heparan sulfate, chondroitin sulfate A, dermatan sulfate, hyaluronic acid, shark cartilage chondroitin sulfate, or bovine serum albumin and adsorbed to BHK-21 cells. Cells were scored for infectivity in a single-round replication assay using indirect immunofluorescence. Preincubation of 181/25 with heparin, heparan sulfate, chondroitin sulfate A, or dermatan sulfate decreased infectivity of BHK-21 cells in a dose-dependent manner (Fig. 1A). Dermatan sulfate and heparan sulfate were the most potent inhibitors of 181/25 infectivity in this assay. Chondroitin sulfate A and heparin were also potent inhibitors of 181/25 infectivity. Hyaluronic acid and a mixture of chondroitin sulfate A/C/E from shark cartilage also inhibited 181/25 in a dose-dependent manner (Table 1 and data not shown). As a control, BSA did not significantly diminish infectivity at any dose tested (Fig. 1A). In addition, heparin inhibited 181/25 plaque formation in a dose-dependent manner using plaque-reduction assays (data not shown). We also tested whether heparin preincubation could inhibit 181/25 produced by C6/36 mosquito cells and found that mosquito-derived virus was inhibited by this soluble GAG in a dose-dependent manner and to an extent similar to that seen with mammalian-derived 181/25 (data not shown). Preincubation of 181/25 with soluble GAGs also inhibited infectivity of CHO-K1 cells (data not shown), indicating that the inhibitory effect of GAGs on 181/25 infectivity is not restricted to BHK-21 cells. Importantly, preincubation of cells with 500 μg/ml of heparin, heparan sulfate, chondroitin sulfate A, dermatan sulfate, and hyaluronic acid prior to viral infection did not inhibit infectivity of 181/25 (data not shown). These results indicate that the inhibitory effect of soluble GAGs is due to interactions with virus and not cells.

In contrast to the 181/25 results, the infectivity of strain SL15649 was not significantly altered in a dose-dependent manner by any of the soluble GAGs tested (Fig. 1B and data not shown). These data indicate that 181/25 and SL15649 differ in susceptibility to inhibition by soluble GAGs and suggest that these CHIKV strains exhibit differential interactions with GAGs, possibly in the affinity for GAGs or in the nature of GAG interactions.

Since the infectivity of strain 181/25 was efficiently inhibited by GAGs, we next tested whether incubation of virus with soluble GAGs blocks binding of 181/25 to BHK-21 cells. Purified 181/25 virions were incubated with soluble GAGs prior to adsorption to BHK-21 cells. Virus binding was assessed using flow cytometry (Fig. 1C). Higher concentrations of GAGs were used in this assay since greater numbers of virion particles are required to detect a fluorescence signal following binding. Similar to the infectivity results, virus binding to BHK-21 cells was effectively blocked by preincubation with each of the GAGs tested in a dose-dependent manner. In this assay, heparin was the most potent inhibitor of binding of 181/25 to BHK-21 cells. Dermatan sulfate and heparan sulfate also inhibited binding, as did chondroitin sulfate A, but at much higher concentrations (Table 1). Differences in the magnitude of inhibition by specific soluble GAGs in the infectivity and binding assays are likely due to differences in assay conditions, including cell number, virus concentration, temperature, and duration of adsorption. Collectively, these data indicate that soluble GAGs inhibit infectivity of strain 181/25, but not SL15649, on BHK-21 cells by blocking 181/25 from binding to the cell surface and suggest that 181/25 and GAGs directly interact.

Inhibition of 181/25 by soluble heparan sulfate occurs prior to endosomal escape. To determine whether inhibition of 181/25 infectivity by soluble GAGs occurs during an early step of the entry process prior to endosomal escape, we defined the temporal window at which heparan sulfate acts by adding the GAG to virus inocula at various times during the adsorption phase. Consistent with our previous observations (Fig. 1A), incubation of 181/25 with heparan sulfate prior to adsorption resulted in almost complete inhibition of 181/25 infectivity (Fig. 2A), whereas incubation with BSA had no effect (data not shown). Inhibition of 181/25 infectivity by heparan sulfate diminished as a function of time following viral adsorption. Notably, almost 50% of the inhibitory effect of heparan sulfate was lost when it was added 20 min post-adsorption (~56% infected cells; $P < 0.01$ compared with the BSA control). When added 45 min after adsorption, heparan sulfate lost almost all inhibitory effect (~88% infected cells; $P < 0.01$ compared with the BSA control). These data indicate that heparan sulfate inhibits 181/25 infectivity early in the infectious cycle.

Since attachment of CHIKV occurs prior to internalization of the virus into the endocytic pathway, we sought to determine the time required for 181/25 to escape the endosome and become resistant to a lysosomotropic agent. We assessed the capacity of

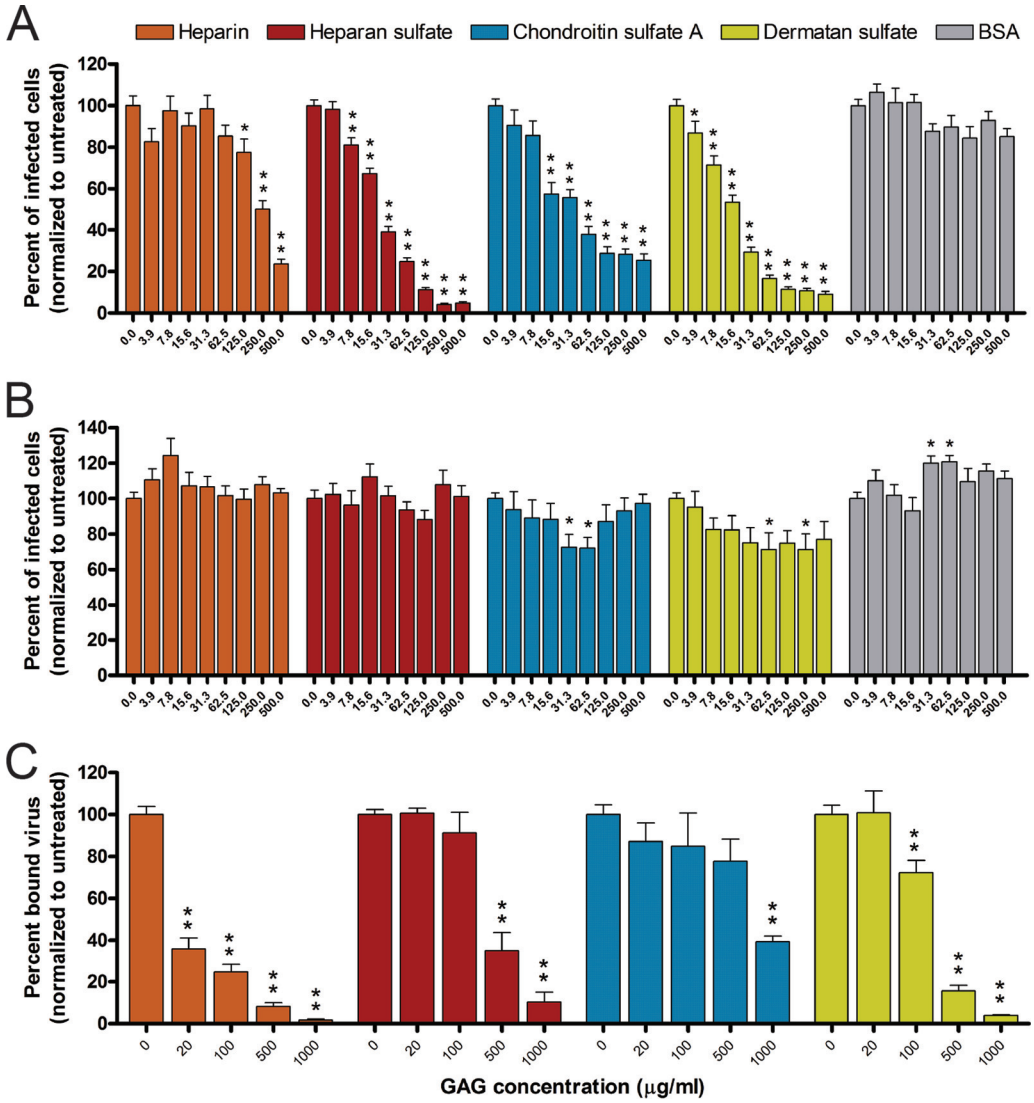

FIG 1 Soluble GAGs inhibit 181/25 infectivity and binding. (A and B) Purified virions of strain 181/25 (A) or SL15649 (B) (MOI of ~2.5 PFU/cell) were incubated with buffer alone or buffer containing heparin, heparan sulfate, chondroitin sulfate A, dermatan sulfate, or bovine serum albumin (BSA) at the concentrations shown at 4°C for 30 min prior to adsorption to BHK-21 cells. At 2 hpi, the inoculum was replaced with medium containing 20 mM NH_4Cl. At 18 hpi, infected cells were detected by indirect immunofluorescence. Results are expressed as the mean percentage of infected cells normalized to untreated controls for three (181/25) or two (SL15649) independent experiments performed in triplicate. Error bars indicate SEM. *, $P < 0.05$; **, $P < 0.01$ (in comparison to untreated controls as determined by one-way ANOVA followed by Dunnett's *post hoc* test). (C) Strain 181/25 (MOI of ~5 PFU/cell) was incubated with buffer alone or buffer containing heparin, heparan sulfate, chondroitin sulfate A, or dermatan sulfate at the concentrations shown at 4°C for 30 min. Virus-GAG mixtures were adsorbed to BHK-21 cells at 4°C for 30 min and stained with a CHIKV-specific antibody. The MFI of each sample was determined by flow cytometry. The data were normalized to the MFI of untreated virus controls for three independent experiments performed in triplicate. Error bars indicate SEM. *, $P < 0.01$ (in comparison to untreated controls as determined by one-way ANOVA followed by Dunnett's *post hoc* test).

NH_4Cl to inhibit 181/25 infectivity of BHK-21 cells when added at various times during the adsorption phase (Fig. 2B). NH_4Cl raises the pH of intracellular organelles within 1 min following addition to the medium (73), thereby allowing inhibition of low-pH-dependent endosomal escape by the virus at defined intervals postinfection. BHK-21 cells were adsorbed with 181/25 virions, and medium containing 20 mM NH_4Cl was added at various intervals after adsorption. The percent infected cells at 18 hours postinfection (hpi) was determined by indirect immunofluorescence and normalized to the infectivity of 181/25 when NH_4Cl was added at 120 min after infection. When NH_4Cl was added at 5 min postadsorption, only 4.5% of cells were infected by 181/25 ($P < 0.01$). Inhibition of 181/25 infectivity by NH_4Cl decreased gradually over time, with approximately half of the inhibitory effect lost by 45 min postadsorption ($P < 0.01$) and all the inhibitory effect lost by 100 min postadsorption ($P > 0.05$). These data confirm previous observations that endosomal acidification is essential for CHIKV infection of cells (13, 31–34) and suggest that inhibition of 181/25 infectivity by heparan sulfate occurs prior to inhibition by NH_4Cl.

CHIKV strains 181/25 and SL15649 require cell-surface GAGs for binding and infectivity. To examine whether GAGs are required for CHIKV infection, we tested 181/25 and SL15649 for the capacity to infect parental CHO-K1 cells and a panel of mutant

TABLE 1 Inhibition of 181/25 infectivity and binding by soluble GAGs

Inhibitor	Infectivity		Binding	
	Inhibition (%)[a]	IC_{50}, μg/ml (95% CI)[b]	Inhibition (%)[c]	IC_{50}, μg/ml (95% CI)[b]
Heparin	76.4 ± 9.8	248.5 (203.6–303.5)	98.3 ± 1.3	7.9 (3.542–17.74)
Heparan sulfate	95.1 ± 3.4	25.3 (23.3–27.5)	90.9 ± 11.4	357.7 (254.0–503.7)
Chondroitin sulfate A	74.6 ± 13.3	44.5 (34.4–57.5)	96.0 ± 0.6	179.1 (130.6–245.7)
Dermatan sulfate	90.9 ± 6.9	17.5 (15.21–19.35)	60.6 ± 6.5	>750[d]
Chondroitin sulfate A/C/E	78.2 ± 11.0	9.0 (6.469–12.52)	ND[e]	ND
Hyaluronic acid	86.7 ± 8.6	112.3 (97.9–128.8)	ND	ND

[a] Percent inhibition of infectivity compared with untreated controls (at a concentration of inhibitor of 500 μg/ml) ± standard error of the mean.
[b] Inhibitory concentration of each GAG that prevents 50% of infectivity (IC_{50}) relative to untreated controls with the 95% confidence interval (CI).
[c] Percent inhibition of binding compared with controls (at a concentration of inhibitor of 1,000 μg/ml) ± standard error of the mean.
[d] Could not be determined accurately due to partial dose response.
[e] ND, not determined.

CHO cells that display various defects in GAG biosynthesis (Fig. 3A). Parental CHO-K1 and mutant cell lines were adsorbed with either strain and scored for infectivity using conditions to allow a single infectious cycle. Cell line pgsA745, which is deficient in xylosyltransferase activity and thus lacks expression of all GAGs (74, 75), was highly resistant to infection by 181/25 (~0.5% infected cells; $P < 0.001$ compared with the CHO-K1 cells), confirming previous observations (76). These cells also were resistant to infection by SL15649 (~18% infected cells; $P < 0.001$ compared with the CHO-K1 cells). pgsA745 cells were less susceptible to strain 181/25 than to strain SL1649 ($P < 0.001$), suggesting that 181/25 is more dependent than SL15649 on GAGs for efficient infection. Cell line pgsB761, which is deficient in galactosyltransferase I and expresses only ~5% of the wild-type levels of heparan sulfate and chondroitin sulfate (75), was highly resistant to 181/25 infection (~7% infected cells; $P < 0.001$) but highly susceptible to SL15649 infection, with the infectivity level nearing that of parental CHO-K1 cells (~97% infected cells; $P > 0.05$). Similarly, cell line pgsD677, which is deficient in both N-acetylglucosaminyltransferase and glucuronosyltransferase activity and produces a 3-fold excess of chondroitin sulfate but no heparan sulfate (77), was highly resistant to 181/25 (~2% infected cells; $P < 0.001$) but susceptible to SL15649 (~70% infected cells; $P < 0.001$), albeit less susceptible than the pgsB761 cell line. These results suggest that both vaccine strain 181/25 and clinical isolate SL15649 depend on cell-surface GAGs for efficient infection but that the specific GAGs or structural specificities of the GAGs used by these viruses may differ.

To determine whether GAGs are required for attachment of 181/25 and SL15649 to CHO cells, we tested both viruses for the capacity to bind parental and mutant CHO cell lines. Cells were incubated with either virus strain and scored for binding using flow cytometry (Fig. 3B). Strain 181/25 did not efficiently bind to any of the mutant cell lines ($P < 0.001$ for pgsA745, pgsB761, and pgsD677 compared with CHO-K1). In contrast, SL15649 bound modestly to both pgsB761 and pgsD677 cells ($P < 0.001$ for both cell lines compared with CHO-K1) but less well to pgsA745 cells ($P < 0.001$ compared with CHO-K1). To confirm that CHO-K1 and mutant cell lines can support viral replication if entry steps are bypassed, we introduced *in vitro*-transcribed 181/25 RNA into both CHO-K1 and pgsA745 cells by electroporation and determined titers of progeny virus in cell supernatants 24 h later. We found that CHO-K1 and pgsA745 cells produce infectious virus to similar extents following viral RNA electroporation (data not

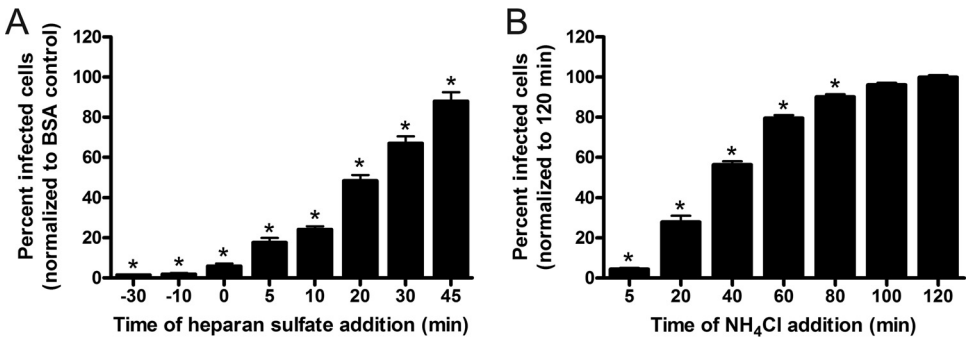

FIG 2 Kinetics of inhibition of 181/25 by heparan sulfate and ammonium chloride. (A) 181/25 virions (MOI of ~2.5 PFU/cell) were adsorbed to BHK-21 cells at 37°C. At the times shown prior to or during adsorption, heparan sulfate (250 μg/ml) was added to the virus inoculum. After 2 h adsorption, unbound virus was removed, and cells were incubated with medium containing 20 mM NH_4Cl. At 18 hpi, infected cells were detected by indirect immunofluorescence. Results are expressed as the mean percentage of infected cells normalized to BSA-treated controls from two independent experiments performed in triplicate. Error bars indicate SEM. *, $P < 0.01$ (in comparison to BSA-treated controls as determined by one-way ANOVA followed by Dunnett's *post hoc* test). (B) 181/25 virions (MOI of ~2.5 PFU/cell) were adsorbed to BHK-21 cells at 37°C. At the times shown following adsorption, the virus inoculum was removed, and cells were incubated with medium containing 20 mM NH_4Cl. At 18 hpi, infected cells were detected by indirect immunofluorescence using a CHIKV-specific polyclonal antibody. Results are expressed as the mean percentage of infected cells normalized to the percentage of infected cells when NH_4Cl was added at 120 min from three independent experiments performed in triplicate. Error bars indicate SEM. *, $P < 0.01$ (in comparison to untreated controls as determined by one-way ANOVA followed by Dunnett's *post hoc* test).

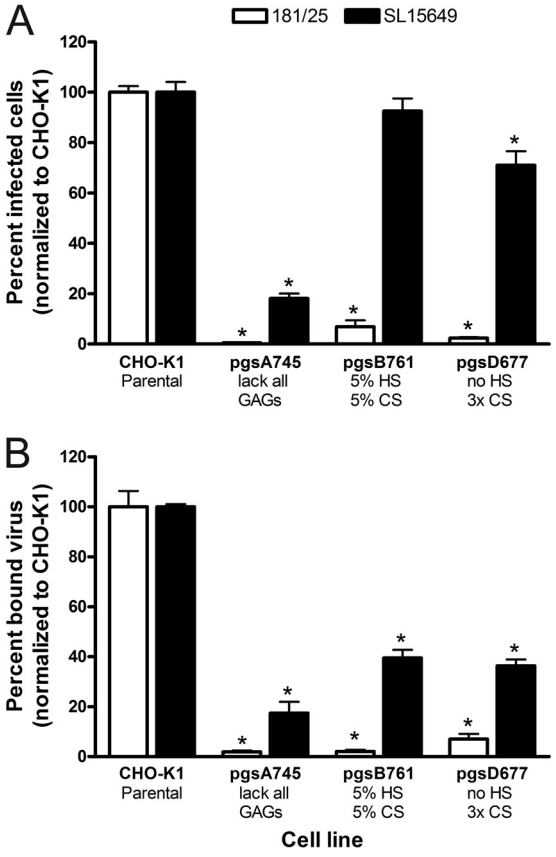

FIG 3 CHIKV 181/25 and SL15649 infectivity of and binding to parental and mutant CHO cells. (A) Parental CHO-K1, pgsA745, pgsB761, and pgsD677 cells were adsorbed with an MOI of ~10 PFU/cell of either 181/25 or SL15649. At 2 hpi, the inocula were replaced with medium containing 20 mM NH_4Cl. At 18 hpi, infected cells were detected by indirect immunofluorescence. Results are expressed as the mean percentage of infected cells normalized to the percentage of infected parental CHO-K1 cells for three (181/25) or two (SL15649) independent experiments performed in triplicate. Error bars indicate SEM. *, $P < 0.001$ (in comparison to the infectivity of the appropriate parental virus in CHO-K1 cells as determined by one-way ANOVA followed by Tukey's multiple-comparison test). (B) Parental CHO-K1, pgsA745, pgsB761, and pgsD677 cells were adsorbed with an MOI of ~5 PFU/cell of either 181/25 or SL15649 at 4°C for 1 h and stained with a CHIKV-specific antibody. The mean fluorescence intensity (MFI) of each sample was determined by flow cytometry. The data were normalized to the MFI of virus bound to parental CHO-K1 cells for three (181/25) or two (SL15649) independent experiments performed in triplicate. Error bars indicate SEM. *, $P < 0.001$ (in comparison to the binding of the appropriate parental virus to CHO-K1 cells as determined by one-way ANOVA followed by Tukey's multiple-comparison test). GAG, glycosaminoglycan; HS, heparan sulfate; CS, chondroitin sulfate.

shown). Together, these data indicate that both vaccine strain 181/25 and clinical isolate SL15649 depend on cell-surface GAGs for infection, specifically at the stage of viral attachment.

E2 residue 82 influences dependence on cell-surface GAGs. Although both 181/25 and SL15649 depend to some extent on cell-surface GAGs for efficient binding and infectivity, these strains display differences in the requirement for GAG utilization and inhibition by soluble GAGs. To identify amino acids responsible for these differences, we compared E2 amino acid sequences of 181/25 and SL15649 and found 16 amino acid polymorphisms (Table 2). Interestingly, 181/25 E2 contains arginines at residues 82 and 318, whereas SL15649 E2 contains glycine and valine residues at these positions, respectively. We were particularly interested in residue 82 because the presence of an arginine at this position is partially responsible for attenuation of virulent strains in some mouse models of CHIKV infection (80). To determine whether differences in GAG utilization between 181/25 and SL15649 are due to polymorphisms at one or both of these positions, we generated isogenic variants in the SL15649 and 181/25 infectious clones containing reciprocal amino acid substitutions at residues 82 and 382 in single- and double-mutant constructs (Table 3). The rescued viruses were viable, producing cytopathic effect (CPE) in BHK-21 cells within 24 h of electroporation and replicating to titers of 10^7 to 10^9 PFU/ml of purified virus, which are comparable to those seen with the parental SL15649 and 181/25 viruses, respectively (Table 3). In these experiments, we observed a correlation between virus titers in Vero cells and the amino acid at position 82. 181/25-E2 R82G and -E2 R82G/R318V virus titers were approximately 6- to 8-fold lower than those of 181/25. Correspondingly, SL15649-E2 G82R and -E2 G82R/V318R virus titers were approximately 5- to 7-fold higher than titers of SL15649. Titers for the reciprocal E2 318 mutants were comparable to those of their parental counterparts. We also observed a small-plaque phenotype for SL15649-E2 G82R and -E2 G82R/V318R compared with SL15649 (data not shown). Of note,

TABLE 3 CHIKV parental and mutant viruses used in this study

Virus	No. of genomes/ml[a]	PFU/ml[b]	Genome/PFU ratio	Normalized ratio[c]
181/25				
WT	1.58×10^{11}	1.4×10^{9}	120	1.0
E2 R82G	7.88×10^{10}	2.2×10^{8}	360	3.2
E2 R318V	7.22×10^{10}	1.0×10^{9}	72	0.62
E2 R82G/R318V	8.83×10^{10}	1.8×10^{8}	500	4.4
SL15649				
WT	7.71×10^{10}	1.7×10^{7}	4400	1.0
E2 G82R	1.93×10^{10}	1.2×10^{8}	160	0.036
E2 V318R	1.51×10^{11}	3.0×10^{7}	5100	1.1
E2 G82R/V318R	2.91×10^{10}	8.3×10^{7}	350	0.079

[a] Genomes/ml data were determined by duplicate real-time quantitative PCRs from three replicate experiments.
[b] Titers were determined by plaque assay using Vero cells. The mean viral titers from three independent plaque assays of a single stock are shown.
[c] Each mutant genome/PFU value was normalized to the parental WT value. The ratio of the relative numbers of genomes to PFU of WT 181/25 to that of WT SL15649 was 0.027.

TABLE 2 Amino acid polymorphisms in the E2 glycoprotein sequences of viruses used in this study

Virus strain	E2 amino acid at position[a]: 2	12	82	118	149	157	164	194	205	255	312	317	318	375	377	384
SL15649	T	T	G	S	K	V	T	G	G	I	M	V	V	T	I	M
181/25	I	I	R	G	R	A	A	S	D	V	T	I	R	S	V	V

[a] Numbered from the N terminus of E2.

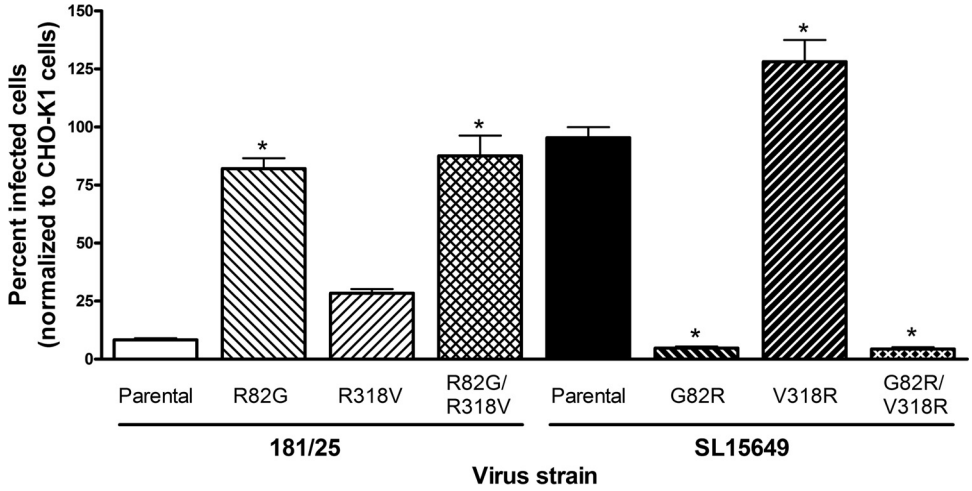

FIG 4 E2 residue 82 is a primary determinant of GAG utilization. Parental CHO-K1 and pgsB761 cells were adsorbed with an MOI of ~10 PFU/cell of each parental virus (181/25 or SL15649) or the E2 mutants shown. At 2 hpi, the inoculum was replaced with medium containing 20 mM NH_4Cl. At 18 hpi, infected cells were detected by indirect immunofluorescence. Results are expressed as the mean percentage of infected pgsB71 cells normalized to parental CHO-K1 cells for each virus for two independent experiments performed in triplicate. Error bars indicate SEM. *, $P < 0.001$ (in comparison to infectivity of the appropriate parental virus in CHO-K1 cells as determined by one-way ANOVA followed by Tukey's multiple-comparison test).

a small-plaque phenotype was originally used as a criterion for selecting clone 181/25 (65). However, plaques formed by 181/25-E2 R82G and -E2 R82G/R318V were not correspondingly larger than those formed by 181/25 (data not shown).

As an additional measure of viral fitness, we determined the genome/PFU ratio for each virus in infectivity assays using Vero cells. The parental strains 181/25 and SL15649 had genome/PFU ratios of 120 and 4,400, respectively (Table 3). E2 318 mutants had genome/PFU ratios similar to those of the parental strains. However, variants 181/25-E2 R82G and 181/25-E2 R82G/R318V had genome/PFU values that were 3.2- and 4.4-fold higher, respectively, than those of 181/25. Correspondingly, SL15469-E2 G82R and SL15649-E2 G82R/V318R had genome/PFU ratios that were 28- and 13-fold lower, respectively, than those of SL15649. Thus, an arginine at position 82 in E2 results in increased viral titers, a decreased genome/PFU ratio, and, in the SL15649 background, a reduction in plaque size, suggesting that a basic residue at position 82 in E2 enhances viral fitness in mammalian cell culture. A small-plaque phenotype (51, 58, 59, 65) and a higher level of infectivity in cell culture (53, 61) have been observed with other GAG-binding alphavirus strains.

To determine whether either of the basic amino acids at E2 82 and 318 affects GAG utilization, parental and mutant viruses were tested for infection of parental CHO-K1 and mutant pgsB761 cells, the cell line in which we observed the greatest difference in infectivity between the two parental strains (Fig. 3A). As before, SL15649 efficiently infected pgsB761 cells (~95% infected), whereas infection of these cells was greatly impaired for 181/25 (~8%) relative to infection of parental CHO-K1 cells ($P < 0.001$ for both viruses) (Fig. 4). Substitution of Arg^{82} with a glycine in 181/25 E2 (181/25-E2 R82G) allowed efficient infection of pgsB761 cells (~82% infected; $P < 0.001$ compared with 181/25), whereas substitution of Gly^{82} in SL15649 E2 with an arginine (SL15649-E2 G82R) resulted in substantially reduced infectivity of these cells (~5% infected; $P < 0.001$ compared with SL15649). Substitution of Arg^{318} in 181/25 E2 with valine (181/25-E2 R318V) or of Val^{318} in SL15649 E2 with arginine (SL15649-E2 V318R) resulted in increased infectivity of pgsB761 cells (~28% or ~128% infected, respectively). The SL15649-E2 G82R/V318R double mutant did not efficiently infect pgsB761 cells (~4% infected; $P < 0.001$ compared with SL15649), whereas the 181/25-E2 R82G/R318V double mutant did (88% infected; $P < 0.001$ compared with 181/25), suggesting that the sequence polymorphism at residue 82 predominates in conferring infectivity of pgsB761 cells. Therefore, an arginine at E2 residue 82 yields a higher degree of dependence on cell-surface GAGs for efficient infection.

E2 R82 mediates a direct interaction with GAGs. Since cell-surface GAGs are required for efficient binding and infectivity by 181/25 and SL15649, we next tested whether CHIKV virions and GAGs directly interact. Equivalent genome copies (5×10^7) of purified 181/25, 181/25-E2 R82G, SL15649, or SL15649-E2 G82R virions were incubated with agarose beads conjugated to heparin or with unconjugated beads as a negative control, and bound material from both heparin-agarose and unconjugated beads was resolved by SDS-PAGE and transferred to a PVDF membrane. Membranes were immunoblotted using an anti-E2 antibody to detect captured virus. We found that 181/25 was efficiently captured by heparin-agarose beads, whereas 181/25-E2 R82G was not (Fig. 5A). Correspondingly, we observed little capture of SL15649 by heparin beads, while SL15649-E2 G82R was more efficiently precipitated (Fig. 5A). We detected no virus capture by beads alone, suggesting that interactions between heparin and virions are specific (Fig. 5B). Densitometric analysis of three independent experiments indicates that ~38% and ~24% of 181/25 and SL15649-E2 G82R, respectively, were captured by heparin-agarose beads (Fig. 5C). In contrast, SL15649 and 181/25-E2 G82R displayed low levels (~5%) of binding to heparin (Fig. 5C). We conclude that CHIKV virions directly interact with heparin and that this interaction is greatly enhanced by the presence of a basic residue at position 82 in the E2 glycoprotein.

Structural and sequence analysis of CHIKV E2 82. Since interactions between GAGs and proteins often occur via electrostatic and hydrogen-bond interactions between anionic (carboxylate and sulfate) groups in GAGs and cationic amino acid side

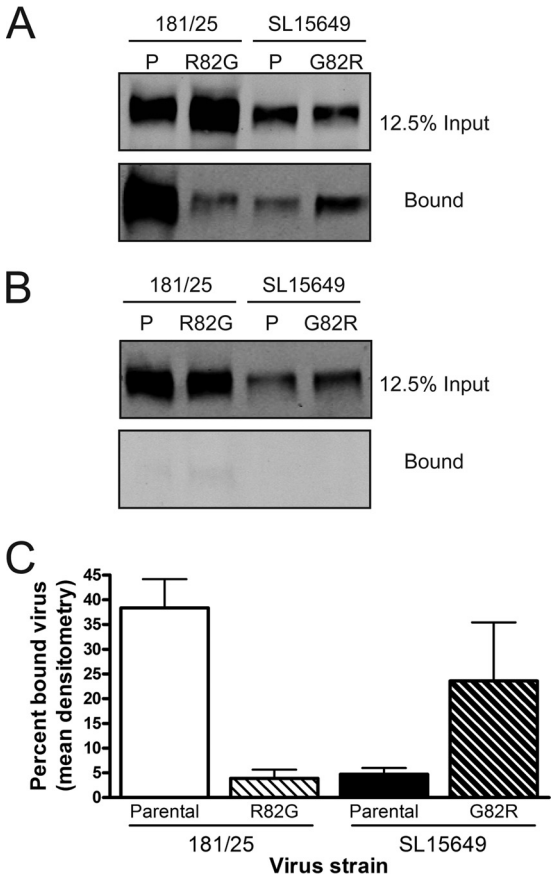

FIG 5 CHIKV E2 R82G mediates a direct interaction with heparin. Approximately 5×10^7 genome equivalents of purified 181/25, 181/25-E2 R82G, SL15649, and SL15649-E2 G82R virions were incubated with 75 μl of washed heparin-agarose beads (A) or unconjugated beads (B) at 4°C for 30 min. Beads were washed three times, and the bound material as well as 12.5% of the input virus was resolved by SDS-PAGE, transferred to a PVDF membrane, and immunoblotted for E2 as a marker for captured virus using a CHIKV-specific monoclonal antibody. The results of an experiment representative of three performed are shown. P, parental virus. (C) Densitometric analysis of virus bound to heparin-agarose beads. Data are expressed as the mean percent bound virus calculated from the densitometric analysis of captured virus divided by the estimated total input virus for three independent experiments. Error bars indicate SEM.

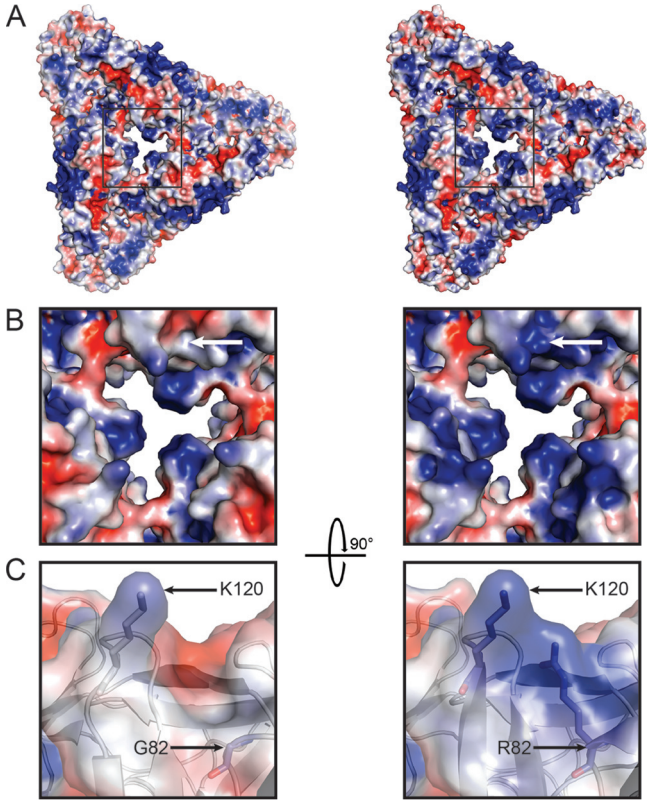

FIG 6 Electrostatic potentials of SL15649 and 181/25 E1/E2 trimers. (A) Top view of the electrostatic potential map displayed on the molecular surface of E1/E2 trimers of SL15649 (left panel) compared with a model of 181/25 (right panel) based on the crystal structure of CHIKV E1/E2 (PDB accession no. 2XFB). Positive potential is depicted in blue, and negative potential is depicted in red. (B) Enlarged view of the boxed areas from panel A highlighting the central cavity of the E1/E2 trimer. A white arrow indicates the position of Gly^{82} in SL15649 (left panel) or Arg^{82} in 181/25 (right panel) in one of the E2 monomers. (C) Enlarged view of the inner cavity rotated by 90° around the horizontal axis from the top view in panel B. A ribbon tracing of E2 is shown with a semitransparent view of the electrostatic surface and amino acids Gly^{82} (SL15649, left panel) or Arg^{82} (181/25, right panel) and Lys^{120} shown in stick representations.

chains, we sought to determine how substitution of Gly^{82} to Arg affects the local electrostatic environment surrounding this residue. Using the crystal structure of the CHIKV E1/E2 trimer (Protein Data Bank [PDB] accession code 2XFB [30]), we modeled the 181/25 E2 structure by substituting 12 residues of the 16 total polymorphisms displayed by the two strains (Table 2) located within the crystal structure, including G82R. The electrostatic charge distribution for each virus was calculated using the PyMol plug-in program APBS (71) and mapped onto a molecular surface representation of the E1/E2 trimer (Fig. 6). In the SL15649 model of the E1/E2 trimer (Fig. 6A and B, left panels), Gly^{82} is located in the "wings" insertion in the BC loop at the top of the immunoglobulin-like β-barrel fold that comprises domain A of E2, which has been implicated in mediating interactions with receptors (30). Gly^{82} is part of a cavity formed by domain A, which is centered on the 3-fold axis of the trimer spike. The three Gly^{82} residues are located at the inner apical surface of the cavity, facing toward the cavity center (Fig. 6A and B). Substitution of glycine with an arginine at residue 82 results in an expected increase in positive charge of the environment surrounding this residue (Fig. 6B). In addition, the additional density of the larger arginine side chain occupies a space adjacent to a conserved lysine at position 120, which is vacant in the SL16549 structure (Fig. 6C). Since residue 82 is part of the central cavity, it is possible that the increase in positive charge at this position in 181/25 results in formation of a GAG-binding pocket at the central cavity apex.

We surveyed the frequency of an arginine or glycine at E2 82 in historical and circulating CHIKV strains. Alignment of the 158 CHIKV E2 protein sequences available in the NIAID ViPR database (72) revealed that 157 of 158 (>99%) sequences contained a glycine at position 82 in E2. The only sequence in the database that contains an arginine at this residue is 181/25 (TSI-GSD-218 [65, 67]). CHIKV11, a strain isolated from an infected patient in Singapore in 2006, is the only other published CHIKV strain that has an arginine at position 82 in E2 (78). CHIKV11 was passaged in Vero cells and may have acquired an arginine at position 82 during cell-culture passage (78). This analysis reveals that a glycine at residue 82 in E2 is highly conserved.

DISCUSSION

The initial events in the replication cycle of CHIKV are not well defined. In this study, we found that CHIKV vaccine strain 181/25 requires cell-surface glycosaminoglycans for efficient attachment to and infection of cells in culture. In addition to pgsA745 cells, which are not susceptible to 181/25 infection (76), pgsB761 cells or pgsD677 cells are likewise not susceptible to 181/25 infection, suggesting that 181/25 is dependent on cell-surface heparan sulfate for efficient infection. We detected decreased cell binding by 181/25 both in the absence of cell-surface GAGs and in the presence of soluble GAGs. Moreover, we found that inhibition of 181/25 infectivity by soluble heparan sulfate occurs prior to endosomal escape. Collectively, these data suggest that 181/25 uses heparan sulfate proteoglycans as attachment receptors.

Our structural analysis suggests that Arg^{82} participates in a solvent-accessible GAG-binding pocket in the central cavity of the E1/E2 trimer of 181/25. Although the precise GAG-binding site cannot be determined without high-resolution structural studies of 181/25 with a soluble GAG, it is likely that a number of basic amino acids in E2 coordinate interactions with GAGs (46, 49, 79). We think it likely that Arg^{82} participates in a network of basic residues, possibly including Lys^{120}, which form a GAG-binding site in 181/25 E2 and enhances the affinity of the glycoprotein for GAGs. In support of this model, 181/25 bound heparin more efficiently than did SL15649. In addition, substitution of Gly^{82} with Arg in SL15649 increased virus binding to heparin, suggesting an increase in E2 affinity for GAGs.

It has been hypothesized that Arg^{82} in E2 of 181/25 contributes to attenuation of the vaccine strain due to GAG binding (76, 80). Our results provide support for this hypothesis. An arginine at position 82 in both 181/25 and SL15649 results in a greater dependence on GAGs for infection in cell culture. In addition, we provide the first evidence for a direct interaction between 181/25 and an immobilized GAG, which is highly dependent on the presence of an arginine at position 82 in E2. In comparison to its parental strain AF15561, 181/25 contains 10 nucleotide differences, including two amino acid polymorphisms in the E2 glycoprotein (T12I and G82R) (80). Genetic analysis reveals that E2 T12I and G82R are responsible for attenuation of both AF15661 and a clinical isolate, CHIKV LR2006 OPY-1 (strain LR), in mouse models of CHIKV virulence (80), indicating that Arg^{82} in E2 functions in attenuation of CHIKV. Although infection of mice with 181/25 results in decreased dissemination and viremia compared with parental strain AF15561 or strain LR (76, 80), mechanisms of virulence attenuation of 181/25 *in vivo* have not been fully elucidated. Similar to other GAG-binding viruses, low levels of viremia during infection with 181/25 may be due to rapid clearance of virus from the bloodstream (55, 58, 81–83).

The conservation of a glycine at position 82 in E2 suggests that this residue contributes importantly to viral fitness. Consistent with this idea, 181/25 infects *A. albopictus* C6/36 cells less efficiently than its parental virus AF15561, which contains Gly^{82} (data not shown), suggesting that an arginine at this position in E2 brings a fitness cost for replication of CHIKV in mosquito cells. In addition, evidence of reversion from Arg to Gly at position 82 in E2 of 181/25 was observed during infections of mice (80) and in one viremic vaccinee during phase II clinical trials (67), indicating that Gly^{82} is selected for *in vivo*. It is possible that the presence of Arg^{82} may alter the tertiary structure of E2, which may affect binding to other mosquito or mammalian cell receptors.

Similar to other low-passage-number isolates of EEEV and VEEV (50, 62), CHIKV SL15649 exhibits dependence on cell-surface GAGs for efficient binding and infection in cell culture. However, GAG binding may not be a property of all CHIKV strains. For example, it has been demonstrated that CHIKV strain LR replicon particles do not depend on cell-surface GAGs for infection (76). It is unclear whether the observed difference between SL15649 and LR in GAG dependence is due to sequence polymorphisms or experimental differences. Sequence analysis of the infectious clone of SL15649 did not reveal the presence of additional basic amino acids in E2 compared with other clinical isolates (data not shown), suggesting that the requirement for cell-surface GAGs for efficient infection of SL15469 is not the result of cell culture adaptation.

Our experiments using CHO cells deficient in various GAGs provide evidence that 181/25 and SL15649 are dependent on GAGs to differing extents for efficient infection. While it is possible that abrogation of GAG expression in mutant CHO cells alters the expression of other cell-surface molecules required for CHIKV binding, we think this is unlikely since CHIKV strain LR readily infects these cells (76). Interestingly, we did not detect inhibition of SL15649 infectivity by soluble GAGs. SL15649 may bind to GAGs only within the context of a proteoglycan or when expressed at the cell surface. However, we observed a low level of binding of SL15649 to immobilized heparin, which is likely due to interactions between virions and heparin and not a consequence of nonspecific binding to beads, since virus did not bind beads alone. Physiologically relevant GAG-protein interactions display affinities that can range from rather weak (dissociation constant $[K_d] > 10^{-6}$ M) to moderately strong ($K_d = \sim 10^{-9}$ M) (46). Although mounting evidence suggests that high-affinity interactions with GAGs diminish alphavirus virulence (50, 55, 57–59, 63), low-affinity interactions with GAGs may be important for replication within hosts (e.g., to mediate attachment in specific tissues) and consequent pathology.

The structural specificity of the interactions between viruses and GAGs is poorly understood (reviewed in references 84 and 85). GAGs are heterogenous and differ in chain lengths, sulfation patterns, and subunit configurations due to the spatiotemporal expression patterns of GAG biosynthesis genes (79, 85, 86). The presence of specific subunits (e.g., iduronic acid) (44, 87) or the extent and position of sulfation of particular GAGs (39, 88, 89) can substantially influence the specificity of virus-GAG interactions. GAG-binding sites on proteins are surface exposed or in shallow grooves containing positively charged amino acids. The precise spacing of cationic clusters and the composition and arrangement of other residues that comprise the local environment of the GAG-binding site are important for specificity of interactions with GAGs (49, 90). Strain variants that contain basic residues that mediate some level of GAG binding among the different alphaviruses map to five surface-exposed regions within E2: residues 1 to 4 (53–55, 62), 70 to 82 (50, 53–55, 58–60), 114 to 120 (53, 55, 62), 157 to 161 (58), and 209 to 218 (51, 55). Although it is thought that alphavirus E1 and E2 trimers adopt similar overall folds (30, 91), it is possible that the spacing and location of the GAG-binding residues and the local amino acid environment of these five regions in E2 contribute to the type and specificity of GAG-E2 interactions. Conserved basic residues are often found

within or near these five sites, which may mediate low-affinity interactions with GAGs. Basic amino acid polymorphisms within these regions of E2 from passaged viruses or natural isolates may increase the affinity of E2 for different GAGs or alter GAG-binding specificity.

Studies of interactions between GAGs and other alphaviruses have mainly focused on heparin or heparan sulfate. However, studies using other soluble GAGs suggest that some strains use GAGs other than heparan sulfate to bind cells. For example, SINV strain Toto1101 binds to and is inhibited by soluble dermatan sulfate in addition to heparin (52). Similarly, a subset of VEEV GAG-binding mutants inhibited by soluble heparin are also inhibited by soluble dermatan sulfate (55). Differences in structural specificities of GAG interactions with alphavirus E2 glycoproteins may influence the tropism and pathology of these GAG-binding viruses. Indeed, this idea is supported by a study of EEEV heparan sulfate-binding mutants (59).

Our data suggest that 181/25 and SL15649 differ in the utilization of individual GAGs or structural specificities of GAGs. Although 181/25 infectivity was inhibited to some extent by all soluble GAGs tested, regardless of type of subunits or level of sulfation, this virus displays greater GAG specificity in cell culture. Based on studies using mutant CHO cell lines, strain 181/25 appears to depend mainly on heparan sulfate in cell culture, whereas SL15649 appears to use chondroitin sulfate, possibly in addition to heparan sulfate, for infection. Whether the amino acid sequences that influence GAG dependence for 181/25 and SL15649 are distinct or contiguous remains to be determined. Interestingly, E2 from 181/25 and SL15469 contains a heparin-binding consensus sequence (47) (from residues 250 to 255 [DRKGKI]) which is solvent accessible and conserved in other circulating CHIKV isolates. Ongoing work to define GAG-binding sites and structural specificity of GAG interactions with CHIKV 181/25 and virulent clinical isolates will enhance an understanding of CHIKV tropism and pathogenesis.

ACKNOWLEDGMENTS

We thank Andrea Pruijssers and Bernardo Mainou for critical reviews of the manuscript. We are grateful to members of the Dermody laboratory for useful suggestions and discussions during the course of the study. We thank Nicole Sexton for technical assistance. We thank Kerstin Reiss and Melanie Dietrich from the laboratory of Thilo Stehle for their assistance with structural analysis. A subset of infectivity assays were conducted at the Vanderbilt High-Throughput Screening Facility. Flow cytometry experiments were performed in the Vanderbilt Cytometry Shared Resource.

This work was supported by Public Health Service awards F32 AI096833 (L.A.S.) and U54 AI057157 for the Southeast Regional Center for Excellence for Emerging Infections and Biodefense (T.S.D.) and the Elizabeth B. Lamb Center for Pediatric Research. Additional support by provided by the Vanderbilt Diabetes Research and Training Center for the Vanderbilt Flow Cytometry Shared Resource (DK058404).

REFERENCES

1. **Burt FJ, Rolph MS, Rulli NE, Mahalingam S, Heise MT.** 2012. Chikungunya: a re-emerging virus. Lancet **379:**662–671. http://dx.doi.org/10.1016/S0140-6736(11)60281-X.
2. **Thiberville SD, Moyen N, Dupuis-Maguiraga L, Nougairede A, Gould EA, Roques P, de Lamballerie X.** 2013. Chikungunya fever: epidemiology, clinical syndrome, pathogenesis and therapy. Antiviral Res. **99:**345–370. http://dx.doi.org/10.1016/j.antiviral.2013.06.009.
3. **Schwartz O, Albert ML.** 2010. Biology and pathogenesis of chikungunya virus. Nat. Rev. Microbiol. **8:**491–500. http://dx.doi.org/10.1038/nrmicro2368.
4. **Borgherini G, Poubeau P, Jossaume A, Gouix A, Cotte L, Michault A, Arvin-Berod C, Paganin F.** 2008. Persistent arthralgia associated with chikungunya virus: a study of 88 adult patients on reunion island. Clin. Infect. Dis. **47:**469–475. http://dx.doi.org/10.1086/590003.
5. **Couturier E, Guillemin F, Mura M, Leon L, Virion JM, Letort MJ, De Valk H, Simon F, Vaillant V.** 2012. Impaired quality of life after chikungunya virus infection: a 2-year follow-up study. Rheumatology (Oxford) **51:**1315–1322. http://dx.doi.org/10.1093/rheumatology/kes015.
6. **Hoarau JJ, Jaffar Bandjee MC, Krejbich Trotot P, Das T, Li-Pat-Yuen G, Dassa B, Denizot M, Guichard E, Ribera A, Henni T, Tallet F, Moiton MP, Gauzere BA, Bruniquet S, Jaffar Bandjee Z, Morbidelli P, Martigny G, Jolivet M, Gay F, Grandadam M, Tolou H, Vieillard V, Debre P, Autran B, Gasque P.** 2010. Persistent chronic inflammation and infection by Chikungunya arthritogenic alphavirus in spite of a robust host immune response. J. Immunol. **184:**5914–5927. http://dx.doi.org/10.4049/jimmunol.0900255.
7. **Schilte C, Staikowsky F, Couderc T, Madec Y, Carpentier F, Kassab S, Albert ML, Lecuit M, Michault A.** 2013. Chikungunya virus-associated long-term arthralgia: a 36-month prospective longitudinal study. PLoS Negl. Trop. Dis. **7:**e2137. http://dx.doi.org/10.1371/journal.pntd.0002137.
8. **Sissoko D, Malvy D, Ezzedine K, Renault P, Moscetti F, Ledrans M, Pierre V.** 2009. Post-epidemic Chikungunya disease on Reunion Island: course of rheumatic manifestations and associated factors over a 15-month period. PLoS Negl. Trop. Dis. **3:**e389. http://dx.doi.org/10.1371/journal.pntd.0000389.
9. **Banerjee K, Mourja DT, Malunjkar AS.** 1988. Susceptibility & transmissibility of different geographical strains of Aedes aegypti mosquitoes to Chikungunya virus. Indian J. Med. Res. **87:**134–138.
10. **Singh KR, Pavri KM.** 1967. Experimental studies with chikungunya virus in Aedes aegypti and Aedes albopictus. Acta Virol. **11:**517–526.
11. **Tesh RB, Gubler DJ, Rosen L.** 1976. Variation among goegraphic strains of Aedes albopictus in susceptibility to infection with chikungunya virus. Am. J. Trop. Med. Hyg. **25:**326–335.
12. **Tsetsarkin KA, Vanlandingham DL, McGee CE, Higgs S.** 2007. A single mutation in chikungunya virus affects vector specificity and epidemic potential. PLoS Pathog. **3:**e201. http://dx.doi.org/10.1371/journal.ppat.0030201.
13. **Sourisseau M, Schilte C, Casartelli N, Trouillet C, Guivel-Benhassine F, Rudnicka D, Sol-Foulon N, Le Roux K, Prevost MC, Fsihi H, Frenkiel MP, Blanchet F, Afonso PV, Ceccaldi PE, Ozden S, Gessain A, Schuffenecker I, Verhasselt B, Zamborlini A, Saib A, Rey FA, Arenzana-Seisdedos F, Despres P, Michault A, Albert ML, Schwartz O.** 2007. Characterization of reemerging chikungunya virus. PLoS Pathog. **3:**e89. http://dx.doi.org/10.1371/journal.ppat.0030089.
14. **Borgherini G, Poubeau P, Staikowsky F, Lory M, Le Moullec N, Becquart JP, Wengling C, Michault A, Paganin F.** 2007. Outbreak of chikungunya on Reunion Island: early clinical and laboratory features in 157 adult patients. Clin. Infect. Dis. **44:**1401–1407. http://dx.doi.org/10.1086/517537.
15. **Economopoulou A, Dominguez M, Helynck B, Sissoko D, Wichmann O, Quenel P, Germonneau P, Quatresous I.** 2009. Atypical Chikungunya virus infections: clinical manifestations, mortality and risk factors for severe disease during the 2005–2006 outbreak on Reunion. Epidemiol. Infect. **137:**534–541. http://dx.doi.org/10.1017/S0950268808001167.
16. **Rajapakse S, Rodrigo C, Rajapakse A.** 2010. Atypical manifestations of chikungunya infection. Trans. R. Soc. Trop. Med. Hyg. **104:**89–96. http://dx.doi.org/10.1016/j.trstmh.2009.07.031.
17. **Das T, Jaffar-Bandjee MC, Hoarau JJ, Krejbich Trotot P, Denizot M, Lee-Pat-Yuen G, Sahoo R, Guiraud P, Ramful D, Robin S, Alessandri JL, Gauzere BA, Gasque P.** 2010. Chikungunya fever: CNS infection and pathologies of a re-emerging arbovirus. Prog. Neurobiol. **91:**121–129. http://dx.doi.org/10.1016/j.pneurobio.2009.12.006.
18. **Dupont-Rouzeyrol M, Caro V, Guillaumot L, Vazeille M, D'Ortenzio E, Thiberge JM, Baroux N, Gourinat AC, Grandadam M, Failloux AB.** 2012. Chikungunya virus and the mosquito vector Aedes aegypti in New Caledonia (South Pacific Region). Vector Borne Zoonotic Dis. **12:**1036–1041. http://dx.doi.org/10.1089/vbz.2011.0937.
19. **Horwood PF, Reimer LJ, Dagina R, Susapu M, Bande G, Katusele M, Koimbu G, Jimmy S, Ropa B, Siba PM, Pavlin BI.** 2013. Outbreak of chikungunya virus infection, Vanimo, Papua New Guinea. Emerg. Infect. Dis. **19:**1535–1538. http://dx.doi.org/10.3201/eid1909.130130.
20. **Mombouli JV, Bitsindou P, Elion DO, Grolla A, Feldmann H, Niama FR, Parra HJ, Munster VJ.** 2013. Chikungunya virus infection, Brazza-

ville, Republic of Congo, 2011. Emerg. Infect. Dis. **19:**1542–1543. http://dx.doi.org/10.3201/eid1909.130451.
21. **Wangchuk S, Chinnawirotpisan P, Dorji T, Tobgay T, Dorji T, Yoon IK, Fernandez S.** 2013. Chikungunya fever outbreak, Bhutan, 2012. Emerg. Infect. Dis. **19:**1681–1684. http://dx.doi.org/10.3201/eid1910.130453.
22. **Wu D, Zhang Y, Zhouhui Q, Kou J, Liang W, Zhang H, Monagin C, Zhang Q, Li W, Zhong H, He J, Li H, Cai S, Ke C, Lin J.** 2013. Chikungunya virus with E1-A226V mutation causing two outbreaks in 2010, Guangdong, China. Virol. J. **10:**174. http://dx.doi.org/10.1186/1743-422X-10-174.
23. **Thiberville SD, Boisson V, Gaudart J, Simon F, Flahault A, de Lamballerie X.** 2013. Chikungunya fever: a clinical and virological investigation of outpatients on Reunion Island, South-West Indian Ocean. PLoS Negl. Trop. Dis. **7:**e2004. http://dx.doi.org/10.1371/journal.pntd.0002004.
24. **Kuhn RJ.** 2007. Togaviridae: the viruses and their replication, p 1001–1022. *In* Knipe DM, Howley PM, Griffin DE, Lamb RA, Martin MA, Roizman B, Straus SE (ed), Fields virology, 5th ed. Lippincott, Williams and Wilkins, New York, NY.
25. **Khan AH, Morita K, Parquet Md Mdel C, Hasebe F, Mathenge EG, Igarashi A.** 2002. Complete nucleotide sequence of chikungunya virus and evidence for an internal polyadenylation site. J. Gen. Virol. **83**(Pt 12)**:**3075–3084.
26. **Fuller SD.** 1987. The T=4 envelope of Sindbis virus is organized by interactions with a complementary T=3 capsid. Cell **48:**923–934. http://dx.doi.org/10.1016/0092-8674(87)90701-X.
27. **Mancini EJ, Clarke M, Gowen BE, Rutten T, Fuller SD.** 2000. Cryo-electron microscopy reveals the functional organization of an enveloped virus, Semliki Forest virus. Mol. Cell **5:**255–266. http://dx.doi.org/10.1016/S1097-2765(00)80421-9.
28. **Sun S, Xiang Y, Akahata W, Holdaway H, Pal P, Zhang X, Diamond MS, Nabel GJ, Rossmann MG.** 2013. Structural analyses at pseudo atomic resolution of Chikungunya virus and antibodies show mechanisms of neutralization. eLife **2:**e00435. http://dx.doi.org/10.7554/eLife.00435.
29. **Jose J, Snyder JE, Kuhn RJ.** 2009. A structural and functional perspective of alphavirus replication and assembly. Future Microbiol. **4:**837–856. http://dx.doi.org/10.2217/fmb.09.59.
30. **Voss JE, Vaney MC, Duquerroy S, Vonrhein C, Girard-Blanc C, Crublet E, Thompson A, Bricogne G, Rey FA.** 2010. Glycoprotein organization of Chikungunya virus particles revealed by X-ray crystallography. Nature **468:**709–712. http://dx.doi.org/10.1038/nature09555.
31. **Kielian M, Chanel-Vos C, Liao M.** 2010. Alphavirus entry and membrane fusion. Viruses **2:**796–825. http://dx.doi.org/10.3390/v2040796.
32. **Bernard E, Solignat M, Gay B, Chazal N, Higgs S, Devaux C, Briant L.** 2010. Endocytosis of chikungunya virus into mammalian cells: role of clathrin and early endosomal compartments. PLoS One **5:**e11479. http://dx.doi.org/10.1371/journal.pone.0011479.
33. **Gay B, Bernard E, Solignat M, Chazal N, Devaux C, Briant L.** 2012. pH-dependent entry of chikungunya virus into Aedes albopictus cells. Infect. Genet. Evol. **12:**1275–1281. http://dx.doi.org/10.1016/j.meegid.2012.02.003.
34. **Lee RC, Hapuarachchi HC, Chen KC, Hussain KM, Chen H, Low SL, Ng LC, Lin R, Ng MM, Chu JJ.** 2013. Mosquito cellular factors and functions in mediating the infectious entry of chikungunya virus. PLoS Negl. Trop. Dis. **7:**e2050. http://dx.doi.org/10.1371/journal.pntd.0002050.
35. **Haywood AM.** 1994. Virus receptors: binding, adhesion strengthening, and changes in viral structure. J. Virol. **68:**1–5.
36. **Mercer J, Schelhaas M, Helenius A.** 2010. Virus entry by endocytosis. Annu. Rev. Biochem. **79:**803–833. http://dx.doi.org/10.1146/annurev-biochem-060208-104626.
37. **Dechecchi MC, Tamanini A, Bonizzato A, Cabrini G.** 2000. Heparan sulfate glycosaminoglycans are involved in adenovirus type 5 and 2-host cell interactions. Virology **268:**382–390. http://dx.doi.org/10.1006/viro.1999.0171.
38. **Zautner AE, Korner U, Henke A, Badorff C, Schmidtke M.** 2003. Heparan sulfates and coxsackievirus-adenovirus receptor: each one mediates coxsackievirus B3 PD infection. J. Virol. **77:**10071–10077. http://dx.doi.org/10.1128/JVI.77.18.10071-10077.2003.
39. **Chen Y, Maguire T, Hileman RE, Fromm JR, Esko JD, Linhardt RJ, Marks RM.** 1997. Dengue virus infectivity depends on envelope protein binding to target cell heparan sulfate. Nat. Med. **3:**866–871. http://dx.doi.org/10.1038/nm0897-866.
40. **Tan CW, Poh CL, Sam IC, Chan YF.** 2013. Enterovirus 71 uses cell surface heparan sulfate glycosaminoglycan as an attachment receptor. J. Virol. **87:**611–620. http://dx.doi.org/10.1128/JVI.02226-12.
41. **WuDunn D, Spear PG.** 1989. Initial interaction of herpes simplex virus with cells is binding to heparan sulfate. J. Virol. **63:**52–58.
42. **Roderiquez G, Oravecz T, Yanagishita M, Bou-Habib DC, Mostowski H, Norcross MA.** 1995. Mediation of human immunodeficiency virus type 1 binding by interaction of cell surface heparan sulfate proteoglycans with the V3 region of envelope gp120-gp41. J. Virol. **69:**2233–2239.
43. **Giroglou T, Florin L, Schafer F, Streeck RE, Sapp M.** 2001. Human papillomavirus infection requires cell surface heparan sulfate. J. Virol. **75:**1565–1570. http://dx.doi.org/10.1128/JVI.75.3.1565-1570.2001.
44. **Hallak LK, Collins PL, Knudson W, Peeples ME.** 2000. Iduronic acid-containing glycosaminoglycans on target cells are required for efficient respiratory syncytial virus infection. Virology **271:**264–275. http://dx.doi.org/10.1006/viro.2000.0293.
45. **Esko JD, Kimata K, Lindahl U.** 2009. Proteoglycans and sulfated glycosaminoglycans, p 229–248. *In* Varki A, Cummings RD, Esko JD, Freeze HH, Stanley P, Bertozzi CR, Hart GW, Etzler ME (ed), Essentials of glycobiology, 2nd ed. Cold Spring Harbor Laboratory Press, Cold Spring Harbor, NY.
46. **Gandhi NS, Mancera RL.** 2008. The structure of glycosaminoglycans and their interactions with proteins. Chem. Biol. Drug Des. **72:**455–482. http://dx.doi.org/10.1111/j.1747-0285.2008.00741.x.
47. **Cardin AD, Weintraub HJ.** 1989. Molecular modeling of protein-glycosaminoglycan interactions. Arteriosclerosis **9:**21–32. http://dx.doi.org/10.1161/01.ATV.9.1.21.
48. **Hileman RE, Fromm JR, Weiler JM, Linhardt RJ.** 1998. Glycosaminoglycan-protein interactions: definition of consensus sites in glycosaminoglycan binding proteins. Bioessays **20:**156–167. http://dx.doi.org/10.1002/(SICI)1521-1878(199802)20:2<156::AID-BIES8>3.0.CO;2-R.
49. **Torrent M, Nogues MV, Andreu D, Boix E.** 2012. The "CPC clip motif": a conserved structural signature for heparin-binding proteins. PLoS One **7:**e42692. http://dx.doi.org/10.1371/journal.pone.0042692.
50. **Gardner CL, Ebel GD, Ryman KD, Klimstra WB.** 2011. Heparan sulfate binding by natural eastern equine encephalitis viruses promotes neurovirulence. Proc. Natl. Acad. Sci. U. S. A. **108:**16026–16031. http://dx.doi.org/10.1073/pnas.1110617108.
51. **Heil ML, Albee A, Strauss JH, Kuhn RJ.** 2001. An amino acid substitution in the coding region of the E2 glycoprotein adapts Ross River virus to utilize heparan sulfate as an attachment moiety. J. Virol. **75:**6303–6309. http://dx.doi.org/10.1128/JVI.75.14.6303-6309.2001.
52. **Byrnes AP, Griffin DE.** 1998. Binding of Sindbis virus to cell surface heparan sulfate. J. Virol. **72:**7349–7356.
53. **Klimstra WB, Ryman KD, Johnston RE.** 1998. Adaptation of Sindbis virus to BHK cells selects for use of heparan sulfate as an attachment receptor. J. Virol. **72:**7357–7366.
54. **Smit JM, Waarts BL, Kimata K, Klimstra WB, Bittman R, Wilschut J.** 2002. Adaptation of alphaviruses to heparan sulfate: interaction of Sindbis and Semliki forest viruses with liposomes containing lipid-conjugated heparin. J. Virol. **76:**10128–10137. http://dx.doi.org/10.1128/JVI.76.20.10128-10137.2002.
55. **Bernard KA, Klimstra WB, Johnston RE.** 2000. Mutations in the E2 glycoprotein of Venezuelan equine encephalitis virus confer heparan sulfate interaction, low morbidity, and rapid clearance from blood of mice. Virology **276:**93–103. http://dx.doi.org/10.1006/viro.2000.0546.
56. **Kerr PJ, Weir RC, Dalgarno L.** 1993. Ross River virus variants selected during passage in chick embryo fibroblasts: serological, genetic, and biological changes. Virology **193:**446–449. http://dx.doi.org/10.1006/viro.1993.1143.
57. **Bear JS, Byrnes AP, Griffin DE.** 2006. Heparin-binding and patterns of virulence for two recombinant strains of Sindbis virus. Virology **347:**183–190. http://dx.doi.org/10.1016/j.virol.2005.11.034.
58. **Byrnes AP, Griffin DE.** 2000. Large-plaque mutants of Sindbis virus show reduced binding to heparan sulfate, heightened viremia, and slower clearance from the circulation. J. Virol. **74:**644–651. http://dx.doi.org/10.1128/JVI.74.2.644-651.2000.
59. **Gardner CL, Choi-Nurvitadhi J, Sun C, Bayer A, Hritz J, Ryman KD, Klimstra WB.** 2013. Natural variation in the heparan sulfate binding domain of the eastern equine encephalitis virus E2 glycoprotein alters interactions with cell surfaces and virulence in mice. J. Virol. **87:**8582–8590. http://dx.doi.org/10.1128/JVI.00937-13.
60. **Klimstra WB, Heidner HW, Johnston RE.** 1999. The furin protease cleavage recognition sequence of Sindbis virus PE2 can mediate virion attachment to cell surface heparan sulfate. J. Virol. **73:**6299–6306.

61. **Ryman KD, Gardner CL, Burke CW, Meier KC, Thompson JM, Klimstra WB.** 2007. Heparan sulfate binding can contribute to the neurovirulence of neuroadapted and nonneuroadapted Sindbis viruses. J. Virol. **81:**3563–3573. http://dx.doi.org/10.1128/JVI.02494-06.
62. **Wang E, Brault AC, Powers AM, Kang W, Weaver SC.** 2003. Glycosaminoglycan binding properties of natural venezuelan equine encephalitis virus isolates. J. Virol. **77:**1204–1210. http://dx.doi.org/10.1128/JVI.77.2.1204-1210.2003.
63. **Klimstra WB, Ryman KD, Bernard KA, Nguyen KB, Biron CA, Johnston RE.** 1999. Infection of neonatal mice with sindbis virus results in a systemic inflammatory response syndrome. J. Virol. **73:**10387–10398.
64. **Morrison TE, Oko L, Montgomery SA, Whitmore AC, Lotstein AR, Gunn BM, Elmore SA, Heise MT.** 2011. A mouse model of chikungunya virus-induced musculoskeletal inflammatory disease: evidence of arthritis, tenosynovitis, myositis, and persistence. Am. J. Pathol. **178:**32–40. http://dx.doi.org/10.1016/j.ajpath.2010.11.018.
65. **Levitt NH, Ramsburg HH, Hasty SE, Repik PM, Cole FE, Jr, Lupton HW.** 1986. Development of an attenuated strain of chikungunya virus for use in vaccine production. Vaccine **4:**157–162. http://dx.doi.org/10.1016/0264-410X(86)90003-4.
66. **Edelman R, Tacket CO, Wasserman SS, Bodison SA, Perry JG, Mangiafico JA.** 2000. Phase II safety and immunogenicity study of live chikungunya virus vaccine TSI-GSD-218. Am. J. Trop. Med. Hyg. **62:**681–685.
67. **Hoke CH, Jr, Pace-Templeton J, Pittman P, Malinoski FJ, Gibbs P, Ulderich T, Mathers M, Fogtman B, Glass P, Vaughn DW.** 2012. US Military contributions to the global response to pandemic chikungunya. Vaccine **30:**6713–6720. http://dx.doi.org/10.1016/j.vaccine.2012.08.025.
68. **Mainou B, Zamora PF, Ashbrook AW, Dorset DC, Kim KS, Dermody TS.** 2013. Reovirus cell entry requires functional microtubules. mBio **4:**e00405–13. http://dx.doi.org/10.1128/mBio.00405-13.
69. **Schneider CA, Rasband WS, Eliceiri KW.** 2012. NIH Image to ImageJ: 25 years of image analysis. Nat. Methods **9:**671–675. http://dx.doi.org/10.1038/nmeth.2089.
70. **Emsley P, Cowtan K.** 2004. Coot: model building tools for molecular graphics. Acta Crystallogr. D Biol. Crystallogr. **60:**2126–2132. http://dx.doi.org/10.1107/S0907444904019158.
71. **Baker NA, Sept D, Joseph S, Holst MJ, McCammon JA.** 2001. Electrostatics of nanosystems: application to microtubules and the ribosome. Proc. Natl. Acad. Sci. U. S. A. **98:**10037–10041. http://dx.doi.org/10.1073/pnas.181342398.
72. **Pickett BE, Sadat EL, Zhang Y, Noronha JM, Squires RB, Hunt V, Liu M, Kumar S, Zaremba S, Gu Z, Zhou L, Larson CN, Dietrich J, Klem EB, Scheuermann RH.** 2012. ViPR: an open bioinformatics database and analysis resource for virology research. Nucleic Acids Res. **40:**D593–D598. http://dx.doi.org/10.1093/nar/gkr859.
73. **Ohkuma S, Poole B.** 1978. Fluorescence probe measurement of the intralysosomal pH in living cells and the perturbation of pH by various agents. Proc. Natl. Acad. Sci. U. S. A. **75:**3327–3331. http://dx.doi.org/10.1073/pnas.75.7.3327.
74. **Esko JD, Stewart TE, Taylor WH.** 1985. Animal cell mutants defective in glycosaminoglycan biosynthesis. Proc. Natl. Acad. Sci. U. S. A. **82:**3197–3201. http://dx.doi.org/10.1073/pnas.82.10.3197.
75. **Esko JD, Weinke JL, Taylor WH, Ekborg G, Roden L, Anantharamaiah G, Gawish A.** 1987. Inhibition of chondroitin and heparan sulfate biosynthesis in Chinese hamster ovary cell mutants defective in galactosyltransferase I. J. Biol. Chem. **262:**12189–12195.
76. **Gardner CL, Burke CW, Higgs ST, Klimstra WB, Ryman KD.** 2012. Interferon-alpha/beta deficiency greatly exacerbates arthritogenic disease in mice infected with wild-type chikungunya virus but not with the cell culture-adapted live-attenuated 181/25 vaccine candidate. Virology **425:**103–112. http://dx.doi.org/10.1016/j.virol.2011.12.020.
77. **Lidholt K, Weinke JL, Kiser CS, Lugemwa FN, Bame KJ, Cheifetz S, Massague J, Lindahl U, Esko JD.** 1992. A single mutation affects both N-acetylglucosaminyltransferase and glucuronosyltransferase activities in a Chinese hamster ovary cell mutant defective in heparan sulfate biosynthesis. Proc. Natl. Acad. Sci. U. S. A. **89:**2267–2271. http://dx.doi.org/10.1073/pnas.89.6.2267.
78. **Lee CY, Kam YW, Fric J, Malleret B, Koh EG, Prakash C, Huang W, Lee WW, Lin C, Lin RT, Renia L, Wang CI, Ng LF, Warter L.** 2011. Chikungunya virus neutralization antigens and direct cell-to-cell transmission are revealed by human antibody-escape mutants. PLoS Pathog. **7:**e1002390. http://dx.doi.org/10.1371/journal.ppat.1002390.
79. **Raman R, Sasisekharan V, Sasisekharan R.** 2005. Structural insights into biological roles of protein-glycosaminoglycan interactions. Chem. Biol. **12:**267–277. http://dx.doi.org/10.1016/j.chembiol.2004.11.020.
80. **Gorchakov R, Wang E, Leal G, Forrester NL, Plante K, Rossi SL, Partidos CD, Adams AP, Seymour RL, Weger J, Borland EM, Sherman MB, Powers AM, Osorio JE, Weaver SC.** 2012. Attenuation of Chikungunya virus vaccine strain 181/clone 25 is determined by two amino acid substitutions in the E2 envelope glycoprotein. J. Virol. **86:**6084–6096. http://dx.doi.org/10.1128/JVI.06449-11.
81. **Lee E, Hall RA, Lobigs M.** 2004. Common E protein determinants for attenuation of glycosaminoglycan-binding variants of Japanese encephalitis and West Nile viruses. J. Virol. **78:**8271–8280. http://dx.doi.org/10.1128/JVI.78.15.8271-8280.2004.
82. **Lee E, Lobigs M.** 2002. Mechanism of virulence attenuation of glycosaminoglycan-binding variants of Japanese encephalitis virus and Murray Valley encephalitis virus. J. Virol. **76:**4901–4911. http://dx.doi.org/10.1128/JVI.76.10.4901-4911.2002.
83. **Lee E, Wright PJ, Davidson A, Lobigs M.** 2006. Virulence attenuation of Dengue virus due to augmented glycosaminoglycan-binding affinity and restriction in extraneural dissemination. J. Gen. Virol. **87:**2791–2801. http://dx.doi.org/10.1099/vir.0.82164-0.
84. **Liu J, Thorp SC.** 2002. Cell surface heparan sulfate and its roles in assisting viral infections. Med. Res. Rev. **22:**1–25. http://dx.doi.org/10.1002/med.1026.
85. **Kamhi E, Joo EJ, Dordick JS, Linhardt RJ.** 2013. Glycosaminoglycans in infectious disease. Biol. Rev. Camb. Philos. Soc. **88:**928–943. http://dx.doi.org/10.1111/brv.12034.
86. **Esko JD, Linhardt RJ.** 2009. Proteins that bind sulfated glycosaminoglycans, p 501–511. *In* Varki A, Esko JD, Freeze HH, Stanley P, Bertozzi CR, Hart GW, Etzler ME (ed), Essentials of glycobiology, 2nd ed. Cold Spring Harbor Press, Cold Spring Harbor, NY.
87. **Thammawat S, Sadlon TA, Hallsworth PG, Gordon DL.** 2008. Role of cellular glycosaminoglycans and charged regions of viral G protein in human metapneumovirus infection. J. Virol. **82:**11767–11774. http://dx.doi.org/10.1128/JVI.01208-08.
88. **Feyzi E, Trybala E, Bergstrom T, Lindahl U, Spillmann D.** 1997. Structural requirement of heparan sulfate for interaction with herpes simplex virus type 1 virions and isolated glycoprotein C. J. Biol. Chem. **272:**24850–24857. http://dx.doi.org/10.1074/jbc.272.40.24850.
89. **Shukla D, Liu J, Blaiklock P, Shworak NW, Bai X, Esko JD, Cohen GH, Eisenberg RJ, Rosenberg RD, Spear PG.** 1999. A novel role for 3-O-sulfated heparan sulfate in herpes simplex virus 1 entry. Cell **99:**13–22. http://dx.doi.org/10.1016/S0092-8674(00)80058-6.
90. **Fromm JR, Hileman RE, Caldwell EE, Weiler JM, Linhardt RJ.** 1997. Pattern and spacing of basic amino acids in heparin binding sites. Arch. Biochem. Biophys. **343:**92–100. http://dx.doi.org/10.1006/abbi.1997.0147.
91. **Li L, Jose J, Xiang Y, Kuhn RJ, Rossmann MG.** 2010. Structural changes of envelope proteins during alphavirus fusion. Nature **468:**705–708. http://dx.doi.org/10.1038/nature09546.

JVI Journals.ASM.org

Residue 82 of the Chikungunya Virus E2 Attachment Protein Modulates Viral Dissemination and Arthritis in Mice

Alison W. Ashbrook,[a,b] Kristina S. Burrack,[c] Laurie A. Silva,[b,d] Stephanie A. Montgomery,[e] Mark T. Heise,[f] Thomas E. Morrison,[c] Terence S. Dermody[a,b,d]

Departments of Pathology, Microbiology, and Immunology,[a] and Pediatrics,[d] and Elizabeth B. Lamb Center for Pediatric Research,[b] Vanderbilt University School of Medicine, Nashville, Tennessee, USA; Department of Microbiology, University of Colorado School of Medicine, Aurora, Colorado, USA[c]; Department of Population Health and Pathobiology, College of Veterinary Medicine, North Carolina State University, Raleigh, North Carolina, USA[e]; and Departments of Genetics and of Microbiology and Immunology, University of North Carolina at Chapel Hill, Chapel Hill, North Carolina, USA[f]

ABSTRACT

Chikungunya virus (CHIKV) is a mosquito-borne alphavirus that has reemerged to cause profound epidemics of fever, rash, and arthralgia throughout sub-Saharan Africa, Southeast Asia, and the Caribbean. Like other arthritogenic alphaviruses, mechanisms of CHIKV pathogenesis are not well defined. Using the attenuated CHIKV strain 181/25 and virulent strain AF15561, we identified a residue in the E2 viral attachment protein that is a critical determinant of viral replication in cultured cells and pathogenesis *in vivo*. Viruses containing an arginine at E2 residue 82 displayed enhanced infectivity in mammalian cells but reduced infectivity in mosquito cells and diminished virulence in a mouse model of CHIKV disease. Mice inoculated with virus containing an arginine at this position exhibited reduced swelling at the site of inoculation with a concomitant decrease in the severity of necrosis in joint-associated tissues. Viruses containing a glycine at E2 residue 82 produced higher titers in the spleen and serum at early times postinfection. Using wild-type and glycosaminoglycan (GAG)-deficient Chinese hamster ovary (CHO) cell lines and soluble GAGs, we found that an arginine at residue 82 conferred greater dependence on GAGs for infection of mammalian cells. These data suggest that CHIKV E2 interactions with GAGs diminish dissemination to lymphoid tissue, establishment of viremia, and activation of inflammatory responses early in infection. Collectively, these results suggest a function for GAG utilization in regulating CHIKV tropism and host responses that contribute to arthritis.

IMPORTANCE

CHIKV is a reemerging alphavirus of global significance with high potential to spread into new, immunologically naive populations. The severity of CHIKV disease, particularly its propensity for chronic musculoskeletal manifestations, emphasizes the need for identification of genetic determinants that dictate CHIKV virulence in the host. To better understand mechanisms of CHIKV pathogenesis, we probed the function of an amino acid polymorphism in the E2 viral attachment protein using a mouse model of CHIKV musculoskeletal disease. In addition to influencing glycosaminoglycan utilization, we identified roles for this polymorphism in differential infection of mammalian and mosquito cells and targeting of CHIKV to specific tissues within infected mice. These studies demonstrate a correlation between CHIKV tissue tropism and virus-induced pathology modulated by a single polymorphism in E2, which in turn illuminates potential targets for vaccine and antiviral drug development.

Chikungunya virus (CHIKV) is a mosquito-borne alphavirus that has reemerged to cause sudden and severe epidemics throughout sub-Saharan Africa, Southeast Asia, and the Caribbean. CHIKV infection causes a rheumatic disease principally characterized by an abrupt onset of fever, rash, headache, and debilitating polyarthralgia and myalgia (1, 2). Although acute symptoms usually subside within 1 to 2 weeks, chronic joint pain and inflammation occur in many patients for months or years after the initial infection (3–7). The occurrence of chronic arthritis is highly variable, ranging between 15 and 70% of infected individuals depending on the specific study cohort and observed most frequently in the elderly and persons with comorbidities (7).

Since 2004, the geographic distribution of CHIKV has increased significantly, reaching immunologically naive populations in islands of the Indian Ocean, Europe, and the Caribbean (8–13). These epidemics are noteworthy for more severe clinical manifestations, including encephalopathy, hepatitis, meningoencephalitis, and ocular disease and represent the first documented cases of fatal infection (14–16). Currently, there are no licensed CHIKV vaccines or antiviral therapies for infected individuals, and only supportive care for clinical symptoms is available.

CHIKV is an Old World alphavirus and member of the Semliki Forest antigenic complex along with the closely related O'nyong-nyong virus (ONNV), Ross River virus (RRV), and Semliki Forest virus (SFV) (17). The alphavirus genome consists of a single, positive-sense RNA molecule approximately 12 kb in length that contains two open reading frames (18, 19). The first open reading

Received 9 June 2014 **Accepted** 12 August 2014
Published ahead of print 20 August 2014
Editor: D. S. Lyles
Address correspondence to Terence S. Dermody, terry.dermody@vanderbilt.edu.

doi:10.1128/JVI.01672-14

frame encodes four nonstructural proteins (nsP1 to nsP4) that form the replicase complex and mediate synthesis of additional copies of the viral genome and the subgenomic RNA (17–19). The subgenomic, second open reading frame encodes a polyprotein containing three major structural proteins, capsid, pE2, and E1, and the small peptides, 6K and TF (17, 19–22). Following translation of the subgenomic RNA, the capsid protein is autoproteolytically cleaved from the polyprotein (18, 23). The remainder is transported through the endoplasmic reticulum (ER) and Golgi apparatus where the 6K peptide is liberated by cellular proteases and the E1 and pE2 proteins are glycosylated (20, 24). During egress, the cellular protease furin cleaves pE2 to release the E3 peptide and generate the mature heterodimer of E1 fusion and E2 attachment proteins (25–27). E1-E2 heterodimers associate as trimers and stud the host-derived lipid bilayer that surrounds the icosahedral capsid (27). The structural proteins encapsidate the viral genome, forming progeny virions near the plasma membrane, which bud from the host cell to infect neighboring cells and disseminate throughout the host (28).

A live, attenuated CHIKV vaccine was developed by passaging a clinical isolate from Thailand, strain AF15561, extensively in mammalian cell culture to produce a highly attenuated virus, strain 181/25 (29, 30). Strains AF15561 and 181/25 differ at only 10 nucleotide positions and 5 amino acid positions across the genome. A previous study identified two polymorphisms in the E2 attachment protein, T12I and G82R, as important mediators of virus strain 181/25 attenuation in both infant CD1 and immunocompromised mice (31). Accumulation of positively charged residues within E2 as a consequence of cell culture passage has been demonstrated for other alphaviruses to confer binding to negatively charged glycosaminoglycans (GAGs) such as heparan sulfate (32–36). We and others have found that strain 181/25 interacts with GAGs to infect host cells and that this interaction is strengthened through the G82R polymorphism in E2 (37, 38). Given the minimal sequence divergence displayed by strains 181/25 and AF15561, it is not known whether they differ in GAG utilization, nor is it clear whether GAG utilization is the sole mechanism that mediates CHIKV 181/25 attenuation.

Heparan sulfate-binding viruses often exhibit reduced viral dissemination and attenuation for disease *in vivo* (34, 39–42). However, such viruses can show increased virulence depending on the route of inoculation, as demonstrated for certain strains of eastern equine encephalitis virus (EEEV) (43, 44). A strategy to introduce attenuating heparan sulfate-binding residues within the CHIKV E2 attachment protein has been established as a model for CHIKV vaccine development (45). Wild-type CHIKV strain LR2006 OPY1 (LR) induced significantly less footpad swelling and proinflammatory cytokine production following substitution of E2 Gly82 with arginine and Glu79 with lysine, the latter of which was identified following serial passage in cell culture (45). Introduction of either substitution enhanced sensitivity to blockade of infection by soluble heparin or salt disruption of ionic interactions (45), suggesting that viruses attenuated by virtue of these mutations exhibit increased dependence on GAGs for infection. However, the roles of E2 residue 82 in CHIKV-induced arthritis and viral tropism are not fully understood. Furthermore, mechanisms by which specific CHIKV residues influence viral pathogenesis remain to be elucidated.

In this study, we defined the contribution of sequence polymorphisms displayed by strains 181/25 and AF15561 to CHIKV pathogenesis using a mouse model of CHIKV-induced arthritis. We engineered a panel of CHIKV variants containing these polymorphisms in the genetic background of each parental strain and screened these viruses for differences in infectivity in mammalian and mosquito cells prior to testing *in vivo*. We found that E2 residue 82 is a determinant of infectivity in mammalian and mosquito cell culture and contributes to CHIKV-induced pathology, including footpad swelling and inflammation and necrosis in the metatarsal muscle ipsilateral to the site of inoculation. In addition, this residue mediates viral dissemination to the spleen and establishment of viremia. Viruses containing an arginine at E2 residue 82 exhibit increased dependence on GAGs for infection of mammalian cells and are more attenuated for musculoskeletal disease. We conclude that CHIKV utilization of GAGs alters viral tropism, tissue inflammation, and tissue injury induced during infection, resulting in attenuated CHIKV disease.

MATERIALS AND METHODS

Cells, viruses, and antibodies. Baby hamster kidney cells (BHK-21; ATCC CCL-10) were maintained in alpha minimal essential medium (αMEM; Gibco) supplemented to contain 10% fetal bovine serum (FBS; Gibco), 10% tryptose phosphate (TP), 2 mM L-glutamine (Gibco), 100 U/ml of penicillin, 100 μg/ml of streptomycin (Gibco), and 25 ng/ml of amphotericin B (Sigma). Vero cells (ATCC CCL-81) were maintained in αMEM supplemented to contain 5% FBS, L-glutamine, penicillin, streptomycin, and amphotericin B. C6/36 cells were maintained in Leibovitz's L-15 medium (Gibco) supplemented to contain 10% FBS, 10% TP, L-glutamine, penicillin, streptomycin, and amphotericin B. Chinese hamster ovary (CHO) CHO-K1 and CHO-pgsA745 cells (46) were maintained in F-12 nutrient mixture (Gibco) supplemented to contain 10% FBS, L-glutamine, penicillin, streptomycin, and amphotericin B. CHO-K1 and CHO-pgsA745 cell lines were provided by Benhur Lee (University of California, Los Angeles).

The CHIKV 181/25 infectious clone plasmid was generated as described previously (47). The CHIKV AF15561 infectious clone and variant clone plasmids were generated using site-directed mutagenesis of the 181/25 infectious clone plasmid.

CHIKV-specific polyclonal antiserum was obtained from the ATCC (VR-1241AF). CHIKV E2-specific monoclonal antibodies (MAbs) CHK-152 and CHK 48-G8 were provided by Michael Diamond (Washington University).

Site-directed mutagenesis. Single-amino-acid substitutions (nsP1 I301T, E2 I12T, E2 R82G, 6K P42C, and E1 V404A) were generated by site-directed mutagenesis of the 181/25 infectious clone plasmid using KOD Hot Start DNA polymerase (Novagen). All five amino acid substitutions were introduced into the 181/25 plasmid to generate the AF15561 infectious clone plasmid. Reciprocal, single-amino-acid substitutions (nsP1 T301I, E2 T12I, E2 G82R, 6K C42P, and E1 A404V) were generated similarly in the AF15561 infectious clone plasmid. cDNA from each clone was sequenced to verify that only the desired mutations were introduced.

Generation of virus stocks from infectious clone plasmids. Infectious clone plasmids were linearized and transcribed *in vitro* using mMessage mMachine SP6 transcription kits (Ambion). BHK-21 cells were electroporated with viral RNA and incubated at 37°C for 24 h. Supernatants containing progeny virus were collected from electroporated cells and stored at −80°C. For some experiments, supernatants were purified by ultracentrifugation through a 20% sucrose cushion in TNE buffer (50 mM Tris-HCl [pH 7.2], 0.1 M NaCl, and 1 mM EDTA) at ~115,000 × *g* in a Beckman 32Ti rotor. Virus pellets were resuspended in virus diluent buffer (VDB) (RPMI medium with HEPES [Gibco] and 1% FBS) and stored at −80°C. Viral titers were determined by plaque assay using Vero cells. All experiments with virus were performed using biosafety level 3 conditions.

CHIKV infectivity assay. Vero, C6/36, CHO-K1, or CHO-pgsA745 cells seeded onto no. 2 glass coverslips (VWR) in 24-well plates or in 96-well plates (Costar) were adsorbed with CHIKV strains in VDB at a multiplicity of infection (MOI) of 1 (Vero and C6/36) or 10 (CHO-K1 and CHO-pgsA745) PFU/cell at 37°C (Vero, CHO-K1, and CHO-pgsA745) or 30°C (C6/36) for 1 h. The inoculum was removed, complete medium was added, and cells were incubated at 37°C or 30°C for an additional hour. The medium was then supplemented to contain 20 mM ammonium chloride to prevent subsequent rounds of infection. After incubation at 37°C or 30°C for 24 h, cells were fixed with ice-cold 100% methanol, washed with phosphate-buffered saline (PBS), and incubated with PBS containing 5% FBS and 0.1% Triton X-100 (TX) at room temperature for 1 h. The cells were incubated with CHIKV-specific polyclonal antiserum (1:1,500) in PBS with FBS and TX at 4°C overnight. The cells were washed three times with PBS and incubated with Alexa Fluor 488-labeled anti-mouse IgG (1:1,000) in PBS with FBS and TX at room temperature for 2 h. The cells were also incubated with 4′,6-diamidino-2-phenylindole (DAPI; Invitrogen) to stain nuclei. The cells and nuclei were visualized by indirect immunofluorescence using an Axiovert 200 fluorescence microscope (Zeiss). CHIKV-positive cells were enumerated in three fields of view with each field of view containing at least 100 cells for triplicate samples. For some experiments, cells were visualized using an ImageXpress Micro XL imaging system (Molecular Devices) at the Vanderbilt High-Throughput Screening Facility. Total and CHIKV-infected cells were quantified using MetaXpress software (Molecular Devices) in four fields of view containing at least 100 cells per field of view for triplicate samples. The number of CHIKV-positive cells was normalized to the total number of cells per field to determine the percentage of infected cells.

Assessment of CHIKV replication by plaque assay. Vero or C6/36 cells were adsorbed with CHIKV strains in VDB at an MOI of 0.01 PFU/cell at 37°C (Vero) or 30°C (C6/36) for 1 h. The inoculum was removed, cells were washed with PBS, and complete medium was added. After incubation at 37°C or 30°C for various intervals, 10% of the cell supernatant was collected and replaced with fresh medium. Viral titers in culture supernatants were determined by plaque assay using Vero cells.

Real-time quantitative RT-PCR. RNA was isolated using a PureLink RNA minikit (Life Technologies). The number of viral genomes/ml for each virus stock was quantified using the qScript XLT one-step reverse transcription-quantitative PCR (RT-qPCR) ToughMix kit (Quanta Biosciences) as described previously (38). CHIKV sequence-specific forward (CHIKVfor [874 5′-AAAGGGCAAGCTTAGCTTCAC-3′]) and reverse (CHIKVrev [961 5′-GCCTGGGCTCATCGTTATTC-3′]) primers were used with an internal fluorogenic probe (CHIKVprobe [899 5′-6-carboxyfluorescein{dFAM}-CGCTGTGATACAGTGGTTTCGTGTG-black hole quencher {BHQ}-3′; Biosearch Technologies). To relate threshold cycle (C_T) values to copies of genomic RNA, standard curves were generated from 10-fold dilutions, from 10^1 to 10^{10} copies, of *in vitro*-transcribed genomic 181/25 RNA.

CHIKV binding assay. Vero cells were adsorbed in suspension with 3×10^{10} genomes of various virus strains in VDB at 4°C for 30 min. The cells were washed with incomplete medium and PBS and fixed in PBS with 1% electron microscopy (EM)-grade paraformaldehyde (Electron Microscopy Sciences). The cells were washed with fluorescence-activated cell sorting (FACS) buffer (PBS with 2% FBS) and incubated with CHIKV E2-specific MAb CHK-152 (1:1,000) in FACS buffer at 4°C for 30 min. The cells were incubated with Alexa Fluor 488-labeled anti-mouse IgG (1:1,000) in FACS buffer at 4°C for 30 min and analyzed using a BD LSRII flow cytometer. Cell staining was quantified using FlowJo software (Tree Star).

Inhibition of CHIKV infection with soluble glycosaminoglycans. Virus was pretreated with soluble heparin (Sigma) or bovine serum albumin (BSA) (Sigma) at 4°C for 30 min. Vero cells were adsorbed with pretreated virus strains at an MOI of 1 PFU/cell at 37°C for 2 h. The inoculum was removed, and complete medium supplemented to contain 20 mM ammonium chloride was added to prevent subsequent rounds of infection. After incubation at 37°C for 24 h, cells were fixed and incubated with CHIKV-specific polyclonal antiserum and DAPI to detect nuclei. Infection was scored by indirect immunofluorescence. CHIKV-positive cells were enumerated in three fields of view for triplicate samples and normalized to the number of total cells per field.

Heparin-agarose binding assay. Heparin-conjugated agarose or unconjugated agarose beads were incubated with 5×10^9 genomes of each virus at 4°C for 30 min as described previously (38). The beads were washed with VDB containing 0.02% Tween 20, and beads or input virus were resuspended in sample buffer (50 mM Tris-HCl [pH 6.8], 2% [wt/vol] sodium dodecyl sulfate [SDS], 1% β-mercaptoethanol, 10% [vol/vol] glycerol, 0.04% [wt/vol] bromophenol blue) and boiled for 10 min. Samples were resolved by SDS-polyacrylamide gel electrophoresis (PAGE) in 10% polyacrylamide gels (Bio-Rad) and transferred to an Immun-Blot polyvinylidene difluoride (PVDF) membrane (Bio-Rad). The membranes were incubated with Tris-buffered saline (TBS) containing 5% milk at room temperature for 1 h followed by incubation with CHIKV-specific MAb CHK 48-G8 (1:2,000) in TBS with 0.1% Tween 20 (TBS-T) at 4°C overnight. The membranes were washed three times with TBS-T and incubated with IRDye 750 CW-labeled goat anti-mouse IgG (1:5,000; LI-COR) in TBS-T at room temperature for 2 h. The membranes were washed three times with TBS-T and once with TBS, and CHIKV-specific signal was detected using an Odyssey imaging system (LI-COR).

Infection of mice. C57BL/6J mice were obtained from The Jackson Laboratory to establish breeding colonies. Mice (20 to 22 days old) were inoculated in the left rear footpad with 10^3 PFU of virus in PBS containing 1% bovine calf serum (BCS) in a 10-μl volume. Mock-infected animals received diluent alone. Mice were monitored for clinical signs of disease and weighed at 24-h intervals. At various intervals following infection, mice were euthanized by isoflurane overdose, blood was collected by cardiac puncture, and mice were perfused by intracardial injection of PBS. Swelling of the feet of both hind limbs was quantified using calipers to measure the height of the feet. For analysis of viral replication, tissues were collected in PBS containing BCS, weighed, homogenized with a MagNA lyser (Roche), and stored at −80°C. Viral titers in tissue homogenates were determined by plaque assay using BHK-21 cells. For RNA analysis, tissues were collected and homogenized in TRIzol reagent (Life Technologies).

Animal husbandry and experiments were performed in accordance with all University of Colorado School of Medicine Institutional Animal Care and Use Committee guidelines. All mouse studies were performed using biosafety level 3 conditions.

Histological analysis. At day 7 postinoculation, mice were euthanized and perfused by intracardial injection of 4% paraformaldehyde (PFA) (pH 7.3). Tissues were resected and incubated in PFA at 4°C for at least 72 h. Fixed tissues were embedded in paraffin, and 5-μm sections were stained with hematoxylin and eosin (H&E) to assess histopathologic changes. Tissues were scored by an observer in a blind manner (unaware of the conditions of the experiment) for the presence, distribution, and severity of histologic lesions. For all tissue changes, the following scoring system was used: 0, no lesions; 1, minimal, 0 to 24% of tissue affected; 2, mild, 25 to 49% of tissue affected; 3, moderate, 50 to 75% of tissue affected; 4, marked, >75% of tissue affected.

Analysis of sequence reversion. RNA was isolated using a PureLink RNA minikit (Life Technologies). cDNA was generated using the SuperScript III first-strand kit (Life Technologies) with random hexamers and used for PCR amplification by KOD polymerase (Novagen) with CHIKV E2 sequence-specific forward (CHIKVE2for [8336 5′-GGGCCGAAGAG TGGAGTCTT-3′]) and reverse (CHIKVE2rev [9089 5′-GACACCCCTG ATCGCACATT-3′]) primers. Amplicons were cloned into a TOPO TA vector (Life Technologies) and sequenced over the mutagenized region of the E2 open reading frame.

Statistical analysis. Mean values for at least duplicate experiments were compared using an unpaired Student's *t* test, one-way analysis of variance (ANOVA) followed by Bonferroni's posthoc test, or Kruskal-

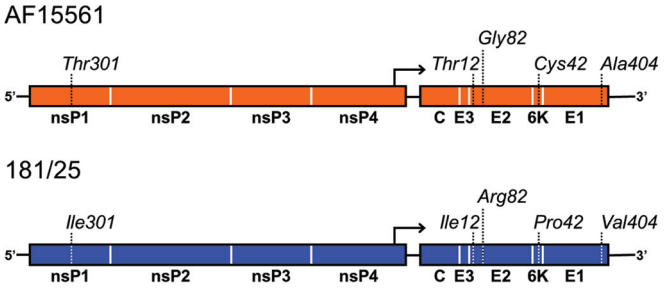

FIG 1 Schematic depiction of polymorphic residues in CHIKV strains AF15561 and 181/25. Distribution of amino acid polymorphisms between strains AF15561 and 181/25 across the ~12-kb genome. Numbers correspond to the amino acid positions within each protein.

Wallis analysis followed by Dunn's posthoc test (GraphPad Prism). *P* values of <0.05 were considered to be statistically significant.

RESULTS

E2 residue 82 is a determinant of CHIKV infectivity in mammalian cell culture. For many viruses, serial passage in mammalian cells enhances viral replicative capacity in cell culture (33, 48–53). To determine whether passage of CHIKV strain AF15561 to generate vaccine strain 181/25 resulted in enhanced replicative capacity, cells were infected with either strain AF15561 or 181/25, and viral titers in culture supernatants were determined by plaque assay over an infectious time course. Relative to strain AF15561, strain 181/25 reached higher titers in several cell lines, including Vero, BHK-21, HeLa, and human brain microvascular endothelial cells (data not shown). These results suggest that strain 181/25 has adapted to mammalian cell culture as a result of cell culture passage, consistent with observations for other passaged viruses.

Virus strains 181/25 and AF15561 differ at five nonsynonymous nucleotides and five synonymous nucleotides across the genome. Polymorphic positions resulting in coding changes in 181/25 are in the nsP1 (T301I), E2 (T12I and G82R), 6K (C42P), and E1 (A404V) proteins (Fig. 1). To define residues that contribute to the replication and infectivity differences observed between strains 181/25 and AF15561, Vero cells were infected at an MOI of 1 PFU/cell with either of the parental strains or viruses containing individual polymorphic residues in the reciprocal genetic background. The percentage of infected cells in each case was quantified after a single round of infection by indirect immunofluorescence (Fig. 2A). As expected, virus strain 181/25 infected a significantly greater percentage of cells than did virus strain AF15561. Substitution of an arginine at E2 residue 82 in the AF15561 background enhanced infectivity to levels even greater than those observed for strain 181/25. Concordantly, substitution of a glycine at E2 residue 82 in the 181/25 background significantly diminished 181/25 infectivity. Interestingly, substituting an isoleucine at E2 residue 12 in the AF15561 background further decreased infectivity relative to AF15561. Introducing any of the other heterologous changes in either background had no effect on infectivity in these cells. To understand how these findings might compare to previous studies with these viruses in mice, the parental and variant viruses were used to infect murine L929 and NIH 3T3 cell lines. As observed in experiments using Vero cells, substitution of an arginine at E2 residue 82 in the AF15561 background enhanced infectivity, whereas substitution of a glycine at E2 residue 82 in the 181/25 background significantly diminished

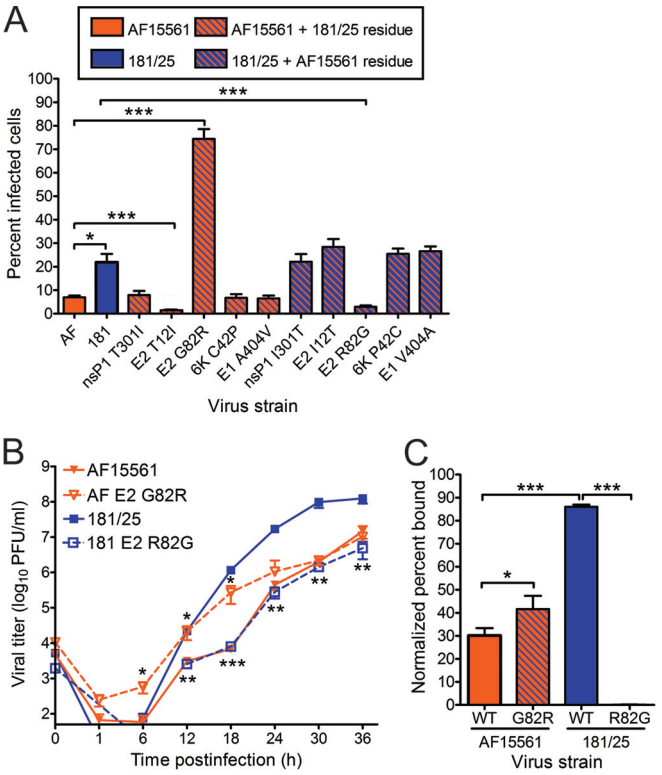

FIG 2 Residue 82 of the E2 attachment protein is a determinant of CHIKV infectivity in mammalian cells. (A) Vero cells were adsorbed with CHIKV strains AF15561 (AF), 181/25 (181), or the variant viruses shown at an MOI of 1 PFU/cell and incubated for 24 h in medium containing 20 mM NH_4Cl. The cells were stained with CHIKV-specific antiserum and DAPI to detect nuclei and imaged by fluorescence microscopy. Results are presented as percent infected cells for triplicate experiments. Error bars indicate standard errors of the means. (B) Vero cells were adsorbed with virus strain AF15561, 181/25, AF15561 E2 G82R, or 181/25 E2 R82G at an MOI of 0.01 PFU/cell. At the times shown, viral titers in culture supernatants were determined by plaque assay using Vero cells. Results are presented as the mean viral titers for triplicate samples. Error bars indicate standard deviations. Titers of virus strains AF15561 and AF15561 E2 G82R were significantly different at 6, 12, and 18 h postinfection, and titers of virus strains 181/25 and 181/25 E2 R82G were significantly different at 12, 18, 24, 30, and 36 h postinfection. (C) Vero cells were adsorbed with ~3 × 10^{10} genomes of wild-type (WT) virus strain AF15561, 181/25, AF15561 E2 G82R, or 181/25 E2 R82G for 30 min. After 30-min incubation, cells were stained with CHIKV E2-specific MAb, and virus-bound cells were quantified by flow cytometry. Results are presented as percent bound cells for triplicate experiments normalized to cell autofluorescence in the absence of CHIKV MAb. No CHIKV-bound cells were detected for virus strain 181/25 E2 R82G. Error bars indicate standard deviations. Values that are significantly different, as determined by ANOVA, followed by Bonferroni's posthoc test (A and C) and Student's *t* test (B), are indicated by asterisks as follows: *, $P < 0.05$; **, $P < 0.01$; ***, $P < 0.001$.

infectivity in these murine cell lines (data not shown). These data suggest that an arginine at residue 82 in the E2 protein confers the enhanced infectivity observed for strain 181/25 in mammalian cells.

Because these virus strains differed substantially in infectivity of Vero cells, we quantified the genome/PFU and genome/fluorescent-focus unit (FFU) ratios for each strain (Table 1). In Vero cells, parental strains AF15561 and 181/25 had genome/PFU ratios of 6,598 and 176, respectively. Similarly, strains AF15561 and 181/25 had genome/FFU ratios of 9.497 × 10^7 and 8.0 × 10^5, respectively. Viral variants containing residues from strain 181/25

TABLE 1 Infectivity of parental and mutant CHIKV strains[a]

Virus strain	Genome/PFU ratio[b]	Genome/FFU ratio[c] ($\times 10^4$) in:	
		Vero cells	C6/36 cells
AF15561	6,598	9,497	980
181/25	176	80	182
AF15561 nsP1 T301I	1,718	2,173	250
AF15561 E2 T12I	1,107	7,621	344
AF15561 E2 G82R	5,656	760	841
AF15561 6K C42P	3,057	4,529	436
AF15561 E1 A404V	4,067	6,255	586
181/25 nsP1 I30T	1,005	455	381
181/25 E2 I12T	99	35	45
181/25 E2 R82G	2,858	9,783	517
181/25 6K P42C	44	17	16
181/25 E1 V404A	121	46	27

[a] Infectivity of virus strains measured in genome equivalents.
[b] Genome copy numbers were determined by real-time quantitative PCRs conducted in triplicate. The number of PFU was determined by plaque assay using Vero cells for three independent replicates for each virus strain.
[c] Fluorescent-focus units (FFU) were determined by indirect immunofluorescence in triplicate for at least two independent experiments.

TABLE 2 Infectivity of purified CHIKV strains[a]

Virus strain	Genome/PFU ratio[b]	Genome/FFU ratio[c] ($\times 10^4$) in:		Ratio[d]
		CHO-K1 cells	CHO-pgsA745 cells	
AF15561	647	1,578	11,795	7.47
AF15561 E2 G82R	498	867	20,494	23.65
181/25	92	310	2,376	7.67
181/25 E2 R82G	316	1,862	8,155	4.38

[a] Infectivity of virus strains measured in genome equivalents.
[b] Genome copy numbers were determined by real-time quantitative PCRs conducted in triplicate. The number of PFU was determined by plaque assay using Vero cells for three independent replicates for each virus strain.
[c] Fluorescent-focus units (FFU) were determined by indirect immunofluorescence in triplicate for at least two independent experiments.
[d] Ratio of the genome/FFU ratio in CHO-pgsA745 cells to the genome/FFU ratio in CHO-K1 cells.

in the AF15561 background had reduced genome/PFU and genome/FFU ratios compared to those of parental strain AF15561. Interestingly, introducing the E2 G82R substitution resulted in the most modest reduction in genome/PFU ratio, but the greatest reduction in genome/FFU ratio. In contrast, introducing the E2 R82G substitution in the 181/25 background resulted in increased genome/PFU and genome/FFU ratios, which were the most dramatic increases of any of the viral variants with AF15561 residues in the 181/25 background. Thus, the E2 82 polymorphism serves as a key determinant of CHIKV infectivity in mammalian cell culture.

To determine whether E2 residue 82 contributes to the production of infectious virus over multiple rounds of infection, Vero cells were infected at an MOI of 0.01 PFU/cell, and viral titers in culture supernatants were determined by plaque assay at 6-h intervals (Fig. 2B). Compared with titers of AF15561, titers of AF15561 E2 G82R were increased 10-fold by 6 h postinfection, 7-fold by 12 h postinfection, and 40-fold by 18 h postinfection. Compared with titers of virus strain 181/25, titers of 181/25 E2 R82G were reduced 145-fold by 18 h postinfection, 60-fold by 24 h postinfection, and 68-fold by 30 h postinfection. Taken together, these data indicate that E2 residue 82 influences both initial and subsequent rounds of CHIKV infection.

Because this determinant of CHIKV infectivity resides in the viral attachment protein, we tested whether E2 residue 82 influences binding to host cells. For these experiments, Vero cells were adsorbed with each parental strain and the reciprocal E2 82 variant strains, and the percentage of virus-bound cells was quantified using flow cytometry (Fig. 2C). A significantly greater proportion of cells were bound by strain 181/25 than by strain AF15561. In agreement with the infectivity data, introducing the E2 G82R substitution in the AF15561 background significantly enhanced cell attachment. In contrast, introducing the E2 R82G polymorphism in the 181/25 background reduced cell binding to undetectable levels. These data suggest that an arginine at position 82 in the E2 attachment protein is required for the enhanced binding and infectivity observed for strain 181/25 in mammalian cells.

E2 residue 82 contributes to CHIKV infectivity in mosquito cells. To determine whether an arginine at E2 residue 82 affects infection and replication in invertebrate cells, we tested the parental and reciprocal E2 82 variant strains for infection and replication in mosquito cells (Fig. 3). *Aedes albopictus* C6/36 cells were infected at an MOI of 1 PFU/cell, and the percentage of infected cells was quantified after a single round of infection by indirect immunofluorescence (Fig. 3A). In sharp contrast to our findings using mammalian cells, strain 181/25 infected significantly fewer C6/36 cells relative to strain AF15561, and substitution of a glycine at E2 residue 82 in the 181/25 background significantly increased 181/25 infectivity in these cells. However, substitution of an arginine at E2 residue 82 in the AF15561 background did not significantly diminish C6/36 infection. Surprisingly, only substitution of isoleucine for threonine at residue 12 in AF15561 E2 was sufficient to reduce infection in these cells, albeit not to the levels observed for strain 181/25. Additionally, AF15561 E2 G82R had a similar genome/FFU ratio compared to that of AF15561, whereas substitutions at the other polymorphic sites with residues from strain 181/25 decreased the genome/FFU ratio. Together, these data indicate that the residue at E2 position 82 provides a fitness advantage for CHIKV infectivity depending on the host cell species.

To assess the role of E2 residue 82 in the production of infectious virus from mosquito cells, C6/36 cells were infected at an MOI of 0.01 PFU/cell, and viral titers in culture supernatants were determined at 6-h intervals (Fig. 3B). Relative to titers of virus strain 181/25, titers of 181/25 E2 R82G were increased 29-fold by 12 h postinfection, 8-fold by 18 h postinfection, and 13-fold by 24 h postinfection. However, relative to titers of virus strain AF15561, there was no decrease in viral titers when an arginine was introduced at E2 82 in the AF15561 strain. These data indicate that E2 Gly82 in the genetic background of strain 181/25 enhances infection of mosquito cells. However, other polymorphisms exhibited by these strains appear to contribute to the enhanced infectivity of AF15561 in mosquito cells in addition to E2 Gly82.

E2 residue 82 influences utilization of glycosaminoglycans. To understand mechanisms by which E2 residue 82 influences CHIKV attachment to mammalian cells, we next investigated the dependence of virus strains 181/25 and AF15561 on GAGs for infectivity. Wild-type CHO-K1 and GAG-deficient CHO-

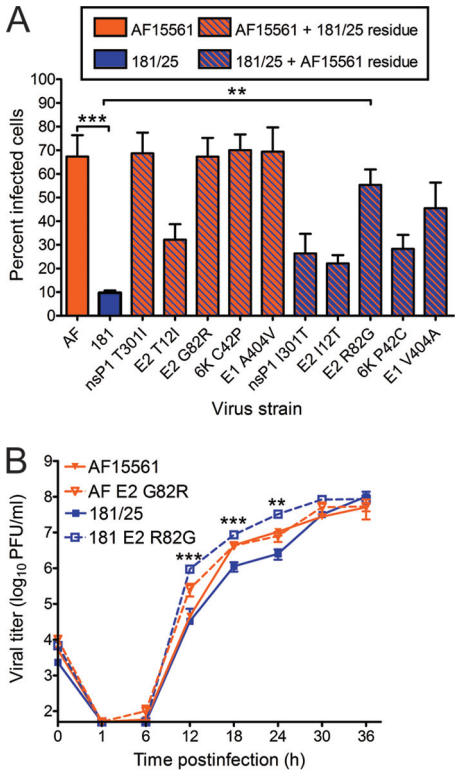

FIG 3 Residue 82 of the E2 attachment protein is a determinant of CHIKV infectivity in mosquito cells. (A) C6/36 mosquito cells were adsorbed with CHIKV strains AF15561 and 181/25 or the variant viruses shown at an MOI of 1 PFU/cell and incubated for 24 h in medium containing 20 mM NH_4Cl. The cells were stained with CHIKV-specific antiserum and DAPI to detect nuclei and imaged by fluorescence microscopy. Results are presented as percent infected cells for quadruplicate experiments. Error bars indicate standard errors of the means. (B) C6/36 cells were adsorbed with virus strain AF15561, 181/25, AF15561 G82R, or 181/25 E2 R82G at an MOI of 0.01 PFU/cell. At the times shown, viral titers in culture supernatants were determined by plaque assay using Vero cells. Results are presented as the mean viral titers for triplicate samples. Error bars indicate standard deviations. The titers of virus strains 181/25 and 181/25 E2 R82G were significantly different at 12, 18, and 24 h postinfection. Values that are significantly different, as determined by ANOVA, followed by Bonferroni's posthoc test (A) and Student's *t* test (B), are indicated by asterisks as follows: **, $P < 0.01$; ***, $P < 0.001$.

pgsA745 cells were infected with purified 181/25, AF15561, 181/25 E2 R82G, or AF15561 E2 G82R at an MOI of 10 PFU/cell. The percentage of infected cells for each virus was quantified after a single round of infection by indirect immunofluorescence (Fig. 4A). The CHO-pgsA745 cells were significantly less susceptible to infection by all four viruses relative to infection of CHO-K1 cells ($P < 0.0001$ for virus strains 181/25 and AF15561, $P < 0.001$ for AF15561 E2 G82R, and $P < 0.05$ for 181/25 E2 R82G). However, the CHO-pgsA745 cells were significantly less susceptible to infection by strain 181/25 relative to strain AF15561. Substitution of E2 Gly82 with arginine in the AF15561 background was sufficient to diminish infectivity in these cells to levels observed for strain 181/25. Furthermore, substitution of E2 Arg82 with glycine in the 181/25 background was sufficient to increase infectivity and mitigate GAG dependence to levels observed for strain AF15561. These data confirm that strain 181/25 is more dependent on GAGs for infection than is AF15561 and that E2 residue 82 mediates this dependence.

We also assessed infectivity by determining genome/PFU ratios using Vero cells and genome/FFU ratios using both CHO-K1 and CHO-pgsA745 cells. We observed a similar trend in the genome/PFU values of purified stocks of the parental and variant viruses used in these experiments. Strain AF15561 had higher genome/PFU ratios than strain 181/25 did in both cell lines, and these differences once again segregated with E2 residue 82. Interestingly, all strains had higher genome/FFU ratios in CHO-pgsA745 cells than in the parental CHO-K1 cells. These data support the hypothesis that viruses containing an arginine at E2 residue 82 are less fit in GAG-deficient cells relative to their glycine-containing counterparts.

On the basis of these and previously published findings (32–36), the GAG dependence mediated by this residue likely occurs at an early step in the infectious life cycle. Therefore, we reasoned that soluble GAGs could act as competitive agonists to block infectivity of GAG-dependent viruses. To test whether competition with soluble GAGs inhibits infection, purified virus was incubated with increasing concentrations of soluble heparin, a highly sulfated GAG, and adsorbed to Vero cells. The percentage of infected cells was quantified after a single round of infection by indirect immunofluorescence (Fig. 4B). Treatment with soluble heparin resulted in a dose-dependent decrease in the percentage of infected cells for all viruses tested. However, this decrease was most substantial for strains 181/25 and AF15561 E2 G82R, for which incubation with the highest concentration of heparin decreased infectivity 15- and 24-fold, respectively. In contrast, incubation of strains AF15561 and 181/25 E2 R82G with the same concentration of heparin resulted in only a 4-fold decrease in infectivity. These findings suggest that CHIKV strains containing an arginine at E2 residue 82 rely on GAGs for efficient cell attachment.

To determine whether the CHIKV strains used in our study interact directly with GAGs, equivalent genome copies of purified parental or variant viruses were incubated with either heparin-conjugated or unconjugated agarose beads. Bound material was resolved by SDS-PAGE and immunoblotted using an E2-specific MAb to detect CHIKV particles (Fig. 4C, left). A significantly greater proportion of strain 181/25 was bound by the heparin-conjugated beads relative to the binding of strain AF15561. Substituting AF15561 E2 Gly82 with arginine increased the proportion of this virus that was bound by the heparin-conjugated beads. Concordantly, substituting strain 181/25 E2 Arg82 with glycine decreased heparin binding. Intensities of the viral protein bands from the particles bound to the heparin-conjugated beads were quantified for three independent experiments and normalized to the intensities of protein bands for input virus (Fig. 4C, right). Approximately 35% and 37% of strains 181/25 and AF15561 E2 G82R, respectively, were captured by the heparin-agarose beads, whereas only 13% and 16% of strains AF15561 and 181/25 E2 R82G, respectively, bound to heparin. These results suggest that CHIKV virions interact directly with GAGs and that these interactions are influenced by E2 residue 82.

CHIKV E2 residue 82 modulates virus-induced pathology. We next investigated whether E2 residue 82 influences CHIKV pathogenesis using a mouse model of CHIKV disease (54). In this model, 3-week-old mice are inoculated subcutaneously in the left rear footpad. Infected mice develop signs of disease similar to those observed in humans infected with CHIKV, including swelling of the feet and ankles, arthritis, myositis, and tenosynovitis. Mice were inoculated with 10^3 PFU of strain 181/25, AF15561,

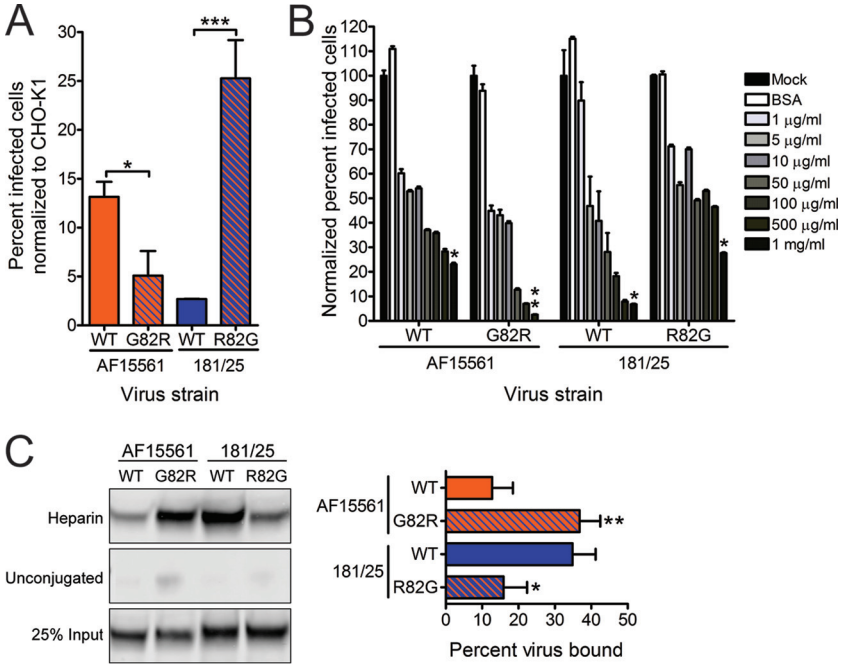

FIG 4 An arginine at E2 residue 82 confers greater dependence on glycosaminoglycans. (A) CHO-K1 and CHO-pgsA745 cells were adsorbed with virus strain AF15561, 181/25, AF1561 E2 G82R, or 181/25 E2 R82G at an MOI of 10 PFU/cell and incubated for 24 h. Wild-type (WT) CHIKV or variant strains containing substitutions at E2 residue 82 were tested. The cells were stained with CHIKV-specific antiserum and DAPI to detect nuclei and imaged by fluorescence microscopy. Results are presented as percent infected cells for triplicate experiments normalized to the values for parental CHO-K1 cells. Error bars indicate standard errors of the means. (B) Strains AF15561, 181/25, AF1561 E2 G82R, and 181/25 E2 R82G were treated with BSA at 1,000 μg/ml or heparin at the concentrations shown for 30 min and adsorbed to Vero cells at an MOI of 2.5 PFU/cell. After incubation for 24 h, cells were stained with CHIKV-specific antiserum and DAPI to detect nuclei and imaged by fluorescence microscopy. Results are presented as percent infected cells for triplicate experiments normalized to the values for mock-treated virus. Error bars indicate standard errors of the means. (C) The virus strains shown at 5×10^9 genome copies each were incubated with heparin-conjugated or unconjugated agarose beads for 30 min, resolved by SDS-PAGE, and detected by immunoblotting with CHIKV E2-specific MAb (left). Twenty-five percent of input virus is shown as a control. The percentage of virus bound to beads was quantified by optical densitometry for triplicate experiments (right). Error bars indicate standard deviations. Values that are significantly different, as determined by Student's *t* test (A and C) and Kruskal-Wallis analysis followed by Dunn's posthoc test (B), are indicated by asterisks as follows: *, $P < 0.05$; **, $P < 0.01$; ***, $P < 0.001$.

181/25 E2 R82G, or AF15561 E2 G82R, and virulence was assessed by weight gain and swelling of feet (Fig. 5). Mice infected with virus strain AF15561 gained less weight than mice infected with virus strain 181/25, indicating that strain AF15561 is more virulent in these animals (Fig. 5A). Mice inoculated with AF15561 E2 G82R gained weight in parallel with mock-infected mice, suggesting that an arginine at E2 residue 82 in the AF15561 background significantly reduces CHIKV virulence. However, mice inoculated with 181/25 E2 R82G did not exhibit impaired weight gain, suggesting that substitution of a glycine at E2 residue 82 in strain 181/25 is not sufficient to recapitulate the virulent phenotype.

To determine the effect of E2 residue 82 on CHIKV-induced arthritis, we assessed swelling of the left and right feet at 1, 3, 5, and 7 days postinoculation (Fig. 5B). At 3, 5, and 7 days postinoculation, mice infected with virus strain AF15561 exhibited significant swelling of the left feet. No swelling was observed in the uninoculated feet of any of the animals. Inoculation with AF15561 E2 G82R resulted in reduced swelling in the left hind limb at 3 and 5 days postinoculation relative to AF15561, whereas inoculation with 181/25 E2 R82G only modestly increased swelling at 5 days postinoculation relative to 181/25. Together, these data suggest that a glycine at E2 residue 82 is necessary but not sufficient for full virulence of strain AF15561, as assessed by weight gain and foot swelling.

To determine whether E2 residue 82 influences the magnitude of pathological injury, left hind limbs of infected mice were processed for histology and assigned a pathology score based on histologic changes (Fig. 6). Tissue damage appeared more severe for mice infected with virus strain AF15561 than for mice infected with virus strain 181/25 at day 7 postinoculation (Fig. 6A and B). In particular, there was slightly more inflammation and necrosis in the metatarsal muscles of AF15561-infected mice compared to those of 181/25-infected mice. However, the levels of myositis and tendonitis induced by these strains were comparable. Substitution of an arginine at E2 82 in the AF15561 strain led to reduced tissue damage, inflammation, and necrosis compared to mice inoculated with the parental AF15561 strain (Fig. 6B). More dramatically, substitution of a glycine at this residue in the 181/25 strain led to consistently more inflammation and necrosis of the metatarsal muscle as well as more severe tendonitis in the hind limb relative to the hind limbs of 181/25-infected mice. These data suggest that E2 residue 82 modulates CHIKV-induced disease and that a glycine at this residue is sufficient to mediate tissue injury in CHIKV-infected mice.

CHIKV titers in the spleen and serum are influenced by E2 residue 82. To determine whether differences in virus-induced pathology are a consequence of differences in viral replication, mice were inoculated subcutaneously in the left rear footpad with 10^3 PFU of virus strain 181/25, AF15561, 181/25 E2 R82G, or

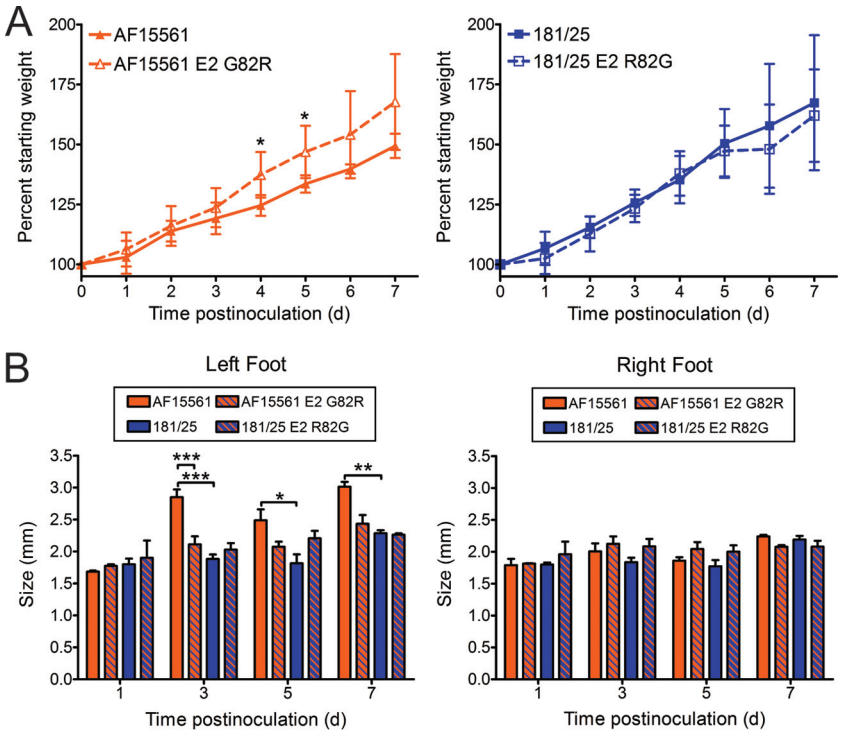

FIG 5 CHIKV E2 residue 82 modulates virus-induced pathology. C57BL/6J mice (20 to 22 days old) were inoculated with 10^3 PFU of CHIKV strain AF15561, 181/25, AF1561 E2 G82R, or 181/25 E2 R82G in the left rear footpad. (A) Mice were weighed at 24-h intervals postinoculation. Results are presented as the mean percent starting weight (weight on day 0). Error bars indicate standard deviations. The number of mice at different time points follow: day 0 to day 1 (D0-D1), $n = 17$; D2-D3, $n = 15$; D4-D5, $n = 8$; D6-D7, $n = 3$. (B) Swelling of the left and right hind feet was quantified using calipers at the times shown (in days). Error bars indicate standard deviations. The number of mice at different time points follow: D1, $n = 2$; D3, $n = 7$; D5, $n = 5$; D7, $n = 3$. Values that are significantly different as determined by ANOVA followed by Bonferroni's posthoc test are indicated by asterisks as follows: *, $P < 0.05$; **, $P < 0.01$; ***, $P < 0.001$.

AF15561 E2 G82R. Tissues were harvested at 1, 3, and 5 days postinoculation, and viral titers were determined by plaque assay (Fig. 7). At 1 day postinoculation, all viruses produced equivalent titers in the left and right hind limbs (Fig. 7A). However, virus strain AF15561 produced higher titers in the spleen and serum relative to virus strain 181/25. The titers of strain AF15561 E2 G82R were reduced in the spleen and serum compared to those of strain AF15561 at 1 day postinoculation, and strain 181/25 E2 R82G produced higher titers in the spleen and serum compared to those of strain 181/25, although this difference was not statistically significant. These data suggest that a glycine at E2 residue 82 contributes to higher viral titers in the spleen and serum at early times postinoculation.

By 3 days postinoculation, all viruses produced comparable titers in the left ankle, but strain AF15561 replicated to significantly higher titers in the left quadriceps and right ankle relative to strain 181/25 (Fig. 7B). However, this difference in replication did not segregate with E2 residue 82, as mice inoculated with AF15561 E2 G82R displayed higher viral titers in the left quadriceps and right ankle relative to 181/25 E2 R82G. Similarly, higher titers of AF15561 E2 G82R were detected in the right quadriceps and serum relative to 181/25 E2 R82G. In the spleen, we observed a trend similar to the day 1 time point with AF15561 E2 G82R producing lower titers in that organ relative to AF15561, and 181/25 E2 R82G producing slightly higher titers relative to 181/25.

By 5 days postinoculation, no virus was detected in the serum. In the left and right quadriceps, titers of virus strain AF15561 E2 G82R were higher relative to those of strain AF15561. In addition, titers of virus strain 181/25 were higher in these tissues relative to those of 181/25 E2 R82G. These data suggest that an arginine at E2 residue 82 correlates with higher viral titers in the quadriceps muscles at later times postinoculation. In contrast, viruses containing a glycine at E2 82 produced higher titers in the spleen at earlier times postinoculation. Thus, residue 82 in the E2 glycoprotein contributes to either viral dissemination to or replication within the hind limbs and spleen and influences establishment of viremia.

A glycine at E2 residue 82 is selected in the spleens of CHIKV-infected mice. Since high mutation rates are associated with replication of positive-sense RNA viruses, we determined the sequences of viral isolates from CHIKV-infected mice to assess the stability of the engineered mutations. RNA was isolated from the spleens of CHIKV-infected mice at 1 day postinoculation, cDNA was generated, and sequences of the E2 open reading frame from multiple clones were determined. Of the clones derived from mice inoculated with strain AF15561 E2 G82R, 21 of 23 clones (91%) encoded a glycine at E2 residue 82. In contrast, only 1 of 7 (14%) of the clones derived from mice inoculated with strain AF15561 encoded an arginine at this position. Viral RNA could not be recovered from the spleens of animals infected with virus strain 181/25 at this early time point, which precluded sequence analysis. To confirm that these mutations were not present in the viral inocula, RNA was isolated from virus stocks, cDNA was generated, and E2 sequences were determined. Of the 20 clones sequenced from each virus stock, all encoded the engineered residues across the E2 open reading frame. These results suggest that

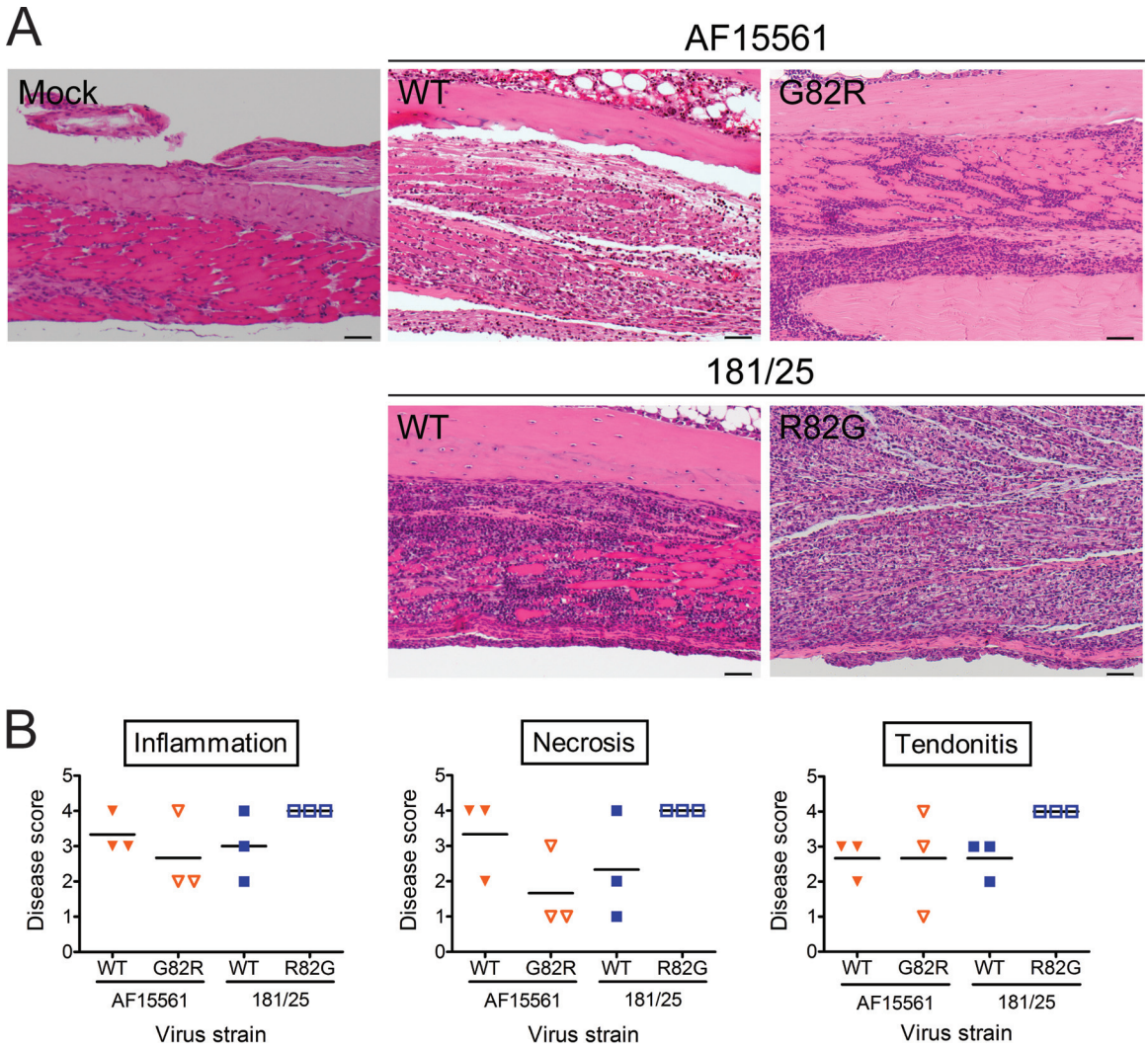

FIG 6 An arginine at E2 residue 82 diminishes CHIKV-induced arthritis. C57BL/6J mice (20 to 22 days old) were inoculated with PBS or 10^3 PFU of virus strain AF15561, 181/25, AF1561 E2 G82R, or 181/25 E2 R82G in the left rear footpad. At day 7 postinoculation, mice were euthanized and perfused with 4% PFA. Consecutive 5-μm sections of the left hind limb were stained with H&E. (A) Representative sections of three mice per group are shown for mock-infected mice or mice inoculated with the parental strains and the reciprocal E2 82 variant strains. Bars, 50 μm. (B) H&E-stained sections were scored for histological evidence of inflammation and necrosis in the metatarsal muscle and tendonitis. Results are expressed as pathology score of tissues from individual animals. Horizontal black lines indicate mean pathology score. Scores were assigned based on the following scale: 0, no lesions; 1, minimal, 0 to 24% of tissue affected; 2, mild, 25 to 49% of tissue affected; 3, moderate, 50 to 75% of tissue affected; 4, marked, >75% of tissue affected.

a glycine at E2 82 is preferentially selected early in CHIKV infection in the spleen, but a residual population of isolates with an arginine at this position is maintained.

DISCUSSION

CHIKV causes both an acute and chronic disease characterized by debilitating joint pain and inflammation (1, 2). However, the viral and host determinants responsible for CHIKV disease have not been fully defined. Additionally, mechanisms of pathogenesis for arthritogenic alphaviruses like CHIKV are not completely understood. CHIKV strain 181/25, which was isolated following serial passage in mammalian cell culture, differs from its closest known parental strain, AF15561, at 5 synonymous and 5 nonsynonymous nucleotide positions. One nonsynonymous polymorphism, G82R in the E2 attachment protein, influences interactions with GAGs (38) and attenuates virulence in some mouse models (31, 45). In this study, we demonstrate a role for E2 residue 82 in the differential infection of mammalian and mosquito cells and in CHIKV-induced musculoskeletal disease. Viruses containing a glycine at E2 82 replicated to higher titers in lymphoid tissues and established higher levels of viremia. Moreover, these viruses induced greater pathological injury, including inflammation and necrosis, in joint-associated tissues compared with viruses containing an arginine at this position. Data presented here expand our knowledge of how CHIKV E2 residue 82 influences virus-cell interactions and provide new information about the function of this residue *in vivo*.

Our results along with previously published data (31, 38, 45) indicate that an arginine at E2 residue 82 enhances utilization of GAGs by CHIKV to infect cultured cells and attenuates the virus in mice. However, it is not clear how an increase in GAG dependence leads to attenuation of CHIKV. For other alphaviruses, such

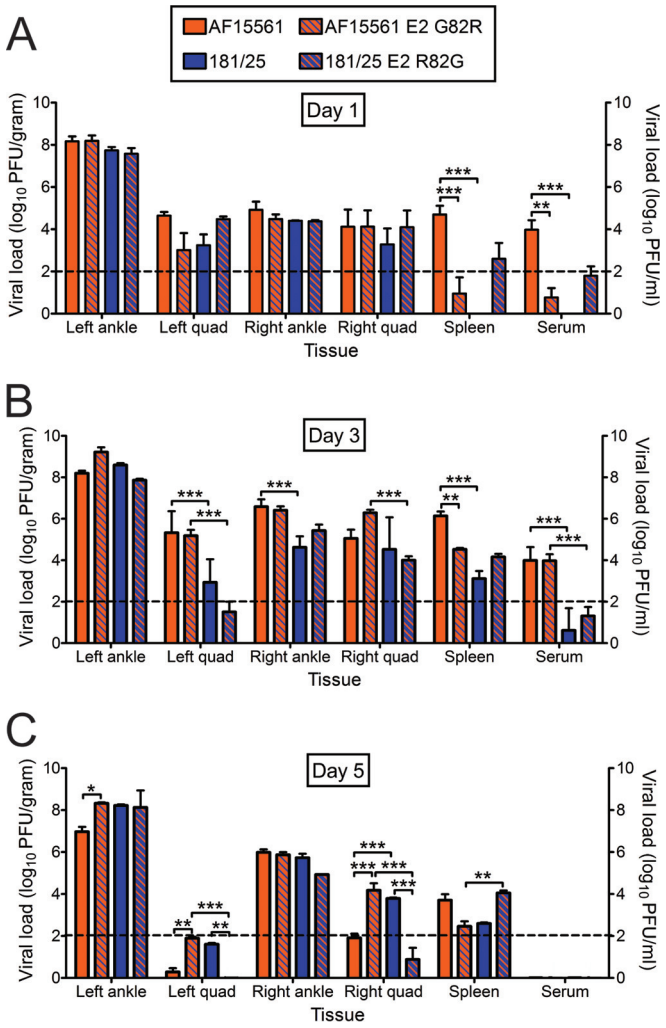

FIG 7 Viral loads following inoculation of parental strains and the reciprocal E2 82 variant strains. C57BL/6J mice (20 to 22 days old) were inoculated with PBS or 10^3 PFU of virus strain AF15561, 181/25, AF1561 E2 G82R, or 181/25 E2 R82G in the left rear footpad. At days 1, 3, and 5 postinoculation, mice were euthanized, their ankles, quadriceps (Quad), and spleens were excised, and serum was collected. Viral titers in tissue and serum homogenates were determined by plaque assay using BHK-21 cells. Results are expressed as the mean PFU/gram (tissue) or PFU/ml (serum). Error bars indicate standard errors of the means. Dashed lines indicate the limit of detection. The number of mice at different time points follow: D1, $n = 5$; D3, $n = 7$; D5, $n = 5$. Values that are significantly different as determined by ANOVA followed by Bonferroni's posthoc test are indicated by asterisks and bars as follows: *, $P < 0.05$; **, $P < 0.01$; ***, $P < 0.001$.

as Sindbis virus and Venezuelan equine encephalitis virus, higher-affinity interactions with GAGs prevent viral spread to sites of secondary replication or facilitate viral clearance from the bloodstream (34, 55, 56). We found that CHIKV strains containing an arginine at E2 82 produce lower titers at sites of secondary replication, including the spleen, and reduced viremia in immunocompetent mice. These findings are consistent with those obtained by Gardner et al. using a similar mouse model (45). Thus, it appears that GAG-dependent strains of CHIKV disseminate less efficiently, are cleared more rapidly, or perhaps both.

E2 residue 82 may also contribute to differences in tissue tropism by both GAG-dependent and GAG-independent mechanisms. Differential distribution and levels of GAGs throughout the body may influence targeting of GAG-dependent viruses to specific tissues or alter the capacity of these viruses to interact with specific cell types. Virus strains 181/25 and AF15561 differ in GAG dependence but not to the extent observed for strain 181/25 and other clinical isolates (37, 38, 45). Strain 181/25 infectivity in CHO-pgsA745 cells, which lack all GAGs, was decreased less than 4-fold relative to strain AF15561. In addition, the 50% inhibitory concentration (IC_{50}) of heparin inhibition for strains 181/25 and AF15561 were comparable (9.4 and 10.8 μg/ml, respectively). These data suggest that additional mechanisms underlie the attenuation of strain 181/25. Since E2 82 is solvent exposed and lies within a putative receptor-binding domain of E2 (27), it is possible that this residue participates in interactions with cellular receptors other than GAGs. Substituting AF15561 E2 Gly82 with an arginine enhances infectivity in Vero cells relative to strain AF15561, likely by promoting interactions with GAGs or other cell surface moieties to mediate attachment. Enhanced viral attachment to the cell surface would facilitate more rapid internalization of the virus and consequent infection. However, infectivity of AF15561 E2 G82R was also significantly greater than that observed for the 181/25 strain in Vero cells, although both strains bound heparin-conjugated agarose beads to a similar extent. Furthermore, substituting AF15561 E2 Gly82 with an arginine only modestly enhanced binding to Vero cells. Thus, these findings suggest that an arginine at this residue in the AF15561 background provides a replication advantage in mammalian cell culture in addition to GAG engagement and attachment to host cells.

As early as 1 day postinoculation of strain AF15561 E2 G82R, nucleotide sequences of most isolates detected in the spleens of infected mice encode a glycine at E2 residue 82. Reversion was also observed by Gorchakov et al. (31) in which 100% isolates in blood encode a glycine at E2 82 by 3 days postinoculation. In contrast, following inoculation with the E2 T12I variant, only 22% of isolates encoded a threonine at E2 residue 12 (31). E2 82 may mediate viral tropism specifically in lymphoid tissues early in infection, and the presence of an arginine at this residue may limit the capacity of the virus to replicate in lymphoid cells. Consistent with this idea, lower levels of viral RNA were detected in the popliteal lymph nodes of mice inoculated with viruses containing an arginine at E2 82 (data not shown). The rapid selection of a glycine at this residue may explain the higher titers of virus strains 181/25 and AF15561 E2 G82R in the spleens and other tissues of infected mice at later times postinoculation and might support a role for this site early in infection. Although viral isolates from the spleens of AF15561-infected mice encoded a glycine at E2 82, the population was not homogeneous, as one clone encoded an arginine at this residue. These data suggest that selection at this position is not absolute *in vivo*.

Residues in E2 regulate virion stability by influencing the folding of the protein and by mediating interactions with the E1 and capsid proteins on the virion surface (57–61). Therefore, changes in E2, such as the nonconservative G82R substitution, may alter the stability of the CHIKV virion as demonstrated for other alphaviruses (57–61). When the E2 Arg82 residue was modeled into the crystal structure of the CHIKV E1/E2 heterodimer (Protein Data Bank [PDB] accession no. 3N42 [27]), this residue closely apposes Glu79, which likely results in the formation of a salt bridge between the cationic guanidinium group of arginine and the anionic carboxylate group of glutamate (data not shown). The formation

of this salt bridge may stabilize the E2 protein and, in turn, promote CHIKV infectivity in cell culture and at sites of initial replication but limit dissemination to sites of secondary replication.

Beyond viral attachment and tissue tropism, E2 82 may contribute to host responses to CHIKV early in infection. Although there were significant differences in swelling and pathology in the left hind limb, titers produced at this site by strains that vary solely at E2 82 were comparable. These data support the hypothesis that differences in pathological injury produced by CHIKV strains with an E2 residue polymorphism result from differences in immune and inflammatory responses. Such responses could be tissue specific and dependent upon replication efficiency in the discrete cell subsets that are targeted within those tissues. Concordant with this hypothesis, relative to the virulent CHIKV LR strain, LR E2 Arg82 induces lower levels of proinflammatory cytokines and chemokines (45). Our data suggest that E2 residue 82 also modulates the induction of necrotic pathways that contribute to differences in swelling elicited by these viruses during infection. Despite similar levels of myositis and tendonitis induced by these strains, viruses containing E2 Arg82 induced less necrosis in the hind limb metatarsal muscle than viruses containing E2 Gly82. In mice deficient for alpha/beta interferon (IFN-α/β) receptors or the signal transducer and activator of transcription factor 1 (STAT1) signal transducer, similar levels of inflammatory infiltrates were observed in the hind limbs following infection with CHIKV strains LR and 181/25, despite reduced swelling in mice infected with strain 181/25 (37). These data suggest a correlation between induction of necrotic pathways and events that contribute to swelling in the infected host, which may occur independently of immune cell infiltration.

Our study demonstrates that a glycine at E2 82 is required for virulence in the AF15561 background but not sufficient to confer virulence to the attenuated 181/25 strain. Substituting 181/25 E2 Arg82 with glycine failed to recapitulate the virulent phenotype, as assessed by weight gain and footpad swelling. However, introducing a glycine at E2 82 was sufficient to induce histopathological injury in the hind limbs of infected mice to levels induced by the parental AF15561 strain. Therefore, the effects of this residue are dependent on the genetic background in which the polymorphism is present. Accordingly, substitution of AF15561 E2 Thr12 with isoleucine from strain 181/25, which infects mammalian cells more efficiently, decreased infectivity to levels less than those observed for AF15561. This substitution was demonstrated previously to contribute to 181/25 attenuation (31) but was not identified in our study in which we used infectivity in mammalian cells as an *in vitro* correlate of virulence to screen viral variants. Therefore, additional polymorphisms displayed by strains AF15561 and 181/25 likely contribute to attenuation of 181/25 in this mouse model of CHIKV disease.

An arginine at E2 residue 82 does not mediate enhancement of infectivity in mosquito cells as in mammalian cells. These data suggest a GAG-independent function for this residue in invertebrate cells. Several mosquito species express the enzymes capable of synthesizing GAGs (62), but a thorough characterization of GAGs expressed by C6/36 cells has not been reported. Additionally, GAGs are present on the surfaces of midgut and salivary gland cells of certain mosquito species (62, 63), but it is not clear whether these molecules contribute to CHIKV infection in the invertebrate host. In contrast to mammalian cells, substituting 181/25 E2 Arg82 with glycine enhances infection of C6/36 cells. This enhancement might result from disrupting interactions with negatively charged GAGs or promoting different or enhanced interactions with other mosquito cell factors either at the cell surface or during later steps in infection. The former would indicate that interactions with GAGs on the surfaces of C6/36 cells impede CHIKV infection. We think this is not the case, as substituting AF15561 E2 Gly82 with arginine does not substantially diminish infection of these cells. Additional cell surface entry mediators may or may not be the same for mammalian and mosquito hosts. The importance of a glycine at this residue for viral fitness is evidenced by its high conservation among CHIKV isolates (38), suggesting that it confers an advantage for replication in mosquitoes.

Understanding mechanisms of virus entry and the interactions that promote dissemination and pathogenesis is critical for development of pathogen-specific therapeutic and prophylactic intervention strategies. Our study suggests that E2 residue 82 is a determinant of infection in both mammalian and mosquito cells and defines a role for E2 residue 82 in GAG engagement and CHIKV virulence *in vivo*. We demonstrate that viruses containing E2 Arg82 display enhanced infectivity in mammalian cells, while viruses containing E2 Gly82 display enhanced infectivity in mosquito cells. The enhancement provided by an arginine at E2 82 was only partly attributable to increased binding, suggesting that this residue promotes interactions with other cell surface molecules or influences steps in the virus life cycle following attachment. In infected mice, viruses encoding an arginine at E2 residue 82 exhibit defects in replication in lymphoid tissues, establishment of viremia, and production of pathological injury in joint-associated muscle. A glycine at E2 82 is under strong selective pressure in the spleens of CHIKV-infected mice, but this residue was not static, as an arginine was also selected at low frequency. Our findings support new functions for E2 residue 82 in host-specific and GAG-independent processes and in the development of joint swelling through necrosis-mediated events. Future studies to understand mechanisms by which E2 residue 82 influences CHIKV tropism and host responses during infection will reveal both viral and host targets to restrict infection and diminish disease.

ACKNOWLEDGMENTS

We thank Jennifer Konopka-Anstadt, Bernardo Mainou, and Clint Smith for critical reviews of the manuscript. We are grateful to members of the Dermody and Morrison laboratories for useful discussions and to John Williams for helpful suggestions during these studies. We thank Halil Aydin and Jonathan Cook from the laboratory of Jeffrey Lee for assistance with structural analysis. A subset of infectivity assays was conducted at the Vanderbilt High-Throughput Screening Facility. The flow cytometry experiments were performed in the Vanderbilt Cytometry Shared Resource.

This work was supported by Public Health Service awards T32 HL07751 (A.W.A.), F32 AI096833 (L.A.S.), and U54 AI057157 (T.S.D.). Additional support was provided by the Elizabeth B. Lamb Center for Pediatric Research.

REFERENCES

1. **Burt FJ, Rolph MS, Rulli NE, Mahalingam S, Heise MT.** 2012. Chikungunya: a re-emerging virus. Lancet **379:**662–671. http://dx.doi.org/10.1016/S0140-6736(11)60281-X.
2. **Suhrbier A, Jaffar-Bandjee MC, Gasque P.** 2012. Arthritogenic alphaviruses–an overview. Nat. Rev. Rheumatol. **8:**420–429. http://dx.doi.org/10.1038/nrrheum.2012.64.
3. **Borgherini G, Poubeau P, Jossaume A, Gouix A, Cotte L, Michault A, Arvin-Berod C, Paganin F.** 2008. Persistent arthralgia associated with Chikungunya virus: a study of 88 adult patients on Reunion Island. Clin. Infect. Dis. **47:**469–475. http://dx.doi.org/10.1086/590003.

4. **Sissoko D, Malvy D, Ezzedine K, Renault P, Moscetti F, Ledrans M, Pierre V.** 2009. Post-epidemic Chikungunya disease on Reunion Island: course of rheumatic manifestations and associated factors over a 15-month period. PLoS Negl. Trop. Dis. **3:**e389. http://dx.doi.org/10.1371/journal.pntd.0000389.
5. **Hoarau JJ, Jaffar Bandjee MC, Krejbich Trotot P, Das T, Li-Pat-Yuen G, Dassa B, Denizot M, Guichard E, Ribera A, Henni T, Tallet F, Moiton MP, Gauzere BA, Bruniquet S, Jaffar Bandjee Z, Morbidelli P, Martigny G, Jolivet M, Gay F, Grandadam M, Tolou H, Vieillard V, Debre P, Autran B, Gasque P.** 2010. Persistent chronic inflammation and infection by Chikungunya arthritogenic alphavirus in spite of a robust host immune response. J. Immunol. **184:**5914–5927. http://dx.doi.org/10.4049/jimmunol.0900255.
6. **Lynch N, Ellis Pegler R.** 2010. Persistent arthritis following Chikungunya virus infection. N. Z. Med. J. **123:**79–81.
7. **Schilte C, Staikowsky F, Couderc T, Madec Y, Carpentier F, Kassab S, Albert ML, Lecuit M, Michault A.** 2013. Chikungunya virus-associated long-term arthralgia: a 36-month prospective longitudinal study. PLoS Negl. Trop. Dis. **7:**e2137. http://dx.doi.org/10.1371/journal.pntd.0002137.
8. **Simon F, Parola P, Grandadam M, Fourcade S, Oliver M, Brouqui P, Hance P, Kraemer P, Ali Mohamed A, de Lamballerie X, Charrel R, Tolou H.** 2007. Chikungunya infection: an emerging rheumatism among travelers returned from Indian Ocean islands. Report of 47 cases. Medicine (Baltimore) **86:**123–137.
9. **Rezza G, Nicoletti L, Angelini R, Romi R, Finarelli AC, Panning M, Cordioli P, Fortuna C, Boros S, Magurano F, Silvi G, Angelini P, Dottori M, Ciufolini MG, Majori GC, Cassone A, CHIKV Study Group.** 2007. Infection with chikungunya virus in Italy: an outbreak in a temperate region. Lancet **370:**1840–1846. http://dx.doi.org/10.1016/S0140-6736(07)61779-6.
10. **Kee AC, Yang S, Tambyah P.** 2010. Atypical Chikungunya virus infections in immunocompromised patients. Emerg. Infect. Dis. **16:**1038–1040. http://dx.doi.org/10.3201/eid1606.091115.
11. **Grandadam M, Caro V, Plumet S, Thiberge JM, Souares Y, Failloux AB, Tolou HJ, Budelot M, Cosserat D, Leparc-Goffart I, Despres P.** 2011. Chikungunya virus, southeastern France. Emerg. Infect. Dis. **17:**910–913. http://dx.doi.org/10.3201/eid1705.101873.
12. **Leparc-Goffart I, Nougairede A, Cassadou S, Prat C, de Lamballerie X.** 2014. Chikungunya in the Americas. Lancet **383:**514. http://dx.doi.org/10.1016/S0140-6736(14)60185-9.
13. **Van Bortel W, Dorleans F, Rosine J, Blateau A, Rousset D, Matheus S, Leparc-Goffart I, Flusin O, Prat C, Cesaire R, Najioullah F, Ardillon V, Balleydier E, Carvalho L, Lemaitre A, Noel H, Servas V, Six C, Zurbaran M, Leon L, Guinard A, van den Kerkhof J, Henry M, Fanoy E, Braks M, Reimerink J, Swaan C, Georges R, Brooks L, Freedman J, Sudre B, Zeller H.** 2014. Chikungunya outbreak in the Caribbean region, December 2013 to March 2014, and the significance for Europe. Euro Surveill. **19(13):** pii=20759. http://www.eurosurveillance.org/ViewArticle.aspx?ArticleId=20759.
14. **Borgherini G, Poubeau P, Staikowsky F, Lory M, Le Moullec N, Becquart JP, Wengling C, Michault A, Paganin F.** 2007. Outbreak of Chikungunya on Reunion Island: early clinical and laboratory features in 157 adult patients. Clin. Infect. Dis. **44:**1401–1407. http://dx.doi.org/10.1086/517537.
15. **Economopoulou A, Dominguez M, Helynck B, Sissoko D, Wichmann O, Quenel P, Germonneau P, Quatresous I.** 2009. Atypical Chikungunya virus infections: clinical manifestations, mortality and risk factors for severe disease during the 2005–2006 outbreak on Reunion. Epidemiol. Infect. **137:**534–541. http://dx.doi.org/10.1017/S0950268808001167.
16. **Das T, Jaffar-Bandjee MC, Hoarau JJ, Krejbich Trotot P, Denizot M, Lee-Pat-Yuen G, Sahoo R, Guiraud P, Ramful D, Robin S, Alessandri JL, Gauzere BA, Gasque P.** 2010. Chikungunya fever: CNS infection and pathologies of a re-emerging arbovirus. Prog. Neurobiol. **91:**121–129. http://dx.doi.org/10.1016/j.pneurobio.2009.12.006.
17. **Griffin DE.** 2001. Alphaviruses, p 917–962. *In* Knipe DM, Howley PM (ed), Fields virology, 4th ed. Lippincott-Raven Press, Philadelphia, PA.
18. **Khan AH, Morita K, Parquet MDC, Hasebe F, Mathenge EG, Igarashi A.** 2002. Complete nucleotide sequence of chikungunya virus and evidence for an internal polyadenylation site. J. Gen. Virol. **83:**3075–3084.
19. **Solignat M, Gay B, Higgs S, Briant L, Devaux C.** 2009. Replication cycle of Chikungunya: a re-emerging arbovirus. Virology **393:**183–197. http://dx.doi.org/10.1016/j.virol.2009.07.024.
20. **Simizu B, Yamamoto K, Hashimoto K, Ogata T.** 1984. Structural proteins of Chikungunya virus. J. Virol. **51:**254–258.
21. **Firth AE, Chung BY, Fleeton MN, Atkins JF.** 2008. Discovery of frameshifting in Alphavirus 6K resolves a 20-year enigma. Virol. J. **5:**108. http://dx.doi.org/10.1186/1743-422X-5-108.
22. **Snyder JE, Kulcsar KA, Schultz KL, Riley CP, Neary JT, Marr S, Jose J, Griffin DE, Kuhn RJ.** 2013. Functional characterization of the alphavirus TF protein. J. Virol. **87:**8511–8523. http://dx.doi.org/10.1128/JVI.00449-13.
23. **Strauss JH, Strauss EG.** 1994. The alphaviruses: gene expression, replication, and evolution. Microbiol. Rev. **58:**491–562.
24. **Konishi E, Hotta S.** 1980. Studies on structural proteins of Chikungunya Virus. I. Separation of three species of proteins and their preliminary characterization. Microbiol. Immunol. **24:**419–428.
25. **de Curtis I, Simons K.** 1988. Dissection of Semliki Forest virus glycoprotein delivery from the trans-Golgi network to the cell surface in permeabilized BHK cells. Proc. Natl. Acad. Sci. U. S. A. **85:**8052–8056. http://dx.doi.org/10.1073/pnas.85.21.8052.
26. **Ozden S, Lucas-Hourani M, Ceccaldi PE, Basak A, Valentine M, Benjannet S, Hamelin J, Jacob Y, Mamchaoui K, Mouly V, Despres P, Gessain A, Butler-Browne G, Chretien M, Tangy F, Vidalain PO, Seidah NG.** 2008. Inhibition of Chikungunya virus infection in cultured human muscle cells by furin inhibitors: impairment of the maturation of the E2 surface glycoprotein. J. Biol. Chem. **283:**21899–21908. http://dx.doi.org/10.1074/jbc.M802444200.
27. **Voss JE, Vaney MC, Duquerroy S, Vonrhein C, Girard-Blanc C, Crublet E, Thompson A, Bricogne G, Rey FA.** 2010. Glycoprotein organization of Chikungunya virus particles revealed by X-ray crystallography. Nature **468:**709–712. http://dx.doi.org/10.1038/nature09555.
28. **Jose J, Snyder JE, Kuhn RJ.** 2009. A structural and functional perspective of alphavirus replication and assembly. Future Microbiol. **4:**837–856. http://dx.doi.org/10.2217/fmb.09.59.
29. **Levitt NH, Ramsburg HH, Hasty SE, Repik PM, Cole FE, Jr, Lupton HW.** 1986. Development of an attenuated strain of Chikungunya virus for use in vaccine production. Vaccine **4:**157–162.
30. **Edelman R, Tacket CO, Wasserman SS, Bodison SA, Perry JG, Mangiafico JA.** 2000. Phase II safety and immunogenicity study of live Chikungunya virus vaccine TSI-GSD-218. Am. J. Trop. Med. Hyg. **62:**681–685.
31. **Gorchakov R, Wang E, Leal G, Forrester NL, Plante K, Rossi SL, Partidos CD, Adams AP, Seymour RL, Weger J, Borland EM, Sherman MB, Powers AM, Osorio JE, Weaver SC.** 2012. Attenuation of Chikungunya virus vaccine strain 181/clone 25 is determined by two amino acid substitutions in the E2 envelope glycoprotein. J. Virol. **86:**6084–6096. http://dx.doi.org/10.1128/JVI.06449-11.
32. **Byrnes AP, Griffin DE.** 1998. Binding of Sindbis virus to cell surface heparan sulfate. J. Virol. **72:**7349–7356.
33. **Klimstra WB, Ryman KD, Johnston RE.** 1998. Adaptation of Sindbis virus to BHK cells selects for use of heparan sulfate as an attachment receptor. J. Virol. **72:**7357–7366.
34. **Bernard KA, Klimstra WB, Johnston RE.** 2000. Mutations in the E2 glycoprotein of Venezuelan equine encephalitis virus confer heparan sulfate interaction, low morbidity, and rapid clearance from blood of mice. Virology **276:**93–103. http://dx.doi.org/10.1006/viro.2000.0546.
35. **Heil ML, Albee A, Strauss JH, Kuhn RJ.** 2001. An amino acid substitution in the coding region of the E2 glycoprotein adapts Ross River virus to utilize heparan sulfate as an attachment moiety. J. Virol. **75:**6303–6309. http://dx.doi.org/10.1128/JVI.75.14.6303-6309.2001.
36. **Smit JM, Waarts BL, Kimata K, Klimstra WB, Bittman R, Wilschut J.** 2002. Adaptation of alphaviruses to heparan sulfate: interaction of Sindbis and Semliki Forest viruses with liposomes containing lipid-conjugated heparin. J. Virol. **76:**10128–10137. http://dx.doi.org/10.1128/JVI.76.20.10128-10137.2002.
37. **Gardner CL, Burke CW, Higgs ST, Klimstra WB, Ryman KD.** 2012. Interferon-alpha/beta deficiency greatly exacerbates arthritogenic disease in mice infected with wild-type Chikungunya virus but not with the cell culture-adapted live-attenuated 181/25 vaccine candidate. Virology **425:**103–112. http://dx.doi.org/10.1016/j.virol.2011.12.020.
38. **Silva LA, Khomandiak S, Ashbrook AW, Weller R, Heise MT, Morrison TE, Dermody TS.** 2014. A single-amino-acid polymorphism in Chikungunya virus E2 glycoprotein influences glycosaminoglycan utilization. J. Virol. **88:**2385–2397. http://dx.doi.org/10.1128/JVI.03116-13.
39. **Ryman KD, Klimstra WB, Johnston RE.** 2004. Attenuation of Sindbis

virus variants incorporating uncleaved PE2 glycoprotein is correlated with attachment to cell-surface heparan sulfate. Virology **322:**1–12. http://dx.doi.org/10.1016/j.virol.2004.01.003.
40. **Bear JS, Byrnes AP, Griffin DE.** 2006. Heparin-binding and patterns of virulence for two recombinant strains of Sindbis virus. Virology **347:**183–190. http://dx.doi.org/10.1016/j.virol.2005.11.034.
41. **Ryman KD, Gardner CL, Burke CW, Meier KC, Thompson JM, Klimstra WB.** 2007. Heparan sulfate binding can contribute to the neurovirulence of neuroadapted and nonneuroadapted Sindbis viruses. J. Virol. **81:**3563–3573. http://dx.doi.org/10.1128/JVI.02494-06.
42. **Lee E, Wright PJ, Davidson A, Lobigs M.** 2006. Virulence attenuation of dengue virus due to augmented glycosaminoglycan-binding affinity and restriction in extraneural dissemination. J. Gen. Virol. **87:**2791–2801. http://dx.doi.org/10.1099/vir.0.82164-0.
43. **Gardner CL, Ebel GD, Ryman KD, Klimstra WB.** 2011. Heparan sulfate binding by natural eastern equine encephalitis viruses promotes neurovirulence. Proc. Natl. Acad. Sci. U. S. A. **108:**16026–16031. http://dx.doi.org/10.1073/pnas.1110617108.
44. **Gardner CL, Choi-Nurvitadhi J, Sun C, Bayer A, Hritz J, Ryman KD, Klimstra WB.** 2013. Natural variation in the heparan sulfate binding domain of the eastern equine encephalitis virus E2 glycoprotein alters interactions with cell surfaces and virulence in mice. J. Virol. **87:**8582–8590. http://dx.doi.org/10.1128/JVI.00937-13.
45. **Gardner CL, Hritz J, Sun C, Vanlandingham DL, Song TY, Ghedin E, Higgs S, Klimstra WB, Ryman KD.** 2014. Deliberate attenuation of Chikungunya virus by adaptation to heparan sulfate-dependent infectivity: a model for rational arboviral vaccine design. PLoS Negl. Trop. Dis. **8:**e2719. http://dx.doi.org/10.1371/journal.pntd.0002719.
46. **Esko JD, Stewart TE, Taylor WH.** 1985. Animal cell mutants defective in glycosaminoglycan biosynthesis. Proc. Natl. Acad. Sci. U. S. A. **82:**3197–3201. http://dx.doi.org/10.1073/pnas.82.10.3197.
47. **Mainou B, Zamora PF, Ashbrook AW, Dorset DC, Kim KS, Dermody TS.** 2013. Reovirus cell entry requires functional microtubules. mBio **4**(4)**:** e00405–13.
48. **Weaver SC, Brault AC, Kang W, Holland JJ.** 1999. Genetic and fitness changes accompanying adaptation of an arbovirus to vertebrate and invertebrate cells. J. Virol. **73:**4316–4326.
49. **Krieger N, Lohmann V, Bartenschlager R.** 2001. Enhancement of hepatitis C virus RNA replication by cell culture-adaptive mutations. J. Virol. **75:**4614–4624. http://dx.doi.org/10.1128/JVI.75.10.4614-4624.2001.
50. **Blaney JE, Jr, Manipon GG, Firestone CY, Johnson DH, Hanson CT, Murphy BR, Whitehead SS.** 2003. Mutations which enhance the replication of dengue virus type 4 and an antigenic chimeric dengue virus type 2/4 vaccine candidate in Vero cells. Vaccine **21:**4317–4327.
51. **Greene IP, Wang E, Deardorff ER, Milleron R, Domingo E, Weaver SC.** 2005. Effect of alternating passage on adaptation of Sindbis virus to vertebrate and invertebrate cells. J. Virol. **79:**14253–14260. http://dx.doi.org/10.1128/JVI.79.22.14253-14260.2005.
52. **Coffey LL, Vignuzzi M.** 2011. Host alternation of Chikungunya virus increases fitness while restricting population diversity and adaptability to novel selective pressures. J. Virol. **85:**1025–1035. http://dx.doi.org/10.1128/JVI.01918-10.
53. **Volchkova VA, Dolnik O, Martinez MJ, Reynard O, Volchkov VE.** 2011. Genomic RNA editing and its impact on Ebola virus adaptation during serial passages in cell culture and infection of guinea pigs. J. Infect. Dis. **204**(Suppl 3)**:**S941–S946. http://dx.doi.org/10.1093/infdis/jir321.
54. **Morrison TE, Oko L, Montgomery SA, Whitmore AC, Lotstein AR, Gunn BM, Elmore SA, Heise MT.** 2011. A mouse model of Chikungunya virus-induced musculoskeletal inflammatory disease: evidence of arthritis, tenosynovitis, myositis, and persistence. Am. J. Pathol. **178:**32–40. http://dx.doi.org/10.1016/j.ajpath.2010.11.018.
55. **Klimstra WB, Ryman KD, Bernard KA, Nguyen KB, Biron CA, Johnston RE.** 1999. Infection of neonatal mice with Sindbis virus results in a systemic inflammatory response syndrome. J. Virol. **73:**10387–10398.
56. **Byrnes AP, Griffin DE.** 2000. Large-plaque mutants of Sindbis virus show reduced binding to heparan sulfate, heightened viremia, and slower clearance from the circulation. J. Virol. **74:**644–651. http://dx.doi.org/10.1128/JVI.74.2.644-651.2000.
57. **Gidwitz S, Polo JM, Davis NL, Johnston RE.** 1988. Differences in virion stability among Sindbis virus pathogenesis mutants. Virus Res. **10:**225–239. http://dx.doi.org/10.1016/0168-1702(88)90018-4.
58. **Snyder AJ, Sokoloski KJ, Mukhopadhyay S.** 2012. Mutating conserved cysteines in the alphavirus E2 glycoprotein causes virus-specific assembly defects. J. Virol. **86:**3100–3111. http://dx.doi.org/10.1128/JVI.06615-11.
59. **Fields W, Kielian M.** 2013. A key interaction between the alphavirus envelope proteins responsible for initial dimer dissociation during fusion. J. Virol. **87:**3774–3781. http://dx.doi.org/10.1128/JVI.03310-12.
60. **Cutler DF, Melancon P, Garoff H.** 1986. Mutants of the membrane-binding region of Semliki Forest virus E2 protein. II. Topology and membrane binding. J. Cell Biol. **102:**902–910.
61. **Lopez S, Yao JS, Kuhn RJ, Strauss EG, Strauss JH.** 1994. Nucleocapsid-glycoprotein interactions required for assembly of alphaviruses. J. Virol. **68:**1316–1323.
62. **Sinnis P, Coppi A, Toida T, Toyoda H, Kinoshita-Toyoda A, Xie J, Kemp MM, Linhardt RJ.** 2007. Mosquito heparan sulfate and its potential role in malaria infection and transmission. J. Biol. Chem. **282:**25376–25384. http://dx.doi.org/10.1074/jbc.M704698200.
63. **Dinglasan RR, Alaganan A, Ghosh AK, Saito A, van Kuppevelt TH, Jacobs-Lorena M.** 2007. Plasmodium falciparum ookinetes require mosquito midgut chondroitin sulfate proteoglycans for cell invasion. Proc. Natl. Acad. Sci. U. S. A. **104:**15882–15887. http://dx.doi.org/10.1073/pnas.0706340104.

Short Article

Cell Host & Microbe

Isolation and Characterization of Broad and Ultrapotent Human Monoclonal Antibodies with Therapeutic Activity against Chikungunya Virus

Graphical Abstract

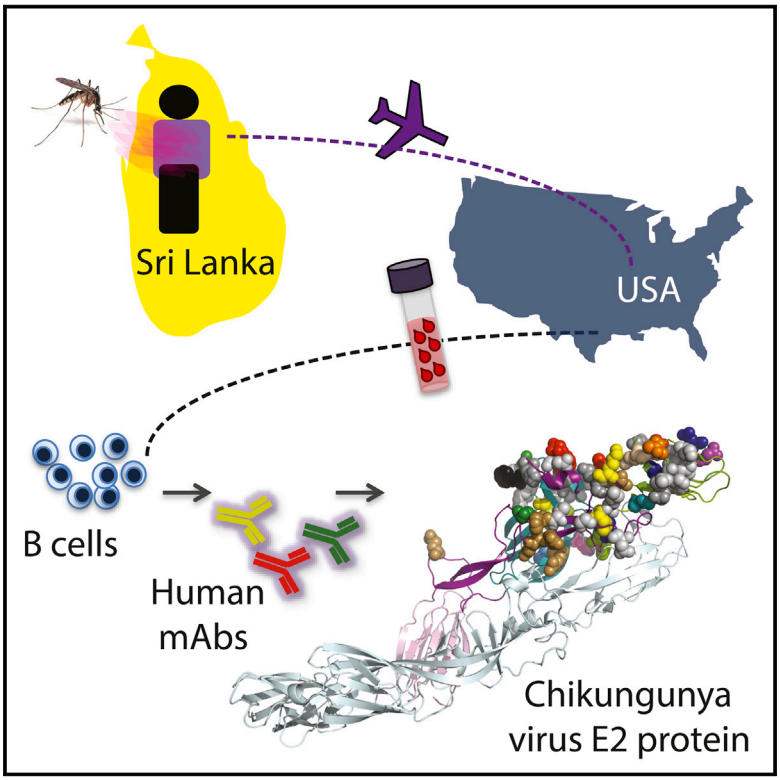

Highlights

- A panel of 30 chikungunya virus-specific antibodies (Abs) isolated from a single donor
- 13 Abs exhibited broad and potent neutralizing activity with IC_{50} < 10 ng/ml
- Potently neutralizing Abs bind to the E2 envelope protein and block viral fusion
- Several Abs exhibited prophylactic and therapeutic activity in a mouse model

Authors

Scott A. Smith, Laurie A. Silva, Julie M. Fox, ..., Michael S. Diamond, Terence S. Dermody, James E. Crowe, Jr.

Correspondence

james.crowe@vanderbilt.edu

In Brief

No effective therapy or vaccine is available for chikungunya virus (CHIKV), a debilitating mosquito-borne pathogen that is spreading globally. Smith et al. isolated and characterized a panel of broad and potent CHIKV-specific human monoclonal antibodies. Several antibodies exhibited prophylactic and therapeutic activity in mice and their mechanism suggests vaccine approaches.

Smith et al., 2015, Cell Host & Microbe *18*, 86–95
July 8, 2015
http://dx.doi.org/10.1016/j.chom.2015.06.009

CellPress

Cell Host & Microbe
Short Article

Isolation and Characterization of Broad and Ultrapotent Human Monoclonal Antibodies with Therapeutic Activity against Chikungunya Virus

Scott A. Smith,[1,5,9] Laurie A. Silva,[2,4,9] Julie M. Fox,[8] Andrew I. Flyak,[3] Nurgun Kose,[5] Gopal Sapparapu,[5] Solomiia Khomadiak,[2,4] Alison W. Ashbrook,[2,3,4] Kristen M. Kahle,[6] Rachel H. Fong,[6] Sherri Swayne,[6] Benjamin J. Doranz,[6] Charles E. McGee,[7] Mark T. Heise,[7] Pankaj Pal,[8] James D. Brien,[8] S. Kyle Austin,[8] Michael S. Diamond,[8] Terence S. Dermody,[2,3,4] and James E. Crowe, Jr.[2,3,5,*]

[1]Department of Medicine
[2]Department of Pediatrics
[3]Department of Pathology, Microbiology, and Immunology
[4]Elizabeth B. Lamb Center for Pediatric Research
[5]Vanderbilt Vaccine Center
Vanderbilt University Medical Center, Vanderbilt University, Nashville, TN 37232, USA
[6]Integral Molecular, Philadelphia, PA 19104, USA
[7]Department of Microbiology and Immunology, University of North Carolina School of Medicine, Chapel Hill, NC 27599, USA
[8]Departments of Medicine, Molecular Microbiology, Pathology & Immunology, Washington University School of Medicine, St. Louis, MO 63110, USA
[9]Co-first author
*Correspondence: james.crowe@vanderbilt.edu
http://dx.doi.org/10.1016/j.chom.2015.06.009

SUMMARY

Chikungunya virus (CHIKV) is a mosquito-transmitted RNA virus that causes acute febrile infection associated with polyarthralgia in humans. Mechanisms of protective immunity against CHIKV are poorly understood, and no effective therapeutics or vaccines are available. We isolated and characterized human monoclonal antibodies (mAbs) that neutralize CHIKV infectivity. Among the 30 mAbs isolated, 13 had broad and ultrapotent neutralizing activity (IC_{50} < 10 ng/ml), and all of these mapped to domain A of the E2 envelope protein. Potent inhibitory mAbs blocked post-attachment steps required for CHIKV membrane fusion, and several were protective in a lethal challenge model in immunocompromised mice, even when administered at late time points after infection. These highly protective mAbs could be considered for prevention or treatment of CHIKV infection, and their epitope location in domain A of E2 could be targeted for rational structure-based vaccine development.

INTRODUCTION

Chikungunya virus (CHIKV) is an enveloped, positive-sense RNA virus in the Alphavirus genus of the *Togaviridae* family and is transmitted by *Aedes* species mosquitoes. The mature CHIKV virion contains two glycoproteins, the E1 fusion protein and the E2 attachment protein, which are generated from a precursor polyprotein, p62-E1, by proteolytic cleavage. In humans, CHIKV infection causes fever and joint pain, which may be severe and last in some cases for years (Schilte et al., 2013; Sissoko et al., 2009; Staples et al., 2009). CHIKV has caused outbreaks in most regions of sub-Saharan Africa and also in parts of Asia, Europe, and the Indian and Pacific Oceans. In December 2013, the first transmission of CHIKV in the Western Hemisphere occurred, with autochthonous cases identified in St. Martin (CDC, 2013). The virus spread rapidly to many islands in the Caribbean as well as Central, South, and North America. In less than 1 year, over a million suspected CHIKV cases in the Western Hemisphere were reported, and endemic transmission in more than 40 countries, including the United States, was documented (CDC, 2014). At present, there is no licensed vaccine or antiviral therapy to prevent or treat CHIKV infection.

Although mechanisms of protective immunity to CHIKV infection in humans are not fully understood, the humoral response controls infection and limits tissue injury (Chu et al., 2013; Hallengärd et al., 2014; Hawman et al., 2013; Kam et al., 2012b; Lum et al., 2013; Pal et al., 2013). Immune human γ-globulin neutralizes infectivity in cultured cells and prevents morbidity in mice when administered up to 24 hr after viral inoculation (Couderc et al., 2009). Several murine monoclonal antibodies (mAbs) that neutralize CHIKV infection have been described (Bréhin et al., 2008; Goh et al., 2013; Masrinoul et al., 2014; Pal et al., 2013, 2014), including some with efficacy when used in combination to treat mice or nonhuman primates following CHIKV challenge (Pal et al., 2013, 2014). In comparison, a limited number of human CHIKV mAbs have been reported, the vast majority of which exhibit modest neutralizing activity (Fong et al., 2014; Fric et al., 2013; Lee et al., 2011; Selvarajah et al., 2013; Warter et al., 2011).

We isolated a large panel of human mAbs that neutralize CHIKV infectivity in cell culture and successfully treated immunodeficient *Ifnar*$^{-/-}$mice (lacking type I interferon receptors) inoculated with a lethal dose of CHIKV, even when administered as late as

60 hr after infection. We identified the A domain of E2 as the major antigenic site for recognition by human mAbs that broadly neutralize CHIKV infection with ultrapotent activity and showed that the principal mechanism of inhibition is to prevent fusion.

RESULTS

Isolation of CHIKV-Specific Human mAbs

We isolated a panel of mAbs from a single individual who acquired CHIKV infection in Sri Lanka in 2006 and presented with fever, arthralgias, and rash (Figure S1). We transformed B cells in two separate experiments from a single blood sample collected from the donor five and a half years following natural infection. We observed a virus-specific B cell frequency of ~0.1% of total B cells and established 30 stable hybridomas from B cell lines secreting antibodies that bound to virus. The mAb panel contained IgGs of multiple subclasses, with 24 IgG1, 3 IgG2, and 2 IgG3; one was not determined due to poor hybridoma growth (Table 1). We determined the nucleotide sequences of the antibody variable gene region using cDNA of expressed antibody mRNAs in the cloned hybridomas. Each of the clones used distinct sequences to encode the associated mAbs, except for mAbs 2B4 and 4J21, which appeared identical in the variable regions and exhibited similar functional activity.

Assessment of mAb Neutralization with SL15649 VRPs

Seventeen of the mAbs exhibited neutralizing activity against Asian CHIKV strain SL15649-GFP virus replicon particles (VRPs) with EC_{50} values < 40 ng/ml, with 7 exhibiting ultrapotent inhibitory activity (defined as EC_{50} values < 10 ng/ml, Table 1). Five mAbs possessed weak inhibitory activity (EC_{50} values in the 0.095 to 5.2 μg/ml range) and 8 of the mAbs had no inhibitory activity at the highest concentration tested (EC_{50} values > 10 μg/ml).

Breadth of Neutralizing Activity with Live Viruses

We determined the EC_{50} values for each mAb against representative infectious CHIKV strains of the East/Central/South African (ECSA) genotype (LR2006 OPY1 [LR] strain), the West African genotype (NI 64 IbH 35 strain), and the Asian genotype (RSU1 and 99659 [2014 Caribbean] strains) using a high-throughput focus reduction neutralization test (FRNT) (Pal et al., 2013). Twenty-five of the mAbs exhibited neutralizing activity against at least one CHIKV strain (EC_{50} values < 10 μg/ml), with 8 mAbs exhibiting neutralization in a potent range (EC_{50} values between 10 and 99 ng/ml), and 13 mAbs exhibiting neutralization in an ultrapotent range (Table 1). For comparative purposes, we also tested the previously reported human mAbs 5F10 and 8B10 against viruses of all three genotypes, and in every case the EC_{50} values were >100 ng/ml. In most cases, the mAbs we isolated exhibited relatively similar neutralizing activity against virus from all three genotypes. Six mAbs (2B4, 2H1, 4J21, 4N12, 5M16, and 9D14) inhibited viruses from all three genotypes with ultrapotent activity. These data indicate that a single individual can develop multiple CHIKV-specific antibodies that are ultrapotent and broadly neutralizing.

Binding to E2 Protein

The CHIKV E2 protein is a dominant target of murine (Goh et al., 2013; Lum et al., 2013), nonhuman primate (Kam et al., 2014), and human (Fong et al., 2014; Kam et al., 2012a, 2012b; Selvarajah et al., 2013) humoral responses. We tested the human mAbs for binding to a monomeric form of the ectodomain of E2 protein expressed in *E. coli* (Pal et al., 2013). Nine mAbs bound strongly to the E2 ectodomain, 6 exhibited moderate binding, 1 bound weakly, and 14 failed to bind above background (Table 1). The capacity to bind purified E2 protein in vitro did not correlate directly with neutralizing potency (Table 1). A subset of 17 human mAbs was tested using a surface plasmon resonance assay for binding to the p62-E1 protein derived from mammalian cells (Voss et al., 2010). All mAbs bound in the nM range, with K_D values from 0.5 to 20 nM. Differences in binding kinetics did not correlate with antigenic specificity or functional activity (Table S1).

Competition-Binding Studies

To identify non-overlapping antigenic regions in recombinant E2 protein recognized by different neutralizing mAbs, we used a quantitative competition-binding assay. For comparison, we also evaluated four previously described murine mAbs (CHK-84, CHK-88, CHK-141, and CHK-265) (Pal et al., 2013) and the previously described human mAb 5F10 (Warter et al., 2011) (Figure S2). The pattern of competition was complex, but three major competition groups were evident, which we designated group 1-3. We also defined a fourth group containing the single human mAb, 5F19. These competition studies suggest that there are at least three major antigenic regions recognized by CHIKV-specific antibodies.

Epitope Mapping Using Alanine-Scanning Mutagenesis

We used an alanine-scanning mutagenesis library coupled with cell-based expression and flow cytometry to identify residues in E2 and E1 proteins of CHIKV strain S27 (ECSA genotype) required for mAb binding (Fong et al., 2014) (Figure S3). Residues required for mAb binding to CHIKV glycoproteins for a subset of 20 human mAbs are listed in Table 1. Mutations affecting binding of these 20 mAbs are indicated in an alignment of the full-length E2 sequences of strain S27 and strains representing all CHIKV genotypes that were used in our study (Figure 1A). The aa in E2 that influence binding are located primarily in the solvent-exposed regions of domains A and B and arches 1 and 2 of the β-ribbon connector, which links domains A and B (Voss et al., 2010) (Figure 1A). Comparison of the antigenic sites identified by loss-of-binding experiments using alanine-scanning mutagenesis with the competition-binding analysis (Figure S2) demonstrated that competition groups 1 and 2 generally corresponded to sites within domain A and the arches, whereas group 3 corresponded to regions in domain B.

Structural Analysis of Antigenic Regions

A large and diverse number of the surface residues in domains A and B and the arches are contacted by at least 1 of the mAbs (Figures 1B and 1C). Two principal antigenic regions in E2 accounted for the binding of multiple mAbs. The first region is located in domain A, between residues 58 and 80, and contains the putative receptor-binding domain (RBD) (Sun et al., 2014; Voss et al., 2010). The second region is located in domain B, between residues 190 and 215. Both sequence regions project away from the viral envelope and are located near the E2 trimer apex (Figures S3 and S4).

Table 1. Characteristics of Chikungunya Virus-Specific Human Monoclonal Antibodies

				Major Antigenic Site				In Vitro Neutralizing Potency and Breadth of CHIKV-Specific Human mAbs			
					Mutagenesis Mapping			Neutralization against CHIKV against Indicated Genotype and Strain* EC_{50}, ng/ml[g] [95% Confidence Interval]			
										Asian Genotype	
mAb[a]	IgG Sub-class[b]	λ/κ Light Chain[b]	ELISA Binding to E2 Ectodomain (10 μg/ml)[c]	Competition Binding Group for Purified E2 Protein[d]	E2 Domain[e]	E2 Residues for which Reduced Binding Was Noted when Altered to Alanine	Neutralization against CHIKV VRP (Strain SL15649)[f] EC_{50} in ng/ml[g] [95% Confidence Interval]	West African Genotype NI 64 IbH 35 Strain	ECSA Genotype LR2006 OPY1 (LR) Strain	RSUI Strain	2014 Caribbean 99659 strain
2H1	IgG2	λ	++	Low binding	E2-DA	R80, T116	8 [6–10]	3.7 (3.3–4.3)	5.6 (4.9–6.3)	5.9 (5.3–6.7)	5.5 (4.7–6.5)
4N12	IgG2	κ	–	NT	Arch	D250	8 [7–10]	2.5 (2.0–3.1)	4.0 (3.3–5.0)	6.5 (5.7–7.3)	7.3 (5.9–9.2)
2B4	IgG1	λ	++	Low binding	NoReduct	–	14 [11–17]	3.2 (2.8–3.7)	5.6 (4.6–6.7)	6.5 (5.6–7.7)	7.0 (6.0–8.2)
4J21	IgG1	λ	++	Low binding	NoReduct	–	5 [4–6]	5.2 (4.3–6.4)	7.4 (6.6–8.3)	7.7 (7.0–8.6)	7.2 (5.3–9.8)
5M16	IgG1	κ	+++	2	Arch	G253	5 [4–6]	6. 0 (5.5–6.6)	5.9 (5.0–6.8)	8.4 (6.7–10.4)	11.7 (9.7–14.1)
9D14	IgG1	λ	+++	2	NoReduct	–	6 [5–7]	2.1 (1.6–2.7)	2.9 (2.3–3.7)	6.3 (4.7–8.4)	86.0 (31.5–235)
1H12	IgG1	λ	+++	1/2	DA/B, Arch	T58, D59, D60, R68, D71, I74, D77, T191, N193, K234	17 [14–20]	3.0 (2.5–3.5)	7.5 (6.7–8.4)	11.7 (9.3–14.8)	11.6 (8.2–16.2)
8E22	IgG1	λ	++	Low binding	DA, Arch	H62, W64, R68, H99, D117, I255	17 [14–19]	8.2 (7.0–9.7)	7.2 (6.4–8.3)	42.5 (30.8–58.5)	138.9 (64.7–298)
8G18	IgG1	λ	++	Low binding	DA	H62, W64, D117	17 [14–19]	4.7 (4.1–5.3)	7.3 (6.3–8.4)	34.9 (24.9–48.9)	52.4 (24.1–114)
10N24	IgG1	κ	–	NT	DA,B	W64, D71, R80, T116, D117, I121, N187, I190	21 [17–26]	7.9 (6.9–9.0)	9.5 (8.2–11.0)	15.9 (13.2–19.2)	23.6 (18.3–30.5)
8I4	IgG1	κ	+++	NSF Ab	DB, Arch	M171, Q184, I190, N193, V197, R198, Y199, G209, L210, K215, K234, V242, I255	8 [5–14]	6.9 (3.8–12.3)	6.2 (4.5–8.4)	153 (78–299)	>
3N23	IgG1	κ	–	NT	DA, Arch	D60, R68, G98, H170, M171, K233, K234	25 [21–30]	6.0 (5.0–7.2)	10.1 (8.9–11.5)	14.1 (11.6–17.1)	8.7 (7.0–10.9)
5O14	IgG1	κ	+++	2	NoReduct	–	38 [30–47]	6.7 (5.5–8.3)	12.1 (10.9–13.5)	17.3 (14.2–21.1)	6.2 (5.3–7.2)
4J14	IgG1	λ	++	Low binding	DA/B	D63, W64, T65, R80, I121, A162, N193	23 [20–26]	12.9 (11.2–15.0)	17.7 (16.1–19.4)	23.1 (20–27)	23.0 (18.5–28.4)
3E23	IgG2	λ	–	NT	DA	W64	11 [9–13]	19.4 (15.2–25.0)	18.7 (16.3–21.5)	36.0 (30.3–42.9)	38.0 (30.3–47.5)
1L1	IgG1	λ	+/–	Low binding	Arch	G253	18 [15–22]	18.6 (15.5–22.4)	24.2 (21.3–27.5)	34.3 (29–40.7)	ND
3B4	IgG3	κ	–	NT	DB	V192, Q195	>	18.7 (10.7–32.8)	29.6 (18.7–46.8)	271 (144–511)	ND
4B8	IgG1	λ	+++	2	NoReduct	–	0.6 [0.4–0.8]	22.8 (12.4–41.8)	28.1 (19.8–39.9)	234 (142–386)	ND
4G20	IgG1	λ	–	NT	DB	D174, R198, Y199, K215	95 [60–160]	22.3 (17.3-29.0)	34.9 (28.2–43.8)	131.4 (88.5–195)	ND
1O5	IgG1	λ	–	NT	DA	W64, T65	138 [110–170]	30.1 (22.6–35.3)	37.6 (32.6–43.4)	48.9 (37.8–63.2)	ND
1O6	IgG3	λ	–	2	DA	R80	5,200 [4,100–6,600]	61.7 (50.8–74.8)	57.5 (48.8–68.1)	ND	ND

(*Continued on next page*)

Table 1. ***Continued***

				Major Antigenic Site			In Vitro Neutralizing Potency and Breadth of CHIKV-Specific Human mAbs				
					Mutagenesis Mapping		Neutralization against CHIKV VRP (Strain SL15649)[f]	Neutralization against CHIKV against Indicated Genotype and Strain* EC_{50}, ng/ml[g] [95% Confidence Interval]			
mAb[a]	IgG Sub-class[b]	λ/κ Light Chain[b]	ELISA Binding to E2 Ectodomain (10 μg/ml)[c]	Competition Binding Group for Purified E2 Protein[d]	E2 Domain[e]	E2 Residues for which Reduced Binding Was Noted when Altered to Alanine	EC_{50} in ng/ml[g] [95% Confidence Interval]	West African Genotype NI 64 IbH 35 Strain	ECSA Genotype LR2006 OPY1 (LR) Strain	Asian Genotype RSUI Strain	Asian Genotype 2014 Caribbean 99659 strain
2L5	NT	NT	–	NT	NoReduct	–	4,600 [2,400–9,500]	1,076 (748–1,548)	2,361 (1,460–3,819)	5,632 (3,904–8,128)	ND
3A2	IgG1	κ	+++	3	DB	I190, R198, Y199, G209, L210, T212	1,300 [830–1,900]	1,566 (1,111–2,207)	1,396 (952–2,046)	>	ND
5F19	IgG1	λ	+++	4	DA	H18	>	>	9,064 (2,911–28,249)	>	ND
1M9	IgG1	κ	–	NT	DA, Arch	R36, H62, R80, Q146, E165, E166, N231, D250, H256	>	>	>	6,187 (2,795–13,709)	ND
1I9	IgG1	κ	–	NT	E2	–	>	>	>	>	ND
4B10	IgG1	κ	–	NT	NoReduct	–	>	>	>	>	ND
2C2	IgG1	λ	–	NT	NoReduct	–	>	>	>	>	ND
2D12	IgG1	κ	–	NT	E2	–	>	>	>	>	ND
5N23	IgG1	λ	+++	1	DA, Arch	E24, D117, I121	>	>	>	>	ND
murine CHK-152	IgG2c	κ	–	NT	E2-DA, E2-DB	D59, W235, A11, M74, G194, N193, T212, H232[h]	3 [2–4]				

[a]Order of antibodies reflects the level of potency degree and breadth of the antibodies in neutralization assays against clinical CHIKV isolates of diverse genotypes.
[b]Immunoglobulin isotype, subtype, and light chain use were determined by ELISA; NT indicates not tested due to poor growth of B cell line.
[c](–) denotes no detectable binding [OD < 0.1]; (+/–) denotes weak binding [OD 0.31–0.499]; (++) denotes moderate binding [OD 0.5–0.99]; (+++) denotes strong binding [OD > 1.0].
[d]Values shown represent combined data from two independent experiments; "Low binding" indicates incomplete mAb binding to E2 on biosensor for assessing competition; NT indicates not tested since Ab did not bind E2 ectodomain in ELISA; "NSF Ab" indicates insufficient supply of mAb.
[e]"-" indicates that the mAb did not react against the wild-type envelope proteins and could not be tested in this system; "NoReduct" indicates the mAb did bind to the wild-type E proteins, but no reduction was noted reproducibly for any mutant; DA indicates domain A; DB indicates domain B; Arch indicates arch 1, arch 2, or both.
[f]Values shown represent combined data from two or more independent experiments.
[g]Concentration (ng/ml) at which 50% of virus was neutralized (EC_{50}); (>) indicates EC_{50} value is greater than the highest mAb concentration tested (10 μg/ml); ND = Not Done.
[h]Residues identified by contacts with mAb in cryo-EM reconstruction (Sun et al., 2013).

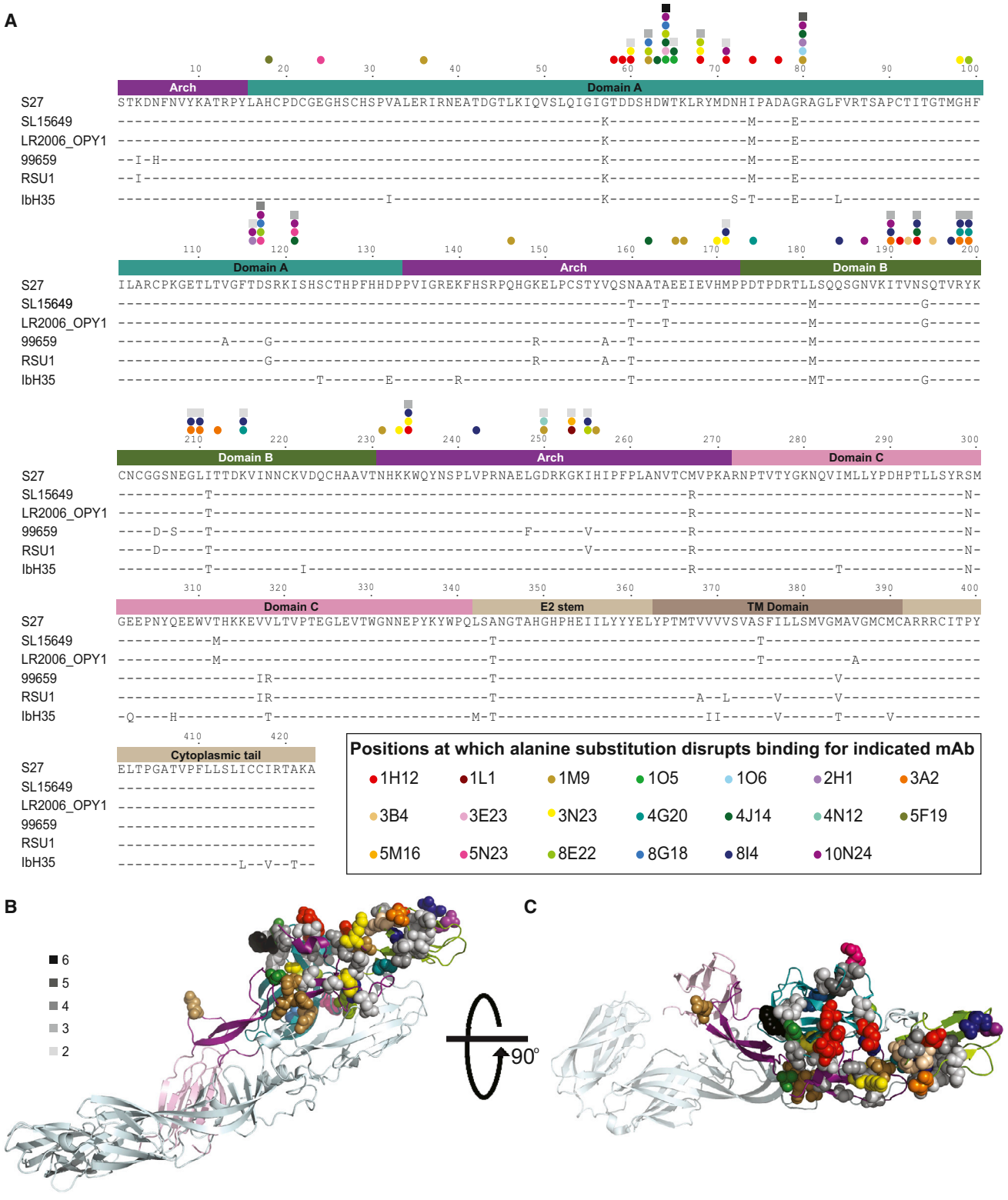

Figure 1. Structural Analysis of E2 Residues Important for mAb Binding

(A) Sequence alignment of E2 from the CHIKV strains (indicated on the left) used in this study. The numbers above the sequence correspond to the aa position in the mature E2 protein. Amino acids identical to strain S27 are indicated by a dash. Domains of E2 determined from the crystal structure of the E2/E1 heterodimer (Voss et al., 2010) are depicted in the diagram above the alignment and are color coded (cyan, domain A; purple, β-ribbon connector; green, domain B; pink, domain C; taupe shades, regions not present in the crystal structure). The position of residues at which alanine substitution disrupts mAb binding, as determined

(legend continued on next page)

Mechanism of Neutralization

We conducted pre- and post-attachment neutralization assays using mAbs displaying a range of inhibitory activities. As expected, all 5 mAbs tested neutralized infection efficiently when pre-incubated with VRPs (Figure 2A). However, mAb 4B8 did not neutralize VRPs completely even at high concentrations, suggesting the presence of a fraction of CHIKV virions resistant to this mAb; this pattern also was observed in assays using viable CHIKV strains corresponding to the three distinct CHIKV genotypes. In contrast, mAbs 3E23, 4J21, 5M16, and 9D14 completely neutralized infection when administered before attachment. All five human mAbs also neutralized CHIKV infection when added following attachment, but we observed three different patterns of activity (Figure 2A). mAb 4B8 was incapable of complete neutralization when added post-attachment, and the fraction of resistant virions was larger compared with that observed following pre-attachment neutralization. mAb 9D14 neutralized VRPs with comparable efficiency whether added before or after attachment. MAbs 3E23, 4J21, and 5M16 displayed complete neutralization of VRPs, but the efficiency of neutralization post-attachment was lower than that following pre-attachment. The mAbs 2H1 and 4N12 also efficiently neutralized VRPs when added prior to or after attachment (data not shown).

Fusion-from-without (FFWO) assay testing (Edwards and Brown, 1986) of five of the ultrapotently neutralizing mAbs (3E23, 4B8, 4J21, 5M16, or 9D14) revealed that all inhibited fusion. In the absence of antibody treatment, a short pulse of acidic pH-buffered medium resulted in infected cells, indicating fusion between the viral envelope and plasma membrane, whereas a pulse of neutral pH resulted in little to no infection as expected (Figure 2B). Notably, all five human mAbs inhibited plasma membrane fusion and infection, with mAb 9D14 exhibiting the greatest potency in this assay. These studies suggest that ultrapotently neutralizing mAbs block CHIKV fusion.

mAb Prophylaxis In Vivo

We tested a subset of mAbs exhibiting diverse levels of neutralizing activity (Table 1) in a lethal infection model with 6-week-old, highly immunodeficient *Ifnar*$^{-/-}$ mice. Mice were pre-treated with a single 50 μg dose (~3 mg/kg) of human anti-CHIKV mAbs or a West Nile virus (WNV)-specific isotype control mAb (WNV hE16) 24 hr before subcutaneous injection with a lethal dose of CHIKV-LR2006. All mice treated with the isotype control mAb succumbed to infection by 4 days post-inoculation. Pretreatment with mAbs 4B8, 4J21, or 5M16 completely protected *Ifnar*$^{-/-}$ mice, whereas treatment with mAbs 3E23 or 9D14 partially protected the infected animals, with 50% and 67% survival rates, respectively (Figure 3A). Surprisingly, mAb 2D12, which weakly neutralized in vitro, protected 80% of the animals.

mAb Post-exposure Therapy In Vivo

Ifnar$^{-/-}$ mice were inoculated with a lethal dose of CHIKV-LR2006 and then administered a single 50 μg (~3 mg/kg) dose of representative mAbs 24 hr following virus inoculation. Therapeutic administration of mAb 4N12 or 5M16 mAbs provided complete protection, whereas the isotype-control mAb provided no protection, and others provided partial protection (Figure 3B). To define further the therapeutic window of efficacy, *Ifnar*$^{-/-}$ mice were administered a single 250 μg (~14 mg/kg) dose of representative mAbs 48 hr after challenge with CHIKV-LR2006. Treatment with 4N12, 5M16, 4J21, and 4B8 protected 100%, 85%, 50%, and 12.5% of the animals, respectively (Figure 3C). Remarkably, monotherapy with 4N12 or 4J21 at the later time point of 60 hr protected 70% and 55% of animals when used at a dose of 500 μg (~28 mg/kg) (Figure 3D). The observed differences in efficacy of the mAbs are likely not due to varying in vivo half-life in mice, as there was no appreciable difference in the rate of clearance in the serum for mAbs 4B8, 5M16, 4N12, and 4J21 (data not shown). These data establish that human mAbs can protect against CHIKV-induced death, even at intervals well after infection is established.

Combination mAb Therapy In Vivo

Given the possibility of resistance selection in vivo in animals treated with a single anti-CHIKV mAb (Pal et al., 2013), we tested whether a combination of two anti-CHIKV human mAbs could protect mice against lethal challenge. We chose pairs of neutralizing mAbs based on the potency of individual mAbs in vitro as well as protective activity in vivo as monotherapy. *Ifnar*$^{-/-}$ mice were administered a single combination antibody treatment dose of the most effective mAbs 60 hr after inoculation. None of the combinations tested at varying doses ([4J21 + 2H1], [4J21 + 5M16], or [4J21 + 4N12]) provided superior protection to 4J21 or 4N12 monotherapy.

DISCUSSION

We report the isolation of a diverse panel of naturally occurring human mAbs from a single individual, the majority of which recognize the CHIKV E2 protein and display remarkable neutralizing activity in vitro and therapeutic efficacy in vivo. As a class, the most inhibitory antibodies also exhibited broad activity, neutralizing viruses from all three CHIKV genotypes, including a strain currently circulating in the Caribbean. The majority of human CHIKV-specific mAbs isolated in this study neutralized the virus at concentrations <100 ng/ml, and many exhibited inhibitory activity at <10 ng/ml. This activity is greater than we have observed in our previous studies of human mAbs against other pathogenic human viruses, including H1, H2, H3, or H5 influenza viruses (Hong et al., 2013; Krause et al., 2010, 2011a, 2011b, 2012; Thornburg et al., 2013; Yu et al., 2008), dengue viruses (Messer et al., 2014; Smith et al., 2012, 2013a, 2013b, 2014),

by alanine-scanning mutagenesis, are designated by color-coded dots for each specific mAb. Residues that influence the binding of multiple antibodies are indicated by squares shaded in gray, with the darker the shade of gray, the greater number of antibodies influenced by substitution at that residue (legend in B). (B) Location of residues required for mAb binding mapped onto the crystal structure of the mature envelope glycoprotein complex (PDB ID 3N41). A side view of a ribbon trace of a single heterodimer of E1/E2 is shown with E1 in light cyan and the domains of E2 colored as in (A). The side chains of the aa required for mAb binding are shown as space-filling forms and color coded for each of the 20 individual antibodies according to the legend in (A).
(C) A top view of the E1/E2 heterodimer, rotated 90° from the structure in (B). Also see Figures S3 and S4.

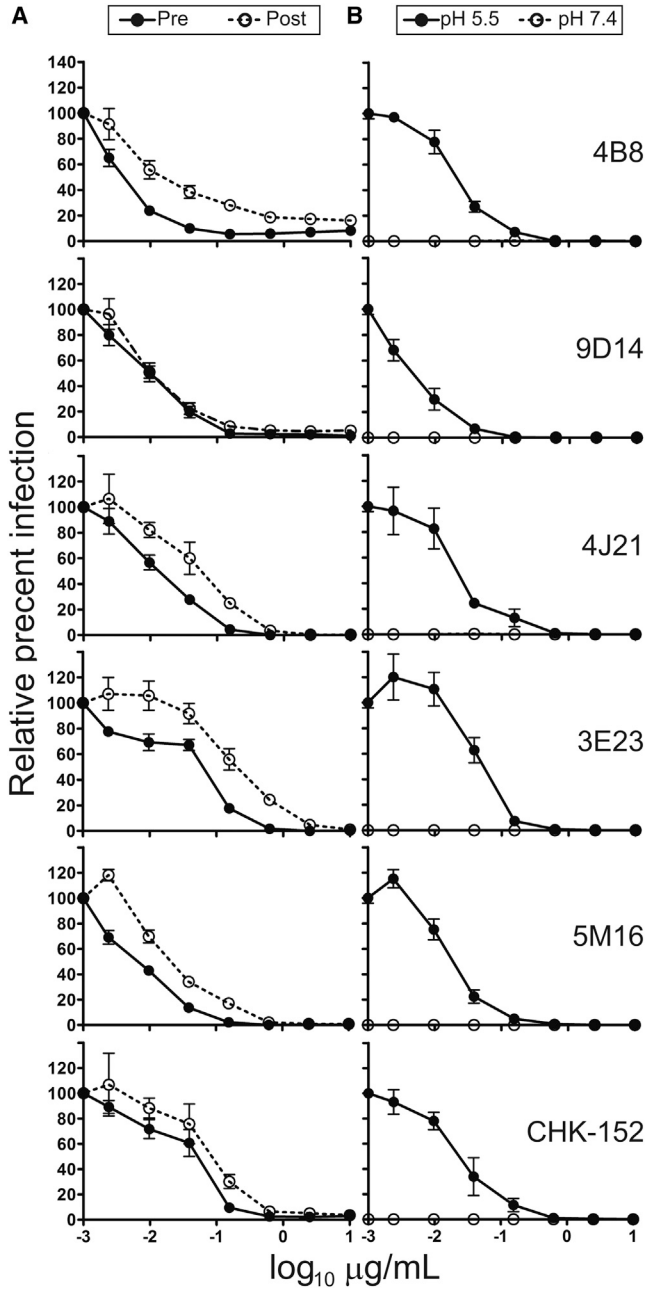

Figure 2. Mechanism of Neutralization by Human Anti-CHIKV mAbs

(A) Pre- and post-attachment neutralization assays. SL15649 VRPs were (1) incubated with the mAbs shown (including CHK-152, a positive control mAb) prior to addition to pre-chilled Vero cells, followed by removal of unbound virus by three washes (pre-attachment; filled circle) or (2) allowed to adsorb to pre-chilled Vero cells followed by addition of the indicated mAbs (post-attachment; open circles). (B) FFWO assay. SL15649 VRPs were adsorbed to pre-chilled Vero cells, followed by addition of the mAbs shown (including CHK-152, a positive control murine mAb). Unbound virus was removed, and cells were exposed to low (pH 5.5 to trigger viral fusion at the plasma membrane; filled circles) or neutral (pH 7.4 as a control; open circles) pH medium at 37°C for 2 min. For both (A) and (B), cells were incubated at 37°C until 18 hr after infection, and GFP-positive cells were quantified using fluorescence microscopy. The data are combined from two independent experiments, each performed in triplicate, and represented as mean ± SEM.

and others. The potency of many human CHIKV mAbs is comparable to or exceeds that of best-in-class murine neutralizing CHIKV mAbs (Fric et al., 2013; Pal et al., 2013; Warter et al., 2011), which were generated after iterative boosting and affinity maturation. Most other neutralizing human mAbs against CHIKV are substantially less potent (Fong et al., 2014; Selvarajah et al., 2013; Warter et al., 2011). A single previously reported human CHIKV-specific mAb (IM-CKV063) displays activity comparable to the ultrapotent neutralizing mAbs reported here (Fong et al., 2014).

We observed a diversity of epitope recognition patterns in E2 by the different neutralizing CHIKV mAbs tested. Fine epitope mapping with alanine-substituted CHIKV glycoproteins showed that recognition of three structural regions in E2 is associated with mAb-mediated neutralization: domain A, which contains the putative RBD (Sun et al., 2013; Voss et al., 2010), domain B, which contacts and shields the fusion loop in E1 (Voss et al., 2010), and arches 1 and 2 of the β-ribbon connector, which contains an acid-sensitive region and links domains A and B (Voss et al., 2010). Of the antibodies mapped to epitopes in E2, the bulk (those in competition groups 1 and 2) preferentially recognized sites in domain A and arches 1 and 2, whereas a smaller group (in competition group 3) recognized sites in domain B. These data suggest that surface-exposed regions in domain A and the arches are dominant antigenic sites that elicit human neutralizing antibody responses. We conclude that the highly conserved region in domain A and arch 2 might elicit a broadly protective immune response and serve as an attractive candidate for epitope-focused vaccine design.

Remarkably, almost a quarter of surface-exposed residues in the critical E2 domains appear to be engaged by one or more mAbs from a single individual. The existence of functionally diverse binding modes on the major antigenic sites is implied by two observations: (1) some mAbs bound to similar epitopes but exhibited inhibitory activity that varied by several orders of magnitude and (2) there was little correlation between neutralization capacity and affinity of binding to E2 protein. Seven of the most potently neutralizing human mAbs (2H1, 3E23, 4B8, 4J21, 4N12, 5M16, and 9D14) inhibited CHIKV infection at a step following attachment, likely via prevention of pH-dependent structural changes, which prevents nucleocapsid penetration into the cytoplasm (Kielian et al., 2010).

As therapeutic efficacy in mice appears to predict treatment outcomes in experimentally induced infection and arthritis in nonhuman primates (Pal et al., 2013, 2014), the data here suggest that prophylaxis of humans with CHIKV-specific human mAbs would prevent infection. Given concerns about selection of resistant variants with monotherapy (Pal et al., 2013), combination therapy using ultrapotent neutralizing antibodies that target different regions of E2 may be desirable. Unexpectedly, we did not observe a superior therapeutic effect for combinations of mAbs compared with monotherapy at late time points in these studies with immunodeficient mice. In fact, the survival in most groups treated with combination therapy trended toward less protection than that of the groups treated with 4J21 or 4N12 alone. Although further study is warranted, the lack of enhanced therapeutic benefit with the particular mAb combinations tested could be due to competition or structural hindrance of binding of individual antibody molecules to adjacent epitopes on E2

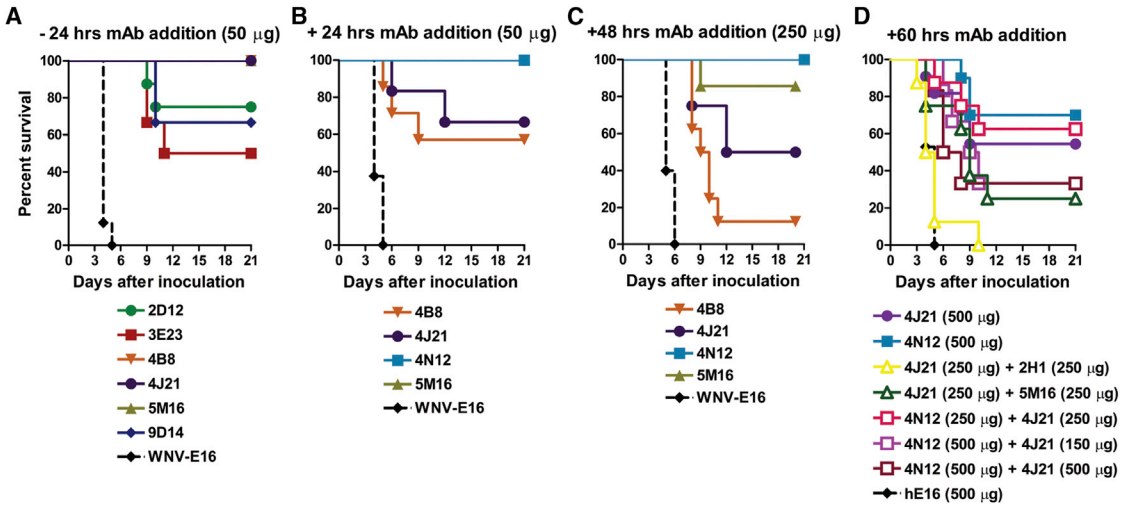

Figure 3. Human mAb Prophylaxis and Therapy against Lethal CHIKV Infection in *Ifnar*$^{-/-}$ Mice

(A–C) Mice were administered either 50 or 250 μg of indicated CHIKV-specific or control mAb by intraperitoneal injection 24 hr before (A; n = 6 to 8 mice per mAb tested) or 24 hr (B; n = 5 to 8 mice per mAb tested) or 48 hr after (C); n = 7 to 10 mice per mAb tested) a lethal challenge of CHIKV.

(D) Mice were administered 150, 250, or 500 μg of indicated CHIKV-specific mAbs in combination by intraperitoneal injection 60 hr after a lethal challenge of CHIKV (n = 6 to 13 mice per mAb combination tested). For monotherapy with 4J21, 4N12, or hE16 (negative control), a single dose of 500 μg was given (n = 10 to 17 mice per mAb tested). All data in this figure were pooled from at least two independent experiments. The following statistical analysis was performed using the Mantel-Cox log rank test: 4N12 versus 4J21, p = 0.39; 4N12 (500 μg) versus 4N12 (250 μg) + 4J21 (250 μg), p = 0.69; 4N12 (500 μg) versus 4N12 (500 μg) + 4J21 (150 μg), p = 0.13; 4N12 (500 μg) versus 4N12 (500 μg) + 4J21 (500 μg), p = 0.06. All Ab administrations with the exception of 4J21 (250 μg) + 2H1 (250 μg) differed significantly from the hE16 control ($p < 0.002$).

proteins on the icosahedral virion surface. In comparison, a prior study with anti-E2 (CHK-152) and anti-E1 (CHK-166) mouse MAbs did show advantage as combination therapy (Pal et al., 2013). Regardless, our data suggest that patient populations at markedly increased risk of severe disease could be targeted for prophylaxis or treatment with human anti-CHIKV mAbs during outbreaks, including those with serious underlying medical conditions (e.g., late-term pregnant women, the immunocompromised, and the elderly). Further clinical testing is planned to determine whether neutralizing human mAbs can prevent or ameliorate established joint disease in humans.

EXPERIMENTAL PROCEDURES

Isolation of Human mAbs

PBMCs were obtained from a human ~5.5 years after documented symptomatic CHIKV infection in Sri Lanka. B cells were transformed with EBV in the presence of CpG. The supernatants from the resulting B cell lymphoblastic cells lines were screened for CHIKV-neutralizing activity using SL15649 VRPS. Positive wells were further selected for the presence of human CHIKV-specific binding antibodies by ELISA using live CHIKV vaccine strain 181/25 virus as antigen. Transformed B cells were collected and fused to a myeloma cell line, distributed into culture plates and expansion, and selected by growth in hypoxanthine-aminopterin-thymidine medium containing ouabain. Hybridomas were cloned by single-cell sorting. Supernatants from cloned hybridomas growing in serum-free medium were collected, purified, and concentrated from clarified medium by protein G chromatography.

Neutralization Assays

Purified IgG mAb proteins were tested for neutralizing activity using CHIKV VRPs or fully infectious CHIKV. VRPs were incubated with serial dilutions of mAbs then inoculated onto Vero 81 cell monolayers for 18 hr; infected cells and total cells (identified with a nuclear marker) were identified with a fluorescence imaging system. Neutralizing activity for four infectious virus strains was determined in a focus reduction neutralization test (Pal et al., 2013). Serial dilutions of mAbs were incubated with 100 focus-forming units of CHIKV and then added to Vero cells. Foci were detected with a mouse anti-CHIKV mAb after cell fixation using immunoperoxidase detection and quantified using an ImmunoSpot 5.0.37 macroanalyzer (Cellular Technologies).

E2 ELISA

Recombinant CHIKV E2 ectodomain protein (corresponding to the CHIKV-LR2006 strain) was generated in *E. coli* (Pal et al., 2013) and adsorbed to microtiter plates. Human mAbs were applied, and bound CHIKV-specific mAbs were detected with biotin-conjugated goat anti-human IgG.

Competition Binding Assay

We identified groups of antibodies binding to the same major antigenic site by competing pairs of antibodies for binding to CHIKV-LR2006 E2 ectodomain protein containing a polyhistidine-tag attached to an Anti-Penta-His biosensor tip (ForteBio 18-5077) in an Octet Red biosensor (ForteBio).

Alanine Scanning Mutagenesis for Epitope Mapping

A CHIKV envelope protein expression construct (strain S27, Uniprot Reference Q8JUX5) with a C-terminal V5 tag was subjected to alanine-scanning mutagenesis to generate a comprehensive mutation library. Primers were designed to mutate each residue within the E2, 6K, and E1 regions of the envelope proteins (residues Y326 to H1248 in the structural polyprotein) to alanine; alanine codons were mutated to serine. In total, 910 CHIKV envelope protein mutants were generated. Loss of binding of mAbs to each construct was determined using an immunofluorescence binding assay, using cellular fluorescence detected with a high-throughput flow cytometer.

Mechanism of Neutralization

MAbs were interacted with VRPs before or after attachment to Vero 81 cells, and then cells were stained, imaged, and analyzed as described for VRP neutralization assays to determine at what stage mAbs exerted the antiviral effect. Fusion-from-without assays were performed as detailed in Supplemental Experimental Procedures.

In Vivo Protection Studies in Mice

Ifnar$^{-/-}$ mice were bred in pathogen-free animal facilities and infection experiments were performed in A-BSL3 facilities. Footpad injections were performed under anesthesia. For prophylaxis studies, human mAbs were administered by intraperitoneal injection to 6-week-old *Ifnar*$^{-/-}$ mice 1 day prior to subcutaneous inoculation in the footpad with 10 FFU of CHIKV-LR. For therapeutic studies, 10 FFU of CHIKV-LR was delivered 24, 48, or 60 hr prior to administration of a single dose of individual or combinations of human mAbs at specified doses.

SUPPLEMENTAL INFORMATION

Supplemental Information includes Supplemental Experimental Procedures, four figures, and one table and can be found with this article online at http://dx.doi.org/10.1016/j.chom.2015.06.009.

AUTHOR CONTRIBUTIONS

S.A.S. and L.A.S. performed initial screening and isolation of antibodies. S.A.S., N.K., and G.S. isolated hybridomas, purified antibodies, and sequenced mAb clones. C.E.M. and M.T.H. devised and executed construction of SL15649 replicon plasmids. L.A.S., S.K., and A.W.A. devised and conducted VRP neutralization and mechanistic assays. J.M.F. and P.P. and M.S.D. devised and performed FRNT assays with infectious virus. S.K.A. and M.S.D. devised and conducted surface plasmon resonance studies. A.F. and J.E.C. devised and performed Octet-based competition binding assays and provided associated data. K.M.K., R.H.F., S.S., and B.J.D. devised and performed alanine-scanning mutagenesis. L.A.S. performed structural analysis of epitope residues. J.M.F., J.D.B., and M.S.D. devised and performed mouse studies. S.A.S., L.A.S., M.S.D., T.S.D., and J.E.C. prepared the manuscript. All authors revised and approved the final version of the manuscript.

ACKNOWLEDGMENTS

We thank Aravinda de Silva (UNC Chapel Hill) for assistance with acquisition of the donor sample, Frances Smith-House at Vanderbilt University for excellent laboratory management support, Melissa Edeling and Katie O'Brien at WUSTL for generating E2 proteins and performing some of the initial mAb binding experiments, Edgar Davidson, Andrew Ettenger, Johnathan Guest, Trevor Barnes, Surabhi Srinivasan, and Bernard Lieberman at Integral Molecular for help with epitope mapping, and Chris Slaughter for assistance with biostatistical analysis of VRP neutralization data. This work was supported by U.S. National Institutes of Health grants R01 AI114816 (J.E.C and M.S.D.), K08 AI103038 (S.A.S.), F32 AI096833 (L.A.S.), T32 HL007751 (A.W.A.), T32 5T32AI007151-33 (C.E.M.) U54 AI057157 (T.S.D.), R01 AI104545 (M.S.D.), and NIH contract HHSN272200900055C (B.J.D.). The work also received support from the Elizabeth B. Lamb Center for Pediatric Research (T.S.D.), Infectious Diseases Society of America Education and Research Foundation (S.A.S.), and National Foundation for Infectious Diseases Young Investigator Award in Vaccine Development sponsored by Pfizer (S.A.S). The project described was supported by the National Center for Research Resources, Grant UL1 RR024975-01 and is now at the National Center for Advancing Translational Sciences, Grant 2 UL1 TR000445-06. The content is solely the responsibility of the authors and does not represent the official views of the NIH. Four of the authors (S.A.S., L.A.S., T.S.D. and J.E.C.) are designated co-inventors on a submitted patent application that includes the human monoclonal antibodies described in this paper.

Received: February 9, 2015
Revised: May 27, 2015
Accepted: June 22, 2015
Published: July 8, 2015

REFERENCES

Bréhin, A.C., Rubrecht, L., Navarro-Sanchez, M.E., Maréchal, V., Frenkiel, M.P., Lapalud, P., Laune, D., Sall, A.A., and Desprès, P. (2008). Production and characterization of mouse monoclonal antibodies reactive to Chikungunya envelope E2 glycoprotein. Virology *371*, 185–195.

CDC (2013). Chikungunya virus (Atlanta, GA: US Department of Health and Human Services). http://www.cdc.gov/media/releases/2013/p1218-chikungunyas.html.

CDC (2014). Chikungunya in the Americas (Atlanta, GA: US Department of Health and Human Services). http://www.cdc.gov/chikungunya/geo/americas.html.

Chu, H., Das, S.C., Fuchs, J.F., Suresh, M., Weaver, S.C., Stinchcomb, D.T., Partidos, C.D., and Osorio, J.E. (2013). Deciphering the protective role of adaptive immunity to CHIKV/IRES a novel candidate vaccine against Chikungunya in the A129 mouse model. Vaccine *31*, 3353–3360.

Couderc, T., Khandoudi, N., Grandadam, M., Visse, C., Gangneux, N., Bagot, S., Prost, J.F., and Lecuit, M. (2009). Prophylaxis and therapy for Chikungunya virus infection. J. Infect. Dis. *200*, 516–523.

Edwards, J., and Brown, D.T. (1986). Sindbis virus-mediated cell fusion from without is a two-step event. J. Gen. Virol. *67*, 377–380.

Fong, R.H., Banik, S.S., Mattia, K., Barnes, T., Tucker, D., Liss, N., Lu, K., Selvarajah, S., Srinivasan, S., Mabila, M., et al. (2014). Exposure of epitope residues on the outer face of the chikungunya virus envelope trimer determines antibody neutralizing efficacy. J. Virol. *88*, 14364–14379.

Fric, J., Bertin-Maghit, S., Wang, C.I., Nardin, A., and Warter, L. (2013). Use of human monoclonal antibodies to treat Chikungunya virus infection. J. Infect. Dis. *207*, 319–322.

Goh, L.Y., Hobson-Peters, J., Prow, N.A., Gardner, J., Bielefeldt-Ohmann, H., Pyke, A.T., Suhrbier, A., and Hall, R.A. (2013). Neutralizing monoclonal antibodies to the E2 protein of chikungunya virus protects against disease in a mouse model. Clin. Immunol. *149*, 487–497.

Hallengärd, D., Lum, F.M., Kümmerer, B.M., Lulla, A., Lulla, V., García-Arriaza, J., Fazakerley, J.K., Roques, P., Le Grand, R., Merits, A., et al. (2014). Prime-boost immunization strategies against Chikungunya virus. J. Virol. *88*, 13333–13343.

Hawman, D.W., Stoermer, K.A., Montgomery, S.A., Pal, P., Oko, L., Diamond, M.S., and Morrison, T.E. (2013). Chronic joint disease caused by persistent Chikungunya virus infection is controlled by the adaptive immune response. J. Virol. *87*, 13878–13888.

Hong, M., Lee, P.S., Hoffman, R.M., Zhu, X., Krause, J.C., Laursen, N.S., Yoon, S.I., Song, L., Tussey, L., Crowe, J.E., Jr., et al. (2013). Antibody recognition of the pandemic H1N1 Influenza virus hemagglutinin receptor binding site. J. Virol. *87*, 12471–12480.

Kam, Y.W., Lee, W.W., Simarmata, D., Harjanto, S., Teng, T.S., Tolou, H., Chow, A., Lin, R.T., Leo, Y.S., Rénia, L., and Ng, L.F. (2012a). Longitudinal analysis of the human antibody response to Chikungunya virus infection: implications for serodiagnosis and vaccine development. J. Virol. *86*, 13005–13015.

Kam, Y.W., Lum, F.M., Teo, T.H., Lee, W.W., Simarmata, D., Harjanto, S., Chua, C.L., Chan, Y.F., Wee, J.K., Chow, A., et al. (2012b). Early neutralizing IgG response to Chikungunya virus in infected patients targets a dominant linear epitope on the E2 glycoprotein. EMBO Mol. Med. *4*, 330–343.

Kam, Y.W., Lee, W.W., Simarmata, D., Le Grand, R., Tolou, H., Merits, A., Roques, P., and Ng, L.F. (2014). Unique epitopes recognized by antibodies induced in Chikungunya virus-infected non-human primates: implications for the study of immunopathology and vaccine development. PLoS ONE *9*, e95647.

Kielian, M., Chanel-Vos, C., and Liao, M. (2010). Alphavirus entry and membrane fusion. Viruses *2*, 796–825.

Krause, J.C., Tumpey, T.M., Huffman, C.J., McGraw, P.A., Pearce, M.B., Tsibane, T., Hai, R., Basler, C.F., and Crowe, J.E., Jr. (2010). Naturally occurring human monoclonal antibodies neutralize both 1918 and 2009 pandemic influenza A (H1N1) viruses. J. Virol. *84*, 3127–3130.

Krause, J.C., Tsibane, T., Tumpey, T.M., Huffman, C.J., Basler, C.F., and Crowe, J.E., Jr. (2011a). A broadly neutralizing human monoclonal antibody that recognizes a conserved, novel epitope on the globular head of the influenza H1N1 virus hemagglutinin. J. Virol. *85*, 10905–10908.

Krause, J.C., Tsibane, T., Tumpey, T.M., Huffman, C.J., Briney, B.S., Smith, S.A., Basler, C.F., and Crowe, J.E., Jr. (2011b). Epitope-specific human influenza antibody repertoires diversify by B cell intraclonal sequence divergence and interclonal convergence. J. Immunol. *187*, 3704–3711.

Krause, J.C., Tsibane, T., Tumpey, T.M., Huffman, C.J., Albrecht, R., Blum, D.L., Ramos, I., Fernandez-Sesma, A., Edwards, K.M., García-Sastre, A., et al. (2012). Human monoclonal antibodies to pandemic 1957 H2N2 and pandemic 1968 H3N2 influenza viruses. J. Virol. *86*, 6334–6340.

Lee, C.Y., Kam, Y.W., Fric, J., Malleret, B., Koh, E.G., Prakash, C., Huang, W., Lee, W.W., Lin, C., Lin, R.T., et al. (2011). Chikungunya virus neutralization antigens and direct cell-to-cell transmission are revealed by human antibody-escape mutants. PLoS Pathog. *7*, e1002390.

Lum, F.M., Teo, T.H., Lee, W.W., Kam, Y.W., Rénia, L., and Ng, L.F. (2013). An essential role of antibodies in the control of Chikungunya virus infection. J. Immunol. *190*, 6295–6302.

Masrinoul, P., Puiprom, O., Tanaka, A., Kuwahara, M., Chaichana, P., Ikuta, K., Ramasoota, P., and Okabayashi, T. (2014). Monoclonal antibody targeting chikungunya virus envelope 1 protein inhibits virus release. Virology *464-465*, 111–117.

Messer, W.B., de Alwis, R., Yount, B.L., Royal, S.R., Huynh, J.P., Smith, S.A., Crowe, J.E., Jr., Doranz, B.J., Kahle, K.M., Pfaff, J.M., et al. (2014). Dengue virus envelope protein domain I/II hinge determines long-lived serotype-specific dengue immunity. Proc. Natl. Acad. Sci. USA *111*, 1939–1944.

Pal, P., Dowd, K.A., Brien, J.D., Edeling, M.A., Gorlatov, S., Johnson, S., Lee, I., Akahata, W., Nabel, G.J., Richter, M.K., et al. (2013). Development of a highly protective combination monoclonal antibody therapy against Chikungunya virus. PLoS Pathog. *9*, e1003312.

Pal, P., Fox, J.M., Hawman, D.W., Huang, Y.J., Messaoudi, I., Kreklywich, C., Denton, M., Legasse, A.W., Smith, P.P., Johnson, S., et al. (2014). Chikungunya viruses that escape monoclonal antibody therapy are clinically attenuated, stable, and not purified in mosquitoes. J. Virol. *88*, 8213–8226.

Schilte, C., Staikowsky, F., Couderc, T., Madec, Y., Carpentier, F., Kassab, S., Albert, M.L., Lecuit, M., and Michault, A. (2013). Chikungunya virus-associated long-term arthralgia: a 36-month prospective longitudinal study. PLoS Negl. Trop. Dis. *7*, e2137.

Selvarajah, S., Sexton, N.R., Kahle, K.M., Fong, R.H., Mattia, K.A., Gardner, J., Lu, K., Liss, N.M., Salvador, B., Tucker, D.F., et al. (2013). A neutralizing monoclonal antibody targeting the acid-sensitive region in chikungunya virus E2 protects from disease. PLoS Negl. Trop. Dis. *7*, e2423.

Sissoko, D., Malvy, D., Ezzedine, K., Renault, P., Moscetti, F., Ledrans, M., and Pierre, V. (2009). Post-epidemic Chikungunya disease on Reunion Island: course of rheumatic manifestations and associated factors over a 15-month period. PLoS Negl. Trop. Dis. *3*, e389.

Smith, S.A., Zhou, Y., Olivarez, N.P., Broadwater, A.H., de Silva, A.M., and Crowe, J.E., Jr. (2012). Persistence of circulating memory B cell clones with potential for dengue virus disease enhancement for decades following infection. J. Virol. *86*, 2665–2675.

Smith, S.A., de Alwis, A.R., Kose, N., Harris, E., Ibarra, K.D., Kahle, K.M., Pfaff, J.M., Xiang, X., Doranz, B.J., de Silva, A.M., et al. (2013a). The potent and broadly neutralizing human dengue virus-specific monoclonal antibody 1C19 reveals a unique cross-reactive epitope on the bc loop of domain II of the envelope protein. MBio *4*, e00873–e13.

Smith, S.A., de Alwis, R., Kose, N., Durbin, A.P., Whitehead, S.S., de Silva, A.M., and Crowe, J.E., Jr. (2013b). Human monoclonal antibodies derived from memory B cells following live attenuated dengue virus vaccination or natural infection exhibit similar characteristics. J. Infect. Dis. *207*, 1898–1908.

Smith, S.A., de Alwis, A.R., Kose, N., Jadi, R.S., de Silva, A.M., and Crowe, J.E., Jr. (2014). Isolation of dengue virus-specific memory B cells with live virus antigen from human subjects following natural infection reveals the presence of diverse novel functional groups of antibody clones. J. Virol. *88*, 12233–12241.

Staples, J.E., Breiman, R.F., and Powers, A.M. (2009). Chikungunya fever: an epidemiological review of a re-emerging infectious disease. Clin. Infect. Dis. *49*, 942–948.

Sun, S., Xiang, Y., Akahata, W., Holdaway, H., Pal, P., Zhang, X., Diamond, M.S., Nabel, G.J., and Rossmann, M.G. (2013). Structural analyses at pseudo atomic resolution of Chikungunya virus and antibodies show mechanisms of neutralization. eLife *2*, e00435.

Sun, C., Gardner, C.L., Watson, A.M., Ryman, K.D., and Klimstra, W.B. (2014). Stable, high-level expression of reporter proteins from improved alphavirus expression vectors to track replication and dissemination during encephalitic and arthritogenic disease. J. Virol. *88*, 2035–2046.

Thornburg, N.J., Nannemann, D.P., Blum, D.L., Belser, J.A., Tumpey, T.M., Deshpande, S., Fritz, G.A., Sapparapu, G., Krause, J.C., Lee, J.H., et al. (2013). Human antibodies that neutralize respiratory droplet transmissible H5N1 influenza viruses. J. Clin. Invest. *123*, 4405–4409.

Voss, J.E., Vaney, M.C., Duquerroy, S., Vonrhein, C., Girard-Blanc, C., Crublet, E., Thompson, A., Bricogne, G., and Rey, F.A. (2010). Glycoprotein organization of Chikungunya virus particles revealed by X-ray crystallography. Nature *468*, 709–712.

Warter, L., Lee, C.Y., Thiagarajan, R., Grandadam, M., Lebecque, S., Lin, R.T., Bertin-Maghit, S., Ng, L.F., Abastado, J.P., Desprès, P., et al. (2011). Chikungunya virus envelope-specific human monoclonal antibodies with broad neutralization potency. J. Immunol. *186*, 3258–3264.

Yu, X., Tsibane, T., McGraw, P.A., House, F.S., Keefer, C.J., Hicar, M.D., Tumpey, T.M., Pappas, C., Perrone, L.A., Martinez, O., et al. (2008). Neutralizing antibodies derived from the B cells of 1918 influenza pandemic survivors. Nature *455*, 532–536.